A Simple Model for The Depolarizing Effects of Rain and Ice on Earth Satellite Links in the 10 to 30 GHz Frequency Range

by

Donald Lawson Runyon, Jr.

Thesis submitted to the Faculty of the
Virginia Polytechnic Institute and State University
in partial fulfillment of the requirements for the degree of

MASTER OF SCIENCE

in

Electrical Engineering

APPROVED:

W. L. Stutzman, Chairman

C. W. Bostian

I. M. Besieris

April, 1983
Blacksburg, Virginia

ACKNOWLEDGEMENTS

I would like to express my appreciation to all those people who assisted me in completing my Master of Science thesis. Special thanks goes to Dr. Warren Stutzman for his guidance throughout the year of work that went into this thesis. I would also like to thank the other members of my committee: Dr. Charles Bostian and Dr. Ioannis Besieris. Their comments and suggestions were greatly appreciated.

In addition, I would like to thank Linda White for her help in preparing this manuscript. The other members of the Satellite Communications Group made my graduate years very enjoyable and I wish to extend my gratitude to all of them.

Last, I would like to thank Libbie Reardon for her constant support during the past two years.

TABLE OF CONTENTS

LIST OF FIGURES

Figure 6-4. XPD vs A calculated at 11 GHz using the multiple scattering model for elevation angles of 10.7° and 45°. An ice layer is included above the rain with an ice content given by (6.2-1).

LIST OF TABLES

Chapter I

INTRODUCTION

There are two basic types of communication system trunks in use today: the terrestrial and the satellite-earth link. Terrestrial links include a variety of trunks such as wire, coaxial cable, microwave link, fiber optic cable, and submarine cable. These trunks must be capable of operating reliably within their environments, and maintenance is required over the length of the transmission medium (wire, cable, or relay stations). Similarly, the satellite-earth link must meet performance requirements to achieve a specified reliability under a variety of atmospheric conditions. In contrast to the terrestrial link, the satellite systems have the advantage of having flexible interconnections between terminals (i.e., direct connectivity is not required). This feature, in addition to several others makes the satellite-earth link an attractive communication medium.

The viability of the satellite-earth link has led to an expanding list of uses for satellite communication systems. Beyond the heavy uses for voice and TV, there is great demand and application for electronic mail, electronic fund transfer, computer interconnections, facsimile, and video teleconferencing. As the costs of implementation decrease

with advances in technology, the demand for greater numbers of communication channels may exceed the available frequency band capacities. In order to avoid this situation in the future, research is currently being carried out to examine alternative techniques for increasing channel capacity.

One area of current research is the use of frequencies above the traditional 4/6 GHz band. The major commercial satellite communication systems began with the INTELSAT series in 1965 operating on a 6 GHz uplink and 4 GHz downlink. In 1981, common international service began using the 14/12 GHz band with the INTELSAT V satellite. The major domestic commercial systems developed in the 1970's include WESTAR (Western Union), SATCOM (RCA), and COMSTAR (AT&T), operating in the 6/4 GHz band. Introduction of the SBS satellite series operating in the 14/12 GHz band occured in 1981. The technology is becoming available to implement systems at frequencies in the 10 to 30 GHz band.

The primary advantage of utilizing the higher frequency bands is the promise of relief for the spectrum crowding and sharing below 6 GHz. However, other benefits arise from using the 10 to 30 GHz band. One advantage is that the allocated bandwidth is much larger in the higher frequency bands. The larger bandwidths enable the exploding information transfer requirements to be accomodated. The bandwidth

allocation is 500 MHz in the 4/6 and 7/8 GHz bands, greater than 500 MHz in the 12/14 GHz band, and 3.5 GHz in the 20/30 GHz band. A second advantage concerns hardware aspects. The same electrical performance of antennas and other microwave devices is possible with smaller size devices at the higher frequencies. The advances in reduction of size and weight requirements enable more devices to be included in a single spacecraft, allowing increased system complexity and flexibility.

Satellite capacities are not measured solely by frequency limitations. There is also a spatial limit to the number of satellites that may serve an area from a geosynchronous orbit. The present INTELSAT system has 12 operational and standby satellites to serve 300 earth stations. This includes 20,000 two-way telephone circuits plus TV and data. In the domestic sector, the major application is TV program distribution to broadcasters and cable systems. The projected growth for domestic satellite system traffic is 15% annually through the year 2000 [Edelson, Cooper, 1982]. This growth has brought concern with respect to the ability to satisfy future demand. An example of the growth and use trends is illustrated in Table 1-1.

Table 1-1

Utilization of frequency bands in the development of geosynchronous satellites (placed into orbit or planned) from 1965 to 1984 [Ippolito, 1981].

Interval	Below 6 GHz	7-9 GHz	11-17 GHz	18-40 GHz
1965-69	14	0	0	0
1970-74	23	0	1	2
1975-79	50	13	8	8
1980-84	54	4	39	6

A consequence of the increase in the number of satellites is not only reflected in the band crowding but also in orbit congestion. For domestic geosynchronous satellites the orbital spacing is 4° at 4/6 GHz and 3° at 12/14 GHz which allows 20 and 27 slots respectively. Presently domestic U.S. and Canadian organizations have (current and committed) 12 slots at 4/6 GHz and 10 slots at 12/14 GHz [Ippolito, 1981]. The Federal Communications Commission (FCC) has proposed 2° orbital spacings at 4/6 and 12/14 GHz.

Several techniques have been proposed to alleviate future limitations. Included in these techniques is frequency reuse employing polarization and spatial diversity. The dual polarization technique involves the transmission of a second channel using an orthogonal polarization, thus effectively doubling the frequency spectrum.

This report focuses on the effects of rain and ice on the polarization reuse technique. More specifically, we will devlop a model to reliably predict the measurable effects of signal degradation due to the cochannel interference created by depolarization of the cross channel. This problem has been reviewed by Cox [1981] and Bostian, et al., [1982] for earth-space paths and Olsen [1981] for terrestrial links.

The frequencies used for satellite communication links were selected for minimum atmospheric absorption to provide reliable operation. Attenuation of RF signals within the earth's atmosphere is due mainly to the presence of oxygen and water vapor. A description of the calculated atmospheric absorption and emission of radiation is given by Smith [1982]. This loss is important in the link power budget and may be considered a static value. However, additional consideration must be given to the effects of heavy rainfall. This time varying influence degrades system performance by lowering the received carrier level and hence the carrier-to-noise ratio (C/N). In order to provide a specified system reliability, adequate power margins must be allocated for the effects of rainfall.

Estimates of the rain margin for a single-polarization system may be determined from data or predictions given as a percent time of a year that a fixed level of attenuation (A) is exceeded. For a specified outage in a year, the C/N margin re-

quired would be the value A corresponding to the percent time that the attenuation was exceeded. Typical outage requirements are 0.1 and 0.01% which correspond to 8.8 hours and 53 minutes per year, respectively. The reliability for these outage values are 99.9 and 99.99%. The INTELSAT reliability objective is 99.99% (0.01% outage) and the SBS objective is 99.5% (0.5% outage).

The addition of the second (cross polarized) communication channel at the same frequency and transmitted on the polarization orthogonal to the cochannel polarization requires consideration of the effects of rain and ice depolarization. The depolarization due to rain alone is highly correlated with the cochannel attenuation and may be modeled as a function of the signal fade. The strict definitions for these measures are described in Section 2.1. Ice depolarization, unlike rain depolarization, is not accompanied by signal attenuation and may occur with or without rain along the path. The effects of ice depolarization for most situations may be provided for by the margin allocated for rain depolarization.

The ability to relate depolarization to rain attenuation provides a method to quantify the effects of the addition of the second polarization communication channel when the attenuation characteristic is known or estimated. This report presents the results in development of a simple model to predict

depolarization as a function of the attenuation due to rain and examines the relationship of attenuation and depolarization from the system reliability standpoint.

The basic background beginning with definitions and the mathematical formalism for depolariztion calculations are presented in Section 2.1. The precipitation medium parameters used in theoretical modeling are briefly discussed in Section 2.2 followed by a historical overview of the development of the model currently prescribed by the CCIR in Section 2.3. Other rain calculation models are reviewed in Section 2.4.

The rigorous multiple scattering model presented in Chapter 3 is used to develop the simple model. Chapter 4 discusses the various methods to present measured data and how the methods relate to theory and to each other. Also, a summary of the world-wide data base for depolarization measurements is presented.

The depolarization versus attenuation relationship is investigated in Chapter 5 beginning with basic parameter sensitivity studies. The general form of the relationship between depolarization and attenuation is discussed in Section 5.2 followed by an extensive parameter study in Section 5.3 to determine the details of the functional form. The proposed simple model is presented in Section 5.4 and it is compared to data in Section 5.5. The prediction accuracy of the proposed simple model is

compared with other models in the next section. Section 5.7 relates the depolarization effects and attenuation to the C/N margin for digital PSK systems using measured and predicted data. Frequency scaling of data is addressed using a result derived from the depolarization - attenuation relationship in Section 5.8.

Chapter 6 deals with the depolarization effects due to ice beginning with the theory required for multiple scattering computations.

Chapter II

MATHEMATICAL FORMALISMS

A dual polarized communication link has an antenna system which ideally has two orthogonally polarized transmit input ports and two orthogonally polarized receive output ports. Normally orthogonal linear or orthogonal circular polarization states are selected. However, the transmit polarization states are never perfectly purely linear (or circular), nor are they exactly orthogonal due to hardware imperfections. These imperfect polarization states cause finite cross-coupling of energy between the two channels. Calculation of this coupling is important to communication system designers. Inclusion of these realistic situations, where the dual polarizations are not purely orthogonal, is provided in the mathematical formalism presented here.

The complete system representation includes the effects of a depolarizing medium existing in the path between the transmit and receive antenna. Figure 2-1 is a representation for the system in which the various system blocks can be described mathematically by matrices. The mathematical formalism for this two channel model is presented in this section.

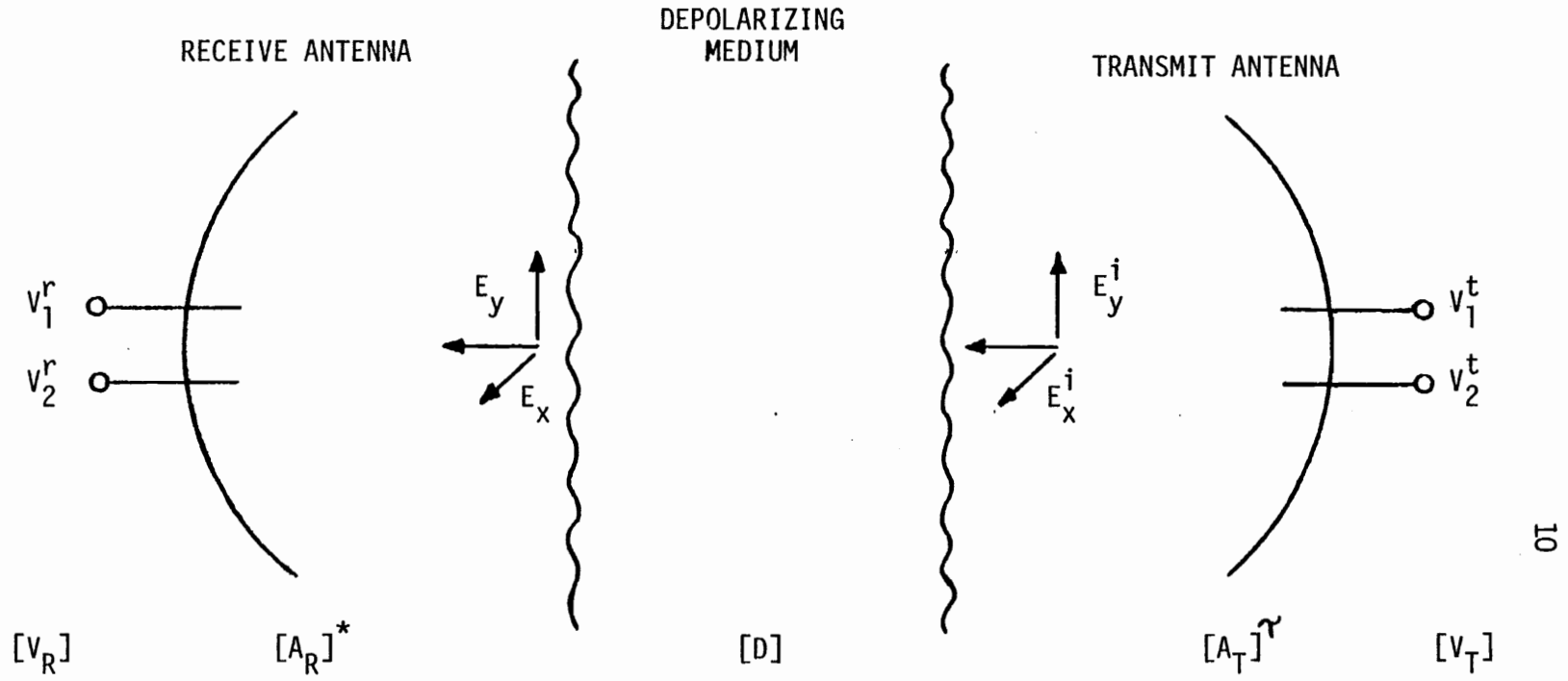

Figure 2-1. Dual polarized transmit-receive system influenced by a depolarizing medium.

2.1 SPECIFYING THE POLARIZATION STATE

The polarization state of any wave can be described through the ellipse traced out by the tip of the instantaneous electric field vector associated with the plane wave. The wave propagation direction is selected to be the z-direction and then the polarization ellipse is in the x-y plane. The x-axis taken as local horizontal. Figure 2-2 shows the polarization ellipse traced out by the tip of the instantaneous electric field vector $\vec{\mathcal{E}}(t)$. The ratio of the maximum to minimum magnitude of the electric field vector is the axial ratio (AR). The sign of AR is defined as + for left-hand sense and - for right hand sense of rotation [Stutzman, 1973].

The polarization state (i.e., shape, orientation of the ellipse and the rotational sense) are completely specified by either of the angle pairs (ε,τ), (γ,δ), where

$$\varepsilon = \cot^{-1}(AR) \qquad 1 \leq |AR| \leq \infty \qquad (2.1\text{-}1)$$

$$\tau = \text{tilt angle} \qquad 0 \leq \tau \leq 180° \qquad (2.1\text{-}2)$$

$$\gamma = \tan^{-1}\frac{E_2}{E_1} \qquad 0 \leq \gamma \leq 90° \qquad (2.1\text{-}3)$$

$$\delta = \text{phase}(E_y) - \text{phase}(E_x) \qquad -180 \leq \delta \leq 180° \qquad (2.1\text{-}4)$$

E_1 and E_2 are the maximum values of the electric field projections onto the x and y axes.

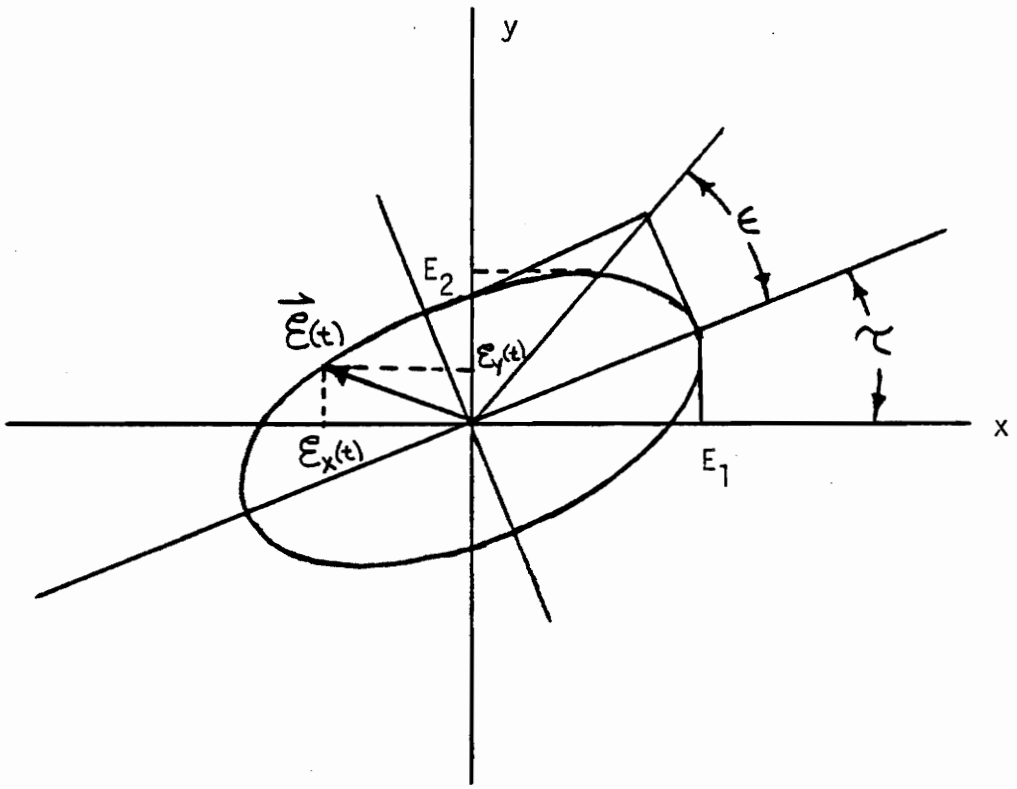

Figure 2-2. Polarization ellipse

The polarization state may be represented by a normalized complex vector. Other methods do exist but the complex vector representation (described in detail by Stutzman [1977]) was chosen because phase is preserved and infinite values are avoided. The complex vector representation is given by

$$\vec{e} = \cos\gamma\,\hat{x} + \sin\gamma\, e^{i\delta}\,\hat{y}. \qquad (2.1\text{-}5)$$

The γ and δ values are found from the more physically descriptive (ε,τ) pair through the transformation

$$\gamma = \left(\frac{1}{2}\right)\cos^{-1}\left[\cos 2\varepsilon \quad \cos 2\tau\right] \qquad (2.1\text{-}6)$$

$$\delta = \tan^{-1}\left[\frac{\tan 2\varepsilon}{\sin 2\tau}\right]. \qquad (2.1\text{-}7)$$

The polarization state of an antenna (either transmitting or receiving) is the same as the polarization state of the wave from the antenna when it is transmitting.

Although the polarization of an antenna is a function of the angular coordinates (θ,ϕ) describing the direction from the antenna, often a knowledge of the polarization state is required only at the peak of the main beam or for a particular (θ,ϕ) direction. Typically the polarization state of an antenna varies slowly throughout the 3-dB beamwidth of the antenna. The model to be developed here is applicable to polarization properties as functions of the space variables

(θ, ϕ) but it will be considered in the context of a fixed direction (such as the antenna main beam axis).

2.2 THE SYSTEM MODEL

The mathematical representation of precipitation effects on radio waves has been studied for a number of years. There is considerable agreement among researchers on the basic approach. There are, however, notational differences. Our research group has been involved in the modeling effort for over ten years. Several theoretical developments and computer programs have been based on a single notational format; therefore, we shall continue to use similar notation. We choose a coordinate system where z is the wave propagation direction and the electric field vector associated with the transmitted signal has components E_x^i and E_y^i The x and y directions are the reference axes discussed in connection with Figure 2.2.

The components of the electric field associated with the wave exiting the medium (and incident upon the receive antenna) are given by

$$\begin{bmatrix} E_x \\ \\ E_y \end{bmatrix} = [D] \begin{bmatrix} E_x^i \\ \\ E_y^i \end{bmatrix} \qquad (2.1\text{-}8)$$

where

$$[D] = \begin{bmatrix} D_{xx} & D_{xy} \\ D_{yx} & D_{yy} \end{bmatrix} \qquad (2.1\text{-}9)$$

is the depolarization matrix for the propagation medium. For the clear air case $[E] = [E^i]$ and $[D]$ is the identity matrix. Any departure from the clear air case can be classified as a propagation event; the matrix accounts for the change of the electric field components and thereby characterizes the medium.

The behavior of the antennas (transmit and receive) in a communication link can be modeled by matrices also. A complete discussion of this is presented in Appendix A. Combining the transmit antenna effects in (A.1-21), the receive antenna effects in (A.1-7), and the medium effects in (2.1-8) yields the complete system equation

$$[V_R]=[C_R][A_R]^*[D][A_T]\tilde{[C_T]}^{-1}\ [V_T]. \qquad (2.1\text{-}10)$$

where

$[V_R] = \begin{bmatrix} V_1^r \\ V_2^r \end{bmatrix}$ = receive phasor voltages at the output ports of a dual polarized communications link

$$[C_R] = \begin{bmatrix} C_1^r & 0 \\ 0 & C_2^r \end{bmatrix} \qquad [C_T]^{-1} = \begin{bmatrix} 1/C_1^t & 0 \\ 0 & 1/C_2^t \end{bmatrix}$$

C_1^r, C_2^r, C_1^t, C_2^t are constants of proportionality required to yield the correct voltage level similar to "effective length of a linearly polarized antenna."

$$[A_R]^* = \begin{bmatrix} \cos \gamma_1^r & \sin \gamma_1^r \; e^{-j\delta_1^r} \\ \cos \gamma_2^r & \sin \gamma_2^r \; e^{-j\delta_2^r} \end{bmatrix}$$

= complex conjugate of receive antenna matrix in which (γ_1^r, δ_1^r) and (γ_2^r, δ_2^r) are the polarization state parameters for channels 1 and 2 of the antenna.

$$[A_T]^\tau = \begin{bmatrix} \cos \gamma_1^t & \cos \gamma_2^t \\ \sin \gamma_1^t \; e^{j\delta_1^t} & \sin \gamma_2^t \; e^{j\delta_2^t} \end{bmatrix}$$

= transpose of transmit antenna matrix

$$[V_T] = \begin{bmatrix} V_1^t \\ V_2^t \end{bmatrix}$$ = transmit phasor voltages exciting ports 1 and 2 of the transmit antenna.

When the antennas on each channel are identical except for the polarization state (this is the case with a dual polarized feed on a common reflector), we have $C_1^t = C_2^t$ and $C_1^r = C_2^r$. If, further, the transmit and receive antennas are identical (except for polarization) (2.1-10) becomes

$$[V_R] = [A_R]^*[D][A_T]^\tau[V_T] \qquad (2.1\text{-}11)$$

If the transmit and receive antennas are not identical, there would be a multiplicative constant (C^r/C^t) in this equation which would not affect our subsequent calculations. Depolarization due to antenna effects alone is found from (2.1-11) with an identity matrix for [D]:

$$\begin{bmatrix} V_1^r \\ V_2^r \end{bmatrix} = \begin{bmatrix} \cos\gamma_1^r \cos\gamma_1^t + \sin\gamma_1^r \sin\gamma_1^t e^{-j(\delta_1^r - \delta_1^t)} & \cos\gamma_1^r \cos\gamma_2^t + \sin\gamma_1^r \sin\gamma_2^t e^{-j(\delta_1^r - \delta_2^t)} \\ \cos\gamma_2^r \cos\gamma_1^t + \sin\gamma_2^r \sin\gamma_1^t e^{-j(\delta_2^r - \delta_1^t)} & \cos\gamma_2^r \cos\gamma_2^t + \sin\gamma_1^r \sin\gamma_2^t e^{-j(\delta_2^r - \delta_2^t)} \end{bmatrix} \begin{bmatrix} V_1^t \\ V_2^t \end{bmatrix} \qquad (2.1\text{-}12)$$

As a simple example consider two identical, circularly polarized antennas (1 - right hand, 2 - left hand, circular

polarization) then ($\gamma_1 = 45°$, $\delta_1 = -90°$ and $\gamma_2 = 45°$, $\delta_2 = 90°$)

$$[A_R] = [A_T] = \frac{1}{\sqrt{2}} \begin{bmatrix} 1 & -j \\ 1 & j \end{bmatrix} \qquad (2.1\text{-}13)$$

If the transmission medium is free space, then

$$[D] = \begin{bmatrix} 1 & 0 \\ 0 & 1 \end{bmatrix} \qquad (2.1\text{-}14)$$

The system equation of (2.1-11) becomes

$$\begin{bmatrix} V_1^r \\ V_2^r \end{bmatrix} = \frac{1}{2} \begin{bmatrix} 1 & j \\ 1 & -j \end{bmatrix} \begin{bmatrix} 1 & 0 \\ 0 & 1 \end{bmatrix} \begin{bmatrix} 1 & 1 \\ -j & j \end{bmatrix} \begin{bmatrix} V_1^t \\ V_2^t \end{bmatrix}$$

$$= \begin{bmatrix} V_1^r \\ V_2^r \end{bmatrix} \qquad (2.1\text{-}15)$$

which is the expected result.

The coupling of signals between channels (due to both antenna and medium effects) degrades the performance of a dual polarized frequency reuse communication systems. This coupling is evaluated by two ratios [Bostian, Stutzman, and Gaines; 1982]. The first is crosspolarization discrimination xpd defined as

$$\text{xpd} = \frac{|V_{11}|}{|V_{21}|} \qquad (2.1\text{-}16)$$

where V_{11} is the voltage received in channel 1 arising from voltage applied to transmit channel 1, and V_{21} is the voltage in receive channel 2 arising also from voltage applied to transmit channel 1. See Figure 2-3. Crosspolarization discrimination is a measure of the shift from state 1 to state 2 when transmit channel 1 is excited. One could consider the xpd for channel 2 also:

$$xpd = \frac{|V_{22}|}{|V_{12}|} \tag{2.1-17}$$

In dB, we have

$$XPD = 20 \log xpd. \tag{2.1-18}$$

The other quantity used to describe channel coupling is crosspolarization isolation xpi defined as

$$xpi = \frac{|V_{11}|}{|V_{12}|} \tag{2.1-19}$$

or

$$xpi = \frac{|V_{22}|}{|V_{21}|} \tag{2.1-20}$$

In dB, we have

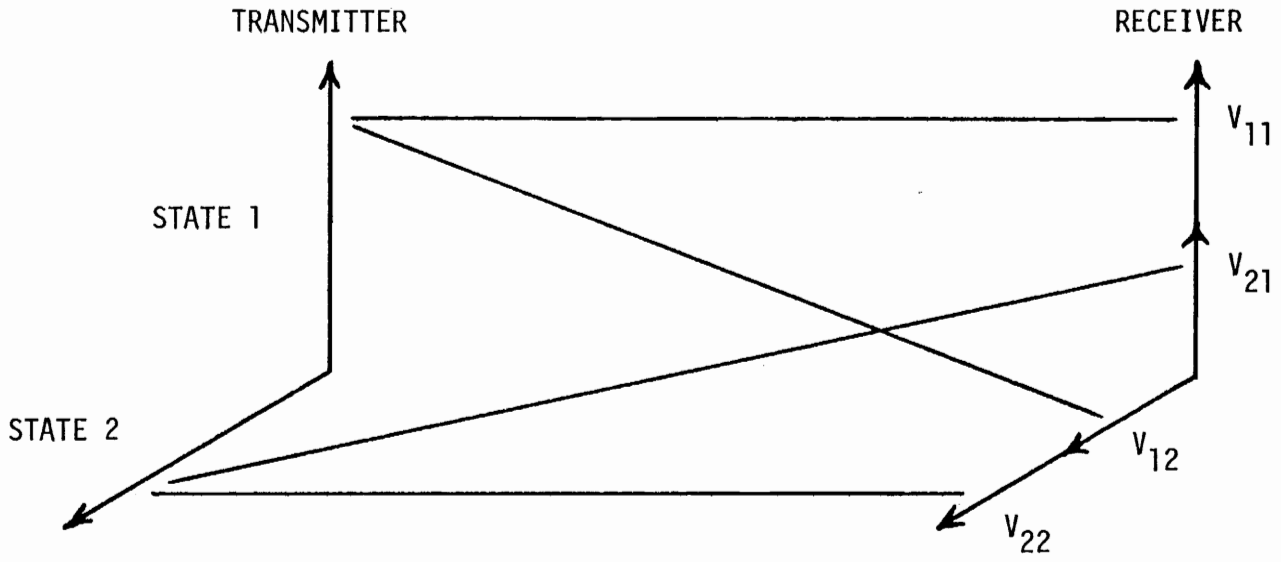

Figure 2-3. Illustration of channel coupling on a dual polarized communication system showing schematically the various voltage phasors.

$$XPI = 20 \log xpi. \qquad (2.1\text{-}21)$$

Crosspolarization isolation is a measure of the immunity to the coupling into a receive channel of signal originally transmitted from a channel of totally different polarization state. This is the typical situation for operational systems where, of course, two transmit channels would be in operation at the same time. xpi is however, difficult to measure because of the steps that must be taken to be able to separate the signal components on the same receive channel which were generated from different transmit channels. Furthermore, in experimental situations there is normally only one transmit channel operational at any instant. (For a system which switches rapidly between two transmit states such as for the COMSTAR satellites it is possible to infer xpi behavior).

Watson and Arbabi [1973] have shown that if the propagation medium contains scatterers with two orthogonal axes of symmetry, then xpd and xpi are equal. This is close to reality for rain media. In most situations the differences between xpd and xpi are not of practical importance. It must be remembered, though, that we are mainly interested in xpi for real communication systems, but we measure and calculate xpd in most research investigations. We shall use

xpd in much of the subsequent work, but we will be actually using xpd to infer xpi.

The xpd and xpi due to antenna effects alone are found from (2.1-11) as

$$\text{xpd} = \frac{|V_1^r|}{|V_2^r|}\Bigg|_{V_1^t = 1,\ V_2^t = 0}$$

$$= \frac{|\cos\gamma_1^r \cos\gamma_1^t + \sin\gamma_1^r \sin\gamma_1^t e^{-j(\delta_1^r - \delta_1^t)}|}{|\cos\gamma_2^r \cos\gamma_1^t + \sin\gamma_2^r \sin\gamma_1^t e^{-j(\delta_2^r - \delta_1^t)}|} \qquad (2.1\text{-}22)$$

$$\text{xpi} = \frac{|V_1^r|\Big|_{V_1^t = 1,\ V_2^t = 0}}{|V_1^r|\Big|_{V_1^t = 0,\ V_2^t = 1}}$$

$$= \frac{|\cos\gamma_1^r \cos\gamma_1^t + \sin\gamma_1^r \sin\gamma_1^t e^{-j(\delta_1^r - \delta_1^t)}|}{|\cos\gamma_1^r \cos\gamma_2^t + \sin\gamma_1^r \sin\gamma_2^t e^{-j(\delta_1^r - \delta_2^t)}|} \qquad (2.1\text{-}23)$$

The crosspolarization discussion and equations (2.1-16) to (2.1-21) apply whether medium effects are present or not. There is one more parameter of interest in communication systems, that of channel fading due to medium effects. Fade, F, is used to measure the amount of signal decrease relative to a clear weather case (identity depolarization matrix). The fade on channel 1 is the ratio of received powers during clear weather relative to the case where a propagation disturbance occurs:

$$F_1 = \frac{P_1}{P_1'} = \frac{|V_1^r|^2}{|V_1^{r'}|^2} \qquad (2.1\text{-}24)$$

and in dB

$$F_{1dB} = 10 \log F_1. \qquad (2.1\text{-}25)$$

Frequently, attenuation is used. This is the signal reduction due to medium effects alone and does not include antenna polarization interaction effects.[Stutzman; 1980] For nearly orthogonal dual polarized systems the differences are extremely small and we can infer that attenuation is the same as fade.

2.3 MODEL PARAMETERS

At the outset of the investigation into precipitation effects on earth-satellite links we must have clearly in mind the parameters of the problem. The parameters can be divided into two types: system parameters associated with the communication link and medium parameters associated with the rain and ice along the propagation path. We will list the parameter types and make several assumptions about their behavior, allowing the introduction of variables to describe the parameter variations.

Figure 2-4 shows the geometry of an earth-satellite link. The system parameters are

Elevation angle

Site elevation above sea level

Frequency of operation

Antenna polarization

The geometry for a single raindrop is shown in Figure 2-5. This, together with the bulk rain medium of Figure 2-4, lead to the following medium parameters:

Raindrop shape

Raindrop size

Raindrop tilt angle

Raindrop temperature

Rain path geometry

Ice quantity

Ice particle orientation

A thorough discussion of raindrop parameters is found in [Stutzman, 1980]. Here only a brief discussion of this subject is given, as required for subsequent depolarization calculations.

Raindrop shape has a significant effect on depolarization. Commonly, raindrops are assumed to be totally oblate spheroidal. This is somewhat simplistic. Although our

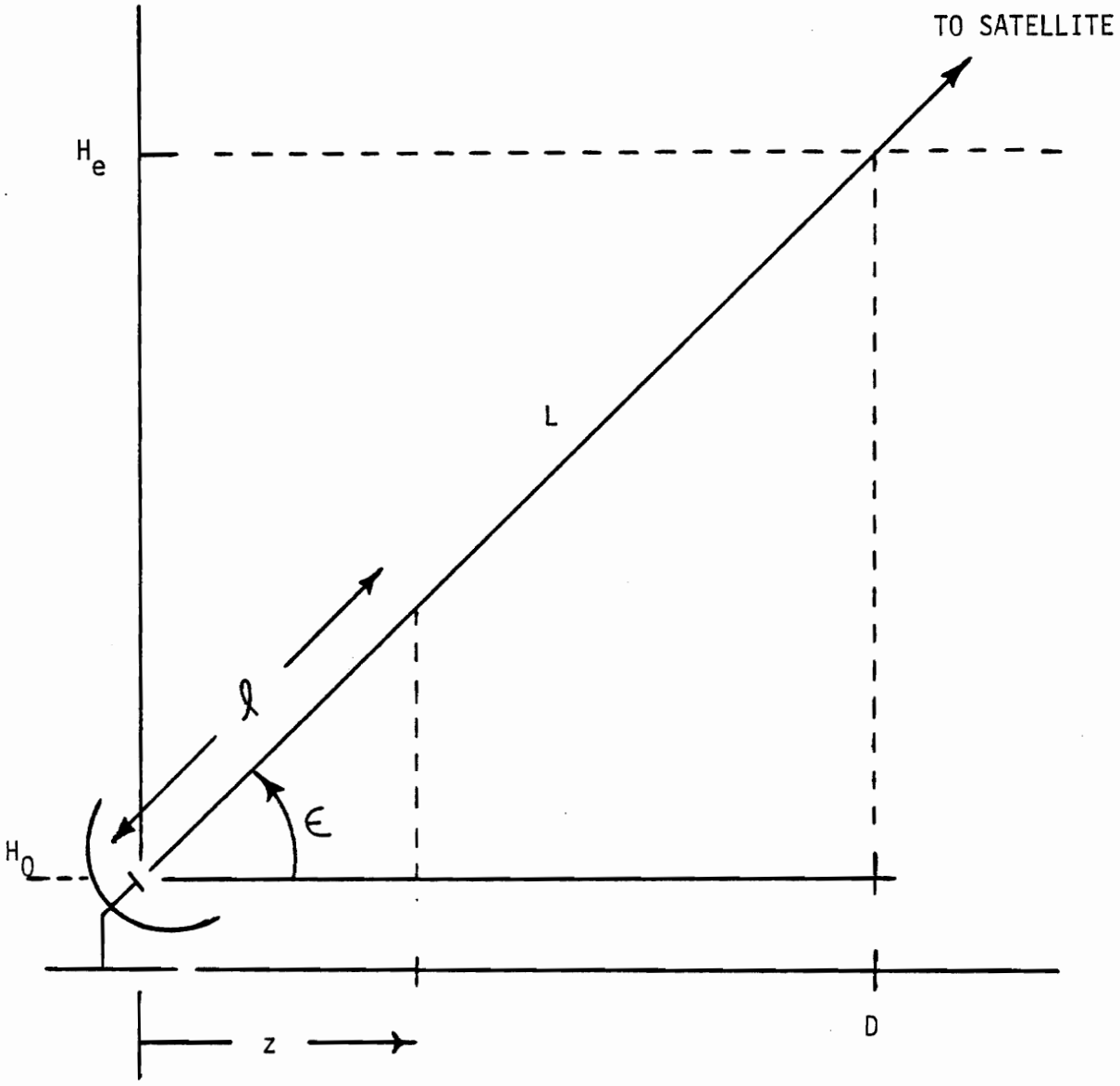

Figure 2-4. Geometry for the earth-satellite link.

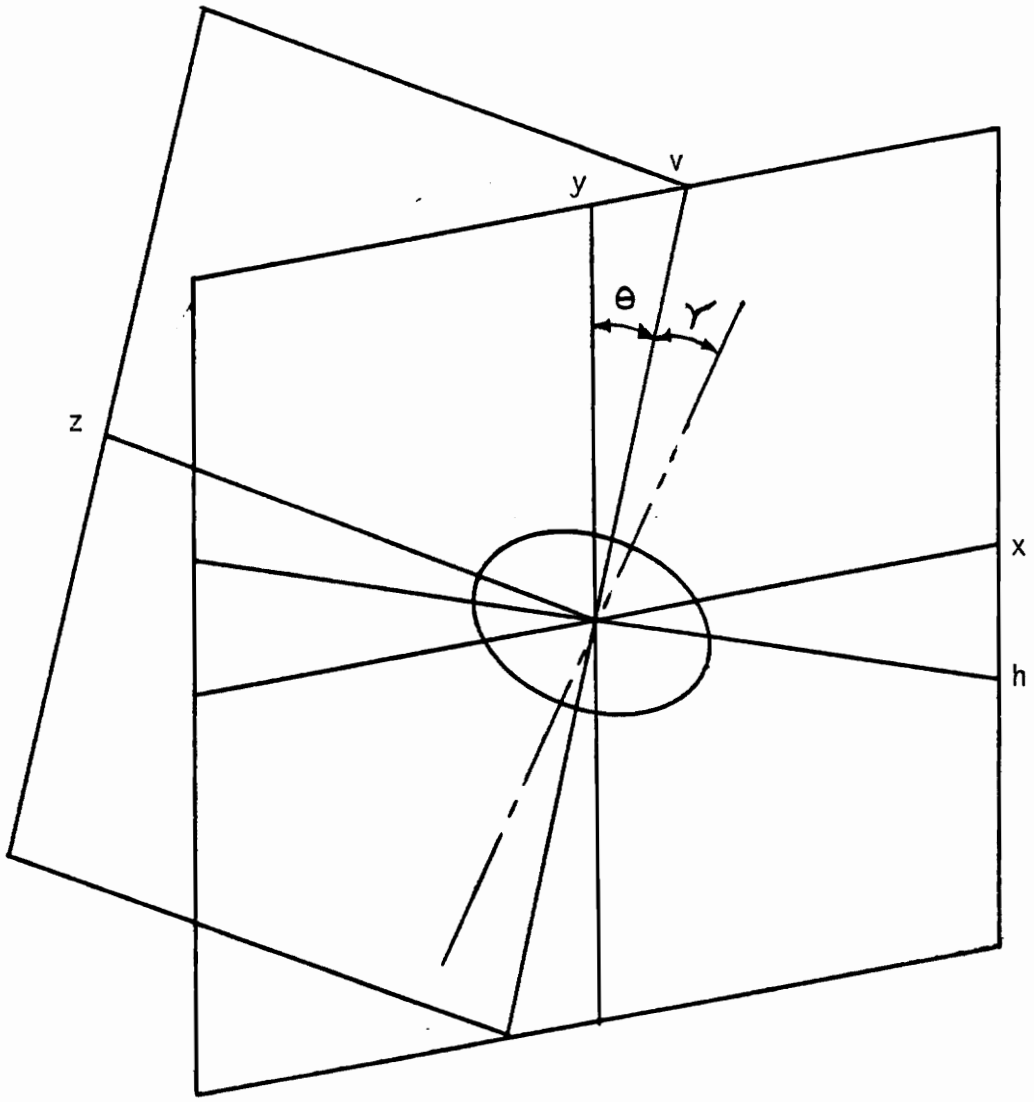

Figure 2-5. Geometry for precipitation particles.

knowledge of raindrop shapes is limited, the shapes can be assumed to be a mixture of spherical, oblate spheroidal, and Pruppacher and Pitter [1971] distorted drops. [Stutzman, 1980]. Oguchi [1977,1981a] investigated the Pruppacher and Pitter shaped raindrops and found that the scattering from them did not differ significantly from that obtained from oblate spheroidal drops. As drops become larger the deformations increase, but the number density of drops decreases tending to reduce the effect. We, therefore, adopt a raindrop shape model which is bimodal, having F_o fraction of the total drops oblate spheroidal in shape, and the remaining fraction $(1-F_o)$ spherical in shape.

The raindrop size distribution can have an effect on attenuation, but is less important for cross polarization calculations and does not normally appear directly in a cross polarization result.

Raindrop temperature is in a category similar to the size distribution and it is not necessary to explicitly include it as a parameter of concern in depolarization modeling.

The orientation of non-spherical raindrops has a strong influence on depolarization. The oblate spheroidal drop orientation can be described (see Figure 2-5) by θ in the plane transverse to the propagation path (in the xy-plane) and the angle γ in the plane containing the axis of symme-

try of the drop (y-axis) and the propagation path (yz-plane). An ensemble of raindrops would have random values of θ and γ. We shall assume that the distributions of θ and γ are independent of each other and of the drop size. [Oguchi, 1981] The effect of γ on cross polarization is less significant than that of θ. [Brussard, 1976; Oguchi, 1977; Olsen, 1981, 1981]. We will assume that the angle γ does not need to enter into the formulation in an explicit manner. Many researchers term θ as an "effective" or "apparent" canting angle. Also, the mean value of γ can be assumed to equal the elevation angle ε, which will appear explicitly.[Olsen, 1982] Thus, we are left with θ, which may be interpreted as the projection of the tilted drops onto the plane transverse to the propagation direction. This is consistent with the idea that the fraction of drops F_o when viewed from the propagation direction appear to be oblate spheroidal and the rest $(1-F_o)$ spherical (such as the end view of a prolate spheroid). All that remains is to pose an analytical form for the distribution over θ. A gaussian distribution with mean $<\theta>$ and standard deviation σ_θ will be assumed.

The final medium parameter for rain is that of the rain path geometry which includes the rain extent and the shape of the rainrate profile along the rain path. It is shown in

Section 5.1 that XPD vs A is relatively insensitive to the rainrate profile. Therefore, no parameters are necessary in the modeling effort for rain path geometry.

The precipitation medium can also contain ice particles. Although little is known about ice particles we shall make the customary assumptions that an ice layer is composed of needles and plates [Bostian and Allnutt, 1981]. Let F_p be the fraction of plates; then $(1-F_p)$ is the fraction of needles. They will be assumed to be gaussian distributed with angle θ_i (analogous to θ for raindrops). The plates have mean $<\theta_{ip}>$ and the needles mean is $<\theta_{in}>$; the associated standard deviations are σ_{ip} and σ_{in}. For needles the azimuthal angle ϕ is also important. Thus, we include a gaussian distribution for it with $<\phi>$ and σ_ϕ. It turns out that for ice calculations the density and thickness of the ice layer in the direction of propagation can be multiplied together forming a single paramenter, IC, or ice content.

Returning now to the system parameters, we can, in light of the discussions of the medium parameters, determine which are necessary. Elevation angle, ε, and frequency, f, are both important mainly because of the dependence of single particle scattering (and, thus, total path depolarization) on ε and f. On the other hand, site elevation H_o is not important because its only influence would be on the rain path

geometry which we have said is of little importance for depolarization.

The final parameter is that of antenna polarization. It will be assumed for these modeling purposes that the transmit and receive antennas are matched in polarization, are aligned, and have ideal polarization characteristics (i.e., pure linear or pure circular). General antenna situations can be handled (see Section 2.1), but the emphasis of this study is on medium effects. Polarization can be closely related to the tilt angle of the medium particles. This is because the physically meaningful quantity is the angle relative to the particle axis. Several investigators have found that this situation is described through the parameter

$$\delta = \begin{cases} |\tau + \langle\theta\rangle| & \text{linear polarization} \\ 45^\circ & \text{circular polarization} \end{cases} \qquad (2.2\text{-}1)$$

where

τ = tilt angle of linearly polarized wave relative to horizontal (see Figure 2.1-2).

$\langle\theta\rangle$ = mean particle canting angle.

The validity of this expression has been checked by computing several cases using the multiple scattering model of Section 3.1.

Based on the preceding discussion we can now summarize the parameters that must be included explicitly in a depolarization model. These are shown in Table 2-1. It is assumed that the parameters not shown in this table are set to some reasonable values. For example, the drop size distribution should be one which yields acceptable attenuation results such as the Marshall-Palmer or Laws-Parsons distributions. Similarly the rain path profile should also be one that yields reasonable path attenuation values (see Section 5.1). In fact, XPD is a function of the path attenuation in addition to the parameters shown in Table 2-1.

Table 2-1

Parameters That Must be Included in a Precipitation Depolarization Model

Parameter	Symbols
Path/System	
Elevation angle	ε
Frequency	f
Rain	
Fraction oblate drops	F_o
Polarization/Canting	$\delta = \begin{cases} \lvert\tau - \langle\theta\rangle\rvert & \text{LP} \\ 45^\circ & \text{CP} \end{cases}$
($\langle\theta\rangle$ = mean canting angle)	
Canting angle spread	σ_θ
Ice	
Ice content	IC
Fraction of plates	F_p
Polarization/Canting	$\delta_{ip} = \begin{cases} \lvert\tau + \langle\theta_{ip}\rangle\rvert & \text{LP} \\ 45^\circ & \text{CP} \end{cases}$
($\langle\theta_{ip}\rangle$ and $\langle\theta_{in}\rangle$ are mean canting angles for plates and needles)	$\delta_{in} = \begin{cases} \lvert\tau + \langle\theta_{ip}\rangle\rvert & \text{LP} \\ 45^\circ & \text{CP} \end{cases}$
Canting angle spread	σ_{ip}, σ_{in}
Azimuthal angle of needles	$\langle\phi\rangle$, σ_ϕ

2.4 RAIN CALCULATION MODELS

Several methods are available for determining the rain medium depolarization matrix [D]. In this section we will review a few of the prominent models (the CCIR Model is discussed separately in Section 2.5).

Olsen [1982] has written an excellent review article on this subject also.

Many researchers choose to include free space in the medium representation. Then a transmission matrix

$$[T] = \begin{bmatrix} T_{11} & T_{12} \\ T_{21} & T_{22} \end{bmatrix} \qquad (2.4\text{-}1)$$

is used instead of a depolarization matrix. The resulting system calculations are, however, the same since only a free space phase shift is introduced (assuming plane wave behavior) and therefore,

$$[T] = e^{-jk_o L} \quad [D] \; . \qquad (2.4\text{-}2)$$

If all raindrops are assumed to be aligned and the rain-rate is uniform throughout the rain volume, the medium can be modeled rather simply. This is often referred to as the differential attenuation - differential phase model (or

constant canting angle model). The medium matrix entries are [Stutzman, 1980]

$$T_{11} = d_h \cos^2\theta + d_v \sin^2\theta$$
$$T_{12} = T_{21} = (d_v - d_h) \sin\theta \cos\theta \qquad (2.4\text{-}3a)$$
$$T_{22} = d_h \sin^2\theta + d_v \cos^2\theta$$

where

$$d_h = e^{-jk_h L}\ ,\ d_v = e^{-jk_h L} \qquad (2.4\text{-}3b)$$

and

$$k_{h,v} = k_o + \frac{2\pi}{k_o} \int f_{n,v}(a)\, n(a)\, da. \qquad (2.4\text{-}3c)$$

The angle θ here is shown in Figure 2.2-1. Many researchers use an angle which is the negative of the one used here. This leads to a sign difference in T_{12}. (See Olsen [1982] for example; he includes a discussion of the origins of this model in the literature.)

The models in use today are more sophisticated than the simple constant canting angle model. These more "exact" models usually include distributions over various parameters to reflect the random nature of the rain medium. In this section some of the more prominent of these models are discussed. For the most part only the results of the models are presented.

2.4.1 The Oguchi Model

Oguchi [1981a] represents the propagation problem with the differential equation

$$\frac{d}{dz}[E] = [M][E] \tag{2.4-4}$$

where

$$M_{11} = -jk_o - j\frac{2\pi}{k_o}\int\int\int [f_h(a, \gamma)\cos^2\theta + f_v(a, \gamma)\sin^2\theta] \cdot n(a, \theta, \gamma)da\, d\theta\, d\gamma$$

$$M_{22} = -jk_o - j\frac{2\pi}{k_o}\int\int\int [f_h(a, \gamma)\sin^2\theta + f_v(a, \gamma)\cos^2\theta] \cdot n(a, \theta, \gamma)da\, d\theta\, d\gamma \tag{2.4-5}$$

$$M_{12} = M_{21} = -j\frac{2\pi}{k_o}\int\int\int [f_h(a, \gamma) - f_v(a, \gamma)]\sin\theta\cos\theta \cdot n(a, \theta, \gamma)da\, d\theta\, d\gamma$$

The transmission matrix is then

$$T_{11} = e^{\lambda 1 L}\cos^2\phi + e^{\lambda 2 L}\sin^2\phi$$

$$T_{22} = e^{\lambda 1 L}\sin^2\phi + e^{\lambda 2 L}\cos^2\phi \tag{2.4-6}$$

$$T_{12} = T_{21} = \frac{1}{2}(e^{\lambda 1 L} - e^{\lambda 2 L})\sin^2\phi$$

where the eigenvalues of [M] are

$$\left.\begin{matrix}\lambda_1 \\ \lambda_2\end{matrix}\right\} = \frac{1}{2}\left\{M_{11} + M_{22} \pm [(M_{11} - M_{22})^2 + (2M_{12})^2]^{1/2}\right\} \qquad (2.4\text{-}7)$$

and

$$\phi = \frac{1}{2} \tan^{-1}\left(\frac{2M_{12}}{M_{11} - M_{22}}\right) \qquad (2.4\text{-}8)$$

In general "angle" ϕ is complex.

In the constant canting angle case,

$$M_{11} = -j(k_o + \frac{2\pi}{k_o}\int [f_h(a)\cos^2\theta + f_v(a)\sin^2\theta]\, n(a)da)$$

$$M_{22} = -j(k_o + \frac{2\pi}{k_o}\int [f_h(a)\sin^2\theta + f_v(a)\cos^2\theta]\, n(a)da) \qquad (2.4\text{-}9)$$

$$M_{12} = M_{21} = -j\frac{2\pi}{k_o}\int [f_h(a) - f_v(a)]\sin\theta\cos\theta\, n(a)da$$

and

$$\lambda_1 = -j(k_o + \frac{2\pi}{k_o}\int f_h(a)\, n(a)\, da) = -jk_h$$

$$\lambda_2 = -j(k_o + \frac{2\pi}{k_o}\int f_v(a)\, n(a)\, da) = -jk_v \qquad (2.4\text{-}10)$$

$\phi = \theta$.

Equation (2.4-6) reduces then to (2.4-3).

Oguchi assumed that the raindrop canting (θ and γ) is statistically independent of the drop size. Further, he assumed that the distributions over angles θ and γ are independent of each other. With these assumptions Oguchi states that ϕ is real and depends only on the distribution of θ. Oguchi [1977] also assumed

$$f_h(a, \gamma) - f_v(a, \gamma) \approx [f_h(a, 0) - f_v(a, 0)] \cos^2\gamma. \qquad (2.4\text{-}11)$$

Then

$$\lambda_1 = -jk_1 \qquad \lambda_2 = -jk_2 \qquad (2.4\text{-}12a)$$

where

$$\left.\begin{matrix} k_1 \\ k_2 \end{matrix}\right\} = \frac{1}{2}\,[k_h + k_v \pm m_\theta\, m_\gamma\, (k_h - k_v)]. \qquad (2.4\text{-}12b)$$

Here k_h and k_v are given by (2.4-3c) and

$$m_\theta = [\langle\cos 2\theta\rangle^2 + \langle\sin 2\theta\rangle^2]^{1/2} \qquad (2.4\text{-}12c)$$

$$m_\gamma = \langle\cos^2\gamma\rangle. \qquad (2.4\text{-}12d)$$

The differential propagation constant is

$$k_1 - k_2 = m_\theta \, m_\gamma \, (k_h - k_v) \qquad (2.4\text{-}13)$$

and "effective canting angle" ϕ is

$$\phi = \frac{1}{2} \tan^{-1} \frac{\langle \sin 2\theta \rangle}{\langle \cos 2\theta \rangle} \qquad (2.4\text{-}14)$$

which is real and depends only on the the θ distribution. Oguchi obtained numerical results by assuming Gaussian distributions for θ and γ giving

$$\begin{aligned} m_\theta &= e^{-2\sigma_\theta^2} \\ m_\gamma &= \frac{1}{2} \left(\cos 2\langle \gamma \rangle \, e^{-2\sigma_\gamma^2} + 1 \right) \\ \phi &= \langle \theta \rangle \end{aligned} \qquad (2.4\text{-}15)$$

Oguchi further set

$$\langle \gamma \rangle = 0 \quad \text{and} \quad \sigma_\gamma = 0 \quad \text{giving } m_\gamma = 1. \qquad (2.4\text{-}16)$$

He noted that the effect of γ on depolarization is less significant than is θ .

Olsen[1982] summarized the work of Osterberg[1976] saying that Osterberg's results were equivalent to those of Oguchi except that Osterberg did not include a distribution over γ.

2.4.2 The Chu Model

Chu[1980a] employs a two-tier Gaussian canting angle model in which there is the usual mean $\langle\theta\rangle$ and standard deviation σ_θ plus a distribution on $\langle\theta\rangle$ (to represent storm-to-storm variation of mean canting angles) which is zero mean and of standard deviation $\sigma_{\langle\theta\rangle}$. The "long-term average" coefficients are then

$$\left.\begin{matrix}\langle|T_{11}|^2\rangle \\ \langle|T_{22}|^2\rangle\end{matrix}\right\} = e^{-(\alpha_1' + \alpha_2')L}\left[D' + \tfrac{1}{2}C'e^{-4\sigma_\theta^2}\right.$$

$$\left.\cdot\,(1 + \cos(4\tau)e^{-8\sigma_{\langle\theta\rangle}^2} \mp E'\cos(2\tau)\,e^{-2(\sigma_\theta^2 + \sigma_{\langle\theta\rangle}^2)}\right] \qquad (2.4\text{-}17a)$$

$$\langle|T_{12}|^2\rangle = \langle|\langle T_{21}\rangle|^2\rangle = e^{-(\alpha_1' + \alpha_2')L}\tfrac{1}{2}C'e^{-\sigma_\theta^2}$$

$$\cdot\,(1 - \cos(4\tau)\,e^{-8\sigma_{\langle\theta\rangle}^2})$$

where τ is the polarization tilt angle and

$$C' = \sinh^2\frac{\Delta\alpha'L}{2} + \sin^2\frac{\Delta\beta'L}{2}$$

$$D' = \cos^2\frac{\Delta\beta'L}{2} + \sinh^2\frac{\Delta\alpha'L}{2} \qquad (2.4\text{-}17b)$$

$$E' = 2\cosh\frac{\Delta\alpha'L}{2}\sinh\frac{\Delta\alpha'L}{2}\ .$$

Here α_1', α_2', and β_1', β_2', are the specific attenuations and phase shifts for the characteristic polarizations along the medium principal axes. Furthermore, [Olsen, 1982]

$$\Delta\alpha' = \alpha_1' - \alpha_2' \approx \mathrm{Im}\,(k_h - k_v)\cos^2\varepsilon$$
$$\Delta\beta' = \beta_1' - \beta_2' \approx -\mathrm{Re}\,(k_h - k_v)\cos^2\varepsilon \qquad (2.4\text{-}18)$$

Chu then gives "power depolarization ratios" for linear polarization

$$\left.\begin{matrix} |\delta_H|^2 \\ |\delta_v|^2 \end{matrix}\right\} = \frac{1}{2}\,\frac{C'}{D'}\,e^{-4\sigma_\theta^2}\,(1 - \cos(4\tau)\,e^{-8\sigma_{<\theta>}^2}) \cdot \left\{\begin{matrix} F_H' \\ F_v' \end{matrix}\right. \qquad (2.4\text{-}19a)$$

where

$$\left.\begin{matrix} F_H' \\ F_v' \end{matrix}\right\} = \left[1 + \frac{1}{2}\,\frac{C'}{D'}\,e^{-4\sigma_\theta^2}\,(1 + \cos(4\tau)\,e^{-8\sigma_{<\theta>}^2}) \mp \frac{E'}{D'}\cos(2\tau)\,e^{-2(\sigma_\theta^2 + \sigma_{<\theta>}^2)}\right]^{-1} \qquad (2.4\text{-}19b)$$

and $\delta_H = T_{21}/T_{11}$ and $\delta_v = T_{12}/T_{22}$. For circular polarization

$$\left|\delta_{\substack{R\\L}}\right|^2 = \frac{C'}{D'} e^{-4\sigma_\theta^2} \quad . \tag{2.4-20}$$

Chu also used the following small argument approximations

$$\frac{C'}{D'} = \frac{1}{4}\left[(\Delta\alpha')^2 + (\Delta\beta')^2\right] L^2$$

$$\left.\begin{matrix} 10 \log F_H' \\ 10 \log F_v' \end{matrix}\right\} = \pm \frac{10}{\ln(10)} \Delta\alpha' L \cos(2\tau)\, e^{-2\sigma_{<\theta>}^2} \tag{2.4-21}$$

Olsen[1982] points out that the fundamental approach used to obtain (2.4-17) is not strictly correct (in the first tier averaging process); however, the impact on the small argument approximations appears to be minimal.

Combining (2.4-18), (2.4-20), and (2.4-21) gives the XPD for circular polarization

$$XPD_c = -20 \log \left[\frac{1}{2} |\Delta k| \cos^2 \varepsilon \, e^{-2\sigma_\theta^2}\right] \qquad (2.4\text{-}22)$$

where

$$|\Delta k| = \sqrt{(\Delta A_o)^2 + (\Delta \phi_o)^2}$$

ΔA_o (in nepers) and $\Delta \phi_o$ (in radians) being the differential attenuation and phase shift in the horizontal direction ($\Delta A_o = Im(k_h - k_v)L$ and $\Delta \phi_o = -Re\,(k_h - k_v)L$). Recently Chu [1982] examined this expression and rewrote it as

$$XPD_c = -20 \log \left(|\Delta k| \frac{f}{A}\right) + 6.02 + 17.37\, \sigma_\theta^2 + 20 \log (f) - 20 \log (A) - 40 \log (\cos \varepsilon) \qquad (2.4\text{-}23)$$

Chu claims that $|\Delta k| \frac{f}{A}$ remains nearly constant over the frequency range of 10 to 30 GHz. Then

$$XPD_c = XPD_o + 20 \log (f) - 20 \log (A) - 40 \log (\cos \varepsilon) \qquad (2.4\text{-}24)$$

where

$$XPD_o = -20 \log \left(|\Delta k| \frac{f}{A}\right) + 6.02 + 17.37\, \sigma_\theta^2$$

is nearly constant with frequency. Through comparisons to measurements Chu fixes the value of XPD_o as

$$XPD_o \approx 11.5 \text{ dB} \tag{2.4-25}$$

From (2.4-19) and (2.4-21) the XPD expression for linear polarization, based on small argument approximations, is

$$XPD_L = -10 \log \left(\frac{C'}{D'} e^{-4\sigma_\theta^2} \right) - 10 \log \left[\frac{1}{2} \left(1 - \cos(4\tau)\, e^{-8\sigma_{<\theta>}^2}\right) \right]$$

$$\pm \frac{10}{\ln(10)} \cos(2\tau)\, e^{-2\sigma_{<\theta>}^2} \Delta\alpha' L \tag{2.4-26}$$

Chu[1980, 1982] also writes this as

$$XPD_L = XPD_c - 10 \log \left[\frac{1}{2} \left(1 - \cos(4\tau)\, e^{-8\sigma_{<\theta>}^2}\right) \right] \pm \frac{\Delta A}{2} \tag{2.4-27}$$

where τ is the polarization angle. Chu claims that $\sigma_{<\theta>}$ is 3^o or less; it should be expressed in radians for use in (2.4-27) though. In practice $\sigma_{<\theta>}$ can appear to be larger for systems with a nonnegligible clear weather residual level. ΔA is the differential attenuation between quasivertical and quasihorizonital polarizations and is

$$\Delta A \approx 0.15 \cos^2\varepsilon \cos 2\tau \, A \quad . \tag{2.4-28}$$

The plus and minus sign in (2.4-27) are for quasivertical and quasihorizontal polarizations, respectively. (Chu's model is discussed further in Section 5.6.)

2.4.3 Modified Two-Tier Gaussian Model

Olsen[1982] noted that Oguchi's approach (see Section 2.4.1) is theoretically sound and Chu's model (see Section 2.4.2) offers the two-tier feature. He, therefore, combined these models and wrote in place of (2.4-17) based on Oguchi's results

$$\left.\begin{matrix} |T_{11}|^2 \\ |T_{22}|^2 \end{matrix}\right\} = e^{-(\alpha_1+\alpha_2)L}\left[D + C\cos^2 2(\langle\theta\rangle - \tau) \mp E \cos 2(\langle\theta\rangle - \tau)\right] \tag{2.4-29a}$$

$$|T_{12}|^2 = |T_{21}|^2 = e^{-(\alpha_1+\alpha_2)L} C \sin^2 2(\langle\theta\rangle - \tau)$$

where

$$C = \sinh^2\left(\frac{\Delta\alpha}{2}L\right) + \sin^2\left(\frac{\Delta\beta}{2}L\right)$$
$$D = \cos^2\left(\frac{\Delta\beta}{2}L\right) + \sinh^2\left(\frac{\Delta\alpha}{2}L\right) \tag{2.4-29b}$$

$$E = 2 \cosh\left(\frac{\Delta\alpha}{2} L\right) \sinh\left(\frac{\Delta\alpha}{2} L\right) \qquad \text{(2.4-29b) cont.}$$

and

$$\alpha_1 + j\beta_1 = jk_1 \qquad \alpha_2 + j\beta_2 = jk_2$$

$$\Delta\alpha = \alpha_1 - \alpha_2 = e^{-2\sigma^2} \Delta\alpha' \qquad \text{(2.4-29c)}$$

$$\Delta\beta = \beta_1 - \beta_2 = e^{-2\sigma^2} \Delta\beta'$$

Note that σ (which is more general and includes random canting in the longitudinal plane) was used in place of σ_θ. The second tier can be added assuming a Gaussian distributed $<\theta>$ with zero mean and standard deviation $\sigma_{<\theta>}$ giving

$$\left.\begin{matrix} <|T_{11}|^2> \\ <|T_{22}|^2> \end{matrix}\right\} = e^{-(\alpha_1 + \alpha_2)L} \left[D + \frac{C}{2} \left(1 + \cos 4\tau\, e^{-8\sigma_{<\theta>}^2}\right) \mp E \cos 2\tau\, e^{-2\sigma_{<\theta>}^2} \right] \qquad \text{(2.4-30)}$$

$$<|T_{12}|^2> = <|T_{21}|^2> = e^{-(\alpha_1 + \alpha_2)L} \frac{C}{2} \left(1 - \cos 4\tau\, e^{-8\sigma_{<\theta>}^2}\right)$$

Then

$$\left.\begin{matrix} |\delta_H|^2 \\ |\delta_V|^2 \end{matrix}\right\} = \frac{1}{2} \frac{C}{D} \left(1 - \cos 4\tau\, e^{-8\sigma_{<\theta>}^2}\right) \cdot \left\{\begin{matrix} F_H \\ F_V \end{matrix}\right. \qquad \text{(2.4-31)}$$

where

$$\left.\begin{matrix} F_H \\ F_V \end{matrix}\right\} = \left[1 + \frac{1}{2}\ \frac{C}{D}\ (1 + \cos\ 4\tau e^{-8\sigma_{<\theta>}^2}) \mp \frac{E}{D} \cos 2\tau e^{-2\sigma_{<\theta>}^2}\right]^{-1}$$

And

$$|\delta_{R,L}|^2 = \frac{C}{D} \tag{2.4-32}$$

The small argument approximations [Olsen, 1982] are

$$\frac{C}{D} = \frac{1}{4}\left[(\Delta\alpha)^2 + (\Delta\beta)^2\right]L^2 \tag{2.4-33}$$

$$\left.\begin{matrix} 10 \log F_H \\ 10 \log F_V \end{matrix}\right\} = \pm\ \frac{10}{\ln(10)}\ \Delta\alpha\ L \cos\ 2\ \tau\ e^{-2\sigma_{<\theta>}^2}$$

These results are equivalent to Chu's, as pointed out by Olsen, since the small argument approximations in both cases are effectively single scattering approximations.

The reformulation of Chu's derivation that Olsen performed can be combined with Chu's recent work on the XPD vs A relationship to obtain a modified result there as well. From (2.4-32), the XPD (in dB) for circular polarization is

$$XPD_C = -10 \log \left|\frac{C}{D}\right|$$

$$= -20 \log \left[\frac{1}{2} \sqrt{(\Delta\alpha L)^2 + (\Delta\beta L)^2} \right] \qquad (2.4\text{-}34)$$

Using (2.4-29c) in (2.4-18) gives

$$\Delta\alpha \approx e^{-2\sigma^2} \text{ Im } (k_h - k_v) \cos^2 \varepsilon$$

$$\Delta\beta \approx -e^{-2\sigma^2} \text{ Re } (k_h - k_v) \cos^2 \varepsilon \qquad (2.4\text{-}35)$$

Then

$$XPD_c = -20 \log \left[\frac{1}{2} |k| \ e^{-2\sigma^2} \cos^2 \varepsilon \right] \qquad (2.4\text{-}36)$$

where $|k|$ is as in (2.4-22). In fact, this result is identical to (2.4-22) with the exception that σ replaces σ_θ here.

2.5 THE CCIR MODEL

In this section we will review the development of the model proposed by the CCIR [1981]. The CCIR model for XPD as a function of A is based on a relation similar to (2.5-5) which was originally developed by Nowland, Olsen, and Shkarofsky [1977] (also see Olsen et al., [1978]). They obtained this result by employing several approximations to the relationship for XPD presented by Oguchi [1977] (see Section 2.4.1) Olsen [1981] reviewed the major steps in the development leading from the (2.5-5) result to the simple CCIR formula (of (2.5-9)); several further approximations were needed. A more detailed development was presented in CCIR Document 5/206-E [1977] and will be reviewed here with emphasis on the approximations involved in obtaining (2.5-5).

From Oguchi[1977] (using (2.4-6)) the expression for XPD due to rain for an arbitrary incident linear polarization can be represented by

$$XPD = 20 \log \left| \frac{e^{\lambda_1 L} \cos^2(\phi - \tau) + e^{\lambda_2 L} \sin^2(\phi - \tau)}{(e^{\lambda_1 L} - e^{\lambda_2 L}) \sin(\phi-\tau)\cos(\phi-\tau)} \right| \qquad (2.5\text{-}1)$$

where

ϕ = effective canting angle

τ = polarization tilt angle relative to horizontal

and λ_1, λ_2 are defined in (2.4-12) to (2.4-15). In order to "simplify" the prediction problem the small argument approximation

$$e^{-j(k_1 - k_2)} \sim 1 - j(k_1 - k_2)L \qquad (2.5\text{-}2)$$

was used with $k_1 \approx k_2$ in (2.5-1) (upon substitution of (2.4-12) and (2.4-13) into (2.5-1)) to give

$$XPD = 10 \log \left[\frac{4\{1 + 2m_\theta m_\gamma \Delta\alpha L \sin^2(\phi-\tau) + [m_\theta m_\gamma (\Delta\alpha^2 + \Delta\beta^2)^{1/2} L \sin^2(\phi-\tau)]^2\}}{m_\theta^2 m_\gamma^2 (\Delta\alpha^2 + \Delta\beta^2) L^2 \sin^2 2(\phi-\tau)} \right] \qquad (2.5\text{-}3)$$

The differential attenuation $\Delta\alpha = \alpha_h - \alpha_v$ and the differential phase shift $\Delta\beta = \beta_h - \beta_v$ are given (using (2.4-13) by

$$k_1 - k_2 = m_\theta m_\gamma (k_h - k_v) = m_\theta m_\gamma (\Delta\beta - j\Delta\alpha) \qquad (2.5\text{-}4)$$

There is some question to the validity of the approximation in (2.5-2) in the application of the final model. Ol-

sen[1982] noted that an approximation of this type is a "single scattering approximation" and the single scattering form must be applied to successive thin layers of the medium to include the forward multiple scattering processes.

A second significant approximation was used to further simplify (2.5-3). The bracketed {} expression in the numerator of (2.5-3) was approximated to unity without justification. The resulting form is then

$$XPD = -20 \log \left[\frac{1}{2} \, m_\theta m_\gamma \, L(\Delta\alpha^2 + \Delta\beta^2)^{1/2} \sin 2|\phi - \tau| \right] \qquad (2.5\text{-}5)$$

This result agrees with that orginally derived by Nowland et al., [1977] if $m_\theta m_\gamma$ is replaced by $m \cos^2 \varepsilon$.

A parallel development was carried out for the co-polar attenuation (CPA) relation. From (2.4-6) we have

$$CPA = -20 \log \left| e^{-\lambda_1 L} \cos^2(\phi - \tau) + e^{\lambda_2 L} \sin^2(\phi - \tau) \right| \qquad (2.5\text{-}6)$$

and using $k_1 \approx k_2$, then (2.5-6) reduces to

$$CPA = -20 \log \left| e^{-j[k_1 \cos^2(\phi - \tau) + k_2 \sin^2(\phi - \tau)]L} \right|$$

$$= \frac{-20L}{\ln(10)} \operatorname{Im} [k_1 \cos^2(\phi - \tau) + k_2 \sin^2(\phi - \tau)] \qquad (2.5\text{-}7)$$

Rewriting (2.5-7) in terms of the specific attenuations A_h and A_v (in dB/unit distance) corresponding to k_h and k_v yields

$$CPA = \tfrac{1}{2} A_h [1 + m_\theta m_\gamma \cos 2(\phi-\tau)] + \tfrac{1}{2} A_v [1 - m_\theta m_\gamma \cos 2(\phi-\tau)]\}L$$

(2.5-8)

Further approximations were applied to (2.5-5) and (2.5-8) to relate XPD as a function of CPA. These are presented by Nowland *et al.*, [1977] and reviewed by Olsen[1981, 1982]. The various parameter variations were curve fitted and presented by Olsen *et al.*, [1978] in the form

$$XPD = 0.0053\, \sigma^2 - 20 \log (\sin 2\, |\phi - \tau|) + 30 \log (f)$$
$$- 40 \log (\cos \varepsilon) - V_1 \log (CPA) \qquad (2.5\text{-}9)$$

where

$V_1 = 20 \qquad 8 \le f \le 15 \quad GHZ$

$= 23 \qquad 15 \le f \le 35 \quad GHZ$.

The relation in (2.5-9) is the form adopted by the CCIR [Doc. 5/5005-E] with the exception of the polarization term (proposed by Chu [1980]) which was replaced by

$$U(\delta) = -10 \log \frac{1}{2} [1 - \cos (4\delta) \, e^{-0.0024 \, \sigma_m^2}] \qquad (2.5\text{-}10)$$

Chapter III

XPD CALCULATION METHODS

The backbone of propagation modeling studies lies in a firm theoretical framework. Parameter studies such as frequency sensitivity, elevation angle variations, etc. require a rigorous theoretical model. The other ingredient is measured data (to be discussed in Chapter 4). A rigorous theoretical model together with measured XPD data can be used to develop simple relationships for calculating XPD in predictive situations different from those available from measurements and rigorous methods.

3.1 THE MULTIPLE SCATTERING MODEL

The multiple scattering approach involves determining the propagation effects on a plane electromagnetic wave passing through a medium of discrete, tenuous scatterers including forward and backward multiple scattering. Multiple scattering analysis has been used by several researchers for a variety of problems (see Ishimaru [1977]). The multiple scattering model presented here for use as a rigorous model was derived in vector form [Tsolakis and Stutzman, 1982; Stutzman, Tsolakis, and Dishman, 1982] which allows for arbitrary polarization of the input wave and receiving antenna. The

only assumptions are that the medium is tenuous and that triple scattering between two scatterers (backscattering of particle 1 onto particle 2 which in turn is forward scattered back to particle 1 and in the forward direction), fourth-order scattering between three scatterers, and so on is negligible. For precipitation media these assumptions hold. As applied to precipitation media the multiple scattering method to be presented offers the following additional features (in addition to the vector formulation): (a) the random distributions of particle size, shape, and orientation are incorporated directly into the model, (b) varying medium density along the propagation path (such as rainrate) is included, (c) the formulation results in calculations that are very easy to implement and evaluate on computers; (d) The model has been shown to give accurate results up to 30 GHz [Tsolakis and Stutzman, 1982] and can probably be extended much higher in frequency, (e) Ice particles as well as rain hydrometeors can be included.

Only the results of the multiple scattering model are given here; the derivation is presented elsewhere [Stutzman, Tsolakis, and Dishman, 1982]. The focus here will be on presentation of the results for clarity in application.

General Formulation

The depolarization matrix for the multiple scattering model is

$$\underline{D} = [e^{-j\underline{k}}] \tag{3.1-1}$$

This can be evaluated after the propagation constant matrix k has been determined from

$$k = \frac{2\pi}{k_o} \int \underline{f}\ n(z',\omega)\ dz'\ d\omega \tag{3.1-2}$$

where $\omega = (a, s, \theta)$ represents the particle variables, namely radius a, shape s, and canting angle θ. The single particle scattering matrix is

$$\underline{f} = \begin{bmatrix} f_{11} & f_{12} \\ f_{21} & f_{22} \end{bmatrix} \tag{3.1-3a}$$

where

$$f_{11} = \frac{1}{2}\left\{f_V(a) + f_H(a) + \cos 2\theta[f_H(a) - f_V(a)]\right\}$$

$$f_{12} = f_{21} = \frac{1}{2}[f_V(a) - f_H(a)] \sin 2\theta \tag{3.1-3b}$$

$$f_{22} = \frac{1}{2}\left\{f_V(a) + f_H(a) + \cos 2\theta\,[f_V(a) - f_H(a)]\right\}$$

$n(z', \omega)$ is the number density of particles as a function of position z along the propagation path and parameters $\omega = (a, s, \theta)$.

The propagation constant expression of (3.1-2) will reduce to that of the differential attenuation - differential phase model of (2.4-3) when the particle density is uniform and all particles are alike and aligned. In this case, parameter variations over z', s, and θ disappear. The depolarization matrix $\underline{D}$ of (3.1-1) would be a solution to a differential equation similar to (2.4-4) in the Oguchi model if the medium particle density were constant (i.e.,if there were no z variation). This, of course, can be a major restriction on the medium. In this section the multiple scattering model will be evaluated using a realistic spatial rainrate distribution.

Continuing now with evaluation of the k matrix, we can write the entries as

$$k_{\ell m} = \frac{2\pi}{k_o} \int f_{\ell m} \; n(z', \omega) \; dz' \; d\omega \tag{3.1-4}$$

$$= \frac{2\pi}{k_o} \int_0^L \int_\theta \int_0^\infty \int_s f_{\ell m} \; n(z', \omega) \; ds \; da \; d\theta \; dz'$$

$$k_{\ell m} = \frac{2\pi}{k_o} \int_0^L \int_0^\infty \int_\theta \left\{ P1 \; f_{\ell m}^{SPH}(a) + P2 \; f_m^{OBL}(a) \right\} \tag{3.1-5}$$

$$p_\theta(\theta) \; d\theta \; n_o(z', a) \; da \; dz'$$

Here we have used the shape distribution of P1 fraction of spherical drops and P2 fraction of oblate spheroidal drops. $p_\theta(\theta)$ is the distribution function of the tilt angles of the oblate drops; $n_o(z', a)$ is the distribution of raindrop sizes (a) as a function of position z' ; and

$$f_m^{SPH} = \begin{cases} f^{SPH}(a) & \ell = m \\ 0 & \ell \neq m \end{cases} \qquad (3.1\text{-}6)$$

$$f_{11}^{OBL}(a) = \frac{1}{2}\left\{f_V(a) + f_H(a) + \cos 2\theta\,[f_H(a) - f_V(a)]\right\}$$

$$f_{12}^{OBL}(a) = f_{21}^{OBL}(a) = \frac{1}{2}\,[f_V(a) - f_H(a)]\,\sin 2\theta \qquad (3.1\text{-}7)$$

$$f_{22}^{OBL}(a) = \frac{1}{2}\left\{f_V(a) + f_H(a) + \cos 2\theta\,[f_V(a) - f_H(a)]\right\}$$

Integration over θ leads to the following replacement

$$\begin{aligned} \sin 2\theta &\rightarrow e^{-2\sigma_\theta^2}\,\sin 2\langle\theta\rangle \\ \cos 2\theta &\rightarrow e^{-2\sigma_\theta^2}\,\cos 2\langle\theta\rangle \end{aligned} \qquad (3.1\text{-}8)$$

Then (3.1-5) reduces to

$$k_{\ell m} = \frac{2\pi}{k_o} \int_0^L \int_0^\infty \left\{ P1\ f_m^{SPH}(a, \langle\theta\rangle) + P2\ f_m^{OBL}(a, \langle\theta\rangle) \right\} n_o(z', a)\, da\, dz' \tag{3.1-9}$$

where

$$f_m^{SPH}(a) = \begin{cases} f^{SPH}(a) & \ell = m \\ 0 & \ell \neq m \end{cases} \tag{3.1-10a}$$

$$f_{11}^{OBL}(a, \langle\theta\rangle) = \frac{1}{2} \left\{ f_V(a) + f_H(a) + e^{-2\sigma_\theta^2} \cos 2\langle\theta\rangle [f_H(a) - f_V(a)] \right\}$$

$$f_{12}^{OBL}(a, \langle\theta\rangle) = f_{21}^{OBL}(a, \langle\theta\rangle) = \frac{1}{2} [f_V(a) - f_H(a)] e^{-2\sigma_\theta^2} \sin 2\langle\theta\rangle \tag{3.1-10b}$$

$$f_{22}^{OBL}(a, \langle\theta\rangle) = \frac{1}{2} \left\{ f_V(a) + f_H(a) + e^{-2\sigma_\theta^2} \cos 2\langle\theta\rangle [f_V(a) - f_H(a)] \right\}$$

Evaluation of the remaining two integrals in (3.1-9) can be somewhat involved depending upon the spatial distribution (in z') of the rain. Furthermore, the single drop scattering coefficients are given in the literature in tabular form. These data, however, can be used to generate polynomi-

al curve fits giving continuous functions that can be integrated. In particular, the single drop coefficients $f^{SPH}(a)$, $f_V(a)$, $f_H(a)$, and $f_{DIF} = f_V(a) - f_H(a)$ are each expressed as a polynomial of the following form,

$$f_q = \sum_{i=0}^{5} \alpha_{iq} a^i \qquad (3.1\text{-}11)$$

Thus, each single drop coefficient is expanded in powers of a up to 5. The expansion coefficients carry an additional subscript, q. This is because the entire range of possible drop radii (0 to 3.5 mm) is broken into intervals over which different polynomial curve fits (and thus coefficient sets) are possible. These intervals are

of	Drop radius, a(mm) lower limits a_{qL}	upper limits a_{qU}
1	0	0.25
2	0.25	1.0
3	1.0	2.0
4	2.0	2.5
5	2.5	3.5

Substitution of (3.1-10) and (3.1-11) into (3.1-9) yields a series of integrals of the following form

$$\mathcal{J} = \int_0^L \int_0^\infty f \; n_o(z',a) \; da \; dz' \tag{3.1-12}$$

$$= \int_0^L \int_0^\infty \sum_{i=0}^{5} \alpha_{iq} \, a^i \; n_o(z',a) \; da \; dz' \tag{3.1-13}$$

The Marshall-Palmer drop size distribution is

$$n_o(z',a) = N_o \, e^{-\rho} \tag{3.1-14}$$

where

$$N_o = 16{,}000$$

and

$$\rho = 8.2 \; [R(z')]^{-0.21}$$

Also, we recognize that the α_{iq} coefficients remain constant only over the q intervals. Thus we break up the integral over a into intervals; this reduces (3.1-13) to

$$\mathcal{I} = N_o \sum_{i=0}^{5} \int_0^L \sum_{q=1}^{5} \alpha_{iq} \int_q a^i e^{-\rho a} \, da \, dz' \tag{3.1-15}$$

$$= N_o \sum_{i=0}^{5} \int_0^L \sum_{q=1}^{5} \left\{ \int a^i e^{-\rho a} \, da \Big|_{a_{qU}} - \int a^i e^{-\rho a} \, da \Big|_{a_{qL}} \right\} da \, dz' \tag{3.1-16}$$

$$= \mathcal{I}_U - \mathcal{I}_L \tag{3.1-17}$$

where

$$\mathcal{I}_{\substack{U \\ L}} = N_o \sum_{q=1}^{5} \sum_{n=0}^{5} \alpha_{nq} \int_0^L \left[\int a^n e^{-\rho a} \, da \right]_{a_{qL}}^{a_{qU}} dz' \tag{3.1-18}$$

The integral over drop size is

$$\mathcal{I}_{aq} = \int a^n e^{-\rho a} \, da \tag{3.1-19}$$

$$= e^{-\rho a} \sum_{m=0}^{n} \frac{n!}{(n-m)!} \frac{a^{n-m}}{(-\rho)^{m+1}} (-1)^m \tag{3.1-20}$$

In the case where $a \leq 0.25$ mm we use the single drop scattering coefficients for $a = 0.25$ mm. Then the integral of (3.1-19) is instead

$$(0.25)^n = \frac{e^{-\rho a}}{-\rho} \tag{3.1-21}$$

As a consequence,

$$\mathcal{J}_{aq} = \frac{e^{-\rho a}}{-\rho} \sum_{m=0}^{n} \frac{n!}{(n-m)!} \frac{a^{n-m}}{(-\rho)^m} (-1)^m \tag{3.1-22}$$

except that when q = 1 the sum reduces to only one term (m = 0) and a = 0.25 inside the sum.

Evaluation for the Exponential Spatial Rain Rate Distribution

The only remaining difficulty is the evaluation of the integral over the spatial variation. This could be done numerically, but an analytical result greatly relieves the computer evaluation phase. This has been done for the piecewise-uniform rainrate model of Persinger et al., [1980]. [Tsolakis and Stutzman, 1982] Recently Stutzman and Dishman [1982] have develped an exponential rainrate model for use with earth-space paths. It was derived and then compared to world wide data sets giving good agreement with attenuation measurements. Since depolarization is much less sensitive to the details of the rainrate distribution along the path, the exponential rainrate distribution can be used

with confidence in this multiple scattering model that is intended for depolarization calculations.

Now we proceed with the multiple scattering model including the exponential spatial distribution. During this derivation the results for a uniform distribution will also be found.

The exponential rainrate distribution is

$$R(z') = \begin{cases} R_o & R_o \le 10 \frac{mm}{hr} \\ R_o \, e^{-\gamma \ln\left(\frac{R_o}{10}\right) \cos \varepsilon \, z'} & R_o > 10 \end{cases} \tag{3.1-23}$$

Then, from (3.1-14),

$$\rho = \begin{cases} 8.2 \, R_o^{-0.21} & R_o \le 10 \frac{mm}{hr} \\ 8.2 \, R_o^{-0.21} \, e^{0.21\gamma \ln \frac{R_o}{10} \cos \varepsilon \, z'} & R_o > 10 \end{cases} \tag{3.1-24}$$

$$= \begin{cases} -C & R_o \le 10 \frac{mm}{hr} \\ -C \, e^{Kz'} & R_o > 10 \end{cases} \tag{3.1-25}$$

where

$$C = -8.2\, R_o^{-0.21}$$

$$K = 0.21\, \gamma \ln \frac{R_o}{10} \cos \varepsilon \qquad (3.1\text{-}26)$$

When $R_o \leq 10$ mm/hr we must evaluate (from (3.1-18)) an integral of the type

$$\int_0^L \frac{e^{-\rho a}}{(-\rho)^{m+1}}\, dz' = \int_0^L \frac{e^{Ca}}{C^{m+1}}\, dz' = \frac{e^{Ca}}{C^{m+1}} L \qquad (3.1\text{-}27)$$

Then,

$$\vartheta_{\substack{U \\ L}} = N_o \sum_{q=1}^{5} \sum_{n=0}^{5} \alpha_{nq} \frac{e^{Ca}}{C} L \sum_{m=0}^{n} \frac{n!}{(n-m)!} \frac{a^{n-m}}{C^m} (-1)^m \qquad (3.1\text{-}28)$$

for R_o 10 mm/hr and where the sum over m reduces to only one term (m = 0) and a = 0.25 inside the sum for q = 1, and where a is a_{qU} or a_{qL} at the upper and lower limits. This is the same result as for a entirely uniform rainrate distribution. In other words, (3.1-28) in (3.1-17) gives the result for a rain of uniform rate and length L along the path.

Now, the exponential rainrate distribution for R_o > 10 mm/hr involves

$$\mathcal{L}_E = \int_0^L \frac{e^{-\rho a}}{(-\rho)^{m+1}}\, dz' = \int_0^L \frac{e^{Ca}\, e^{Kz'}}{C^{m+1}\, e^{(m+1)Kz'}}\, dz' \qquad (3.1\text{-}29)$$

Changing variables to

$$u = e^{Kz'} \qquad du = Ku\, dz'$$

gives

$$\mathcal{L}_E = \int_1^{e^{kL}} \frac{e^{Cau}}{C^{m+1}\, u^{m+1}}\, \frac{du}{Ku} = \frac{1}{K\, C^{m+1}} \int_1^{e^{KL}} \frac{e^{Cau}}{u^{m+2}}\, du \qquad (3.1\text{-}30)$$

From Gradshteyn and Ryzhik [1980], we obtain

$$\int \frac{e^{ax}}{x^n}\,dx = -e^{ax} \sum_{j=1}^{n-1} \left[\frac{a^{j-1}}{(n-1)(n-2)\cdots(n-j)x^{n-j}} + \frac{a^{n-1}}{(n-1)!}\,Ei(ax) \right] \tag{3.1-31}$$

where

$$Ei(ax) = 0.577216 + \ln|ax| + \sum_{j=1}^{\infty} \frac{(ax)^j}{j \cdot (j)!}$$

Then

$$\begin{aligned}
\mathcal{J}_E &= \frac{1}{K\,C^{m+1}} \left[-e^{Cau} \sum_{\ell=1}^{m+1} \frac{(Ca)^{\ell-1}}{(m+2-1)(m+2-2)\cdots(m+2-e)u^{m+2-\ell}} \right. \\
&\qquad \left. + \frac{(Ca)^{m+1}}{(m+1)!}\,Ei(Cau) \right]_{u=1}^{u=e^{KL}} \\
&= \frac{1}{K\,C^{m+1}} \left[-e^{Cau} \sum_{\ell=1}^{m+1} \frac{(m+1-\ell)!}{(m+1)!} \frac{(Ca)^{\ell-1}}{u^{m+2-\ell}} \right. \\
&\qquad \left. + \frac{(Ca)^{m+1}}{(m+1)!}\,Ei(Cau) \right]_{u=1}^{u=e^{KL}} \\
&= \frac{1}{K\,C^{m+1}\Gamma(m+2)} \left[e^{-Cau} \sum_{\ell=1}^{m+1} \Gamma(m+2-\ell) \frac{(Ca)^{\ell-1}}{u^{m+2-\ell}} \right. \\
&\qquad \left. + (Ca)^{m+1}\,Ei(Cau) \right]_{u=1}^{u=e^{KL}}
\end{aligned} \tag{3.1-32}$$

since $\Gamma(n) = (n-1)!$. Using this result together with (3.1-22) in (3.1-18) gives

$$\mathcal{J}_{\substack{U\\L}} = N_o \sum_{q=1}^{5} \sum_{n=0}^{5} \alpha_{nq} \sum_{m=0}^{n} \frac{n!}{(n-m)!} (-1)^m a^{n-m}$$

$$\cdot \frac{1}{K C^{m+1} \Gamma(m+2)} \left[-e^{Cau} \sum_{\ell=1}^{m+1} \Gamma(m+2-\ell) \frac{(Ca)^{\ell-1}}{u^{m+2-\ell}} \right.$$

$$\left. + (Ca)^{m+1} \, Ei(Cau) \right]_{u=1}^{u=e^{KL}} \qquad (3.1\text{-}33)$$

for R_o > 10 mm/hr and where the sum over m reduces to only one term (m=0) and a = 0.25 inside this sum for q=1, and where a is a_{qU} or a_{qL} at the upper and lower limits.

Combining our results, we have

$$\mathcal{J}_{\substack{U\\L}} = N_o \sum_{q=1}^{5} \sum_{n=0}^{5} \alpha_{nq} \sum_{m=0}^{n} G_{mq} \qquad (3.1\text{-}34)$$

where for (q=1)

$$G_{m1} = \frac{e^{Ca}}{C} L \, (0.25)^n \qquad \text{for} \quad \begin{matrix} R_o \quad 10 \frac{mm}{hr} & \text{exponential} \\ \text{any } R_o & \text{uniform} \end{matrix}$$

and for $2 \leq q \leq 5$

$$G_{mq} = \frac{n!}{(n-m)!} \frac{(1)^m}{C^{m+1}} a^{n-m} H_m$$

in which

$$H_m = e^{Ca} L \qquad \text{and} \qquad \begin{matrix} R_o \leq 10 \frac{mm}{hr} & \text{exponential} \\ \text{any } R_o & \text{uniform} \end{matrix}$$

$$H_m = \frac{1}{K \Gamma(m+2)} \left[-e^{Cau} \sum_{\ell=1}^{m+1} \Gamma(m+2-\ell) \frac{(Ca)^{\ell-1}}{x^{m+2-\ell}} + (Ca)^{m+1} Ei(Cax) \right]_{x=1}^{x=e^{KL}} \qquad R_o > 10 \frac{mm}{hr} \text{ exponential}$$

The multiple scattering model has been computer programmed. A description of the program and the statement listing are given in Appendix C.

3.2 COMPARISONS OF THE MULTIPLE SCATTERING MODEL TO OTHER MODELS

Several comparisons of multiple scattering routine predictions with other methods have been made. One such comparison was with the work by Oguchi [1981b]. Oguchi examined the frequency characteristics of crosspolarization for a 1 km terrestrial propagation path with a uniform rainrate distribution along the path. The calculations were made for 100% oblate spheroidal raindrops that were equi-oriented with a mean canting angle < > of 5 degrees. Results of the comparison between calculations from the multiple scattering routine and Oguchi are shown in Figure 3-1 for vertical and horizontal linear polarizations. Good agreement was found between the two models for the various rainrates. The largest deviation between the two models was 2.2 dB at R=25 mm/hr and a frequency of 6 GHz. The frequency characteristics of the two models were essentially the same, with the slopes of the curves determined by regression to be 20.0 $\log_{10}(f)$ for the Oguchi model and 21.3 $\log_{10}(f)$ for the multiple scattering routine.

A resonance effect was reported by Holt et al., [1977] in the forward-scattering amplitudes for equivolumetric drop radii of about 3 mm in the 6 GHz range. This resonance effect for the larger drops is apparent in Figure 3-1 at 6 GHz for R = 150 mm/hr which would contain a significant amount

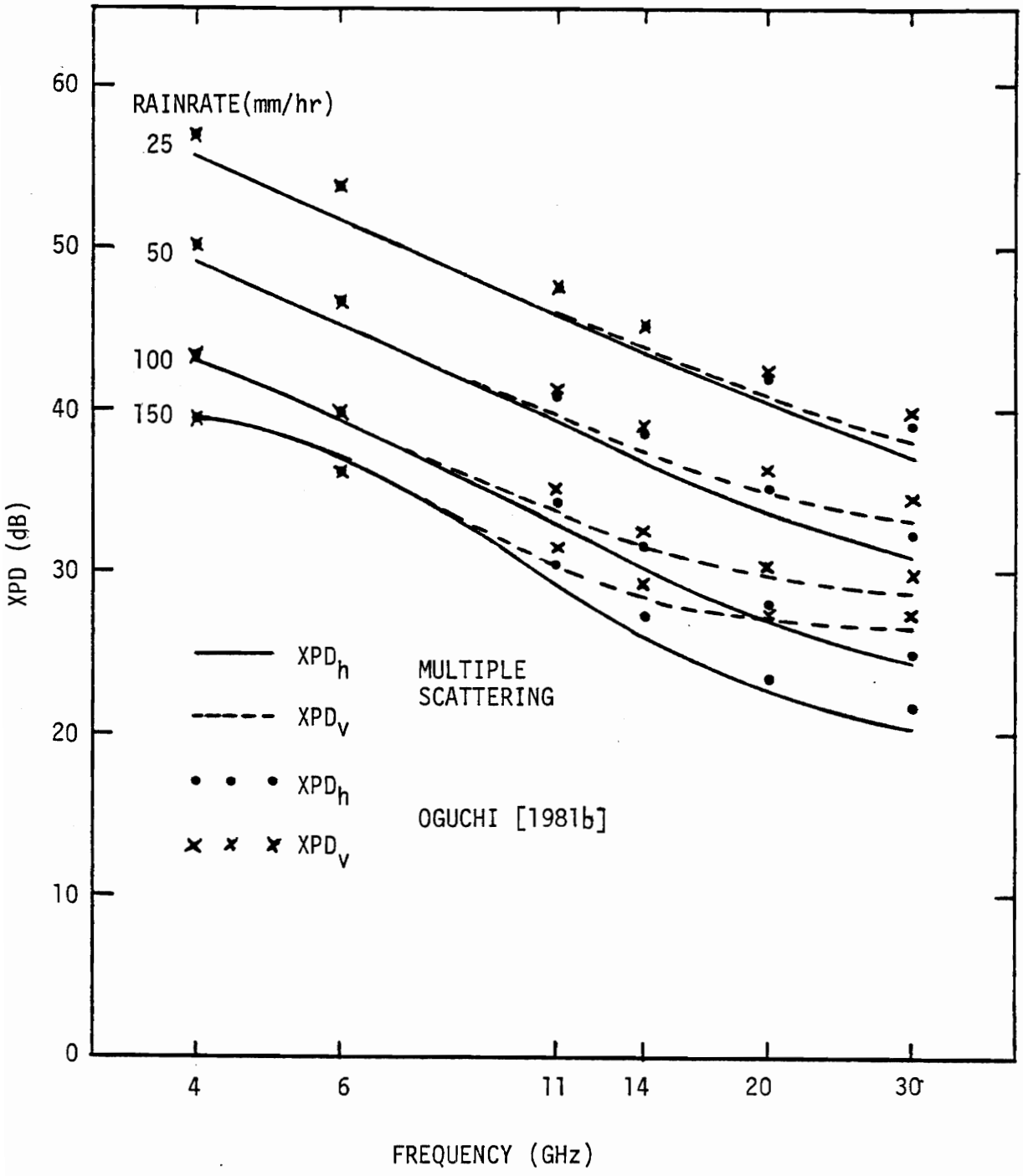

Figure 3-1. Comparison of multiple scattering model results to Oguchi [1981b]

of large drops in drop size distribution. At the higher frequency ranges, this resonance is not significant due to damping [Oguchi, p. 388, 1981b].

It is evident from Figure 3.2-1 that XPD degrades with higher frequency and higher rainrate. Cross-polar discrimination also becomes worse for longer propagation path lengths as does co-polar attenuation (A). When XPD versus A is considered we will see in Section 5.1 that over the frequency range of 10-30 GHz this relationship is relatively independent of path length and that XPD becomes better for higher frequencies when compared to attenuation.

3.3 OTHER SCATTERING FORMULATIONS

The complete multiple scattering formulation is general and easy to apply. Previous results have involved less general formulations. For example, if only the first two terms of the Taylor series expansion of (3.1-1) are retained the single-scattering approximation result is obtained:

$$\underline{D} \approx \underline{I} - j\underline{k} \qquad (3.3\text{-}1)$$

The corresponding physical process is one in which the wave progressing through the medium encounters particles only once; scattering off of a particle and onto another particle and on to the receiver is not considered. This approxima-

tion is valid only if $\underline{k}$ is small [Tsolakis, p. 23, 1982], such as when the particle density is low (very low rainrates and a narrow rain slab) or when $\underline{f}$ is small (as for low frequencies). In single scattering the attenuation due to absorption is essentially neglected [Ishimaru, 1977]. Therefore, only very slightly attenuating media are candidates for application of the single-scattering formula. In the case of rain media the single-scattering approximation is virtually useless. This is illustrated in Figure 3-2 which shows XPD as a function of rainrate (attenuation is small: 0.46 dB at 125 mm/hr as computed using the multiple scattering model). The exponential rainrate profile of SAM (see Section 3.1) is used. The single and multiple scattering calculations agree only at very low rainrates (very tenuous media cases). The single scattering approximation degrades further for higher frequencies.

The single scattering result can be useful if the medium is subdivided into slabs, each being tenuous, and we use the output of each slab as input to the next. This yields a first-order multiple scattering approximation. Rogers and Olsen [1976] have shown that successive application of the single-scattering approximation to infinitely thin layers results in all orders of forward multiple scattering being retained for the whole medium. One form of first order mul-

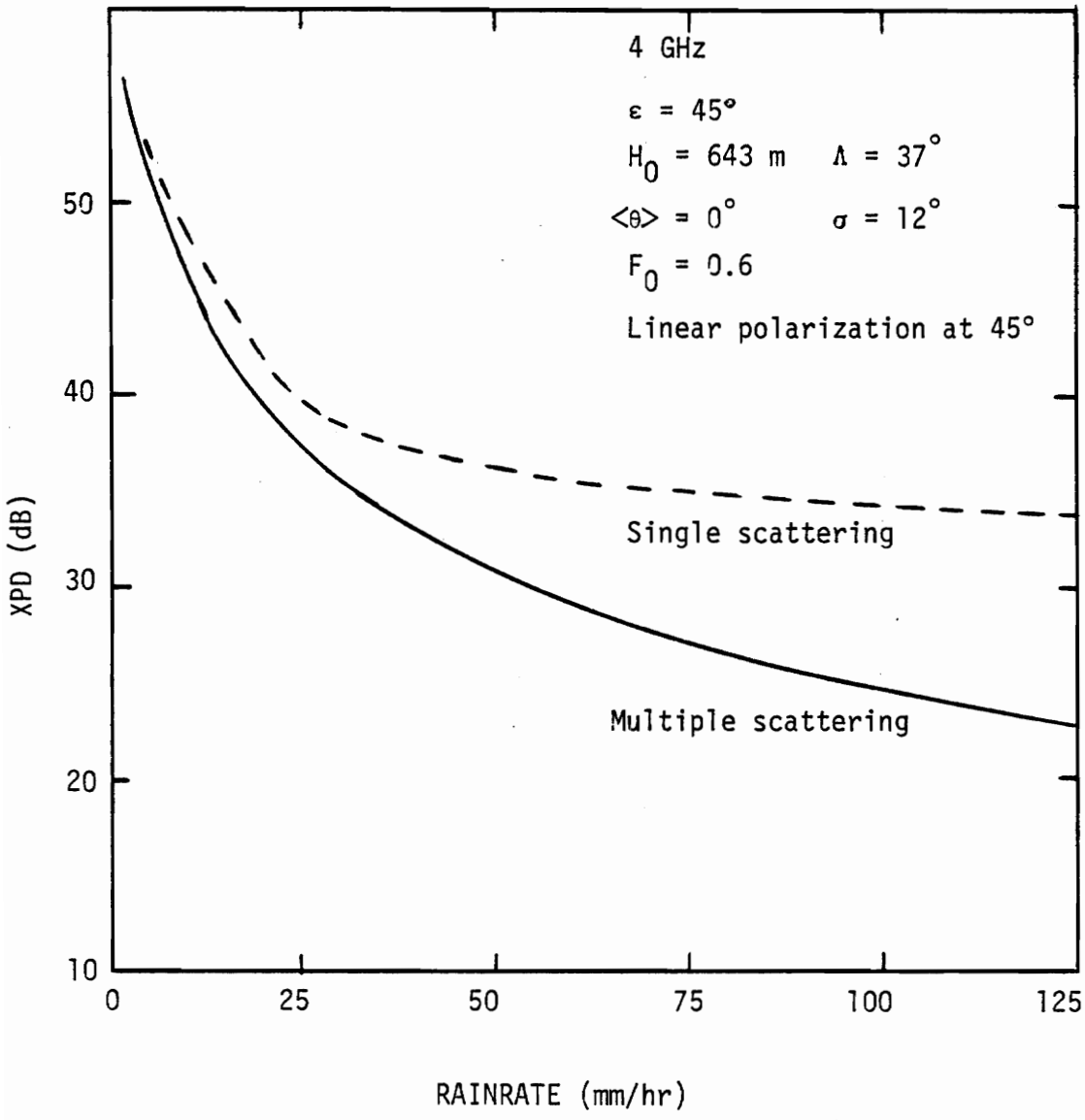

Figure 3-2. XPD versus rainrate at 4 GHz along a slant path at an elevation angle 45°. The exponential rain rate profile of SAM is used.

tiple scattering computations has been used by Persinger and Stutzman [1978]. The associated computer program is referred to as RPP (Rain Propagation Prediction) program. Results from this program and those of the complete multiple scattering have been compared. [Tsolakis and Stutzman, 1982]. The XPD and attenuation values predicted agree very closely up to at least 30 GHz.

Chapter IV

XPD MEASUREMENT

4.1 METHODS OF XPD DATA DISPLAY

XPD measurements can be presented as a function of local point rainrate, as a function of percent time, or as a function of path attenuation. Usually XPD is shown as a function of A because of its relative invariance with time. XPD as a function of rainrate or percent time, however, fluctuates widely as the point-to-path rainrate varies. XPD as a function of attenuation is, however, nearly independent of point rainrate. In fact, XPD as a function A is shown in Section 5.1 to be insensitive to many rain parameters along the propagation path. XPD as a function of A is a valuable relationship that can be used in the predictions of XPD from either attenuation measurements or calculations.

In typical research experiments attenuation and XPD data pair values (with time as a parameter) are measured and recorded. These XPD and A data pairs are processed in one of the following ways:

MEAN - for integer values of A the corresponding values of XPD are linearly averaged.

MEDIAN - For integerized values of A and XPD, the median XPD value for each A value is identified.

EQUIPROBABLE - Measured XPD and A data are often shown as separate statistics in the form of attenuation exceedance (the percent time that attenuation exceeds at specified value a, or P(A>a) and XPD lessance (the percent time that XPD is less than a specified value x, or P(XPD<x)). These statistics indicate the percent time that system performance is unsatisfactory. They can be combined for equal percent times to yield the "equiprobable" XPD vs A result.

JOINT PROBABILITY - The above three methods are basically XPD vs A results. However, the XPD and A data pairs (usually integerized) contain more information. This information is revealed with one of several contour type plots with XPD and A as the axes and joint probability values as the contour.

In this chapter the XPD vs A relationship is examined. The mean, median, and equiprobable methods are examined in detail in Section 4.2. The available worldwide data base is reviewed in Section 4.3. The joint XPD and A data display method is discussed in Section 4.4.

4.2 METHODS OF XPD DATA ANALYSIS

Many XPD experiments have been performed. However, little attention has been given to the variety of ways in which XPD data can be processed or to the sensitivitiy of data processing to experiment characteristics. A meaningful way to display the atmospheric effects on a dual polarized radio system is through an XPD vs A plot. The XPD vs A relationship is useful in modeling studies and for speculation on performance of similar radio systems. Our discussion will focus on earth-space link measurements of rain and ice depolarization, but the ideas apply to terrestrial links as well.

There are at least three methods of analyzing data from a dual polarized radio link to produce an XPD vs A relationship. (The joint probability distribution of XPD and A is also used and is discussed in Section 4.4.) For particular attenuation values the associated XPD values can be combined to yield the mean or the median (50% occurrence level). Me-

dian values are reported more often than are mean values, but we shall show that they are essentially identical. The third approach is the equiprobable method which is more sensitive to medium and measurement characteristics and should be used with caution. This, as well as the mean and median methods, are discussed in more detail and are compared to measured data in this section.

4.2.1 Mean and Median XPD vs A Data

The most direct approach to generating an XPD vs A relationship from measured data is to perform statistical analyses on recorded pairs of XPD and A values. For a given A value, the mean and median XPD values are the most popular measures of XPD. The median value is usually reported; this is probably because many available statistical software packages provide median as an output. A secondary benefit is that these packages also allow examination of deviations from the median (50% occurrence) such as 25-75% and 10-90% occurrence levels. On the other hand, the mean value is the commonly accepted measure of "average" behavior. Often standard deviation is given along with the mean to quantify the spread about the mean.

Mean and median are reasonable measures of the XPD vs A relationship and both are in use. It is desirable to compare data from different experiments employing mean and median data representations. To date no information exists on how reliably mean and median data sets can be compared. In fact, Cox [1981] has not considered mean data sets together with median data because of its unknown relationship to median data. In this section we show that mean and median values of XPD vs A are nearly identical.

When the distribution function for a measured data set is symmetrical mean and median agree exactly. We have examined measured XPD vs A data sets and found that mean and median always agree very closely. The first illustration of this is with data collected at VPI&SU using the SIRIO satellite. [Towner et al., 1982] The satellite transmits right-hand circular polarization at 11.6 GHz. The receiving system at Blacksburg, Va, consists of two separate earth terminals (site 1 employs a 3.7 m antenna and site 2 which is 7.2 km away has a 3.1 m antenna) operating at a 10.7° elevation angle. At this low elevation angle significant rain and ice depolarization occur. One year of data (15 July 1980 - 30 June 1981) has been carefully processed to remove spurious satellite signal fluctuations associated with the SIRIO beacon, signal drifts, etc. These data were processed for mean

and median XPD vs A and are shown in Figure 4-1. Note that mean and median are nearly identical for both receiving sites.

Similar studies were performed on one year data sets at different frequencies, elevation angles, and polarizations. Data from one year of the VPI&SU experiment with the CTS satellite were processed on an events-only basis. The CTS satellite beacon was operated at 11.7 GHz with right-hand circular polarization. The Blacksburg earth terminal viewed the satellite at 33 elevation angle and the data collected for July 1978 through June 1979 are plotted in Figure 4-2. The mean and median data curves are nearly identical.

VPI&SU has also collected data from the COMSTAR satellite beacons operating at 19.04 and 28.56 GHz with linear polarization. [Andrews et al., 1982] One year of events-only data with the COMSTAR experiment at an elevation angle of 46 at both 19 and 28 GHz also revealed excellent agreement between the mean and median values of XPD for all ranges of A values measured.

We can now conclude that mean and median are interchangeable measures of XPD vs A data.

The deviation of the measured data from the mean or median values are also of interest. Figure 4-3 illustrates two approaches using the SIRIO data. Note that the median to-

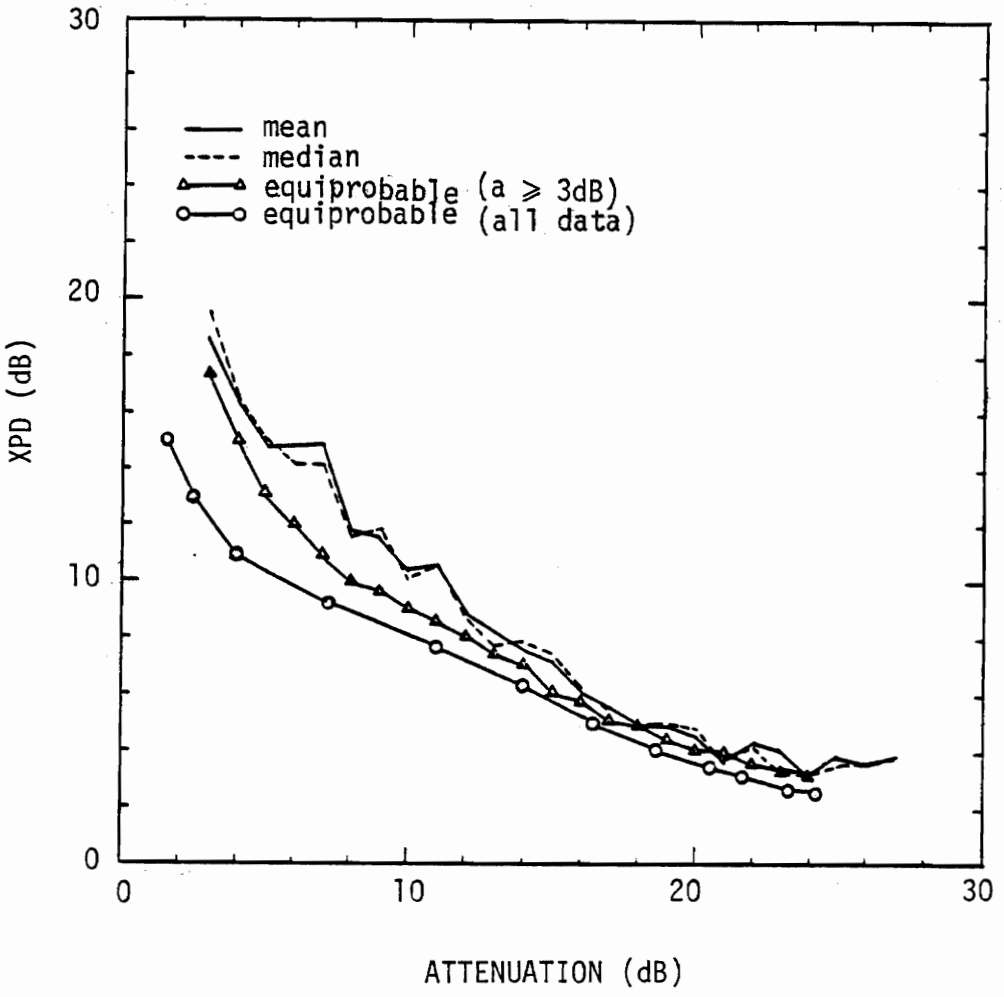

Figure 4-1. XPD vs attenuation data measured at Blacksburg, VA, at an elevation angle of 10.7° using the SIRIO satellite circularly polarized, 11.6 GHz beacon for the time period July 15,1980 - June 30,1981. Comparisons of the following four methods of data display are shown: mean (——), median (----), equiprobable for all data (o——o), and equiprobable for data with A ≥ 3dB (Δ——Δ).

(a) Main site

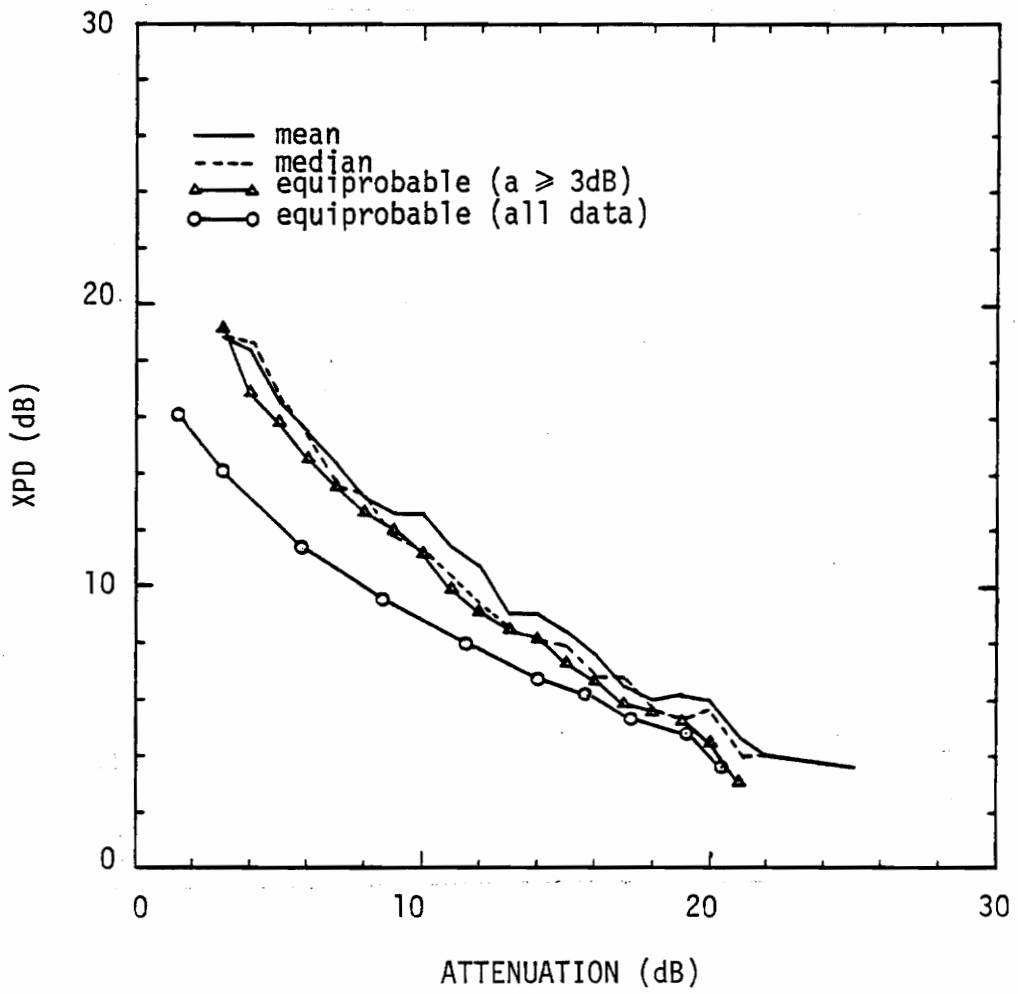

Figure 4-1. (b) Remote site

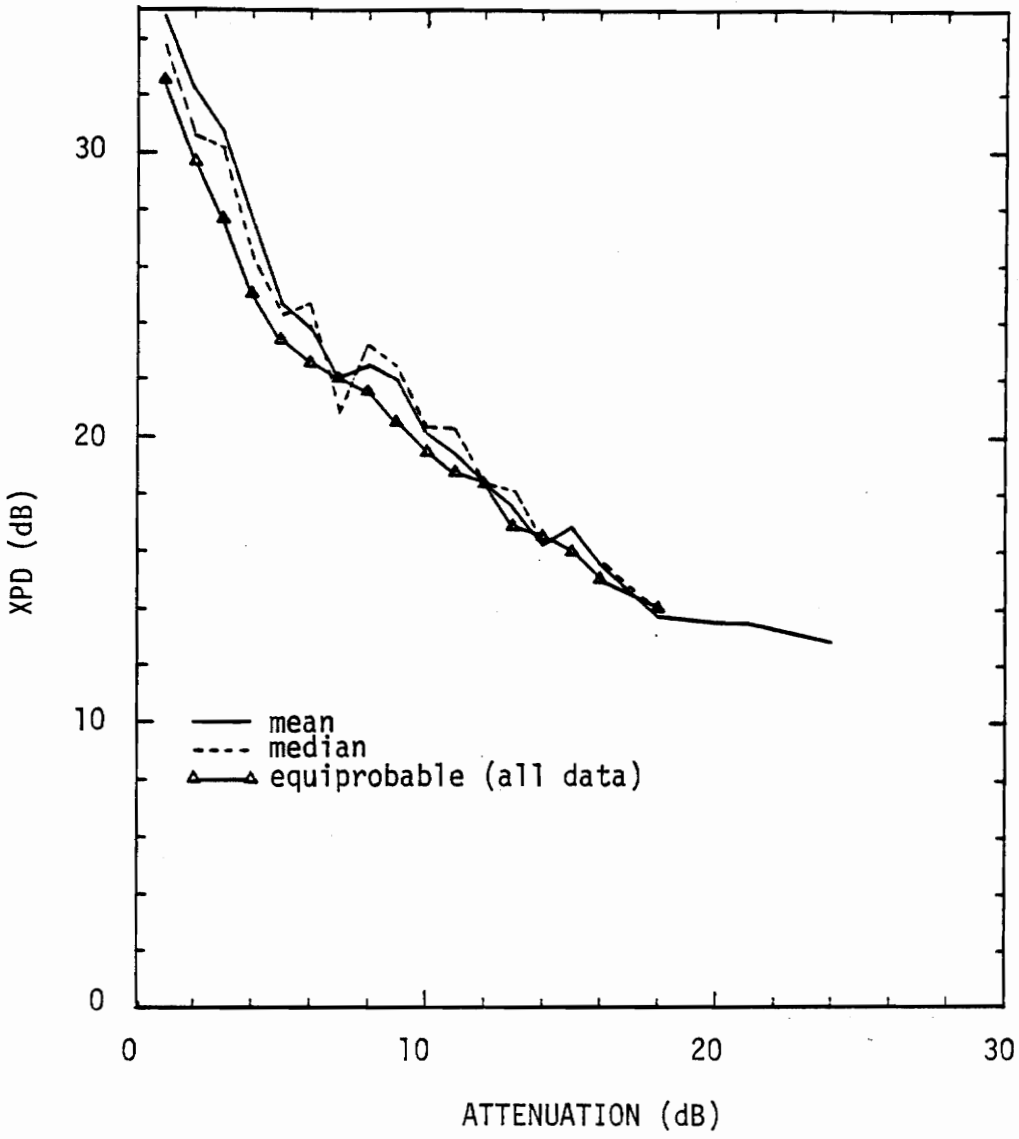

Figure 4-2. XPD vs attenuation data measured at Blacksburg, VA, at an elevation angle of 33° using the CTS satellite circularly polarized, 11.7 GHz beacon for the time period July 1978-June 1979. Comparisons of the following three methods of data display are shown: mean (——), median (----), equiprobable for all data (△——△).

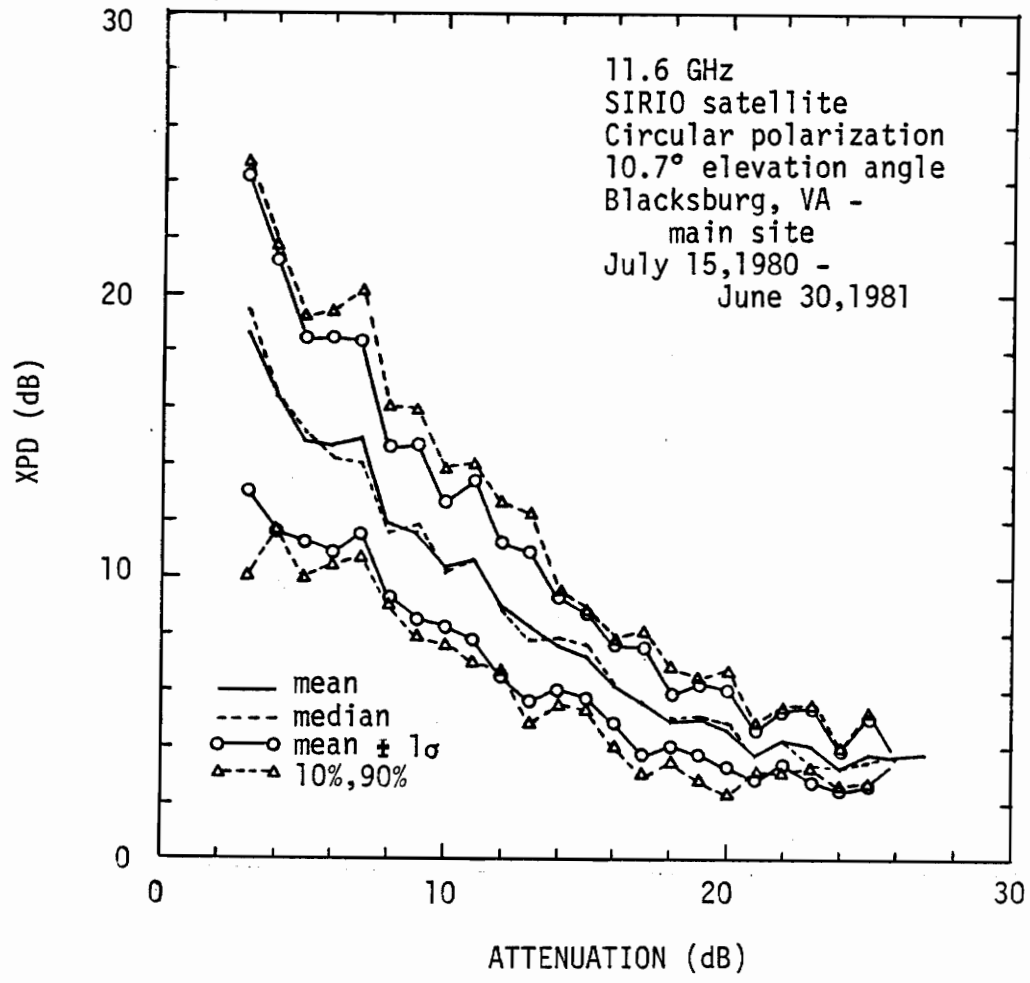

Figure 4-3. Data from Figure 4-1 showing the median value of XPD vs A data along with 10%, 90% occurrence levels (dashed curves). Also shown are mean and one standard deviation levels (solid curves).

(a) Main site

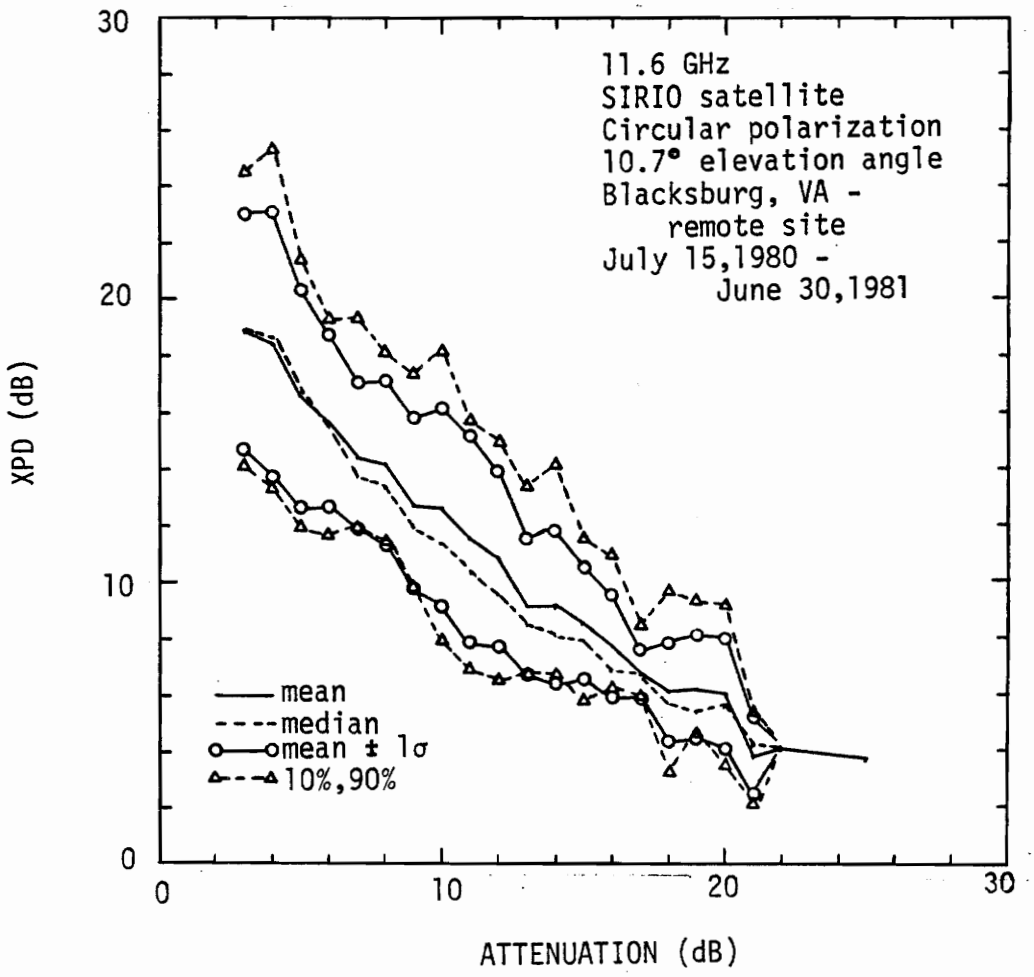

Figure 4-3. (b) Remote site

gether with 10%-90% occurrence levels and the mean together with one standard deviation reflect the deviations in the data sets in a very similar way.

4.2.2 Equiprobable XPD vs A Data

Mean and median XPD vs A data analysis require simultaneous XPD and A data pairs. Frequently these pairs are not recorded or are not available. Instead the individual XPD and A statistics are reported. As mentioned earlier the XPD vs A relationship can be generated from these on an equiprobable basis. The question then is how this result compares to mean and median and what problems arise because simultaneous data pair information is not needed. Some theoretical analysis is necessary as a background to this question.

The density functions for attenuation and XPD statistics are based on discrete samples. However, we will for simplicity assume that the density functions are continuous. This discussion does not depend upon the type of density function, but for the sake of argument we shall use functions that have been presented in the literature. In particular, long-term attenuation and XPD statistics can be modeled by the normal (Gaussian) density function:

$$f(r) = \frac{1}{\sigma_r\sqrt{2\pi}}\, e^{-(r - \langle r\rangle)^2/2\sigma_r^2} \qquad (4.2\text{-}1)$$

where <r> is the mean value of r and σ_r is the standard deviation about the mean.

Attenuation statistics are usually presented for a period which includes all time - both clear weather and rain periods. (If clear weather is excluded form the time base, a log-normal density function provides good results. [Lin, 1973].) We will use a one-sided normal density function; then from (4.2-1) with <a> = 0:

$$f(a) = \frac{2}{\sigma_a\sqrt{2\pi}} \; e^{-a^2/2\sigma_a^2} \; U(a) \qquad (4.2\text{-}2)$$

where U(a) = 0 for a < 0 and 1 for a $\geqslant$ 0. Reemphasizing, some adjustments to this model may be required to fit actual data, but (4.2-2) describes the behavior of attenuation and is sufficient for the points we wish to make. The cumulative (or exceedance) distribution associated with the attenuation density of (4.2-2) is

$$P(A > a) = \frac{2}{\sigma_a\sqrt{2\pi}} \int_a^{\infty} e^{-a^2/2\sigma_a^2} \, da \qquad (4.2\text{-}3)$$

The XPD density function is also modelled by the normal density function [Kanellopoulous and Clarke, 1981]. For high quality systems the XPD is maximum at some clear weather value X_c and only degrades from that during propagation

events. The density function is then a truncated form of (4.2-1) with $\langle r \rangle = X_c$, or

$$f(x) = \frac{2}{\sigma_x \sqrt{2\pi}} \; e^{-(x - X_c)^2/2\sigma_x^2} \qquad -\infty \leq x < X_c \tag{4.2-4}$$

The cumulative (lessance) distribution function for XPD is then

$$P(XPD < x) = \frac{2}{\sigma_x \sqrt{2\pi}} \int_{-\infty}^{x} e^{-(x - X_c)^2/2\sigma_x^2} \; dx \tag{4.2-5}$$

for $x < X_c$.

Equiprobable results are obtained by equating the cumulative distributions of (4.2-3) and (4.2-4); i.e. when

$$P(A > a) = P(XPD < x) \tag{4.2-6}$$

Then a and x form data pairs from which the XPD vs A relationship can be generated. This is represented in Figure 4-4 where the shaded portions indicate equal areas, or equal probabilities as in (4.2-6).

It is obvious that, if the measured cumulative distributions are in error, all equiprobable values will be affected; i.e., inaccuracies <u>anywhere</u> in the A or XPD distribution will affect <u>all</u> points on the equiprobable XPD vs A relationship. Error sources include inaccurate clear weather time duration, antenna effects on XPD, receiver drift effects on A, or any measurement error.

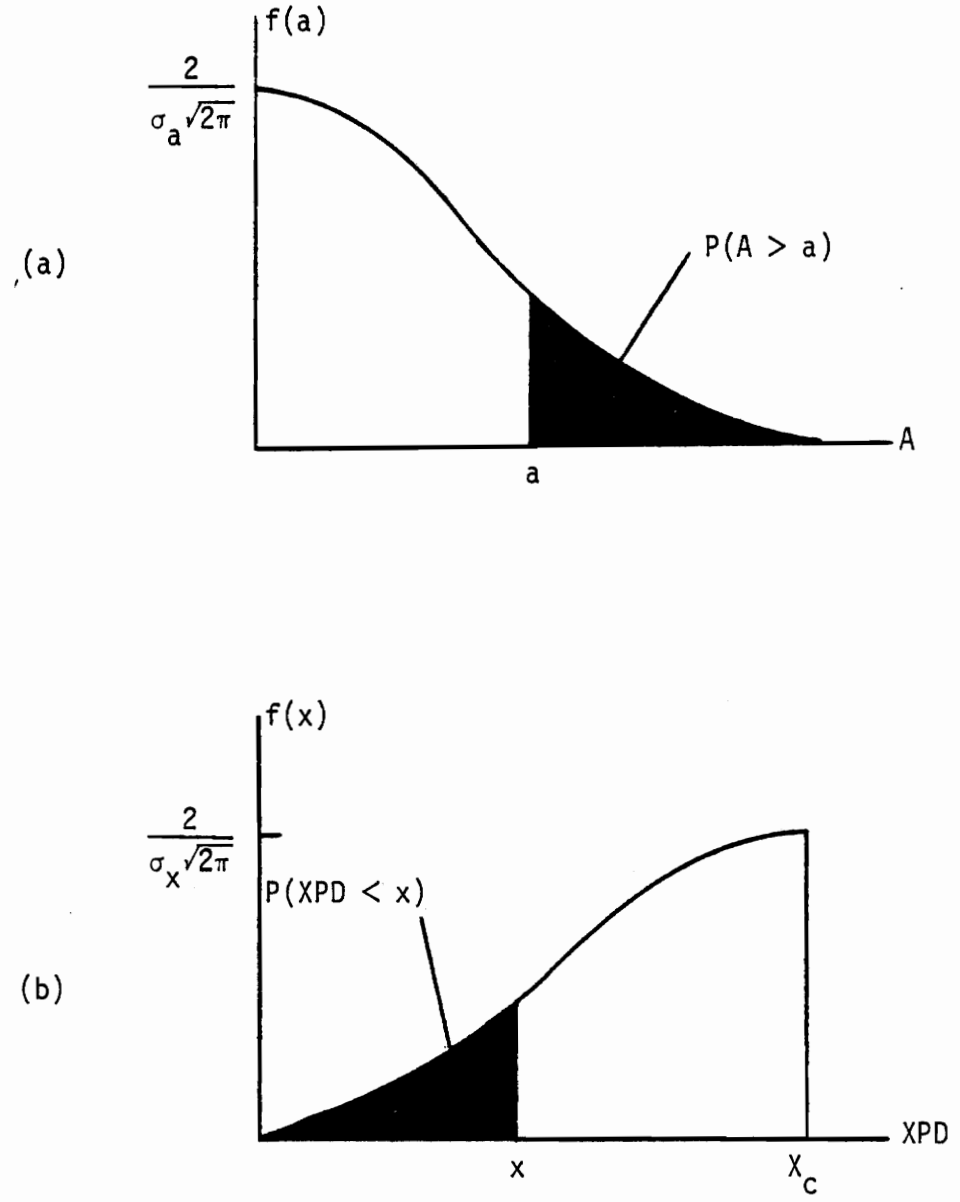

Figure 4-4. Illustration of equiprobable values of attenuation, a, and crosspolar discrimination, x:

$P(A > a) = P(XPD < x)$.

(a) The distribution of attenuation values.

(b) The distribution of XPD values.

The SIRIO, CTS, and COMSTAR data considered in this study were analyzed for the total data base available at VPI&SU. The error sources previously mentioned introduced problems with the equiprobable relationship in addition to the mean and median results. The data were reprocessed on an events-only basis for the one year periods presented. The reprocessed data resulted in cleaner mean and median XPD vs A relationships in addition to better agreement with the equiprobable results.

A medium effect which also impacts equiprobable results is ice depolarization. Suppose that XPD is degraded in the absence of any effect on attenuation due to ice clouds over the time period of the statistics. In this case there is a new value of standard deviation on XPD, σ_x' , such that $\sigma_x' > \sigma_x$ and the tail of the f(x) curve in Figure 4.2-4b extends to lower values of x. Then, equiprobable values result for A and XPD$'$ where XPD$'$ < XPD, for any value of A. Thus, we see that ice depolarization will shift the entire XPD vs A relationship even though it occurred for zero attenuation. This shift is greater at the higher probability levels because the area changes in the density functions are more sensitive to the parameters σ_a and σ_x at the high probability ends.

On the other hand, the mean and median XPD vs A relationship is affected by ice depolarization only at those values

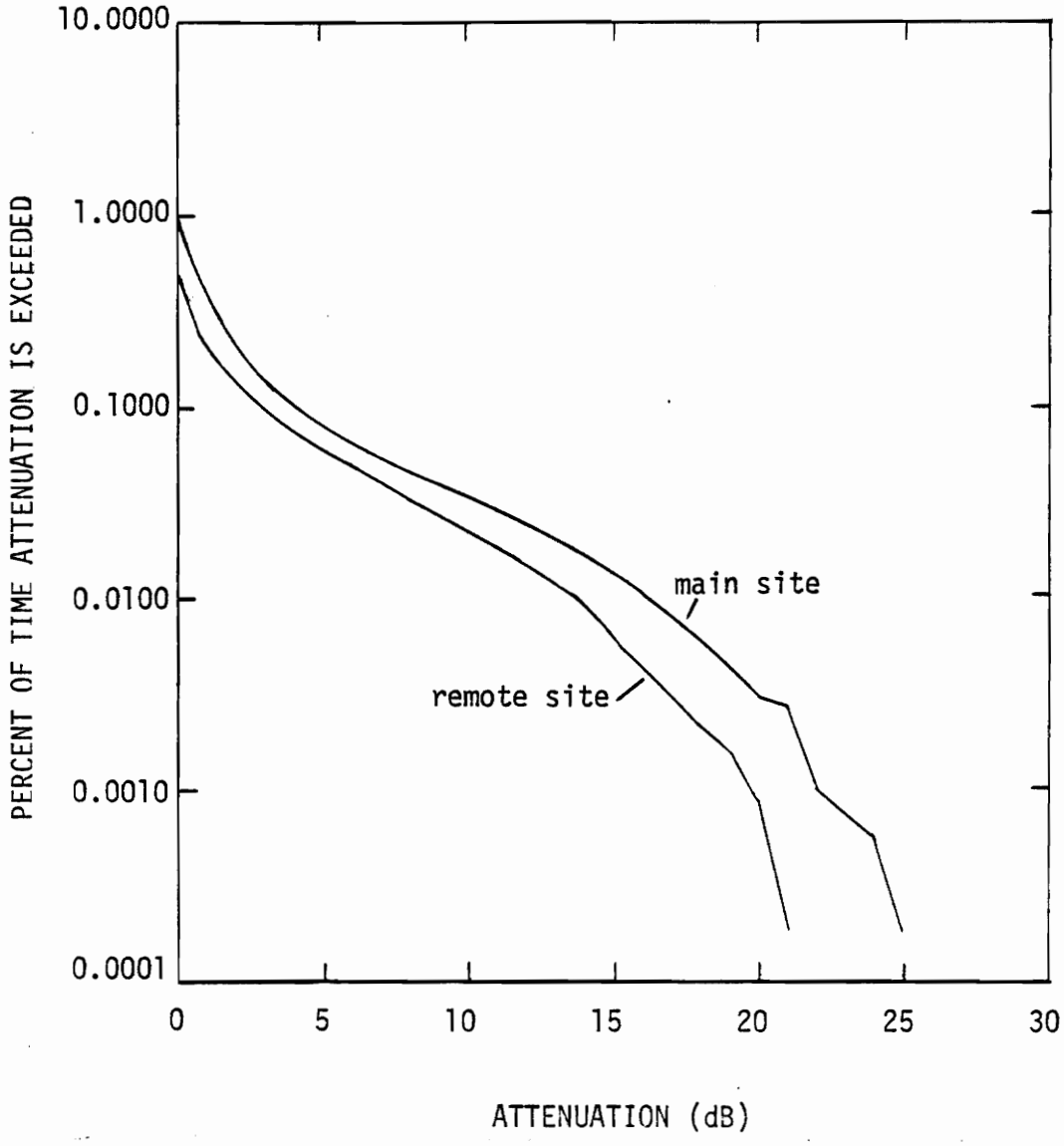

Figure 4-5. Marginal statistics measured at Blacksburg, VA, at an elevation angle of 10.7° using the SIRIO satellite circularly polarized, 11.6 GHz beacon for the time period July 15,1980 - June 30,1981.

(a) Marginal attenuation statistics

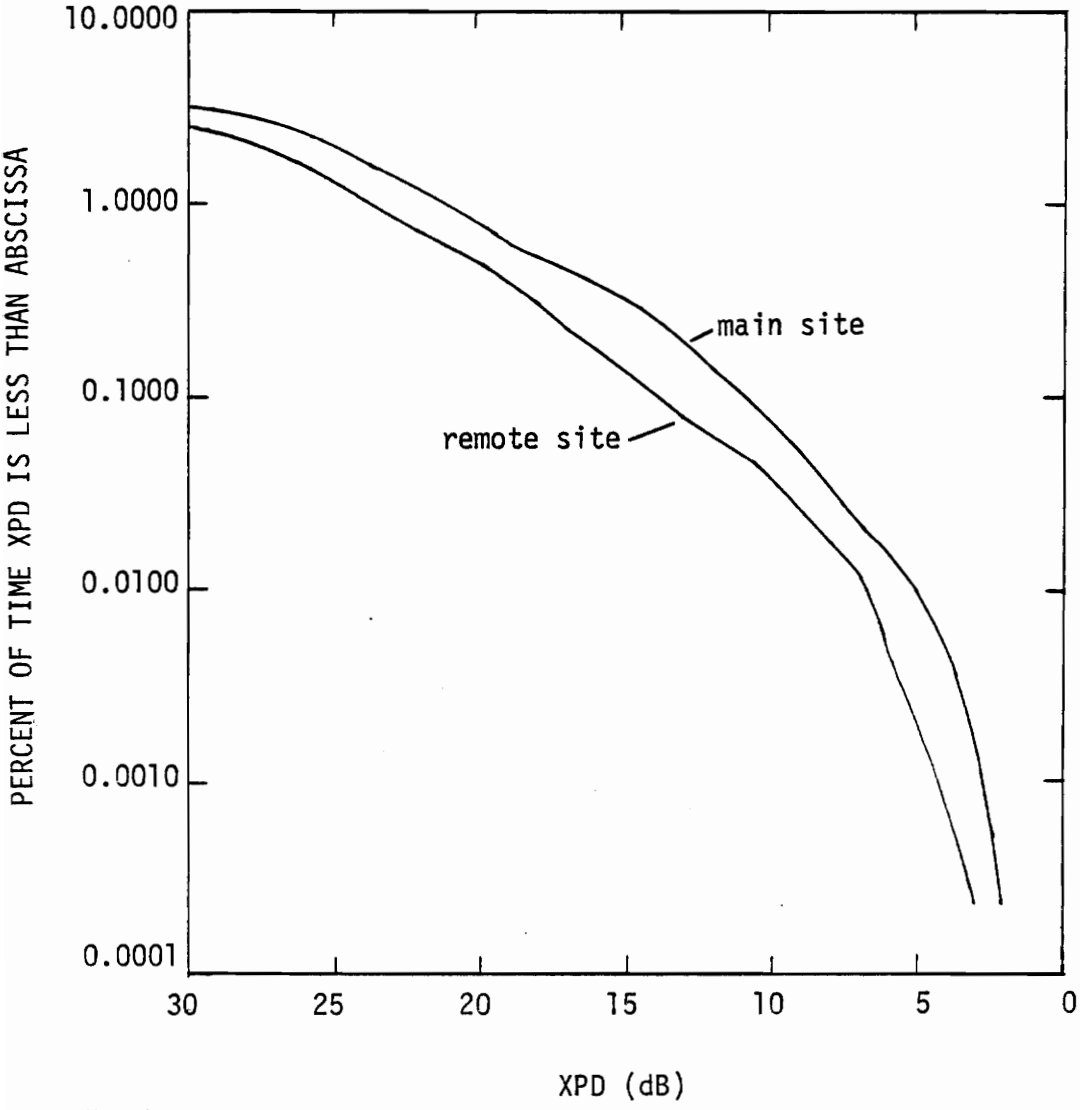

Figure 4-5. (b) Marginal XPD statistics

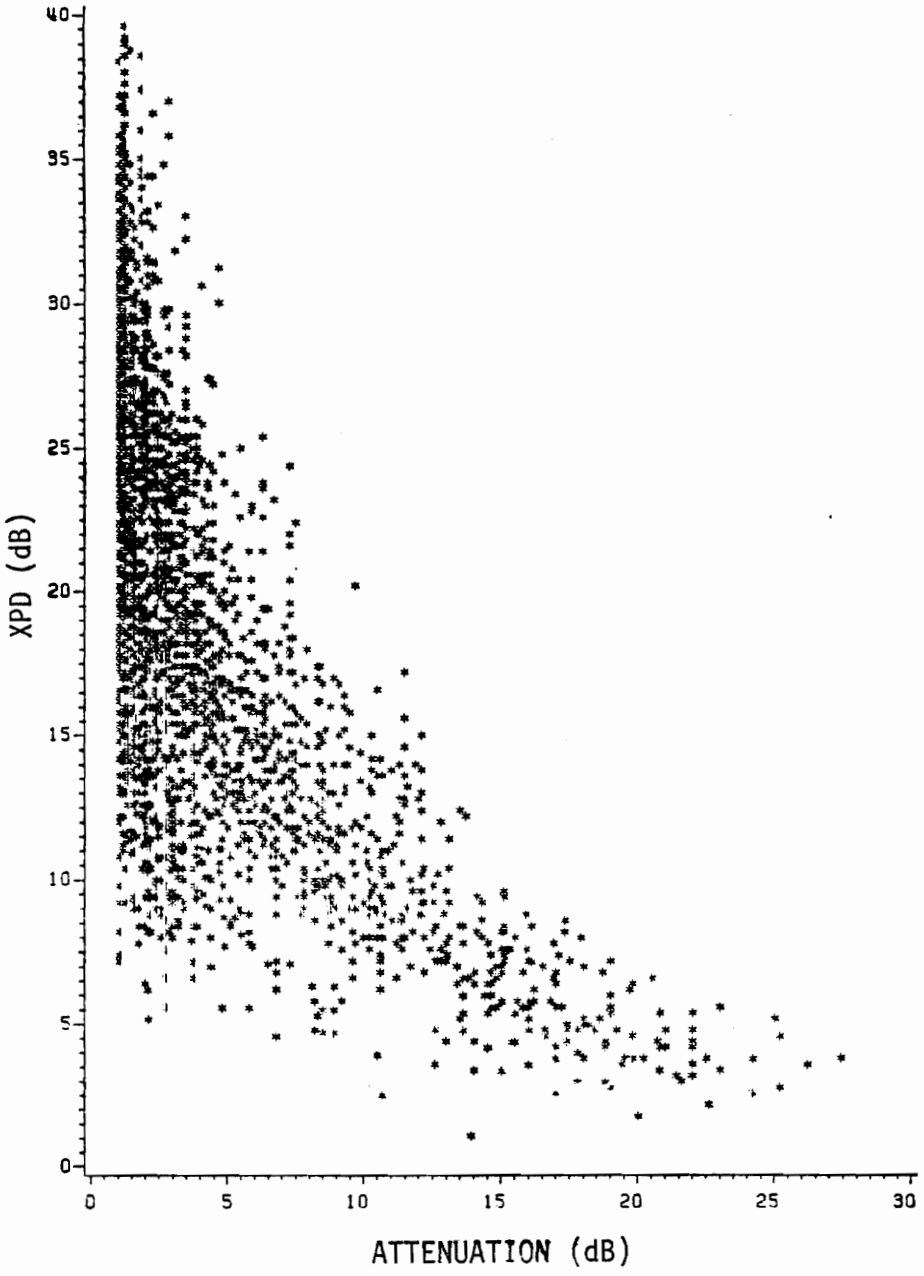

Figure 4-6. Scatter plot of event only data measured at Blacksburg,VA, at an elevation angle of 10.7° using the SIRIO satellite circularly polarized, 11.6 GHz beacon for the time period July 15,1980 - June 30,1981.

(a) Main site

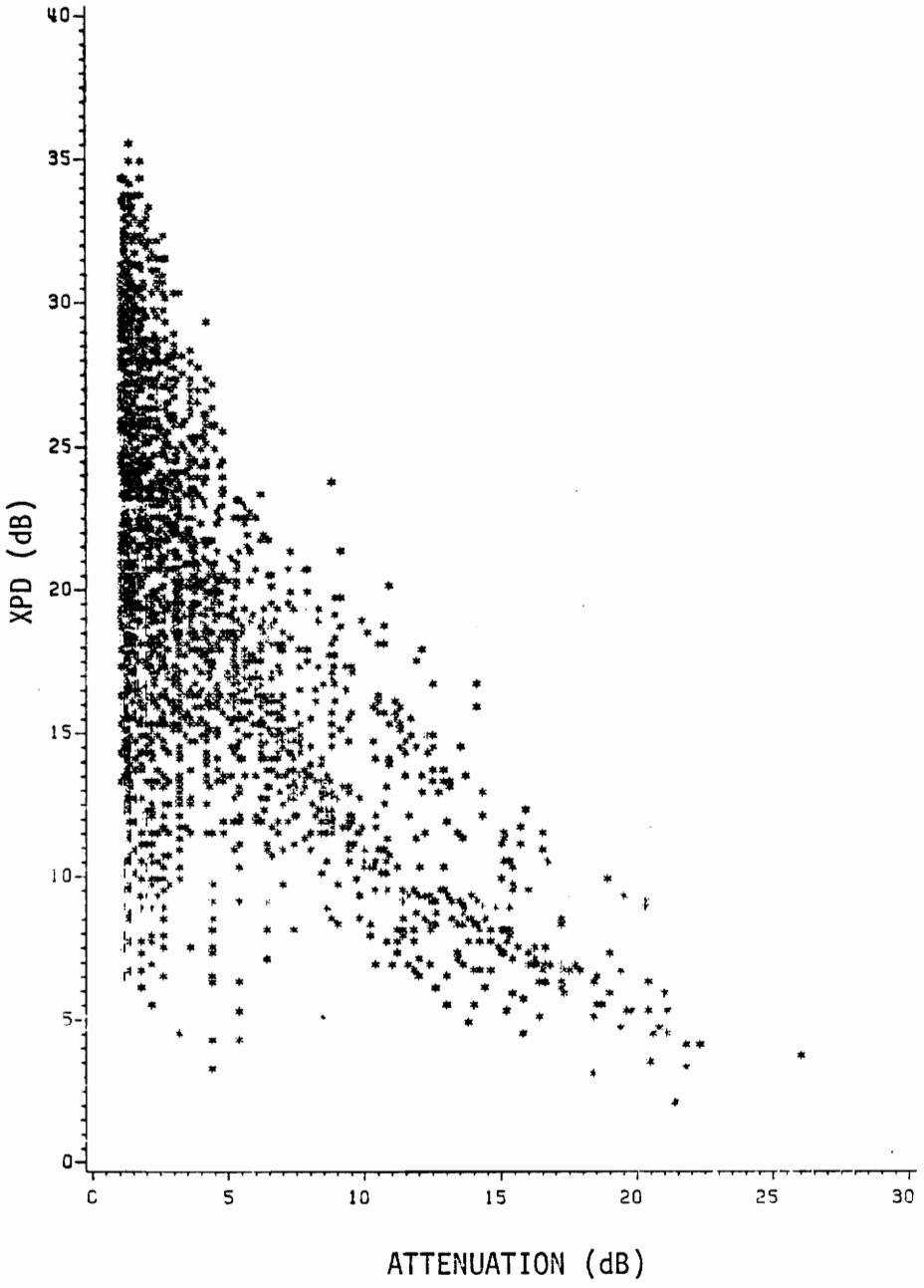

Figure 4-6. (b) Remote site

of A for which ice contributes to depolarization. This together with general sensitivity to error sources, leads to the conclusion that mean or median values are preferred over equiprobable for the XPD vs A relationship, especially when ice depolarization contributions are suspected.

The deviation of equiprobable XPD vs A from mean and median values is illustrated with measured data. The marginal statistics used to generate the equiprobable relationship for the SIRIO data are shown in Figure 4-5. Equiprobable data set results for the SIRIO experiments are shown in Figure 4-1. The presence of ice in these data sets was confirmed. [Stutzman, et al., 1983]

The scatter plots for the SIRIO data are shown in Figure 4-6. Ice effects are easily identified in the points occurring with significant depolarization and low values of attenuation.

Equiprobable results for all data fall significantly below the mean and median results at both SIRIO receiving sites (see Figures 4-1a and 4-1b) as predicted above. The situation can be improved somewhat by including only attenuation data greater than 3 dB, in an attempt to remove the ice affected data. The corresponding XPD vs A curves (see Figures 4-1a and 4-1b) are closer to the mean and median data curves, but are still noticeably pessimistic. Cox

[1981] and Vogel [1979] compared equiprobable and median XPD vs A data sets, at 19 and 11.7 GHz respectively. They noted small deviations, but their elevation angles were much higher (27° and 50°) where ice effects are greatly diminished.

The CTS experiment at 11.7 GHz had an elevation angle of 33° from Blacksburg. The scatter plot of the one year period is shown in Figure 4-7. The XPD vs A relationship produced by the scatter data is much tighter than that observed for the SIRIO experiment. Consequently, the agreement between the equiprobable and mean (or median) relationships seen in Figure 4-2 is very good.

We have examined three methods of displaying measured XPD vs A data, and shown that the mean and median value methods are essentially identical. On the other hand, equiprobable values based on the separate attenuation exceedance and XPD lessance statistics are sensitive to many errors. Ice depolarization alone or imbedded in rain depolarization can shift the entire XPD vs A relationship for equiprobable values.

XPD vs A data sets from different experiments can be compared with confidence when a mixture of mean and median values are present. However, caution should be used with equiprobable data sets, especially when ice effects are suspected.

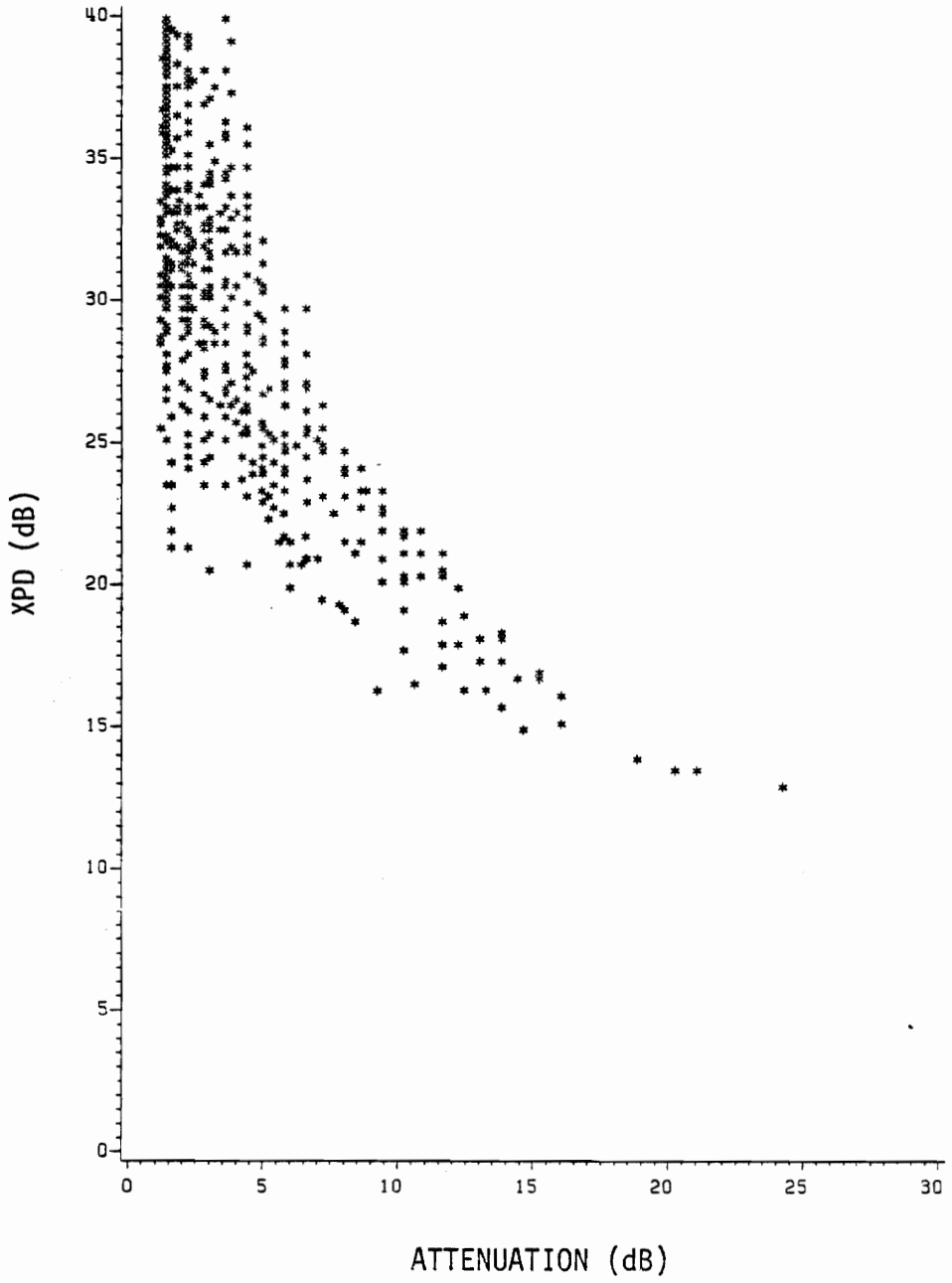

Figure 4-7. Scatter plot of event only data measured at Blacksburg,VA, at an elevation angle of 33° using the CTS satellite circularly polarized, 11.7 GHz beacon for the time period July 1978 - June 1979.

4.3 SUMMARY OF WORLDWIDE DATA BASE

Propagation data experiments for dual polarized earth-space links have been carried out all over the world. Most of these data have been presented in the form of marginal statistics for XPD and A. In Section 4.2 it was shown that the equiprobable XPD vs A relationship is sensitive to errors in the data and is inaccurate when significant ice effects are present. Data from several experiments have been reported in the literature as marginal statistics or as equiprobable XPD vs A data. Unfortunately, many reports do not include adequate justification for the accuracy of equiprobable data. It is important to have reliable data sets when constructing a universal model. Therefore, we limit our study to those experiments that present mean or median relationships. This limitation reduces the number of experiments to only a few in the continental U.S. plus one in U.K. A total of four experiment sites make up the data base: Blacksburg, Virginia; Austin, Texas; Crawford Hill, New Jersey; and Martlesham Heath, U.K. A summary of the experiments at these locations that used mean or median data is given in Table 4-1. This limited set of available data does, however, span the frequency range of interest (i.e. 10-30 GHz) with experiments at 11.6, 11.7, 14.5, 19.04, and 28.56 GHz. The data from the experiments listed in Table

Table 4-1

Summary of Data Base Experiment Characteristics

Data Set Number	Location	Frequency (GHz)	Polarization	Elevation Angle	Latitude	Site Altitude	Satellite	Time Interval	Reference
1	Martlesham Heath, U.K.	11.575	LP, τ=11.8°	29.9°	56.02°	0[3] M	OTS	Jul 1978 - Sep 1981	[Howell, et.al.,1982]
2	Blacksburg, VA[1]	11.6	CP	10.7°	37.00°	643	SIRIO	Jul 15,1980-Jun 30,1981	*
3	Blacksburg, VA[2]	11.6	CP	10.7°	37.00°	643	SIRIO	Jul 15,1980-Jun 30,1981	*
4	Austin, TX	11.7	CP	50.0°	30.39°	230	CTS	Feb 1978 - Jan 1979	[Vogel, 1979]
5	Austin, TX	11.7	CP	50.0°	30.39°	230	CTS	Jun 16,1976-Jun 15,1979	[Vogel, 1982]
6	Blacksburg, VA	11.7	CP	33.0°	37.00°	643	CTS	Jul 1978 - Jun 1979	*
7	Crawford Hill, N.J.	11.7	CP	27.0°	40.39°	115	CTS	Apr 26,1976-Apr 26,1977	[Cox, 1981]
8	Crawford Hill, N.J.	11.7	CP	27.0°	40.39°	115[3]	CTS	Apr 1977 - Jan 1979	[Rustako, 1982]
9	Martlesham Heath, U.K.	11.793	CP	29.9°	56.02°	0[3]	OTS	Jul 1978 - Sep 1981	[Howell, et. al.,1982]
10	Martlesham Heath, U.K.	14.455	CP	29.9°	56.02°	0[3]	OTS	Jul 1978 - Sep 1981	[Howell, et. al.,1982]
11	Blacksburg, VA	19.04	LP, τ=52.5°	46.0°	37.00°	643	COMSTAR D3	Oct 1978 - Sep 1979	*
12	Crawford Hill, N.J.	19.04	LP, τ=69.0°	38.6°	40.39°	115	COMSTAR D2	May 18,1977-May 18,1978	[Cox, et. al,1982]
13	Blacksburg, VA	28.56	LP, τ=52.5°	46.0°	37.00°	643	COMSTAR D3	Oct 1978 - Sep 1979	*
14	Crawford Hill, N.J.	28.57	LP, τ=69.0°	38.6°	40.39°	115	COMSTAR D2	May 18,1977-May 18,1978	[Cox, et. al,1982]

[1] Main site

[2] Remote site

[3] assumed value

* This data was reprocessed on an events only basis for this study.

4-I are used for comparison to the proposal model in Section 5.5 and with other models in Section 5.6.

4.4 JOINT XPD AND ATTENUATION DATA STATISTICS

The reliability of the dual-polarized satellite communication link is affected by degradations of both attenuation and cross-polar discrimination. To accurately assess the fade margin it is necessary to examine the statistics of simultaneous values of attenuation and isolation. Two methods of presenting the joint statistics have been suggested in the literature and these will be discussed and compared in this section using measured data.

4.4.1 The OR Conditional Joint Distribution

Joint statistics may be derived from a two-dimensional density function of sampled instantaneous pairs of crosspolarization discrimination (XPD) and co-polar attenuation (A). The approach suggested by Arnold and Cox [Cox, 1981] uses a density function t(A,X) based on the time in minutes that the integerized values (accuracy with 0.5 dB) of the XPD (X) - attenuation (A) pair occurred. The joint distribution T(a,x) is determined by the sum

$$T(a, x) = \sum_{\substack{A>a \\ \text{all } X}} t(A, X) + \sum_{\substack{X<x \\ A<a}} t(A, X) \qquad (4.4\text{-}1)$$

This sum may be examined by considering T(a,x) for the hypothetical scatter plot of simultaneous XPD and attenuation pairs in Figure 4-8 . Consider the distribution at the point (a' , x'). The first term in (4.4-1) is the cumulative distribution of attenuation exceedance (in minutes) determined by summing all of the observations to the right of the vertical dashed line at a'. The second term in (4.4-1) is the sum of the observations below the horizontal dashed line at x' and to the left of the vertical dashed line at a'. The two terms together represent all the observations less than x' or greater than a' .

Several characteristics of the joint distribution T(a,x) should be noted. The second term of (4.4-1) is zero for the joint distribution at the point (a' , x'') and the joint distribution is equal to the cumulative attenuation exceedance distribution at a'. Therefore, the joint distribution is equal to the cumulative attenuation exceedance distribution for all points in the XPD-attenuation plane where there are no observations X < x for a given a. A second feature is that the first term of (4.4-1) is zero for the joint distribution at the point (a'', x') and the joint distribution is equal to the cumulative XPD lessance distribution at x'.

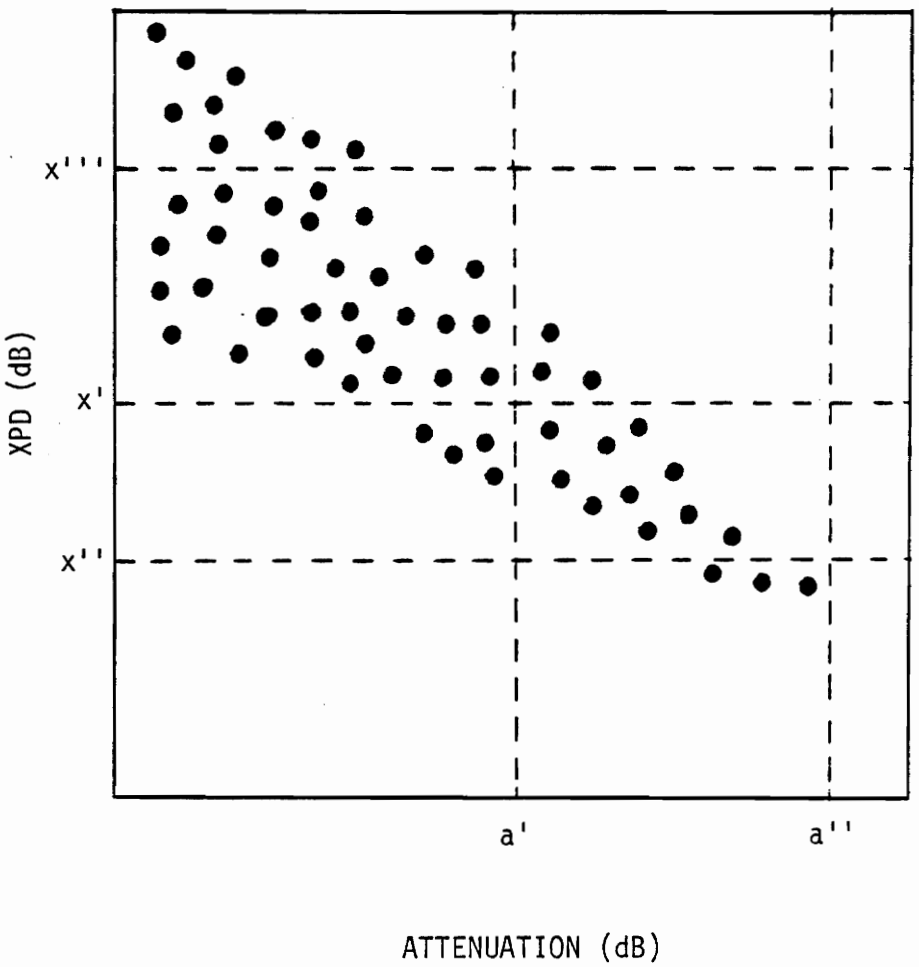

Figure 4-8. Hypothetical scatter plot of simultaneous XPD and attenuation data.

This is true for all values of X at a'' because all of the observations satisfy the condition that attenuation is less than a'' in the second term of (4.4-1). Therefore, the joint distribution is equal to the cumulative XPD lessance distribution for all points in the XPD-attenuation plane where all observations satisfy the condition A < a'' .

Cumulative probabilities are normally expressed as a fraction (or percent time) of the year for the marginal distributions for attenuation exceedance or XPD lessance. To convert the distribution in (4.4-1) from time in minutes to fraction of time requires only that the values of the joint distribution T(a,x) be divided by the total number of minutes comprising the observation period. Also, cumulative probabilities may be defined for the conditions of greater (less) than or equal to some fixed value rather than the exceedance (lessance). For a continuous density function the two definitions are identically equal, but the discrete density function yields a different result. This difference must be considered when comparisons are made between different techniques. For the cumulative distribution of one variable (i.e., the marginal distribution) based on a discrete density function, the calculated results are the same but shifted by one value (an integer in this case) of the observation variable. Similarly, the two variable joint cumula-

tive distribution is shifted one value in each dimension. The definition in (4.4-1) may be rewritten in this case as

$$T(a, x) = \sum_{\substack{A \geq a \\ \text{all } X}} t(A, X) + \sum_{\substack{X \leq x \\ A < a}} t(A, X) \qquad (4.4\text{-}2)$$

for comparison. When (4.4-2) is expressed as a probability (fraction of time rather than time in minutes) it is described as $P(A \geq a \text{ or } X \leq x)$.

Consider next the joint distribution in (4.4-1) for a deterministic relationship between XPD and attenuation which is approximately the case of rain depolarization during the "low percentage" large co-polar signal fades. A hypothetical scatter plot for this relationship is shown in Figure 4-9. The joint distribution $T(a,x)$ is equal to the cumulative attenuation exceedance distribution and also the cumulative XPD lessance distribution at the point (a', x'). This point is the equal probability value of XPD and A. The value of the joint distribution is the same for any value of A (such as a', a'', or a''') for the fixed value $X = x'$. If A is fixed at a', the variation of the variable X yields an increase in the value of the joint distribution for $X \leq x'$ but cannot drop below the value determined at the point $(a',$

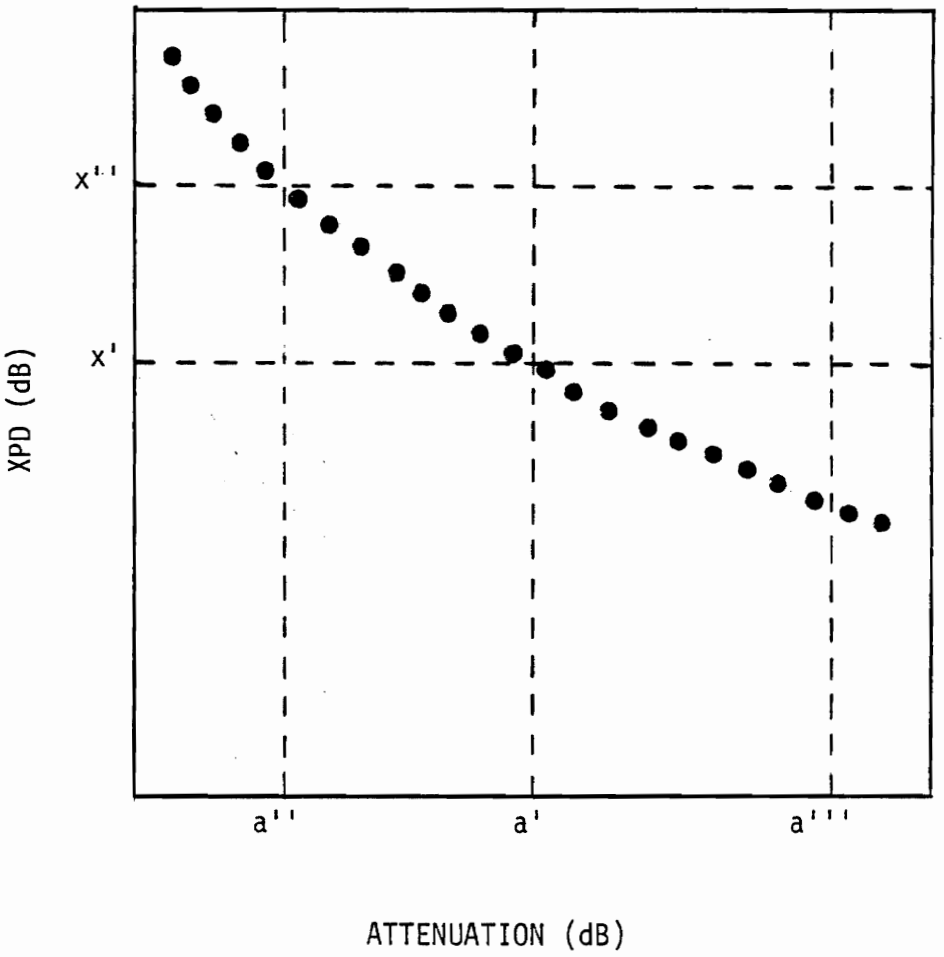

Figure 4-9. Hypothetical scatter plot of deterministic simultaneous XPD and attenuation data.

x'). Thus, for a fixed a we have the cumulative XPD lessance distribution for values of $X > x'$ and the cumulative attenuation exceedance at a' for values of $X \leq x'$

Several display formats may be considered for the representation of the joint distribution. The method used by Cox [1981] to display the distribution of (4.4-1) is a plot of time ($A > a$ or $X < x$) in minutes versus attenuation. The ordinate values of time are scaled logarithmically. A family of curves are generated for fixed values of X. The purely deterministic relationship between XPD and A would result in a set of curves like those in Figure 4-10 when displayed in the format prescribed by Cox. The curve bounding the constant XPD contours is the cumulative attenuation exceedance curve and the vertical spacing for the constant XPD contours is described by the cumulative XPD lessance distribution. A nondeterministic relationship between XPD and A would yield constant XPD contours which curve upward to meet the cumulative attenuation exceedance boundary at a higher time value than the deterministic relationship. The joint statistics provide additional information about the occurrence of the (A, X) pairs that is not observable with the marginal statistics. This additional information is given by the deviation in the constant XPD contours from that which is described by the marginal distributions (i.e., the attenuation exceedance and XPD lessance boundaries).

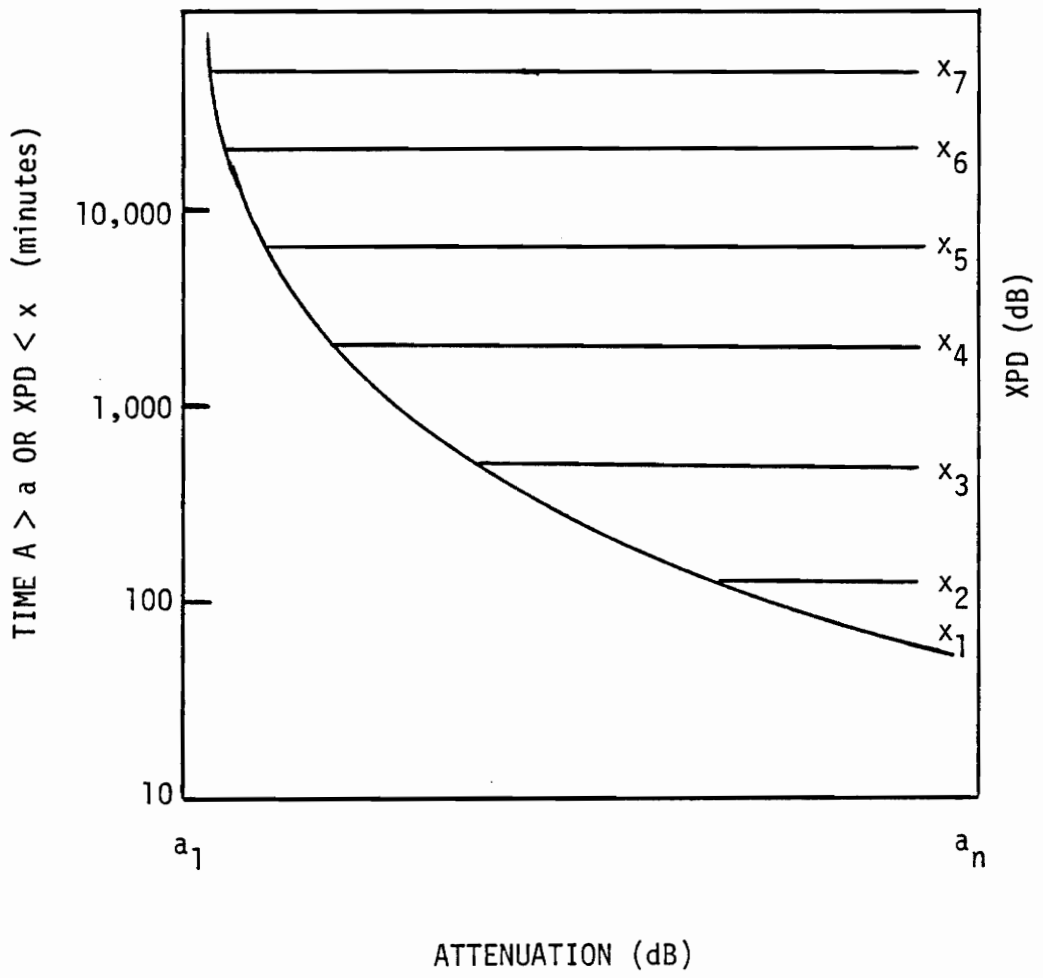

Figure 4-10. Characteristic joint distribution for a deterministic XPD vs A relationship using the display format of Cox [1981].

An alternative display format is to present contours of P(A > a or X < x) on a plot of XPD vs A. A characteristic plot of this type is shown in Figure 4-11 for a deterministic relationship between XPD and A. The contour bends (or "knees") represent the locus of equal probability values of XPD and A and may be determined from the marginal distributions. Also, this equal probability relationship overlays the deterministic functional relationship between XPD and A. When the XPD vs A relationship is not deterministic the sharp bends become rounded and take on a curvature dependent upon the density of the data observations.

4.4.2 The AND Conditional Joint Distribution

An alternate definition for the joint statistics was suggested by Thirlwell and Howell [1982] which is also derived from a two-dimensional density function of XPD and attenuation. Their technique incorporates a density function n(A,X) based on the number of observations that the integerized values of the XPD (X) and attenuation (A) pair occurred. The joint distribution P(a,x) is determined by

$$P(a,\ x) = P(A > a,\ X < x) = \frac{\sum\limits_{\substack{A> a \\ X< x}} n(A,X)}{\sum\limits_{\substack{all \\ A,X}} n(A,X)} \qquad (4.4\text{-}3)$$

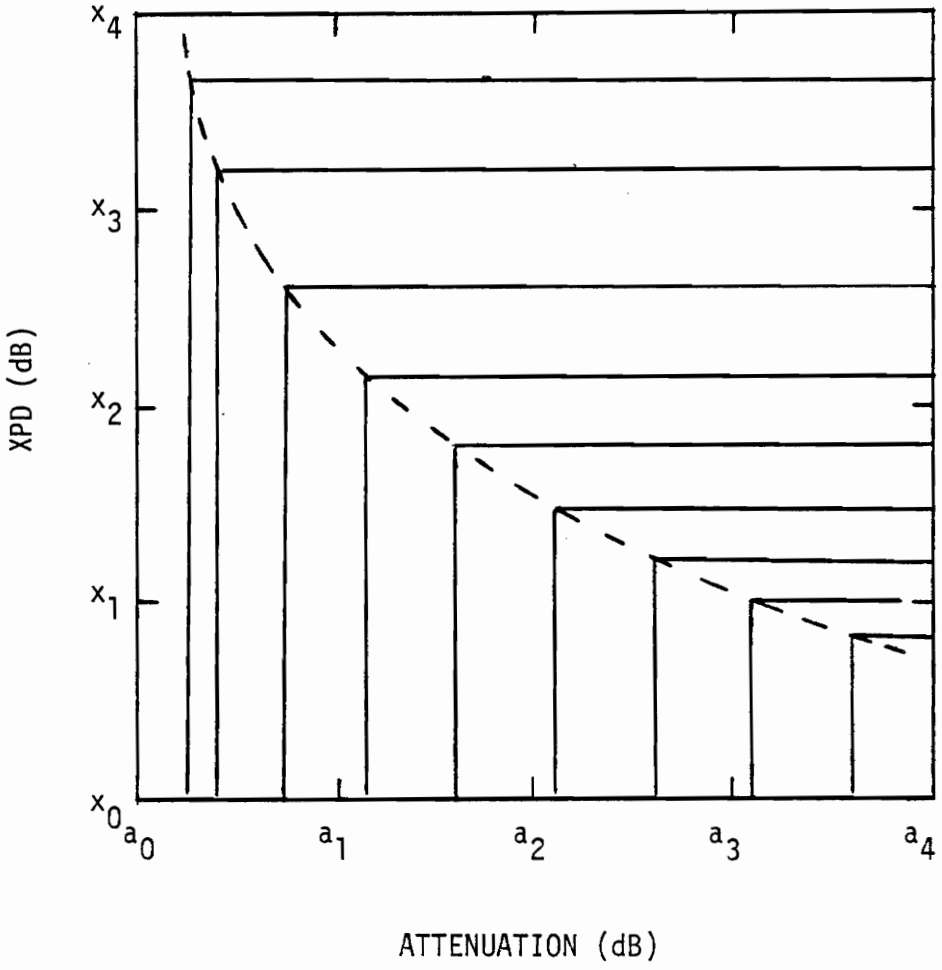

Figure 4-11. Characteristic joint distribution for a deterministic XPD vs A relationship. Contours of constant fraction of time that $A > a$ or $X < x$. Dashed line is the locus of equiprobable values (identical to the deterministic relationship).

The distribution given by (4.4-3) is defined as the fraction of time that A is greater than the value a and XPD is less than to the value x. The definition by Arnold et al., in (4.4-1) has the or condition in contrast to the and in (4.4-3).

The distribution may be illustrated by examining the hypothetical scatter plot of XPD and attenuation data in Figure 4-8. Consider the distribution at the point (a', x'). The numerator in (4.4-3) is the sum of all of the observations which are to the right of the vertical dashed line at a' and are below the horizontal dashed line at x'. The denominator is simply the total number of observations in the attenuation - XPD plane, therefore normalizing the two-dimensional distribution to a maximum value of unity.

The method chosen by Thirlwell and Howell to display the joint distribution is on a plot of XPD versus attenuation with contours of constant joint fraction of time P(a, x). This format is useful for several reasons that will be demonstrated in the following discussion.

Again referring to Figure 4-8, the joint distribution at the point (a', x''') is equal to the cumulative attenuation exceedance distribution at a' because all of the XPD observations are less than x''' for the values of attenuation

greater than a'. Therefore, along the top of the display format $P(A > a, X < x) = P(A > a)$ when the ordinate axis value x is greater than all of the observed values of (A,X) pairs for $A > a$. The result is straight vertical contours distributed horizontally according to the cumulative attenuation exceedance distribution entering from the top of the display until data points are encountered. Once data are encountered the contours deviate according to the density of the scatter data.

The joint distribution at the point (a', x'') is equal to the cumulative XPD lessance distribution at x'' because all of the attenuation observations are greater than a' for the values of XPD less than x''. Therefore, along the left-hand portion of the display format $P(A > a, X < x) = P(X < x)$ when the abscissa value a is less than all of the (A,X) pairs for XPD less than x. The result is straight horizontal contours distributed vertically according to the cumulative XPD lessance distribution entering from the vertical axis at $A = 0$ until data are encountered. This contour joins the contour described originating from the top of the display format.

Consider the joint distribution for a deterministic relationship between XPD and attenuation shown in Figure 4-9. The joint distribution P(a,x) is equal to the cumulative at-

tenuation exceedance distribution and also the cumulative XPD lessance distribution at the point (a', x'). This is the equal-probability point and the locus of these points forms the deterministic relationship between XPD and A. The value of the joint distribution for a fixed x' is the same for any attenuation value less than a'. Similarly, for a fixed value of a', the distribution is the same for any XPD value greater than x'. Therefore, we see that the joint distribution for a deterministic relationship between XPD and A yields straight line contours of constant fraction of time with the corners describing the equal probability values of XPD and A. This was first noted by Gaines and Bostian [1982]. A typical set of contours for a deterministic relationship is shown in Figure 4-12. A nondeterministic relationship between XPD and A yields contours which deviate from the straight contours defined by the equal probability points. This deviation is the additional information available with joint statistics over that using the marginal statistics.

The joint distribution P(a,x) may be defined in a manner similar to (4.4-2) as the fraction of time that attenuation is greater than or equal to the value a and XPD less than or equal to the value x. Under these conditions (4.4-3) is written

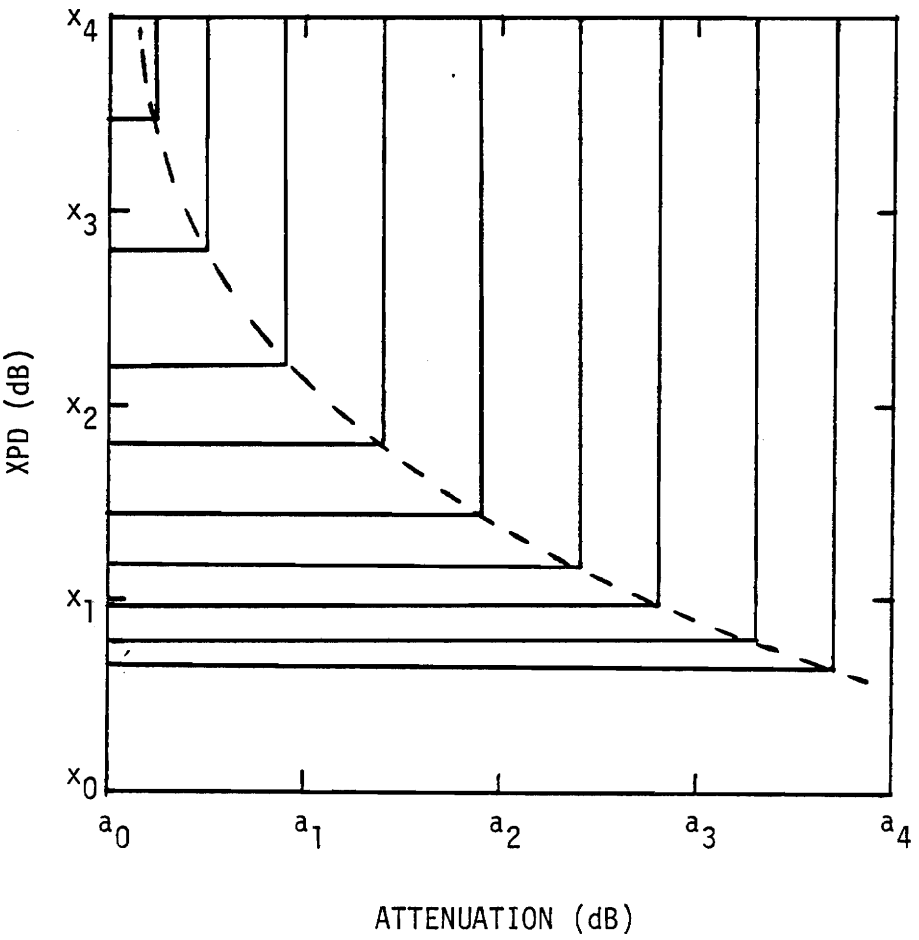

Figure 4-12. Characteristic joint distribution for a deterministic XPD vs A relationship. Contours of constant fraction of time that $A > a$ and $X < x$. Dashed line is the locus of equiprobable values (identical to the deterministic relationship).

$$P(a,\ x) = P(A \geq a,\ X \leq x) = \frac{\sum\limits_{\substack{A \geq a \\ X \leq x}} n(A,X)}{\sum\limits_{\substack{all \\ A,X}} n(A,X)} \qquad (4.4\text{-}4)$$

There is no difference between (4.4-3) and (4.4-4) for a continuous density function. The differences for a discrete density function were discussed in Section 4.4.1.

4.4.3 The Effect of Scattered XPD and A Data Pairs

In Section 4.2 it was shown that uncorrelated activity between attenuation and XPD due to ice depolarization in the absence of significant attenuation causes a shift in the entire XPD lessance distribution. When the XPD vs A relationship is generated by matching equal probable pairs of XPD and A data, the shift affected the complete relationship. The joint distribution defined using (4.4-1) is susceptable to the same problems because of the or condition between the attenuation exceedance and XPD lessance. Any significant ice depolarization in the absence of significant attenuation causes a shift in the joint distribution for all values of attenuation when the value of XPD being considered is greater than that recorded for the ice depolarization. Consider a given data set with and without the significant uncorrelated activity due to ice depolarization for low attenuation

values. When a given (XPD, A) data pair is examined for A greater than the values of attenuation affected by the ice data, it is determined that the joint distribution has a larger fraction of time value when the ice data is included than without. The or condition in (4.4-1) permits data occurring for attenuations less than the value at the point being considered to influence the distribution. This characteristic would not be a problem if the XPD vs A relationship was purely deterministic, in which case the marginal statistics would provide all the information. Therefore, the definitions in (4.4-1) and (4.4-2) are not recommended to represent the joint statistics of attenuation and XPD data.

The second definition for the joint statistics given in (4.4-3) or (4.4-4) has the and condition between the attenuation exceedance and XPD lessance. This definition permits only the data greater than (or equal) to a fixed value of attenuation and less than (or equal) to a fixed value of XPD to be used to calculate the joint distribution. Therefore, ice depolarization data for low attenuation values affects the joint distribution only for those values of attenuation for which the depolarization occurred. This characteristic represents the simultaneous data pair in the manner in which it occurred. A hypothetical joint distribution contour of

constant fraction of time is shown in Figure 4-13 with and without the influence of ice depolarization data at low values of attenuation. The effect on the probability relationship is also shown.

The definitions in (4.4-3) or (4.4-4) have direct significance for system design of a dual polarized communication link. The designer is interested in information pertaining to the behavior of attenuation and XPD simultaneously. The attenuation exceedance and channel discrimination degradation play a role together to cause system failure for a fixed C/N. Joint statistics that do not reflect the simultaneous behavior of XPD and A may be misleading and predict insufficient or excessive margin required for a given reliability. The margin required for a digital PSK system is discussed in Section 5.7.

4.4.4 Comparison of Joint Distribution Data

The joint statistics defined by (4.4-1) and (4.4-3) were calcualted for the same data set to provide a direct comparison of the techniques. The data used were collected at Crawford Hill, N.J. for the period from May 19,1977 to May 18, 1978 of the COMSTAR experiment at 19.04 GHz [Cox, Arnold, 1982]. The polarization was linear at 21° from vertical and the elevation angle was 38.6° at the site. These

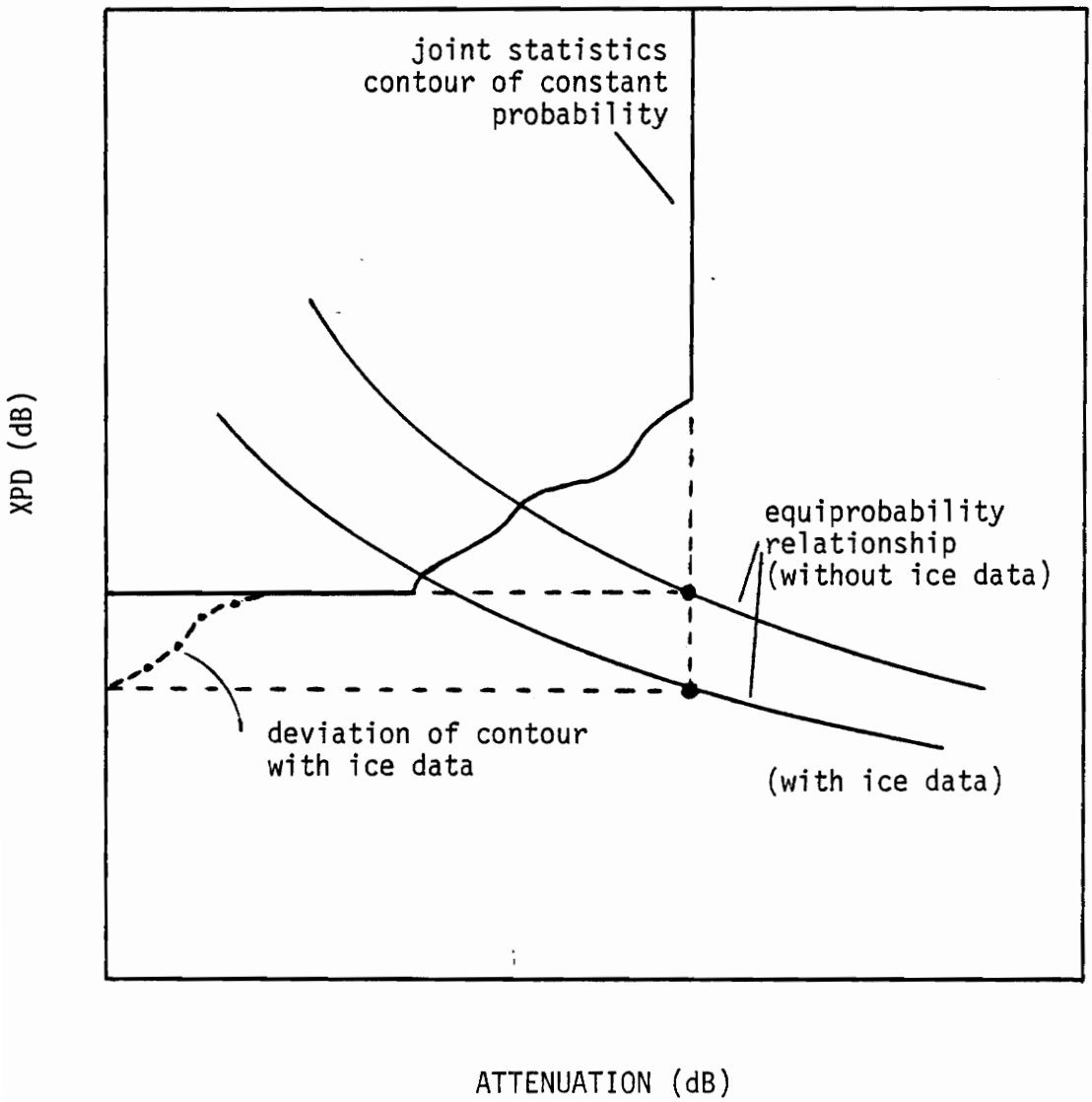

Figure 4-13. Typical joint statistics relationship for a fixed joint probability value with and without ice depolarization data.

data were presented by Cox and Arnold using the joint statistics of the form (4.4-1) in the display format of Figure 4-10. In this comparison, the display format was chosen to be the XPD vs A plot with contours of constant joint percentage of time. The results are shown in Figures 4-14 and 4-15 for the joint statistics using (4.4-1) and (4.4-3), respectively. The number associated with each contour corresponds to the percentage of time of one year or the time in minutes found in Table 4-2 that the joint condition occurred.

The marginal statistics may be determined from the joint statistics for both definitions from the joint statistics for both definitions. In Figure 4-14 the cumulative attenuation exceedance distribution is found along the horizontal axis at XPD = 0 dB, and the cumulative XPD lessance distribution is found along the vertical axis at A = 40 dB. The equiprobable values of XPD and A (usually determined from the marginal statistics) may be determined by constructing straight lines perpendicular to these axis for a fixed joint percentage of time. The intersection of the constructed contours defines the (A,X) pair satisfying the equal probability condition. Similarly in Figure 4-15, the cumulative attenuation distribution is found along the horizontal axis at XPD = 40 dB and the cumulative XPD lessance distribution

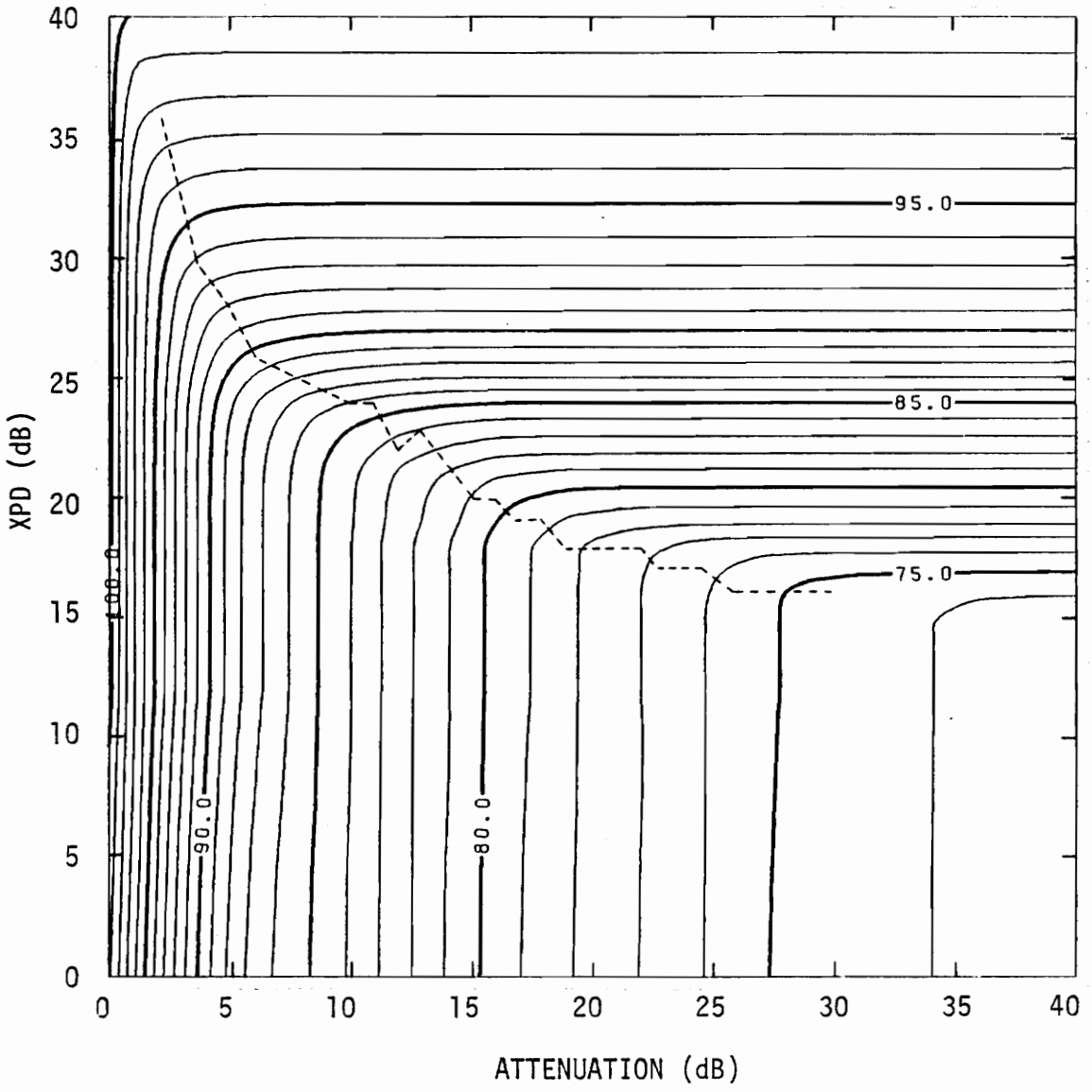

Figure 4-14. Joint statistics (OR condition) measured at Crawford Hill, NJ, at an elevation angle of 38.6° using the COMSTAR D2 satellite linearly polarized (τ = 69°), 19.04 GHz beacon for the time period May 18,1977 - May 18,1978.

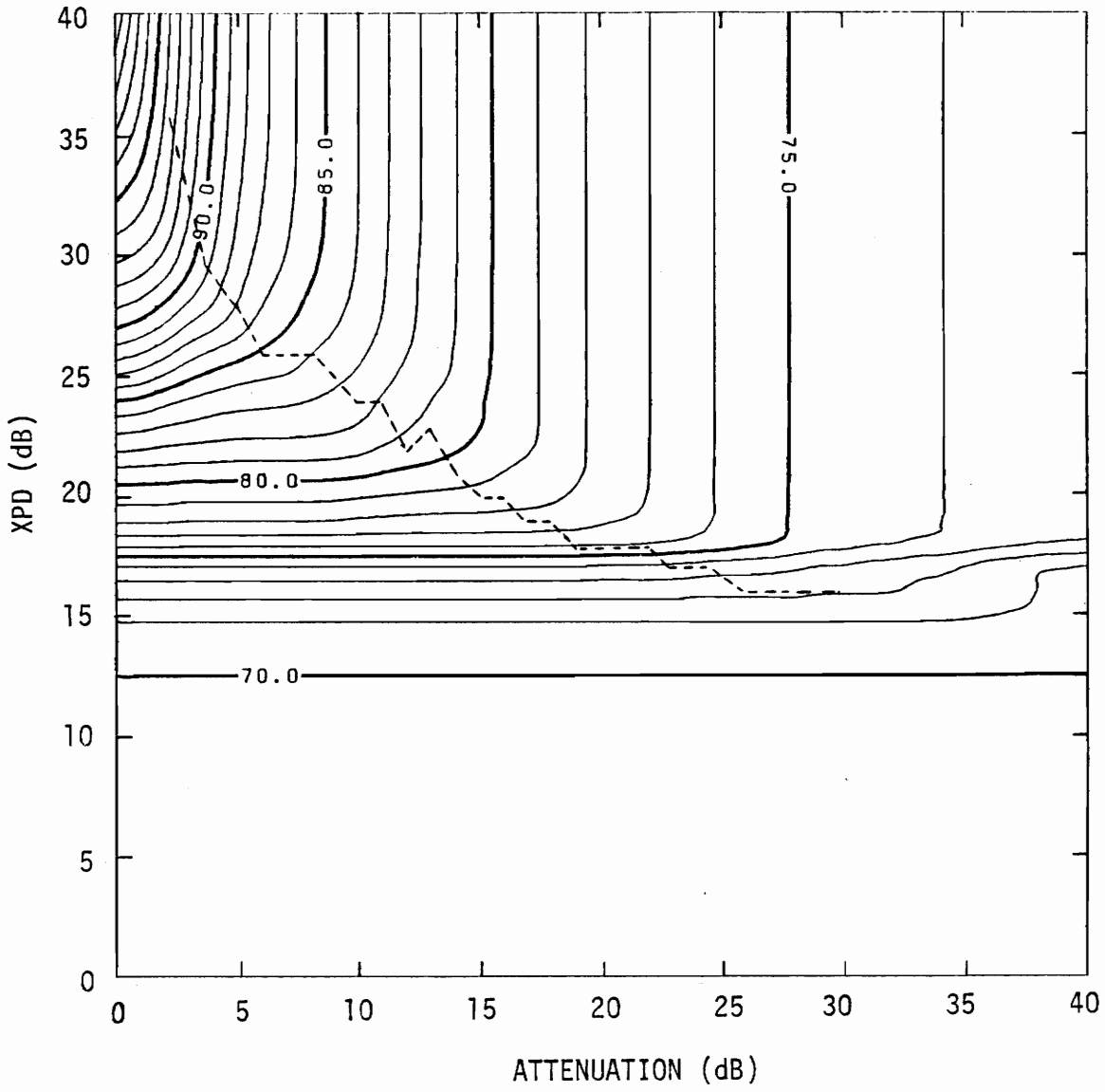

Figure 4-15. Joint statistics (AND condition) measured at Crawford Hill, NJ, at an elevation angle of 38.6° using the COMSTAR D2 satellite linearly polarized (τ = 69°), 19.04 GHz beacon for the time period May 18,1977 - May 18,1978.

Table 4-2

Contour Values for Contours in Figures 4-14 and 15

Contour Number	Percent Time	Minutes Per Year
70	0.0019	10.0
71	0.0024	12.6
72	0.0030	15.8
73	0.0038	20.0
74	0.0048	25.1
75	0.0060	31.6
76	0.0076	39.8
77	0.0095	50.1
78	0.0120	63.1
79	0.0151	79.4
80	0.0190	100.0
81	0.0240	126.0
82	0.0302	159.0
83	0.0380	200.0
84	0.0478	251.0
85	0.0602	316.0
86	0.0757	398.0
87	0.0954	501.0
88	0.1200	631.0
89	0.1511	794.0
90	0.1903	1000.0
91	0.2395	1259.0
92	0.3015	1585.0
93	0.3796	1995.0
94	0.4779	2512.0
95	0.6017	3162.0
96	0.7574	3981.0
97	0.9536	5012.0
98	1.2005	6310.0
99	1.5113	7943.0

is found along the vertical axis at A = 0 dB. Both definitions yield the same locus of equal probable values of XPD and A that would be found on the basis of marginal statistics alone.

The joint statistics defined by (4.4-3) were calculated for the one year period of SIRIO data presented in Section 4.2. These are shown in Figure 4-16 for both sites. The associated contour values are given in Table 4-3. The distortive effect of ice depolarization on the contours occurring at the low values of attenuation is easily observed as discussed in Section 4.4.3.

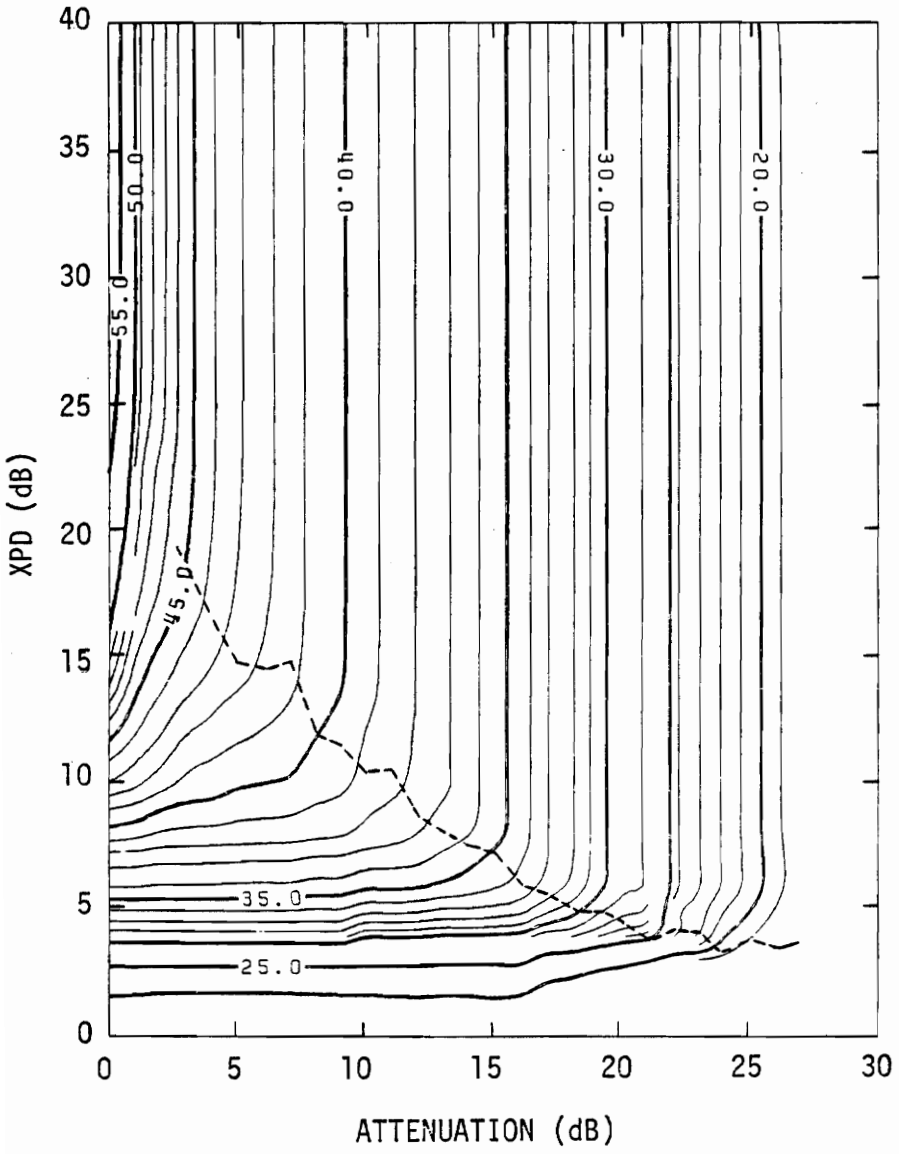

Figure 4-16. Joint statistics measured at Blacksburg,VA, at an elevation angle of 10.7° using the SIRIO satellite circularly polarized, 11.6 GHz beacon for the time period July 15,1980 - June 30,1981.

(a) Main site

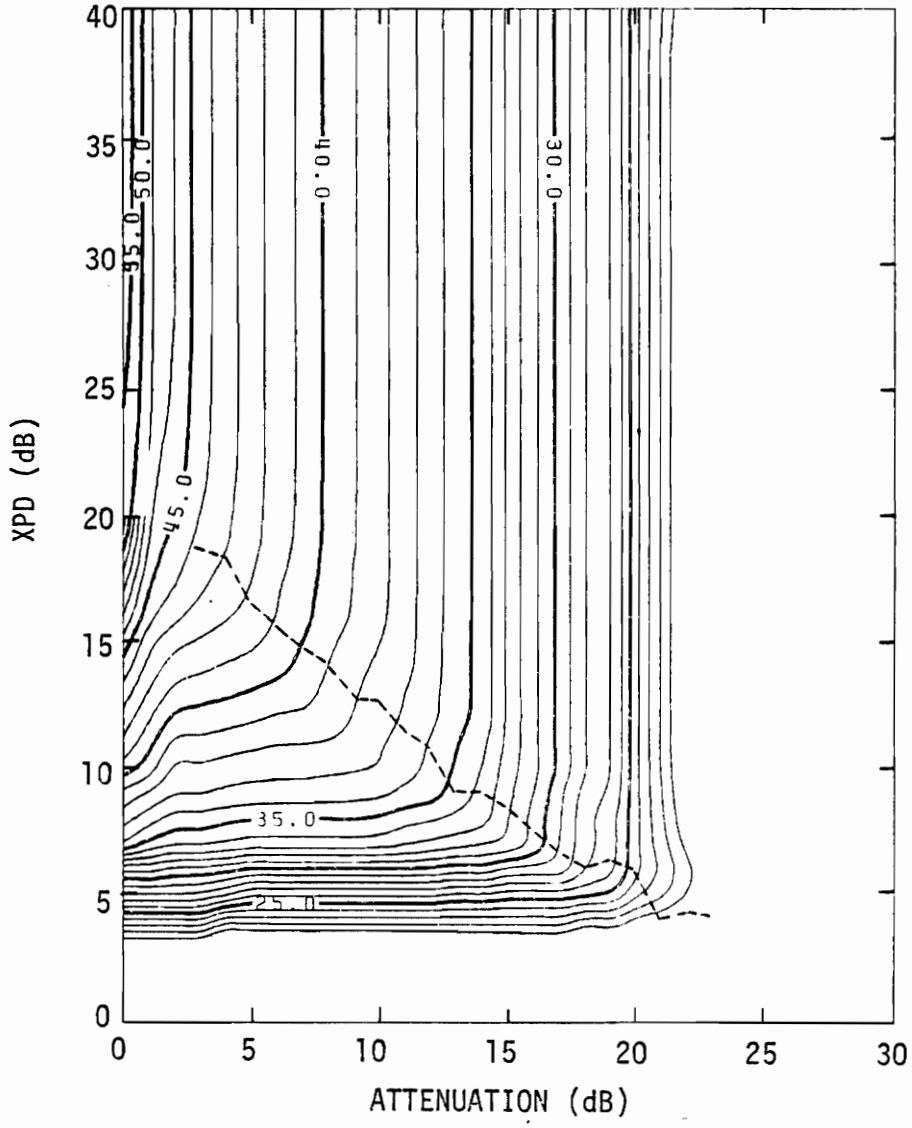

Figure 4-16. (b) Remote site

Table 4-3a

Contour Values for Contours in Figure 4-16a

Contour Number	Percent Time	Minutes Per Year
19	0.00030	1.5
20	0.00038	2.0
21	0.00048	2.5
22	0.00060	3.2
23	0.00076	4.0
24	0.00095	5.0
25	0.00120	6.3
26	0.00151	7.9
27	0.00190	10.0
28	0.00239	12.6
29	0.00301	15.8
30	0.00379	19.9
31	0.00477	25.1
32	0.00600	31.5
33	0.00756	39.7
34	0.00950	49.9
35	0.01200	63.1
36	0.01510	79.4
37	0.01900	99.9
38	0.02390	126.0
39	0.03010	158.0
40	0.03790	199.0
41	0.04770	251.0
42	0.06000	315.0
43	0.07560	397.0
44	0.09510	500.0
45	0.11980	630.0
46	0.15100	794.0
47	0.19000	999.0
48	0.23900	1256.0
49	0.30000	1577.0
50	0.37900	1992.0
55	1.19800	6297.0

Table 4-3b

Contour Values for Contours in Figure 4-16b

Contour Number	Percent Time	Minutes Per Year
21	0.00042	2.2
22	0.00053	2.8
23	0.00067	3.5
24	0.00085	4.5
25	0.00107	5.6
26	0.00134	7.0
27	0.00169	8.9
28	0.00213	11.2
29	0.00268	14.1
30	0.00337	17.7
31	0.00424	22.3
32	0.00530	27.9
33	0.00670	35.2
34	0.00850	44.7
35	0.01070	56.2
36	0.01340	70.4
37	0.01690	88.8
38	0.02130	112.0
39	0.02680	141.0
40	0.03370	177.0
41	0.04240	223.0
42	0.05340	281.0
43	0.06720	353.0
44	0.08460	445.0
45	0.10650	560.0
46	0.13410	705.0
47	0.16900	888.0
48	0.21300	1120.0
49	0.26800	1409.0
50	0.33700	1771.0
55	1.06500	1598.0

The dashed curve in Figures 4-14, 15, and 16 is the median and mean XPD vs A relationship. It is apparent that the mean (or median) relationship follows the knees in the contours. We will show in Section 5.7 that the knee of the contours, when using the definition in (4.4-3) is the important region of the joint statistics for calculation of C/N margin. The close relationship between the mean XPD vs A curve and the contour knees will permit use of the proposed predictive technique established in Section 5.7 to be used.

Chapter V

INVESTIGATION OF THE XPD VS A RELATIONSHIP

In this chapter we bring together the theoretical methods of Chapter 3 and the available measurement results from Chapter 4 in order to build a simple XPD vs A relationship.

5.1 EXAMINATION OF THE SENSITIVITY OF XPD VS A TO RAINRATE DISTRIBUTION SHAPE AND EXTENT

Before a detailed examination of the parameter dependence of the XPD vs A relationship, we can eliminate one major parameter from the study - the rainrate distribution. We will show that although attenuation and XPD alone are strongly dependent on the rainrate distribution, XPD as a function of A is not. This allows us to use a reasonable rainrate distribution and to exclude parameters associated with the rainrate distribution (such as path length, and form factors for a spatial profile).

XPD variation with path length and rainrate spatial profile

The path length and rainrate distribution profile along the propagation path play a dominant role in the predictive modeling of total path atttenuation and of XPD when they are calculated as a function of point rainrate. However, the dependence of A and XPD on path length is similar in the

frequency range from 10 to 30 GHz. Because the behavior is similar for both A and XPD, the XPD vs A relationship is relatively insensitive to path length.

This point is illustrated with a uniform rainrate path profile. Predictions of XPD vs A are calculated using the multiple scattering model for 6, 11, 20 and 30 GHz for different path lengths. The results of this study are shown in Figures 5-1 and 5-2 for 6 and 11 GHz, respectively. At 6 GHz there is a significant difference in the relationship for the three path lengths shown (Figure 5-1). This effect is due primarily to the differential phase-shift mechanism becoming the dominant depolarization source. As frequency increases, the differential phase-shift effect decreases and different attenuation becomes dominant. This is apparent at 11 GHz (Figure 5-2) where there is very little difference in the relationship for the different path lengths. As frequency increases beyond 11 GHz the difference becomes even smaller. The XPD vs A relationship is essentially independent of path length at 20 and 30 GHz.

Chu [1974] examined the XPD vs A relationship for sensitivity to rainrate. He calculated the XPD value corresponding to the fixed value A = 20 dB for $11 \leq f \leq 100$ GHz and rainrates of 5, 25 and 100 mm/hr. He apparently varied the path lengths with a uniform rainrate distribution to obtain

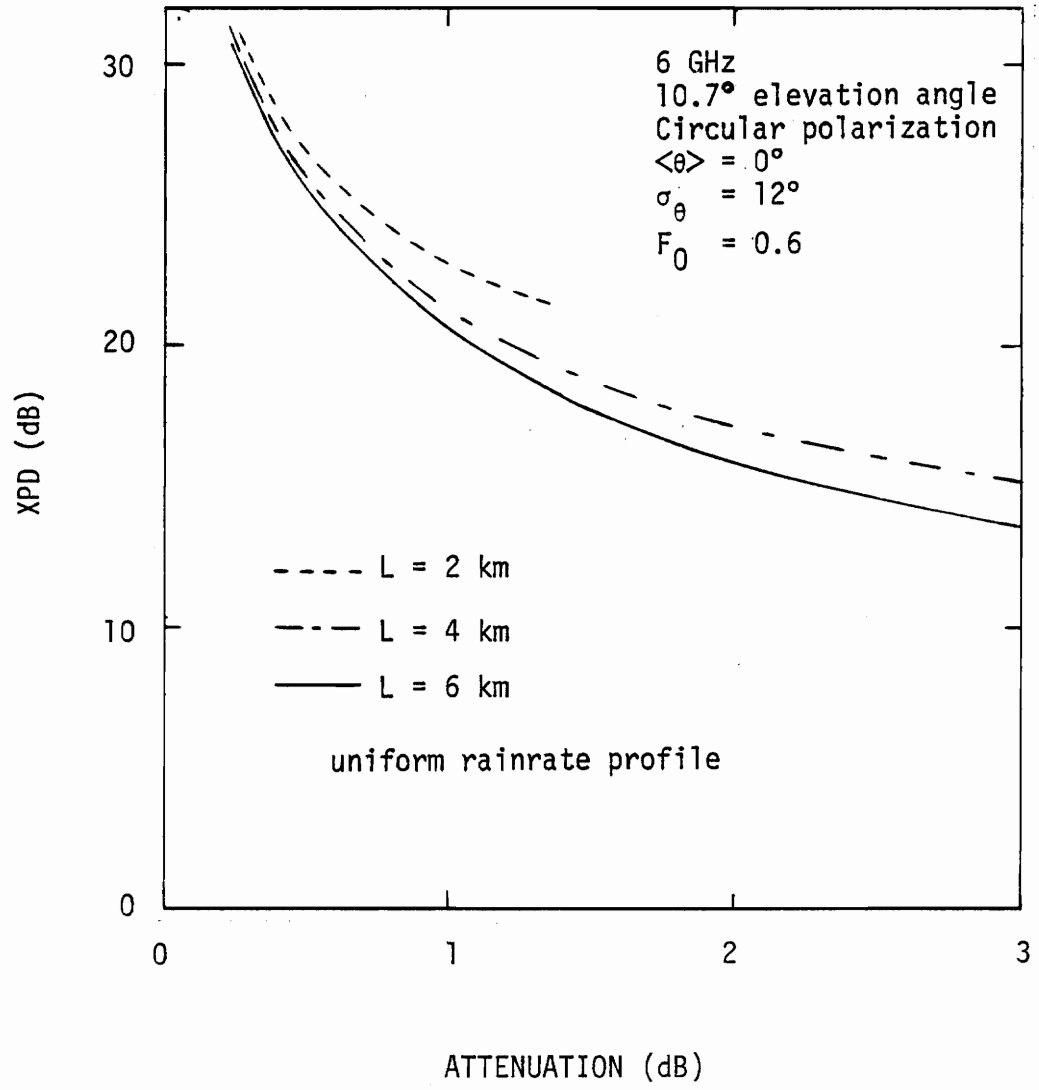

Figure 5-1. Predicted XPD vs A relationship at 6 GHz for a uniform rainrate profile with path length as a parameter.

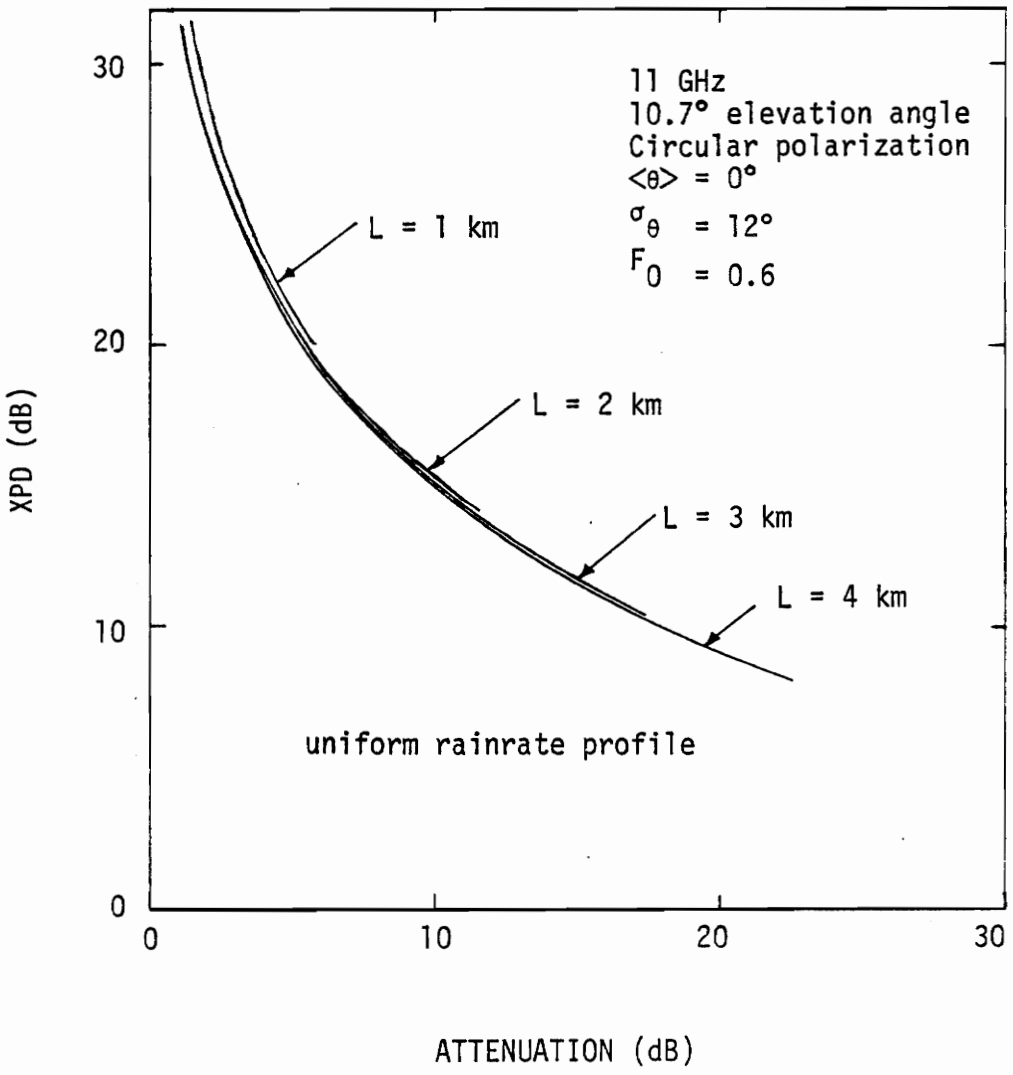

Figure 5-2. Predicted XPD vs A relationship at 11 GHz for a uniform rainrate profile with path length as a parameter.

the fade of 20 dB for a fixed rainrate, but the path lengths used were not specified. Nevertheless, his results suggest that XPD vs A is relatively insensitive to rainrate in the 10 to 100 GHz frequency range. This conclusion that Chu reached based on a fixed attenuation level calculation would assume also a path length independence.

We conducted a study of the effect of the rainrate spatial profile shape or the XPD vs A relationship using the exponential rainrate distribution and the uniform rainrate distribution in the multiple scattering model. Predictions were calculated using the exponential rainrate distribution and the uniform path profile with the same path length L and average rainrate [Stutzman and Dishman, 1982]

$$R_{ave} = \frac{1}{D} \int_0^D R(z)\, dz$$

$$= \begin{cases} R_o & R_o \leq 10 \frac{mm}{hr} \\ R_o \dfrac{1 - e^{-\gamma \ln [R_o/10] D}}{\gamma \ln [R_o/10] D} & R_o > 10 \frac{mm}{hr} \end{cases} \qquad (5.1\text{-}1)$$

where $D = L\cos\varepsilon$ and R_o is point rainrate.

This investigation revealed that the XPD vs A relationship is independent of the shape of the spatial rainrate profile. In other words, the XPD vs A relationship is insensitive to the details of how rain is distributed along a path. Note that for a fixed point rainrate, the XPD and A values calculated using the exponential distribution and those values for the uniform rainrate profile with the same point rainrate are different. Calculations of this type were performed at the frequencies of 11, 14, 20 and 30 GHz; the above conclusion was found in each case.

XPD variation with the parameter γ

The effective rain profile used in the multiple scattering model contains a single constant γ. In the Simple Attenuation Model (SAM) of Stutzman and Dishman [1982] this constant was determined to be 1/22 by comparing predicted results to measured attenuation data. The constant $\gamma = 1/22$ used in the SAM model, however, is not necessarily the optimal value to use in the multiple scattering model. The two models are different in several respects. The SAM model is based on the path integral concept of computing the total attenuation due to rain by integrating the specific attenuation over the entire path. The multiple scattering model, on the other hand, is based on the more rigorous methods described in Section 3.1. SAM assumes 100% spherical rain-

drops where the multiple scattering model includes both spherical and oblate raindrops. In addition to the drop shape differences, the forward scattering coefficients are at 0 C in SAM and 20 C in the multiple scattering program. These differences prompted an examination of the variation of the predicted XPD (using the multiple scattering program) as a function of the constant parameter γ.

Predictions of XPD and A were calculated as functions of the rainrate R_o at 11, 14 and 30 GHz for values γ = 1/17, 1/22, and 1/27 at each frequency. As expected, it was found that the calculated values of A increased as γ was decreased. In addition, there was a corresponding decrease in XPD which left the XPD vs A relationship unchanged. This was verified by plotting the XPD vs A relationship and performing curve fits on the predicted values as is discussed in Section 5.2. The conclusion drawn from this investigation is that the XPD vs A relationship is insensitive to the constant γ. However, if accurate attenuation predictions are to be made using the multiple scattering model a study would be necessary to determine the appropriate shape factor and γ combination. As a secondary conclusion, we can now say that although the γ value of 1/22 was developed for an attenuation-only application using medium parameters different from those in the multiple scattering model, there is no impact on the XPD vs A calculations.

5.2 THE BASIC XPD = U - V LOG A RELATIONSHIP

From the several depolarization experiments it has been found that rain induced depolarization is highly correlated with attenuation along the path. There is little purpose in attempting to relate depolarization to point rainrate [Watson, 1981]. It is also noted that if ice occurs along the propagation path it will create depolarization with an accompanying attenuation much lower than that which rain would generate at the same XPD level. Ice effects can be handled separately (see Chapter 6).

In Chapter 4 several methods were examined for presenting the XPD vs A relationship. If "average" behavior is desired median or mean values of XPD show a strong correlation to A for rain dominated data. This average XPD vs A relationship has been found to be well described by (see Section 2.3, Dissanayake et al., [1980], and Ippolito [1981]).

$$XPD = U - V \log A \tag{5.2-1}$$

where all quantities are in dB and log is base 10. U and V are functions of several parameters. In Section 2.2 the parameter dependences of XPD were identified as given in Table 2.2-1; thus

$$U = U(\varepsilon, f, \delta, \sigma, F_o) \tag{5.2-2a}$$

$$V = V(\varepsilon, f, \delta, \sigma, F_o) \tag{5.2-2b}$$

Coefficients U and V for (5.2-1) may be computed from (XPD, A) data pairs using a least squares error regression analysis for the equation (see Appendix B). Regression analysis weights the curve fit so the accuracy is greatest at the lower values of attenuation where there are more observations by experiment. The preferred technique is an equal weighting of all values of A using the mean or median value of XPD.

The technique of using experimental data alone has some obvious shortcomings. It is not feasible to construct the number of experiments necessary to accumulate a data base sufficient to extract the parameter variations. Therefore, it is necessary to employ theoretical modeling techniques (in addition to experiments) in order to gain the necessary insight to be able to estimate XPD reliably for a variety of location conditions. The rain parameters allow adjustments in the model predictions to obtain agreement with experimental data.

The multiple scattering model has the capability of predicting XPD as a function of A for a variety of conditions. The model in its rigorous form is unattractive for practical use because of the requirement for scattering coefficients for a variety of conditions and the access to a digital com-

puter. However, the multiple scattering model can be used to extract the parameter variations from which functional forms can be found to approximate the U and V functions in (5.2-1). We shall refer to this as the simple model (SIM). This extraction process is described in the following section.

5.3 DETERMINATION OF PARAMETER VARIATIONS

To characterize the functional relationship between predicted values of XPD and A described by (5.2-1) the least squares error regression analysis (Appendix B) was incorporated into the multiple scattering program. This routine computes a pair of constant coefficients U and V from the predictions corresponding to a specific set of program input parameters. In addition, a figure of merit of the fit called the coefficient of determination, r^2, is evaluated. The coefficients U and V can then be studied for a variety of input parameter variations.

Frequency Variation

At this stage a preliminary selection of appropriate rain parameters was necessary. Examination of meteorological research (photographs by Jones[1959]) indicate that rain drop shapes as viewed in one direction can be divided into 60% oblate spheroidal and 40% spherical. Based on this and oth-

er research discussed by Stutzman [1980] the following raindrop parameters were chosen:

$$\langle\theta\rangle = 0^\circ \qquad \sigma_\theta = 12^\circ \qquad F_o = 0.60$$

A series of predictions were computed and compared to measured data in order to validate the selection of the rain parameters about which the sensitivity studies were to be made. Preliminary comparisons between multiple scattering model calculations using these values and measured data showed good agreement. More detailed comparisons to data in Section 5.5 will reveal that minor adjustments in these values will improve the fit to data.

In addition to the rain prameters a set of location parameters were chosen as a standard. Since the frequency f was limited to the available single raindrop forward scattering coefficients at 4, 6, 11, 14, 20 and 30 GHz a decision was made to execute the parameter studies at all the above frequencies. The elevation angle of the slant path was taken to be 45° when all other parameter variations were exercised. The polarization of the transmit and receive antennas for the study was limited to ideal linear and circular polarizations. The polarization of the transmit and receive antennas was taken to be circular during tests of all other parameters.

The frequency variation of XPD for fixed rainrates was investigated using the standard parameters described above. The results of this study are shown in Figure 5-3. The results using the exponential rainrate profile are similar (see Figure 3-1). The dashed line in Figure 5-3 represents the contour of predicted A values of 35 dB. It should be noted that the XPD values as a function of rainrate in Figure 5-3 have not been compared to data. The prediction of XPD and/or A as a function of rainrate in this study has not been fine tuned via the the parameter γ (taken as 1/22) in the exponential rainrate profile as was done in the SAM model [Dishman and Stutzman, 1982] in accordance with experimental data. However, the frequency variation is accurate in addition to the XPD vs A relationship which was proven in as series of tests to be insensitive to the value of γ.

A set of curve fits of the form

$$XPD = a_1 \log(f) + a_o \qquad (5.3\text{-}1)$$

were performed on the predicted data for rainrates from 15 to 100 mm/hr. All fits had an r^2 greater than 0.99 for values of A < 40 dB. The constant coefficient a_1 was determined to be between the value -20 to -21 with the lower value -20 occurring for higher rainrates and the value -21 at the low rainrates. The average value of -20.5 was found at

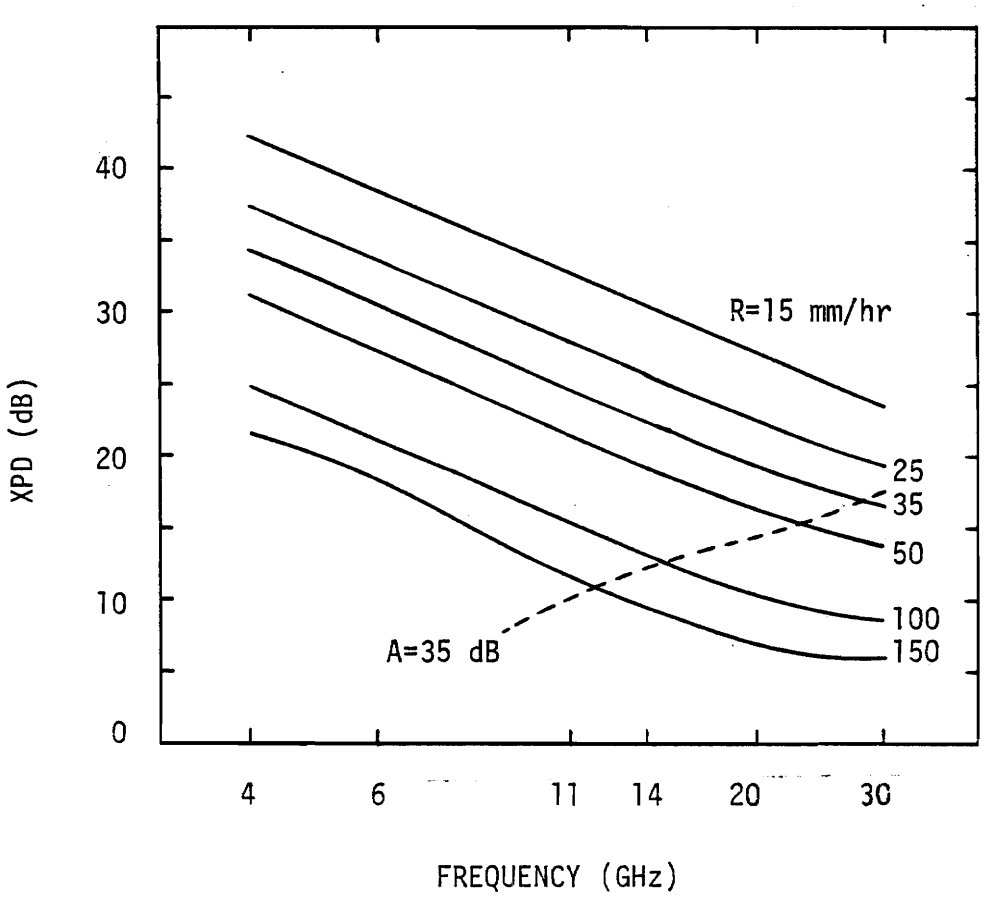

Figure 5-3. Frequency variation of XPD with rainrate as a parameter.

about 50 mm/hr. Using this result we may write the relationship for the frequency scaling of XPD for fixed rainrates as

$$XPD_2 - XPD_1 = -\beta \log\left(\frac{f_2}{f_1}\right) \qquad (5.3\text{-}2)$$

where β may be nominally taken as 20.5. The above result agrees with that found by curve fitting the data of Oguchi [1981b] for a uniform rainrate profile and the same frequency range shown in Figure 3-1. From the Oguchi data, β varies from 20.0 to 20.6 with 20.0 determined at 50 mm/hr with all $r^2 > 0.99$. For frequencies greater than 30 GHz the slope of the curves by Oguchi [1981b] begin to level off. Cox [1981] used the results of Chu to get an approximate value of 20. In the preliminary investigations it was determined that the equation of the form (5.2-1) relating XPD to A would have to be limited to modeling the behavior for frequencies from 10 to 30 GHz. Sufficient attenuation at 4 and 6 GHz does not occur for reasonable rainrates to warrant development of a relationship for the estimation of XPD as a function of attenuation. If modeling in the 4/6 GHz band were to be pursued, XPD should be related to rainrate. The focus here shall remain on characterizing XPD as a function of the attenuation.

Several frequency characteristics of XPD should be noted between 10 and 30 GHz. It was illustrated in Figure 5-3 that the amount of depolarization for a fixed rainrate increases as frequency increases. However we will show that depolarization for a fixed attenuation decreases as frequency increases. This is a significant effect in system design and will be addressed in Section 5.7.

The coefficients U and V were computed from the multiple scattering model prediction for XPD and A for rainrates from 5 to 150 mm/hr. The results of the fits for the standard input parameters are given in Table 5-1. The V values show a small variation as a function of f. It would be attractive for modeling purposes to set V(f) = constant. In order to minimize the errors associated with having a constant V, the decision was made to adjust the value of U so that the adjusted coefficients gave the same value of XPD for A = 10 dB. A study was conducted to determine the value of V that would yield the smallest maximum error between the adjusted and the original fitted curves for the four frequencies. Between the coefficients V = 18, 19, or 20 the constant V = 19 gave a maximum error of XPD = 0.5 dB, which occurs at A = 3 dB for f = 11 GHz. The adjusted coefficients U' and V' are shown in Table 5-1.

Table 5-1

Variation of U and V as a Function of Frequency for the Standard Parameters

Frequency (GHz)	U(f)	V(f)	r^2	U'(f)	V'(f)
11	38.06	18.02	.9996	39.04	19.0
14	42.86	19.82	.9995	42.04	19.0
20	45.01	19.87	.9998	44.14	19.0
30	46.76	18.87	.9998	46.89	19.0

The A values for the 20 and 30 GHz predictions are beyond reasonable levels for the higher rainrates. The curve fits were for rainrates of 5 to 150 mm/hr. If rainrates of 5 to 100 mm/hr are used the r^2 is greater and both U and V have a slightly smaller value. The adjusted U' for $V' = 19$, however, is the same as those shown above to within 0.01.

When the other parameter variations were examined, including the frequency variation with other input parameters, it was found that the coefficient V remained relatively constant. The decision to fix V=19 and adjust U accordingly for all the variations was made to simplify the extractions. The amount of error induced by doing this is believed to be minimal.

The coefficients for $U'(f)$ were modeled by performing a curve fit of the form

$$U'(f) = a_1 \log(f) + a_0 \qquad (5.3\text{-}3)$$

The form of this fit is revealed by plotting $U'(f)$ vs f on a semi-log format as shown in Figure 5-4. The coefficient a_1 is 17.27 with $r^2 = 0.977$. It is important to note that the value found for a_1 is independent of the fixed V' value selected. The coefficient a_o is independent of frequency but is dependent upon the other input parameters. It then follows from (5.3-3) that the change in U' for different frequencies (f_2 and f_1) is

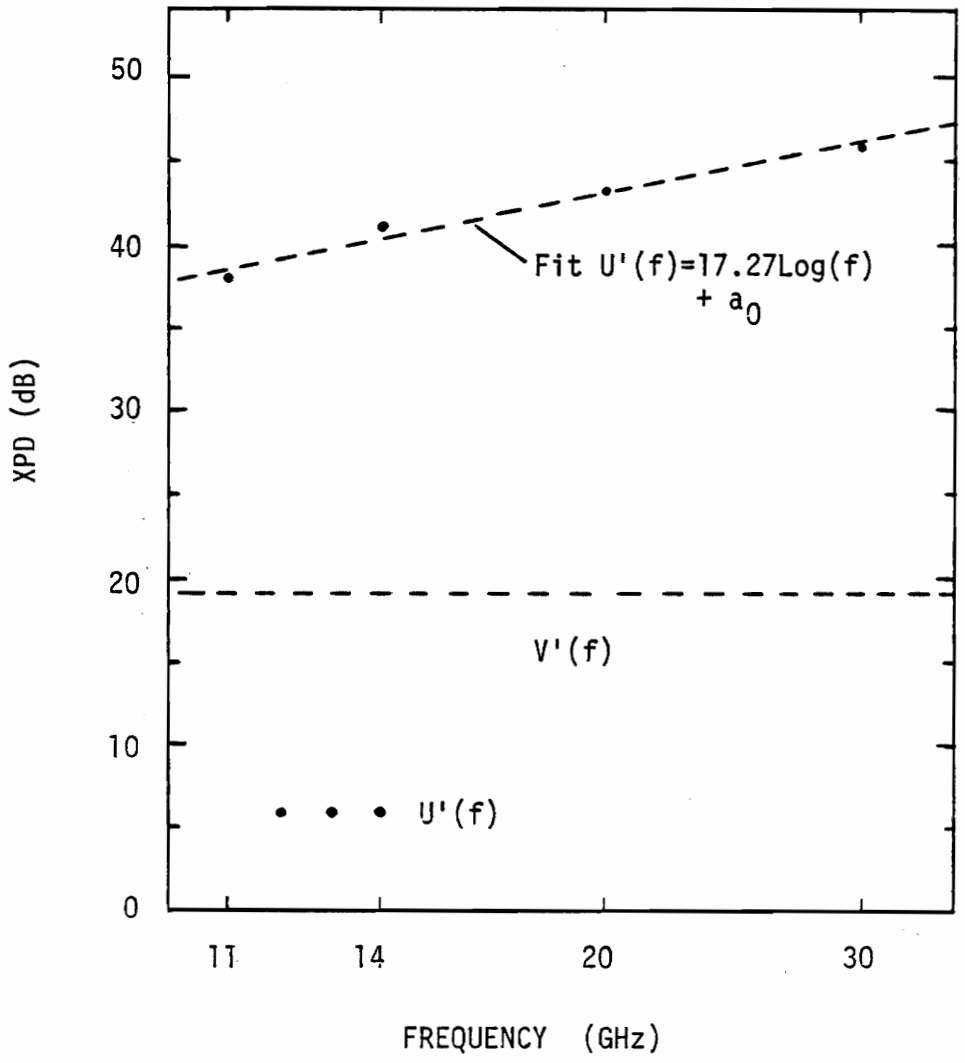

Figure 5-4. Coefficient U'(f) plotted versus frequency with curve fit.

$$U'(f_2) - U(f_1) = \alpha \log \frac{f_2}{f_1} \qquad (5.3\text{-}4)$$

where $\alpha = a_1$ and all other path parameters are the same.

To be complete, the parameter sensitivity analysis should involve the study of a single parameter under all possible combinations of the other parameter influences. In the process of computing XPD while varying the individual parameters in turn, it was observed that over the parameter ranges of greatest interest the variation of each was relatively unaffected by the chosen fixed values of the remaining parameters. The assumption of parameter independence is valid except under extreme conditions.

The U' and V' values of Table 5-1 were established for the fixed values of

$$\langle\theta\rangle = 0° \qquad \sigma_\theta = 12° \qquad F_o = 0.60 \qquad (5.3\text{-}5a)$$

and

$$\varepsilon = 45° \qquad \delta = 45° \qquad (5.3\text{-}5b)$$

which we have called the standard parameters. We determined that $V' = 19.0$ and that U' had a linear dependence with the logarithm of frequency as given in (5.3-3). This relationship, however, will vary as the rain and path parameters are changed. Thus we write (5.3-3) as

$$U' = 17.3 \log(f) + a_o(\varepsilon, \delta, \sigma_\theta, F_o) \qquad (5.3\text{-}6)$$

In the remainder of this section we will determine the functional form of a_o by examining the various parameter dependencies. Also, when the form of a_o is established we will reexamine the 17.3 value of a_1 for its sensitivity to the parameter variations contained in a_o to verify the assumption of parameter independence.

Elevation angle variation

The elevation angle sensitivity study was conducted with the elevation angle varied from 5 to 85 degrees and with the standard parameters input for the remaining variables.

The predictions were computed for the four frequencies available. The results of the study are tabulated in Tables 5-2 to 5-5. Note that the coefficient $V(\varepsilon)$ over the wide range of ε remains essentially constant for all frequencies except 30 GHz. At 30 GHz the coefficient $V(\varepsilon)$ in Table 5-5 is fairly constant for elevation angles greater than 20°. Although there are large variations of V at the low elevation angles, the effective path length is large as well as the associated attenuation values, even for low rainrates. Thus, at these low elevation angle points we are normally at attenuaton levels larger than the nominal range of model ap-

Table 5-2

Variation of U and V as a Function of the Elevation Angle ε at 11 GHz

ε	$U(\varepsilon)$	$V(\varepsilon)$	r^2	$U'(\varepsilon)$
5°	30.08	17.76	.9980	31.32
10	31.30	18.24	.9985	32.06
15	31.92	18.19	.9987	32.73
20	32.55	18.10	.9990	33.45
25	33.55	18.22	.9993	34.33
30	34.40	18.14	.9994	35.30
35	35.42	18.08	.9994	36.34
40	36.63	18.04	.9995	37.59
45	38.06	18.02	.9996	39.04
50	39.74	18.00	.9996	40.74
55	41.74	17.98	.9996	42.76
60	44.25	18.08	.9996	45.17
65	47.16	18.08	.9995	48.08
70	50.80	18.08	.9996	51.72
75	55.57	18.08	.9995	56.49
80	62.33	18.09	.9994	63.24
85	73.75	18.08	.9994	74.67

Table 5-3

Variation of U and V as a Function of Elevation Angle at 14 GHz

ε	$U(\varepsilon)$	$V(\varepsilon)$	r^2	$U'(\varepsilon)$
5°	37.19	20.43	.9990	35.76
10	37.34	20.33	.9989	36.01
15	37.56	20.20	.9990	36.36
20	39.97	20.09	.9992	36.88
25	38.54	20.00	.9993	37.54
30	39.32	19.94	.9993	38.38
35	40.28	19.84	.9994	39.39
40	41.45	19.85	.9995	40.60
45	42.86	19.82	.9995	42.04
50	44.53	19.80	.9995	43.73
55	46.52	19.79	.9995	45.73
60	48.91	19.78	.9996	48.13
65	52.08	19.96	.9996	51.12
70	55.72	19.95	.9996	54.77
75	60.49	19.95	.9996	59.54
80	67.25	19.96	.9996	66.29
85	78.67	19.96	.9995	77.71

Table 5-4

Variation of U and V as a Function of Elevation Angle at 20 GHz

ε	$U(\varepsilon)$	$V(\varepsilon)$	r^2	$U'(\varepsilon)$
5°	34.17	17.11	.9782	36.06
10	36.93	18.42	.9913	37.51
15	38.28	19.00	.9963	38.28
20	39.34	19.37	.9984	38.97
25	40.31	19.60	.9994	39.71
30	41.29	19.74	.9997	40.55
35	42.37	19.82	.9998	41.55
40	43.59	19.86	.9998	42.73
45	45.01	19.87	.9998	44.14
50	46.67	19.87	.9998	45.80
55	48.64	19.86	.9998	47.78
60	51.00	19.85	.9998	50.15
65	53.89	19.83	.9998	53.06
70	57.51	19.81	.9998	56.70
75	62.25	19.80	.9998	61.45
80	68.99	19.79	.9998	68.20
85	80.36	19.76	.9998	79.60

Table 5-5

Variation of U and V as a Function of Elevation Angle at 30 GHz

ε	$U(\varepsilon)$	$V(\varepsilon)$	r^2	$U'(\varepsilon)$
5°	22.93	10.05	.8592	31.88
10	31.32	13.72	.9516	36.60
15	35.14	15.40	.9774	38.74
20	37.78	16.54	.9892	40.24
25	39.87	17.34	.9950	41.53
30	41.66	17.93	.9978	42.73
35	43.34	18.34	.9991	44.00
40	45.00	18.65	.9996	45.35
45	46.76	18.87	.9999	46.89
50	48.66	19.01	.9998	48.65
55	50.80	19.11	.9998	50.69
60	53.29	19.17	.9997	53.12
65	56.26	19.21	.9996	56.05
70	59.94	19.23	.9995	59.71
75	64.74	19.24	.9995	64.50
80	71.49	19.24	.9994	71.25
85	82.47	19.05	.9994	82.42

plication and the deviations of V from a constant are not significant in practice.

The coefficients $U'(\varepsilon)$ were determined in the same manner as $U'(f)$ by forcing $V'(\varepsilon) = 19.0$ and matching the results at A = 10 dB. The variation of $U'(\varepsilon)$ was found to be accurately modeled by the functional variation used in the CCIR model (Section 2.3) for:

$$U'(\varepsilon) = b_1 \log(\cos \varepsilon) + b_o \qquad (5.3\text{-}7)$$

The value of b_1 was determined at the four frequencies and over two different ranges of elevation angles: $15^\circ \leq \varepsilon \leq 55^\circ$ and $25^\circ \leq \varepsilon \leq 55^\circ$. The corresponding b_1 values are given in Table 5-6.

Table 5-6

Coefficient b_1 as a Function of Frequency and Elevation Angle Range

Frequency (GHz)	$15 \leq \varepsilon \leq 55^\circ$ b_1	r^2	$25 \leq \varepsilon \leq 55^\circ$ b_1	r^2
11	-43.70	.9974	-42.17	.9995
14	-41.42	.9999	-41.22	.9999
20	-41.40	.9990	-40.54	.9999
30	-50.29	.9804	-45.53	.9967

The value $b_1 = -42$ was chosen as a compromise. The difference between using the coefficient $b_1 = -42$ and that prescribed by the CCIR model, which is $b_1 = -40$, is 0.30 at $\varepsilon = 45°$ and 0.03 at $\varepsilon = 15°$.

Polarization dependence

XPD will, of course, depend strongly upon the polarization state of the communication link relative to the medium orientation. As discussed in Section 2.2, the parameter

$$\delta = \begin{cases} |\tau - \langle\theta\rangle| & \text{Linear polarization} \\ 45° & \text{Circular polarization} \end{cases}$$

is the only one required to represent the polarization and medium canting angle. The sign on $\langle\theta\rangle$ has been changed here because θ will now be defined opposite to that previously; i.e., θ is positive upward from horizontal. This definition is consistent with common usage. Figure 5-5 shows XPD as a function of δ at frequencies of 11, 14, 20, and 30 GHz for the standard parameter values. Note that XPD is not a symmetric function of δ. However, XPD is nearly symmetric about $\delta = 45°$, and XPD at $\delta = 45°$ is close to the maximum XPD value. This point is often confused in the literature and these approximations are presented as exact. XPD be-

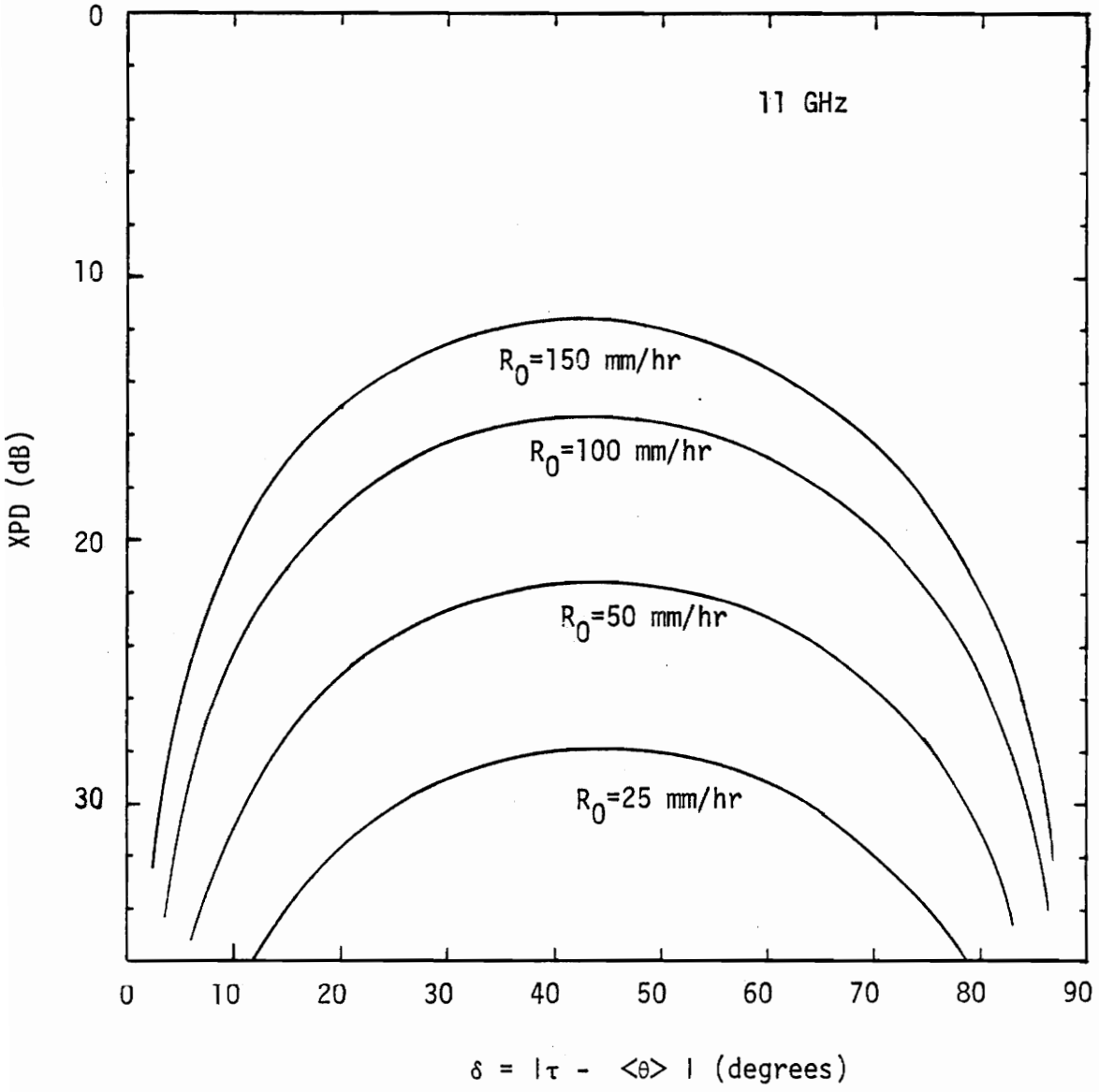

Figure 5-5. XPD variation with polarization parameter δ with rainrate as a parameter.

(a) 11 GHz

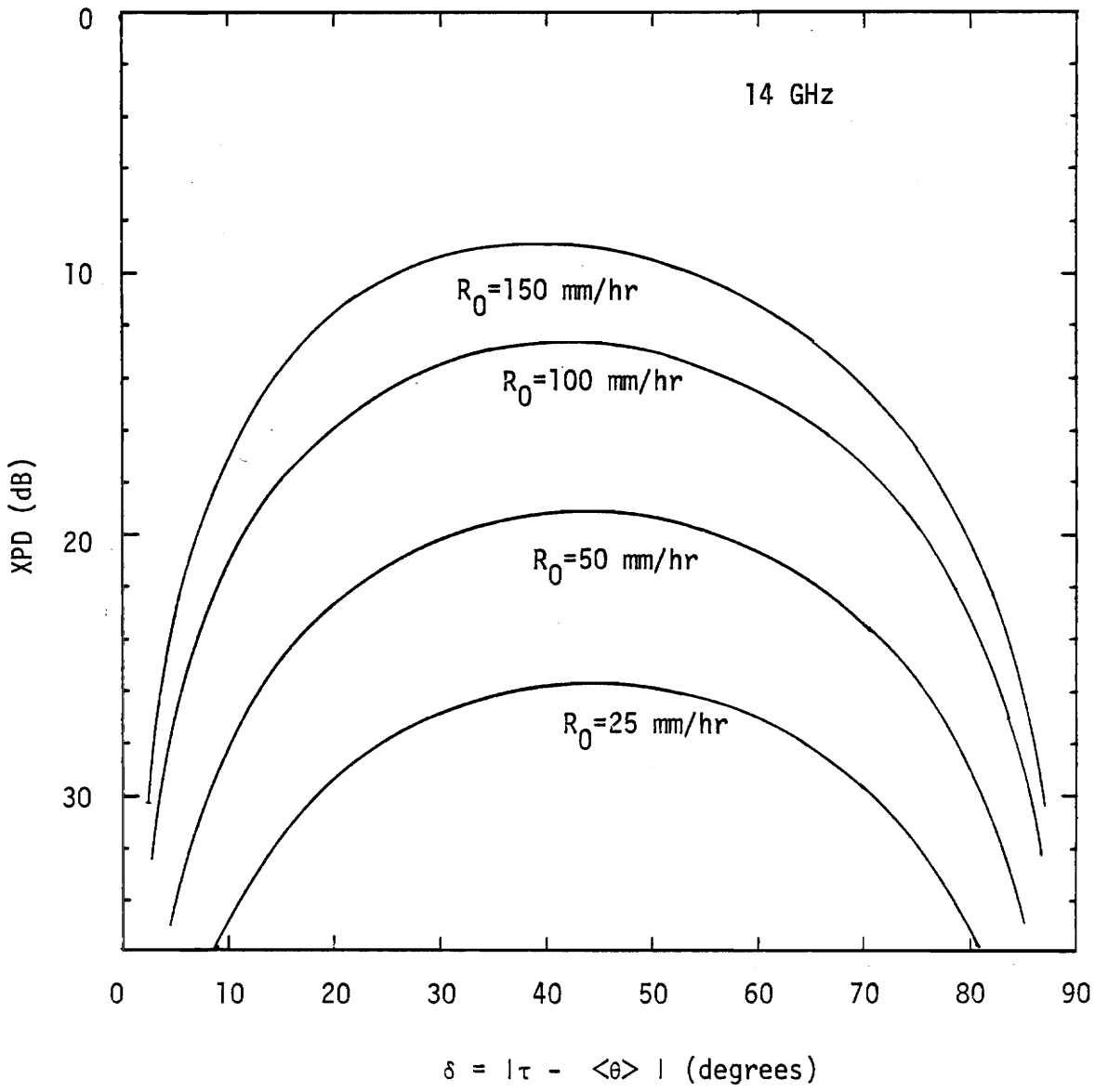

Figure 5-5. (b) 14 GHz

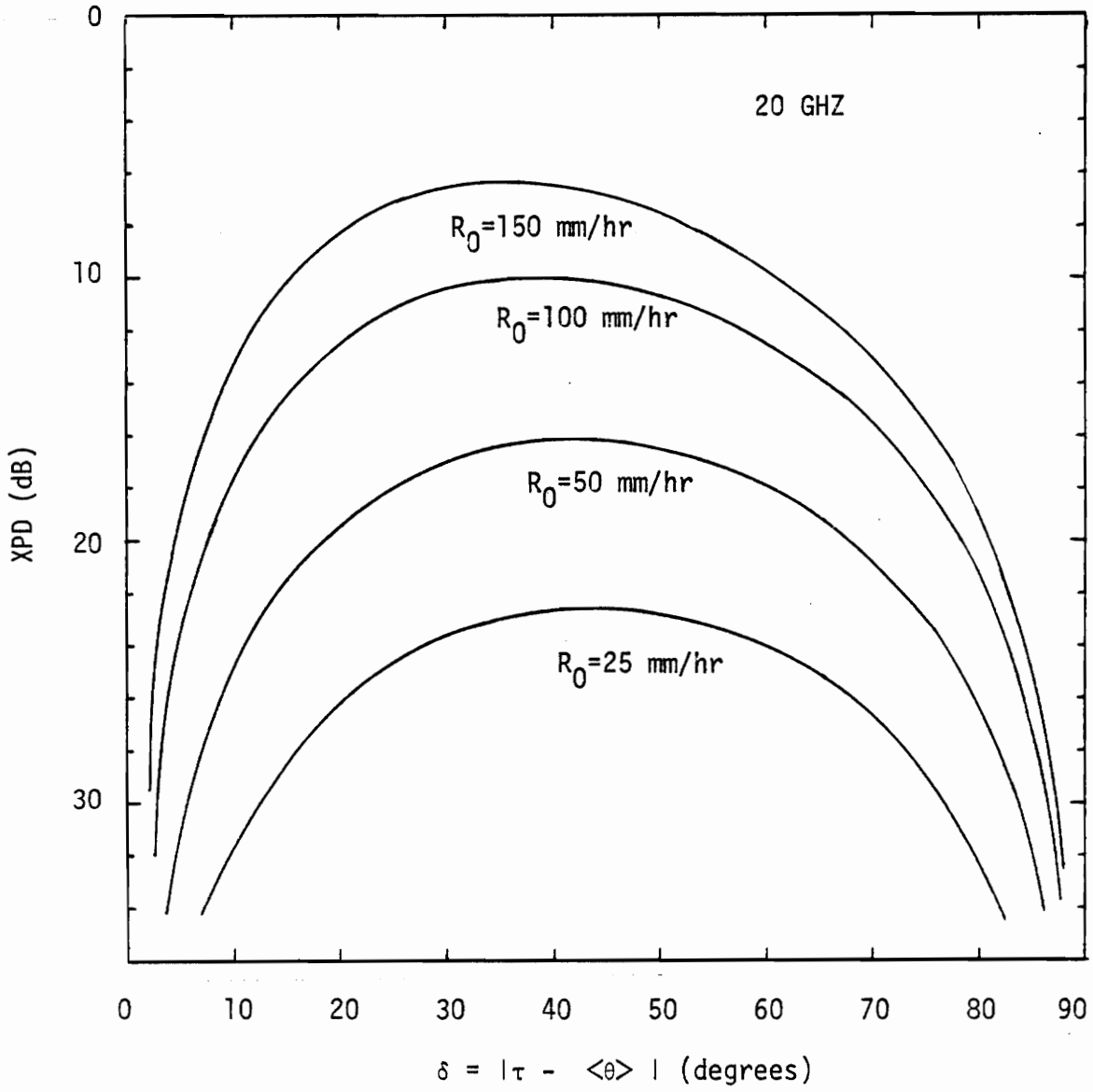

Figure 5-5. (c) 20 GHz

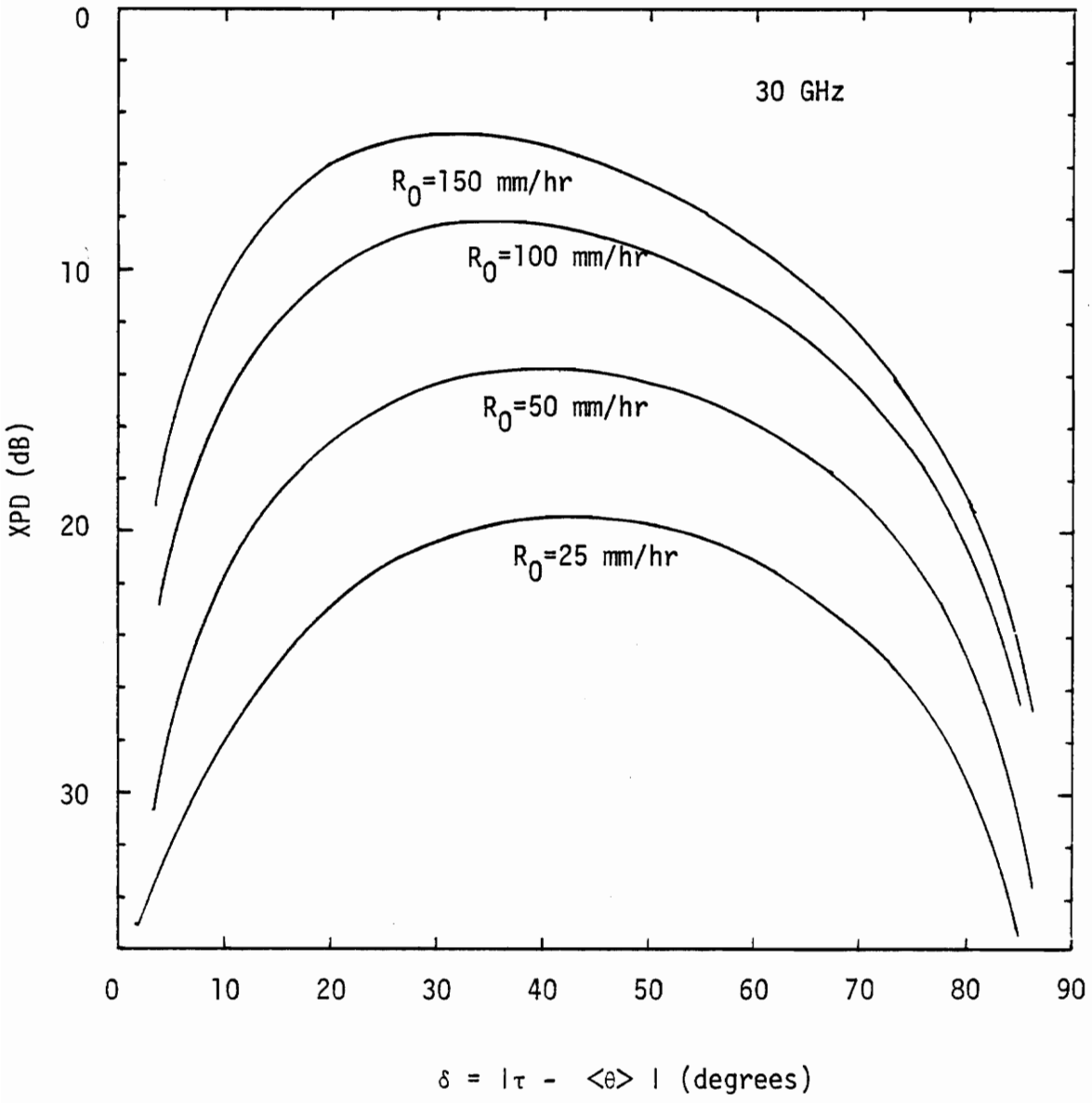

Figure 5-5. (d) 30 GHz

comes asymmetric only when attenuation is large (for high rainrate and/or high frequency). Thus, under normal operating conditions it is a good approximation to assume XPD is symmetric about $\delta = 45°$ and that it is maximum there.

The XPD vs δ results are for a fixed rainrate. The corresponding attenuation would change due to polarization changes. In the study at hand we are interested in XPD changes for fixed attenuation. Thus, we proceed as we did with elevation angle. XPD vs A is examined as a function of δ; the results are tabulated in Tables 5-7 to 5-10 for the four frequencies. Since attenuation is a function of polarization there will be a dependence of V on δ. The tables reveal that this dependence is relatively mild. Therefore, the fit using $V' = 19$ can be used to essentially force the mild δ dependence into U'.

The last column in Tables 5-7 to 5-10 is $U'(\delta) - U'(\delta = 45°)$ reveal the deviation from circular polarization (or, equivalently, linear polarization 45° from the axis of symmetry of the rain). These values also reveal the symmetry of $U'(\delta)$ about $\delta = 45°$. At 11 GHz U' is nearly symmetric, but as frequency increases it becomes more asymmetric. This asymmetry was created by the fitting process that spanned the range of rainrates up to 150 mm/hr. At such high rainrates attenuations become very large at high frequencies,

Table 5-7

Variation of U and V as a Function of
the Polarization Parameter δ at 11 GHz

$\delta = \tau - \langle\theta\rangle$	$U(\delta)$	$V(\delta)$	r^2	$U'(\delta)$	$U'(\delta)-U'(\delta=45°)$
5	53.66	18.55	.9990	54.11	15.07
10	47.76	18.53	.9990	48.23	9.19
15	44.43	18.50	.9991	44.93	5.89
20	42.22	18.45	.9991	42.77	3.73
25	40.65	18.39	.9992	41.26	2.22
30	39.53	18.32	.9993	40.21	1.17
35	38.76	18.23	.9994	39.53	0.49
40	38.27	18.13	.9994	39.14	0.10
45	38.06	18.02	.9996	39.04	0.00
50	38.11	17.90	.9997	39.21	0.17
55	38.43	17.78	.9997	39.65	0.61
60	39.06	17.66	.9998	40.40	1.36
65	40.05	17.56	.9998	41.49	2.45
70	41.50	17.46	.9998	43.04	3.83
75	43.63	17.38	.9999	45.25	6.04
80	46.88	17.32	.9998	48.53	9.52
85	52.75	17.29	.9998	54.46	15.42

Table 5-8

Variation of U and V as a Function of the Polarization Parameter δ at 14 GHz

$\delta = \tau - \langle\theta\rangle$	$U(\delta)$	$V(\delta)$	r^2	$U'(\delta)$	$U'(\delta)-U'(\delta=45°)$
5	58.83	20.80	.9981	57.03	14.99
10	52.91	20.77	.9982	51.14	9.10
15	49.57	20.71	.9982	47.86	5.82
20	47.32	20.62	.9984	45.70	3.66
25	45.70	20.50	.9986	44.20	2.16
30	44.53	20.36	.9988	43.17	1.13
35	43.69	20.20	.9990	42.49	0.45
40	43.14	20.02	.9993	42.12	0.08
45	42.86	19.82	.9995	42.04	0.00
50	42.83	19.62	.9997	42.21	0.17
55	43.09	19.43	.9998	42.66	0.62
60	43.65	19.24	.9998	43.41	1.37
65	44.59	19.07	.9998	44.52	2.48
70	46.00	18.92	.9998	46.08	4.04
75	48.09	18.80	.9997	48.29	6.25
80	51.32	18.71	.9996	51.61	9.57
85	57.17	18.65	.9995	57.52	15.48

Table 5-9

Variation of U and V as a Function of the Polarization Parameter δ at 20 GHz

$\delta = \tau - \langle\theta\rangle$	U(δ)	V(δ)	r^2	U'(δ)	U'(δ)-U'(δ=45°)
5	63.31	22.06	.9971	59.25	15.11
10	56.33	21.97	.9974	53.36	9.22
15	52.87	21.81	.9978	50.06	5.92
20	50.48	21.59	.9982	47.89	3.75
25	48.69	21.31	.9987	46.38	2.24
30	47.32	20.99	.9992	45.33	1.19
35	46.27	20.63	.9995	44.64	0.50
40	45.51	20.25	.9998	44.26	0.12
45	45.01	19.87	.9998	44.14	0.00
50	44.80	19.50	.9998	44.30	0.16
55	44.87	19.14	.9994	44.73	0.59
60	45.29	18.82	.9990	45.47	1.33
65	46.09	18.54	.9985	46.55	2.41
70	47.40	18.29	.9980	48.11	3.97
75	49.41	18.10	.9975	50.31	6.17
80	52.58	17.96	.9972	53.62	9.48
85	58.39	17.88	.9968	59.51	15.37

Table 5-10

Variation of U and V as a Function
of the Polarization Parameter δ at 30 GHz

$\delta = \tau - \langle\theta\rangle$	$U(\delta)$	$V(\delta)$	r^2	$U'(\delta)$	$U'(\delta) - U'(\delta=45°)$
5	66.62	22.73	.9931	62.89	16.00
10	60.47	22.52	.9938	56.95	10.06
15	56.74	22.18	.9949	53.56	6.67
20	54.02	21.73	.9961	51.29	4.40
25	51.86	21.21	.9974	49.65	2.76
30	50.09	20.63	.9985	48.46	1.57
35	48.67	20.03	.9993	47.64	0.75
40	47.56	19.44	.9997	47.12	0.23
45	46.76	18.87	.9999	46.89	0.00
50	46.27	18.33	.9995	46.94	0.05
55	46.11	17.84	.9991	47.27	0.38
60	46.34	17.41	.9984	47.93	1.04
65	46.98	17.03	.9977	48.95	2.06
70	48.17	16.73	.9969	50.44	3.55
75	50.08	16.49	.9963	52.59	5.70
80	53.20	16.32	.9959	55.88	8.99
85	58.97	16.21	.9954	61.76	14.87

and, thus, of little practical significance. Therefore, we will assume U' to be symmetric about 45° with little error. For example, the difference between the calculated XPD values at 11 GHz at $\delta = 85°$ and $\delta = 5°$ is 0.35 dB for A = 10 dB, 0.73 dB for A = 20 dB, and 0.95 dB for A = 30 dB.

The following analytical function (proposed by Chu [1980b]) has been found to perform well:

$$U'(\delta) - U'(\delta = 45°) = -10 \log \frac{1}{2} [1 - \cos (4\delta)] \qquad (5.3\text{-}8)$$

Values calculated using (5.3-8) are tabulated in Table 5-11 for direct comparison to those in the last column of Tables 5-7 to 5-10. Very good agreement is found at the four frequencies.

Table 5-11

Tabulated Values of Equation (5.3-8) as a Function of the Polarization Parameter δ.

δ	$-10\log 1/2\,[1-\cos(4\delta)]$
5°	15.21
10	9.32
15	6.02
20	3.84
25	2.31
30	1.25
35	0.54
40	0.13
45	0.00
50	0.13
55	0.54
60	1.25
65	2.31
70	3.84
75	6.02
80	9.32
85	15.21

Canting angle variation

The sensitivity study of the deviation of the normal distribution about the mean canting angle was performed for σ_θ varying from 0° to 45°. The standard parameters were again used for the other program inputs. The results of this study are tabulated in Tables 5-12 to 5-15. Again $V(\sigma_\theta)$ was essentially constant over the wide range of σ_θ tested. The condition $V'(\sigma_\theta) = 19.0$ was enforced and the values of $U'(\sigma_\theta)$ were determined to give the same value of XPD at A = 10 dB. The modeling of the $U'(\sigma_\theta)$ variation took the form

Table 5-12

Variation of U and V as a Function of the Canting Angle Standard Deviation σ_θ at 11 GHz

σ_θ	$U(\sigma_\theta)$	$V(\sigma_\theta)$	r^2	$U'(\sigma_\theta)$
0°	37.31	18.03	.9996	38.28
3	37.35	18.02	.9995	38.33
6	37.50	18.02	.9995	38.48
9	37.73	18.03	.9996	38.70
12	38.06	18.02	.9996	39.04
15	38.49	18.01	.9996	39.48
18	39.00	18.01	.9996	39.99
21	39.62	18.00	.9997	40.62
24	40.32	17.99	.9996	41.33
27	41.14	17.99	.9996	42.15
30	42.04	17.98	.9996	43.06
33	43.03	17.98	.9996	44.05
36	44.12	17.98	.9995	45.14
39	45.31	17.97	.9995	46.34
42	46.60	17.97	.9995	47.63
45	47.97	17.97	.9995	49.00

Table 5-13

Variation of U and V as a Function of the Canting Angle Standard Deviation σ_θ at 14 GHz

σ_θ	$U(\sigma_\theta)$	$V(\sigma_\theta)$	r^2	$U'(\sigma_\theta)$
0°	42.10	19.83	.9995	41.27
3	42.15	19.83	.9995	41.32
6	42.29	19.83	.9995	41.46
9	42.52	19.83	.9995	41.69
12	42.86	19.82	.9995	42.04
15	43.28	19.82	.9995	42.46
18	43.80	19.81	.9995	42.99
21	44.41	19.81	.9995	43.60
24	45.12	19.80	.9995	44.32
27	45.93	19.79	.9995	45.14
30	46.83	19.79	.9995	46.04
33	47.83	19.79	.9995	47.04
36	48.92	19.78	.9995	48.14
39	50.10	19.78	.9995	49.32
42	51.39	19.77	.9995	50.62
45	52.77	19.77	.9996	52.00

Table 5-14

Variation of U and V as a Function of the Canting Angle Standard Deviation σ_θ at 20 GHz

σ_θ	$U(\sigma_\theta)$	$V(\sigma_\theta)$	r^2	$U'(\sigma_\theta)$
0°	44.23	19.86	.9999	43.37
3	44.28	19.86	.9998	43.42
6	44.43	19.86	.9999	43.57
9	44.67	19.87	.9999	43.80
12	45.01	19.87	.9998	44.14
15	45.45	19.88	.9999	44.57
18	45.98	19.89	.9999	45.09
21	46.61	19.90	.9998	45.71
24	47.33	19.90	.9999	46.43
27	48.15	19.91	.9999	47.24
30	49.06	19.92	.9999	48.14
33	50.07	19.92	.9998	49.15
36	51.17	19.93	.9998	50.24
39	52.36	19.93	.9998	51.43
42	53.65	19.93	.9998	52.72
45	55.03	19.94	.9998	54.09

Table 5-15

Variation of U and V as a Function of the Canting Angle Standard Deviation σ_θ at 30 GHz

σ_θ	$U(\sigma_\theta)$	$V(\sigma_\theta)$	r^2	$U'(\sigma_\theta)$
0°	45.89	18.79	.9998	46.11
3	45.95	18.79	.9998	46.16
6	46.11	18.81	.9997	46.30
9	46.38	18.83	.9998	46.55
12	46.76	18.87	.9999	46.89
15	47.23	18.90	.9998	47.33
18	47.81	18.94	.9998	47.87
21	48.49	18.99	.9998	48.50
24	49.26	19.03	.9997	49.23
27	50.12	19.07	.9998	50.05
30	51.08	19.11	.9998	50.97
33	52.12	19.14	.9997	51.98
36	53.25	19.17	.9996	53.08
39	54.48	19.19	.9996	54.29
42	56.79	19.21	.9996	55.58
45	57.19	19.23	.9996	56.96

$$U'(\sigma_\theta) = d_1 \ \sigma_\theta^2 + d_o \qquad (5.3\text{-}9)$$

A set of curve fits of the form (5.3-9) were performed and the results are shown in Table 5-16.

Table 5-16

Coefficient d_1 as a Function of Frequency

Frequency (GHz)	d_1	r^2
11	0.0052967	1.0000
14	0.0052988	1.0000
20	0.0052954	1.0000
30	0.0053653	1.0000

For modeling purposes $d_1 = 0.0053$ is sufficient. This is the same coefficient for the parameter variation of the form (5.3-9) proposed by Olsen and Nowland [1978].

Raindrop shape distribution dependence

A similar procedure was carried out for variations of the fraction of oblate raindrops, F_o, from 0.4 to 1.0. The results are tabulated in Table 5-17. The analytic function which best describes the behavior is

$$U'(F_o) = e_1 \log(F_o) + e_o \qquad (5.3\text{-}10)$$

Table 5-17

Variation of U and V as a Function of the Shape Parameter F_o for 11, 14, 20, and 30 GHz

f (GHz)	F_o	$U(F_o)$	$V(F_o)$	r^2	$U'(F_o)$
11	0.40	41.52	17.96	.9996	42.56
	0.50	39.61	17.99	.9996	40.62
	0.60	38.06	18.02	.9996	39.04
	0.70	36.76	18.05	.9996	37.71
	0.80	35.63	18.09	.9995	36.54
	0.90	34.65	18.13	.9994	35.52
	1.00	33.78	18.18	.9994	34.60
14	0.40	46.42	19.77	.9995	45.65
	0.50	44.46	19.80	.9995	43.66
	0.60	42.86	19.82	.9995	42.04
	0.70	41.50	19.85	.9995	40.65
	0.80	40.32	19.89	.9995	39.43
	0.90	39.28	19.92	.9995	38.36
	1.00	38.34	19.96	.9994	37.38
20	0.40	48.56	19.86	.9998	47.70
	0.50	46.61	19.87	.9998	45.74
	0.60	45.01	19.87	.9998	44.14
	0.70	43.65	19.87	.9998	42.78
	0.80	42.46	19.86	.9998	41.60
	0.90	41.39	19.84	.9998	40.55
	1.00	40.43	19.81	.9997	39.62
30	0.40	50.60	19.06	.9998	50.54
	0.50	48.51	18.97	.9997	48.54
	0.60	46.76	18.87	.9998	46.89
	0.70	45.21	18.74	.9997	45.47
	0.80	43.83	18.54	.9995	44.23
	0.90	42.54	18.42	.9991	43.12
	1.00	41.35	18.24	.9987	42.11

Results of curve fitting (5.3-10) are shown in Table 5-18 for the four frequencies. A reasonable value to use for modeling is $e_1 = -20$.

Table 5-18

Coefficient e_1 as a Function of Frequency

Frequency (GHz)	e_1	r^2
11	-19.995	1.0000
14	-20.765	1.0000
20	-20.308	1.0000
30	-21.173	0.9999

A final look at the a_1 value

Our initial assumption incorporated into (5.3-3) was that a_1 equalled 17.3 independent of the other parameter values. Having established the functional variation of a_o with parameters ε, δ, σ_θ, and F_o we can verify that a_1 is not affected by these parameters as well. To do this we use the U' values calculated in tables presented in this section for a fixed value of one parameter (ε, δ, σ_θ, or F_o) at the four frequencies to form the curve fit (5.3-3). The resulting a_1 values are given in Table 5-19.

Table 5-19 reveals that the variation in a_1 introduced by varying the individual parameters in turn is rather mild.

The total impact of the assumption that a_1 is strictly constant at a value of 17.3 upon the predictions of XPD can only be assessed by comparison with experimental data. This will be done in Section 5.5. In the next section we collect our findings in this section and form a proposed XPD vs A model.

Table 5-19
The Variation of the Coefficient a_1 as a Function of ε, δ, σ_θ and F_o in the Relation

$$U' = a_1 \log(f) + a_o$$

(a) Elevation angle dependence ($\delta = 45°$, $F_o = .6$, $\sigma_\theta = 12$)

ε	a_1	r^2
30°	16.37	0.961
40	17.09	0.974
45	17.27	0.977
50	17.39	0.978
60	17.46	0.980

(b) Polarization parameter dependence ($\varepsilon = 45°$, $F_o = .6$, $\sigma = 12°$)

δ	a_1	r^2
10°	19.23	0.989
20	18.80	0.987
30	18.19	0.984
40	17.58	0.980
45	17.27	0.977
50	17.00	0.975
60	16.55	0.970
70	16.24	0.965
80	16.10	0.961

(c) Shape parameter dependence ($\varepsilon = 45°$, $\delta = 45°$, $\sigma = 12°$)

F_o	a_1	r^2
0.40	17.49	0.975
0.50	17.40	0.976
0.60	17.27	0.977
0.70	17.10	0.978
0.80	17.00	0.978
0.90	16.83	0.979
1.00	16.68	0.979

Table 5-19 (continued)

(d) Standard deviation dependence (σ_θ) ($\varepsilon = 45°$, $\delta = 45°$, $F_o = .6$)

σ_θ	a_1	r^2
0	17.23	0.977
12	17.27	0.977
24	17.39	0.978
36	17.46	0.978
45	17.50	0.979

5.4 A PROPOSED XPD VS A MODEL

In the previous section, the parameter variations of the multiple scattering model were determined by fitting analytic functions to predicted results. The proposed model of the form (5.2-1) may be written using the results from Section 5.3 as

$$XPD = U - V \log(A) \qquad (5.4\text{-}1)$$

where the coefficients U and V are

$$U(f, \varepsilon, \delta, \sigma_\theta, F_o) = a_1 \log(f) + b_1 \log(\cos \varepsilon) + C_1 \log \tfrac{1}{2}[1 - \cos(4\delta)] + d_1 \sigma_\theta^2 + e_1 \log(F_o) + U_o \qquad (5.4\text{-}2a)$$

$$V = 19.0 \qquad (5.4\text{-}2b)$$

This is the Simple Isolation Model (SIM). The constant coefficients in (5.4-2a) were determined to be

$$\begin{aligned} a_1 &= 17.3 \\ b_1 &= -42.0 \\ c_1 &= -10. \\ d_1 &= 0.0053 \\ e_1 &= -20.0 \end{aligned} \qquad (5.4\text{-}3)$$

The coefficient U_o determined using the standard parameters and f = 11 GHz is

$$U_o = 9.5 \qquad (5.4\text{-}4)$$

The difference between the above constant determined at 11 GHz and that using 30 GHz is 0.31. A comparison of the accuracy of (5.4-2a) using (5.4-3) and (5.4-4) with the tabulated results in Section 5.3 showed good agreement over a wide range of input parameters.

The model is limited, however, to the frequency range $10 \leqslant f \leqslant 30$ GHz. Extending the application above and below these limits requires caution since it has not been tested using the multiple scattering model in the regions of 8 and 35

GHz, respectively. The elevation angle dependence is most accurate for $10^\circ \leq \varepsilon \leq 60^\circ$.

The polarization term $U(\delta)$ in (5.4-2) is inadequate for cases when the polarization is near vertical or horizontal linear (δ close to 0° or 90°). In fact, if δ equals 0° or 90° the term $U(\delta)$ is undefined. Chu [1980] proposed a second tier in the canting angle distribution to account for this difficiency (see Section 2.4). He introduced a normal distribution of the mean canting angle with variance σ_m^2 to account for the variation from storm to storm. The second distribution yields a finite value of XPD for δ equal to 0° or 90°. This second tier resulted in the following polarization term in his simple model

$$U(\delta) = -10 \log \frac{1}{2} \left[1 - \cos(4\delta)\, e^{-0.0024\sigma_m^2}\right] \qquad (5.4\text{-}5)$$

where σ_m is in degrees. We found previously that (5.3-8) agreed very well with the results from the multiple scattering model when $\sigma_m = 0^\circ$. We will adopt this modification for our proposed simple model to provide modeling completeness. The appropriate value of σ_m to use is not clear in the literature. Chu [1982] suggests that $\sigma_m = 3^\circ$, which yields a 19.7 dB improvement of vertical or horizontal polarization (when $\langle\theta\rangle = 0^\circ$) over circular polarization. The CCIR [Doc

515005-E, 1981] adopted Chu's polarization term for their simple model while stating that a value of $\sigma_m = 5°$ appears to give a sufficiently conservative maximum improvement of XPD = 15.4 dB. The term $U(\delta)$, however, yields essentially the same numbers for $20° \leq \delta \leq 70°$ over the practical range $0° \leq \sigma_m \leq 6°$. Only as δ nears 0° or 90° does the factor from the second tier have significant influence on XPD. Sufficient data to establish the appropriate value for δ is not available at this time. Two months of XPD vs A data for 19.04 GHz at Crawford Hill, NJ were recently published for linear polarization 4° from vertical [Arnold, et al., 1982]. The proposed simple model agreed very well with these preliminary data using a value of $\sigma_m = 3°$ for $A \leq 25$ dB. The data approached the noise level of the experiment for $A \geq 22$ dB. Recent measurements at 12 GHz made at Marthesham Heath, U.K. [Howell, R. G. et al., 1982] using the OTS satellite indicate an improvement of about 8 dB for linear polarization at 11.8° from horizontal over circular polarization. Values of $\sigma_m = 0°$ and 3° yield improvements of 7.95 and 7.76 dB respectively. Although the length of the data period is significant, the maximum fade was only 10 dB and the tilt angle was not close enough to 0° to make a precise conclusion. At this preliminary stage we suggest $\sigma_m = 3°$, noting that this yields identical predictions to

those using $\sigma_m = 0^\circ$ for the experiments (excluding the OTS linear experiment) in Table 4.3-1.

The proposed model is based on a rigorous modeling technique where no approximations of the type used in the development of the CCIR model have been used. The accuracy of the proposed model will be demonstrated in Section 5.5 and the improvement over the CCIR model are shown in Section 5.6.

5.5 COMPARISONS OF NEW MODEL TO DATA

We are now in a position to test the new model as presented in the previous section against measured data. Table 4.3-1 lists the worldwide data sets available for model testing. All sets in that table will be compared to predictions, except for data set numbers 4 and 7; these are eliminated because they are for short time periods that are included in data set numbers 6 and 8, respectively. Data for the 12 data sets are plotted in Figures 5-6 through 5-17. Also shown in the figures are SIM predictions using (5.4-2) and the rain parameters:

$$\langle\theta\rangle = 0^\circ \qquad \sigma_\theta = 12^\circ \qquad F_o = 0.65$$

There is excellent agreement between the SIM predictions and measured mean (or median) data. A detailed numerical com-

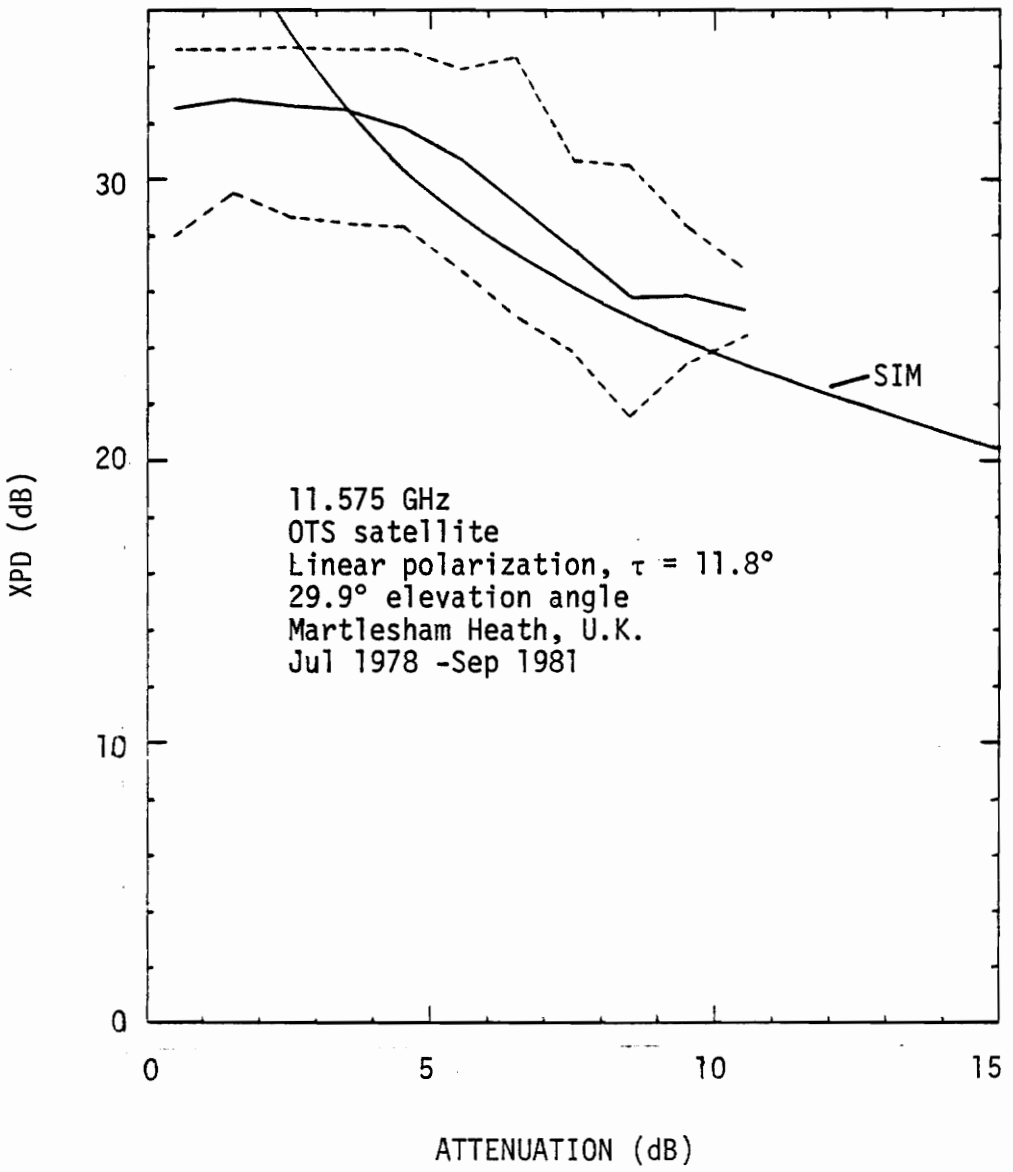

Figure 5-6. Comparison between simple isolation model and measured data set 1. Data quantities shown are: median (——), 10%,90% occurrence levels (----).

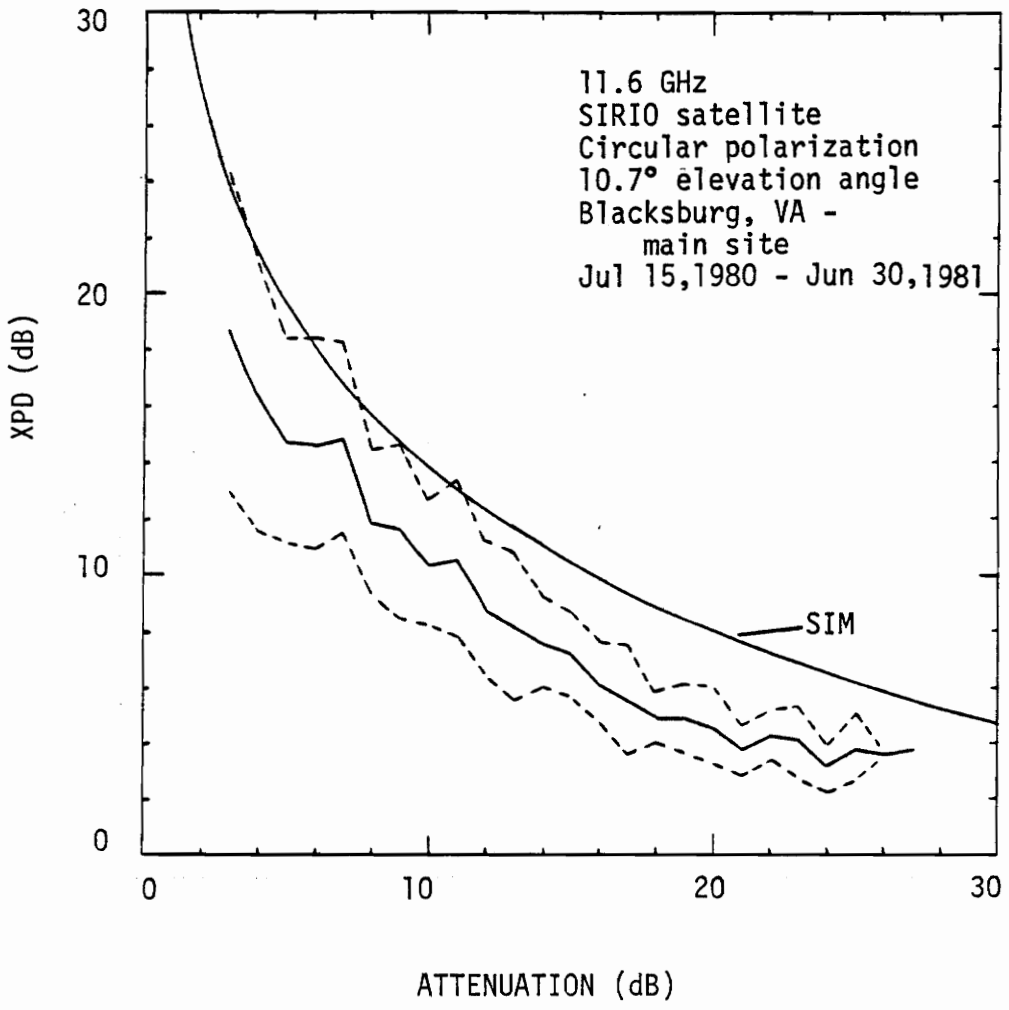

Figure 5-7. Comparison between simple isolation model and measured data set 2. Data quantities shown are: mean (——), mean and one standard deviation (----).

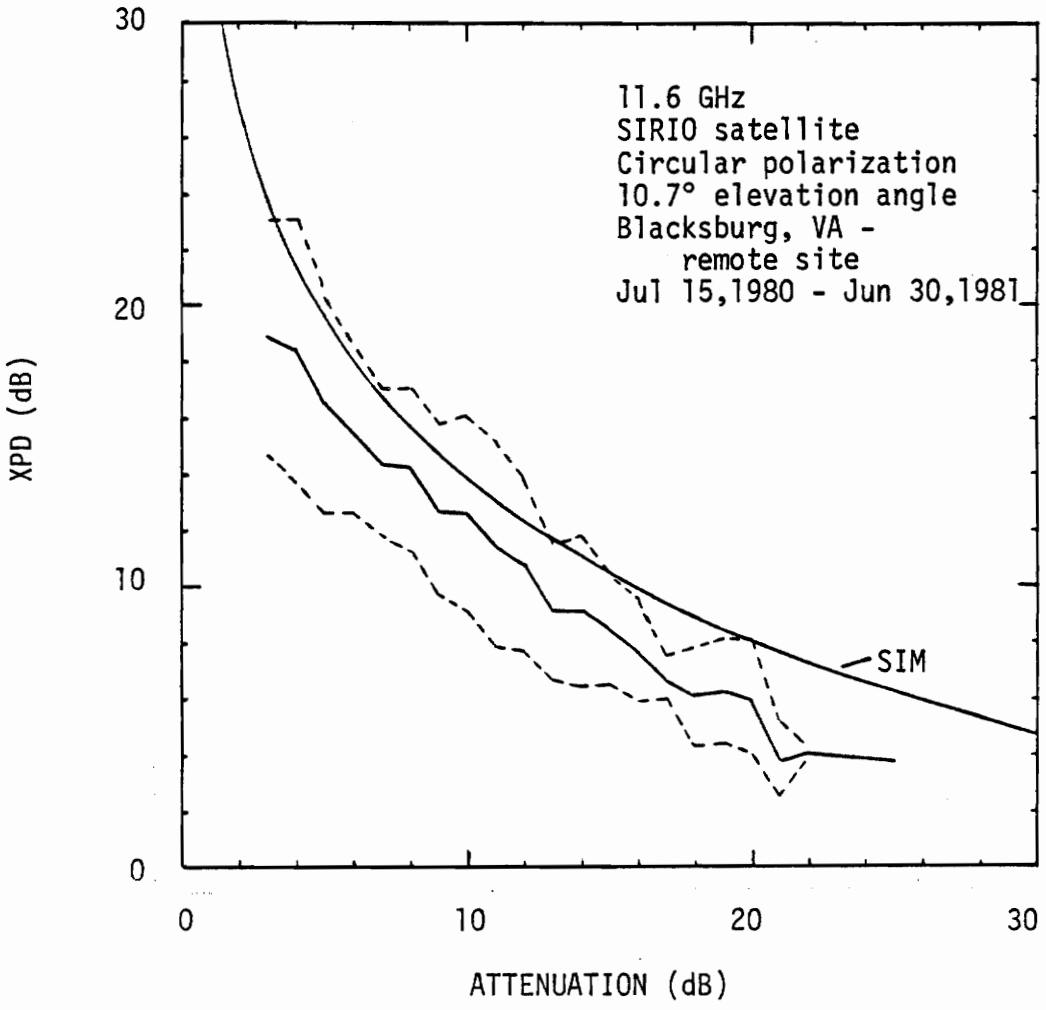

Figure 5-8. Comparison between simple isolation model and measured data set 3. Data quantities shown are: mean (——), mean and one standard deviation (----).

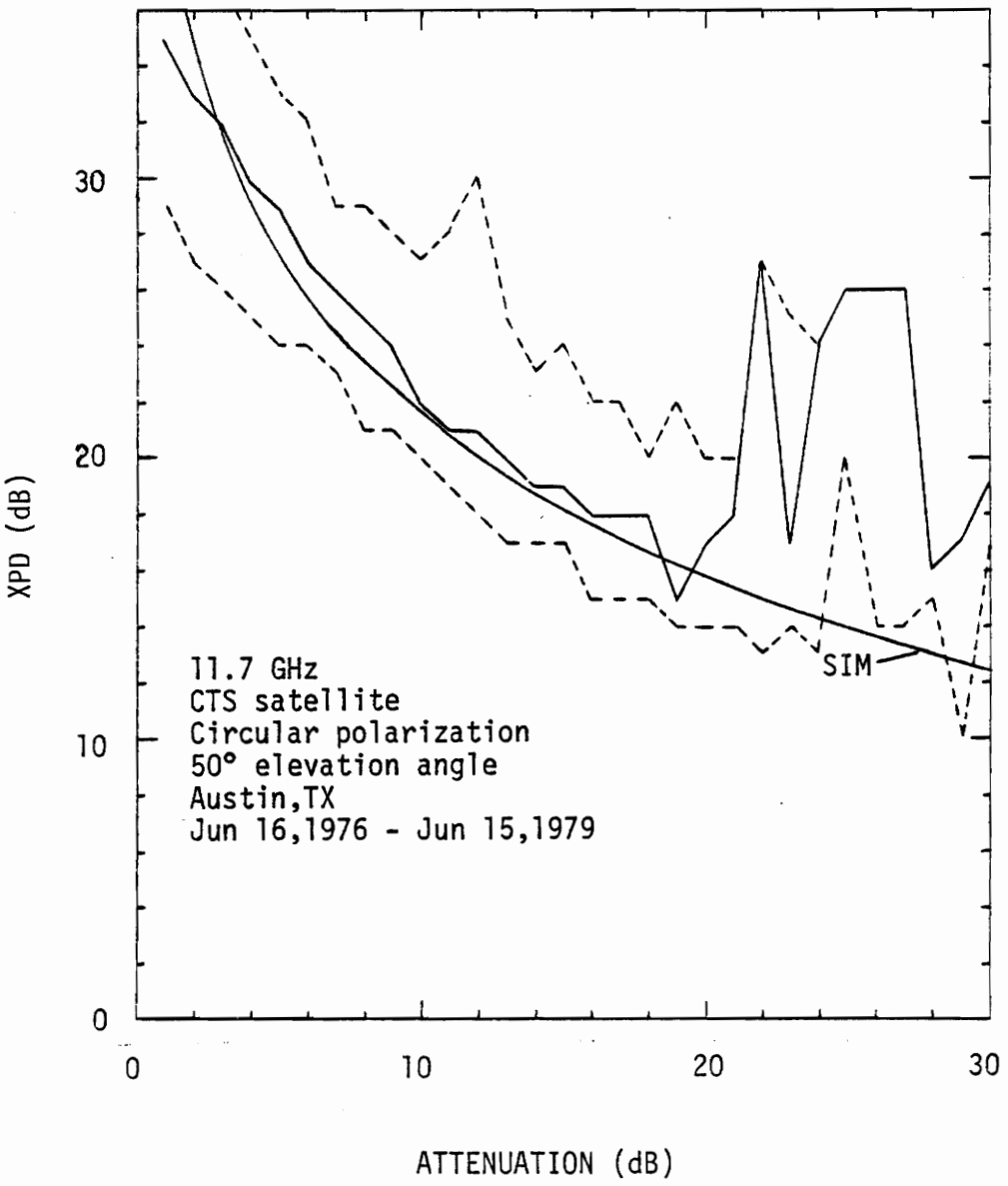

Figure 5-9. Comparison between simple isolation model and measured data set 5. Data quantities shown are: median (——), 10%,90% occurrence levels (----).

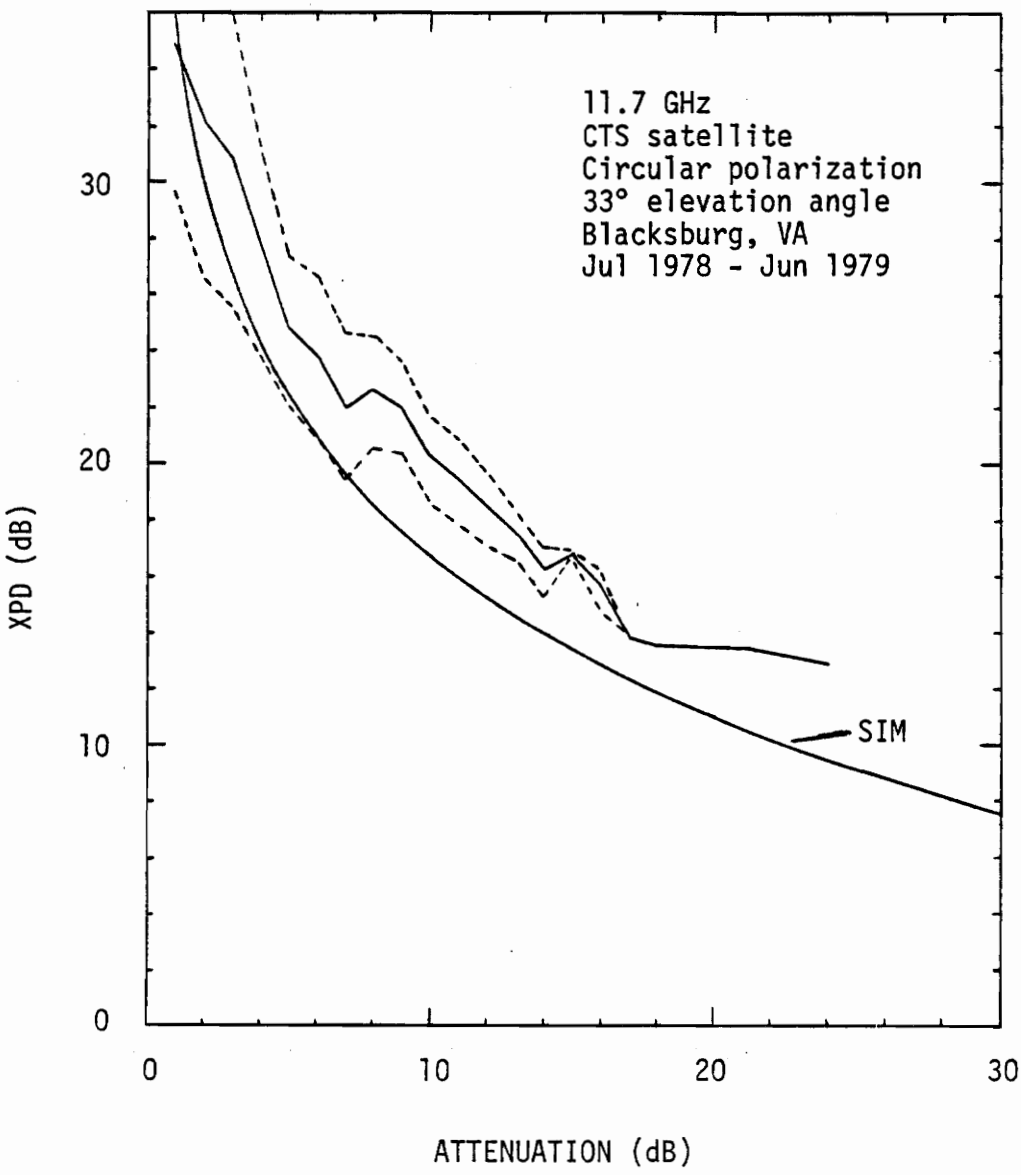

Figure 5-10. Comparison between simple isolation model and measured data set 6. Data quantities shown are: mean (——), mean and one standard deviation (----).

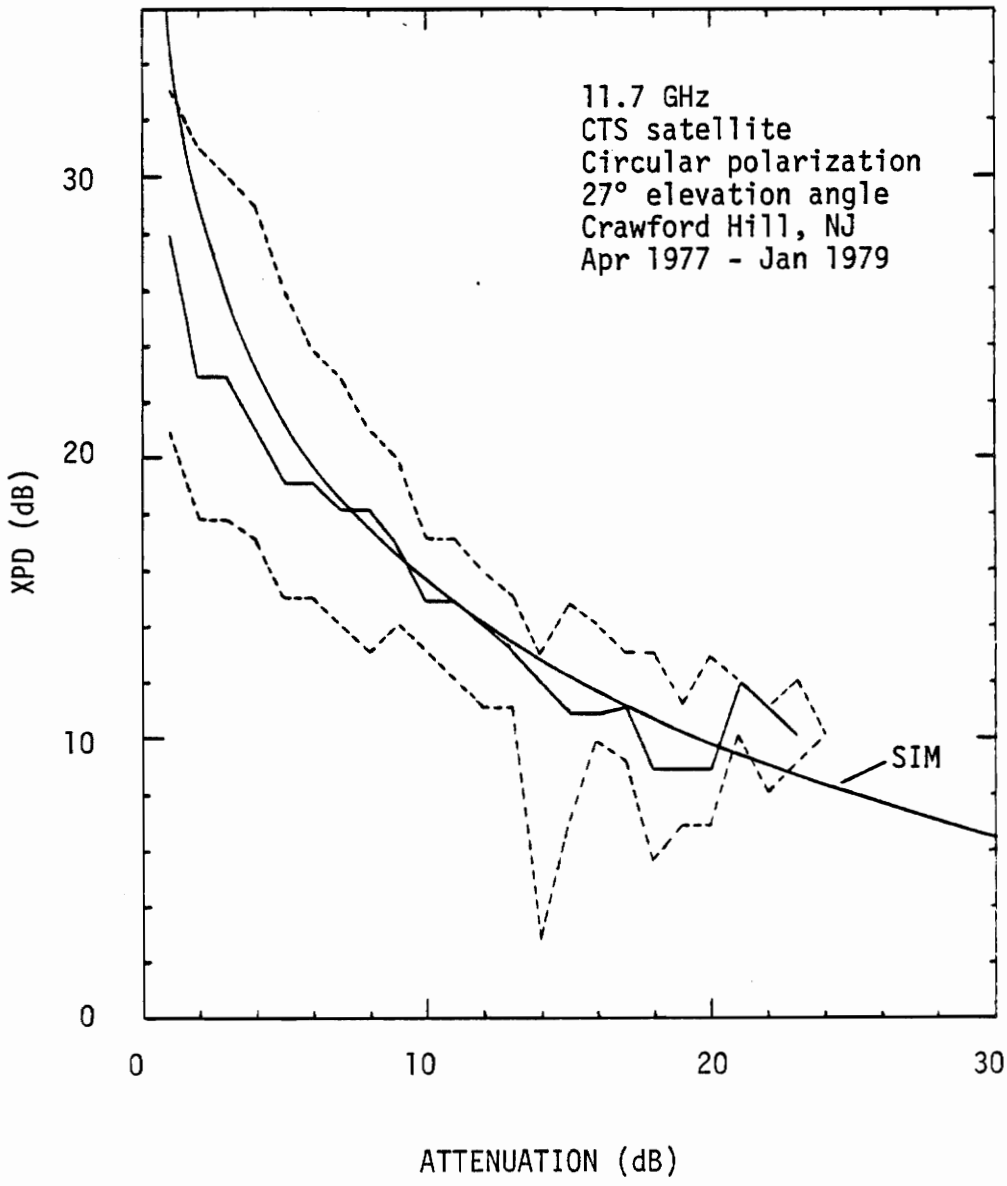

Figure 5-11. Comparison between simple isolation model and measured data set 8. Data quantities shown are: median (——), 10%,90% occurrence levels (----).

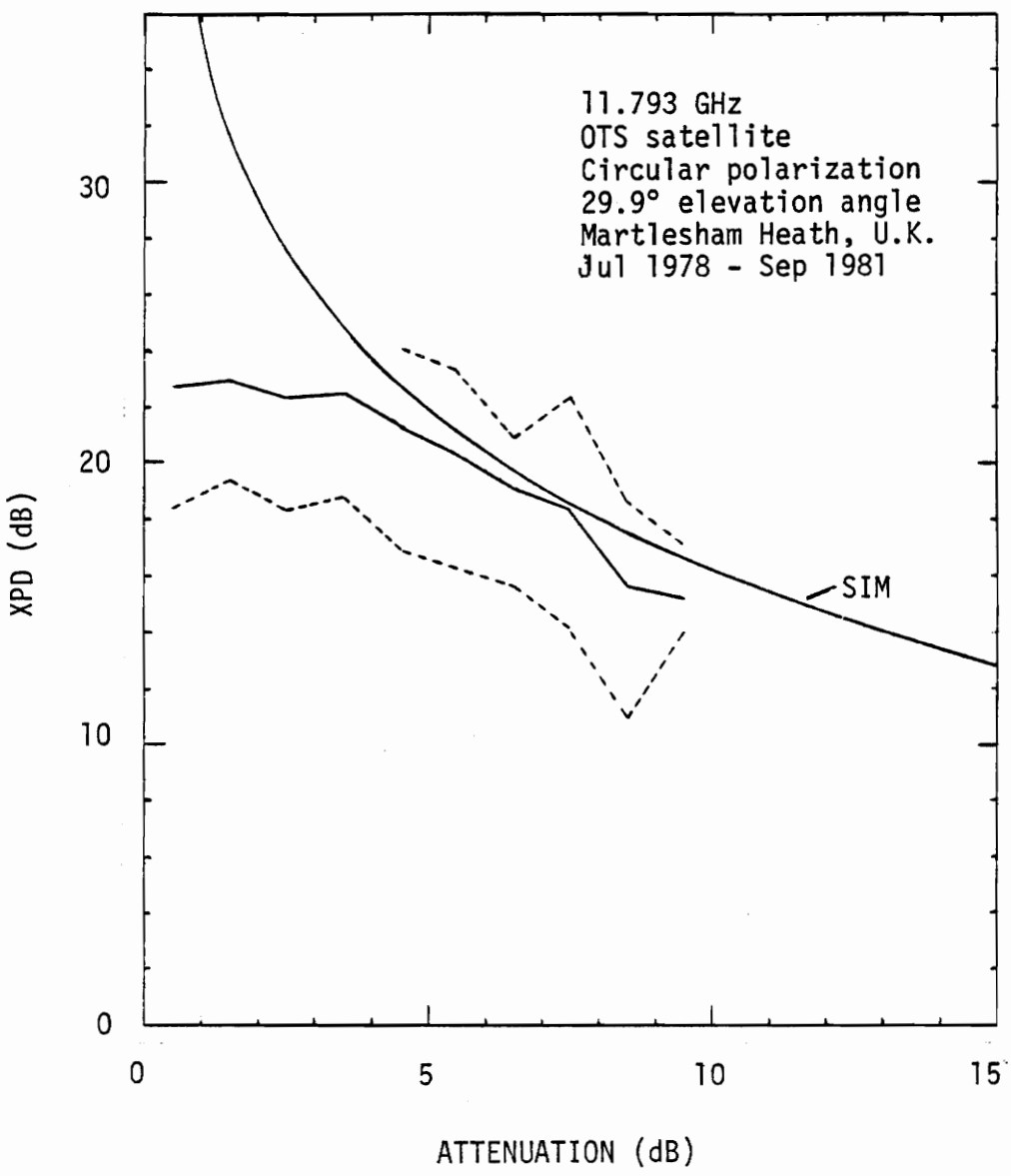

Figure 5-12. Comparison between simple isolation model and measured data set 9. Data quantities shown are: median (——), 10%,90% occurrence levels (----).

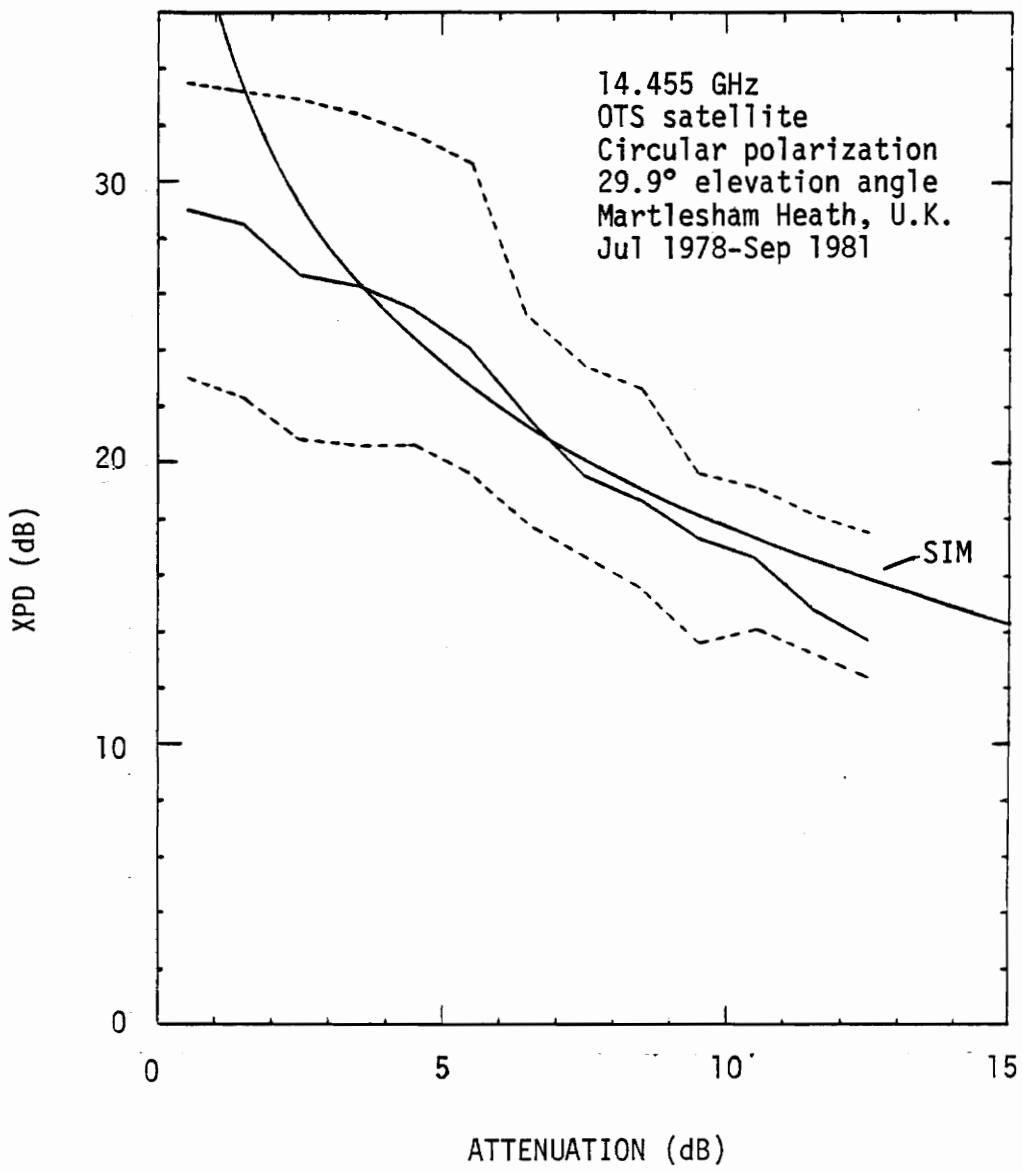

Figure 5-13. Comparison between simple isolation model and measured data set 10. Data quantities shown are: median (——), 10%,90% occurrence levels (----).

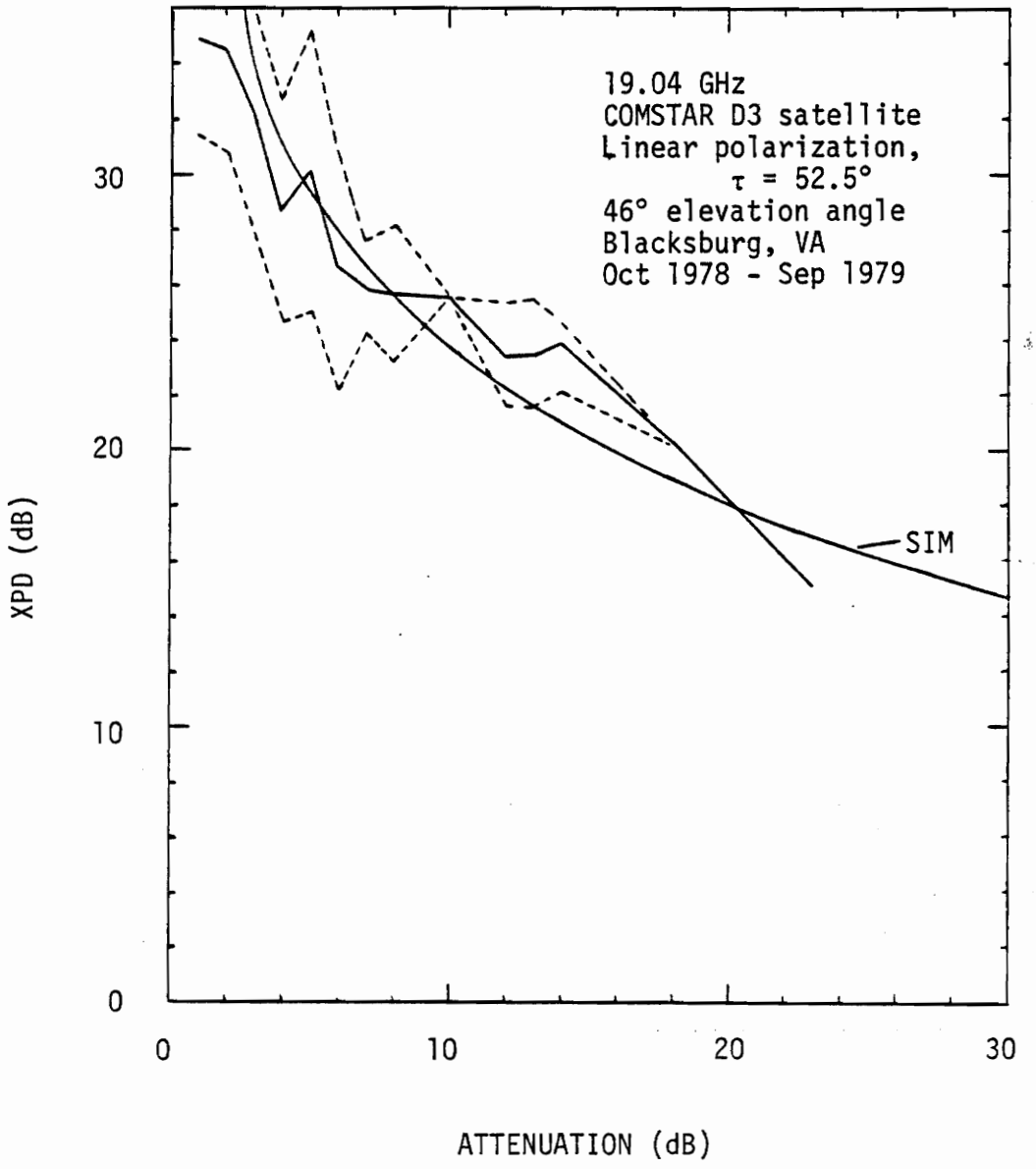

Figure 5-14. Comparison between simple isolation model and measured data set 11. Data quantities shown are: mean (——), mean and one standard deviation (----).

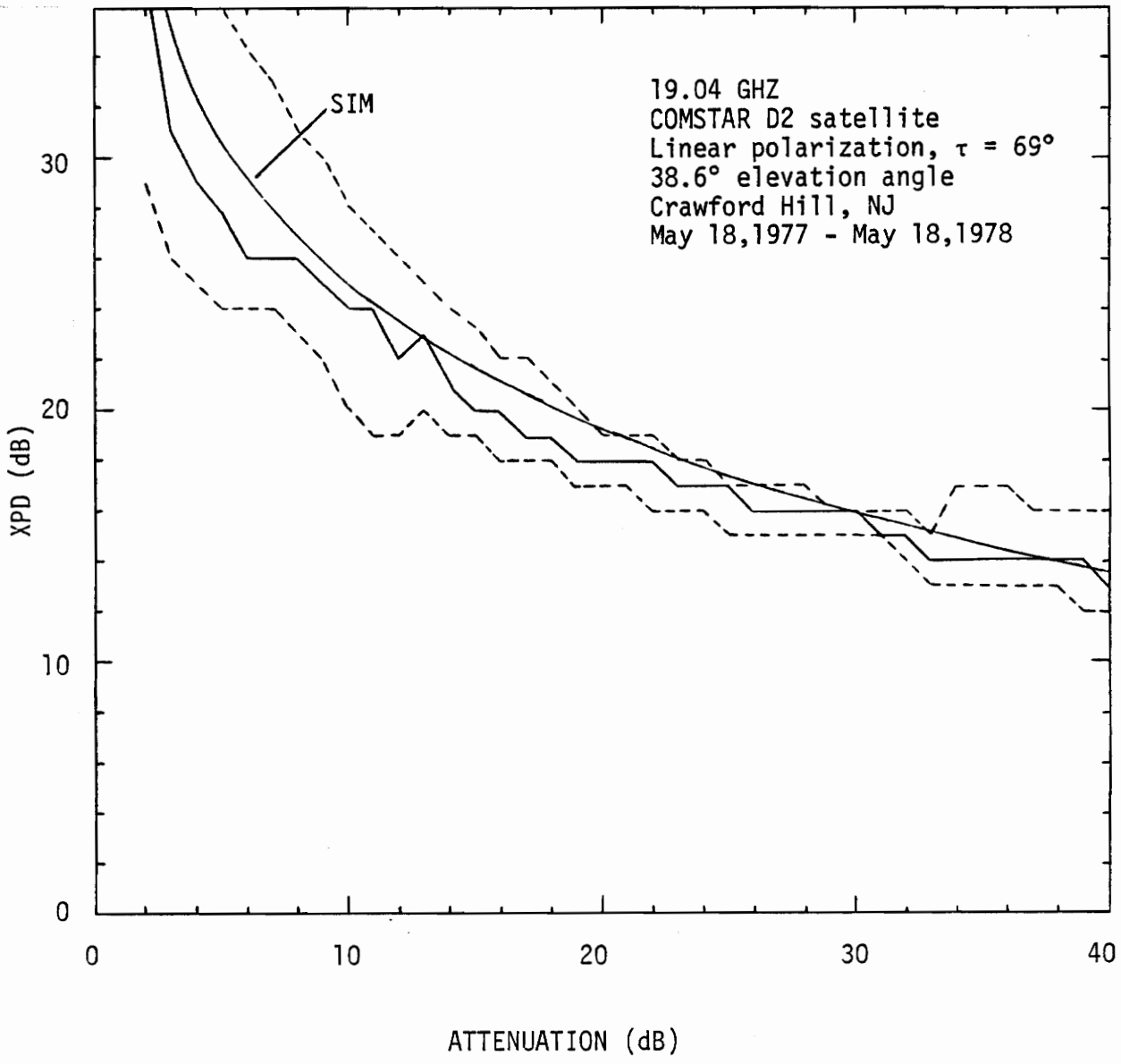

Figure 5-15. Comparison between simple isolation model and measured data set 12. Data quantities shown are: median (——), 10%,90% occurrence levels (----).

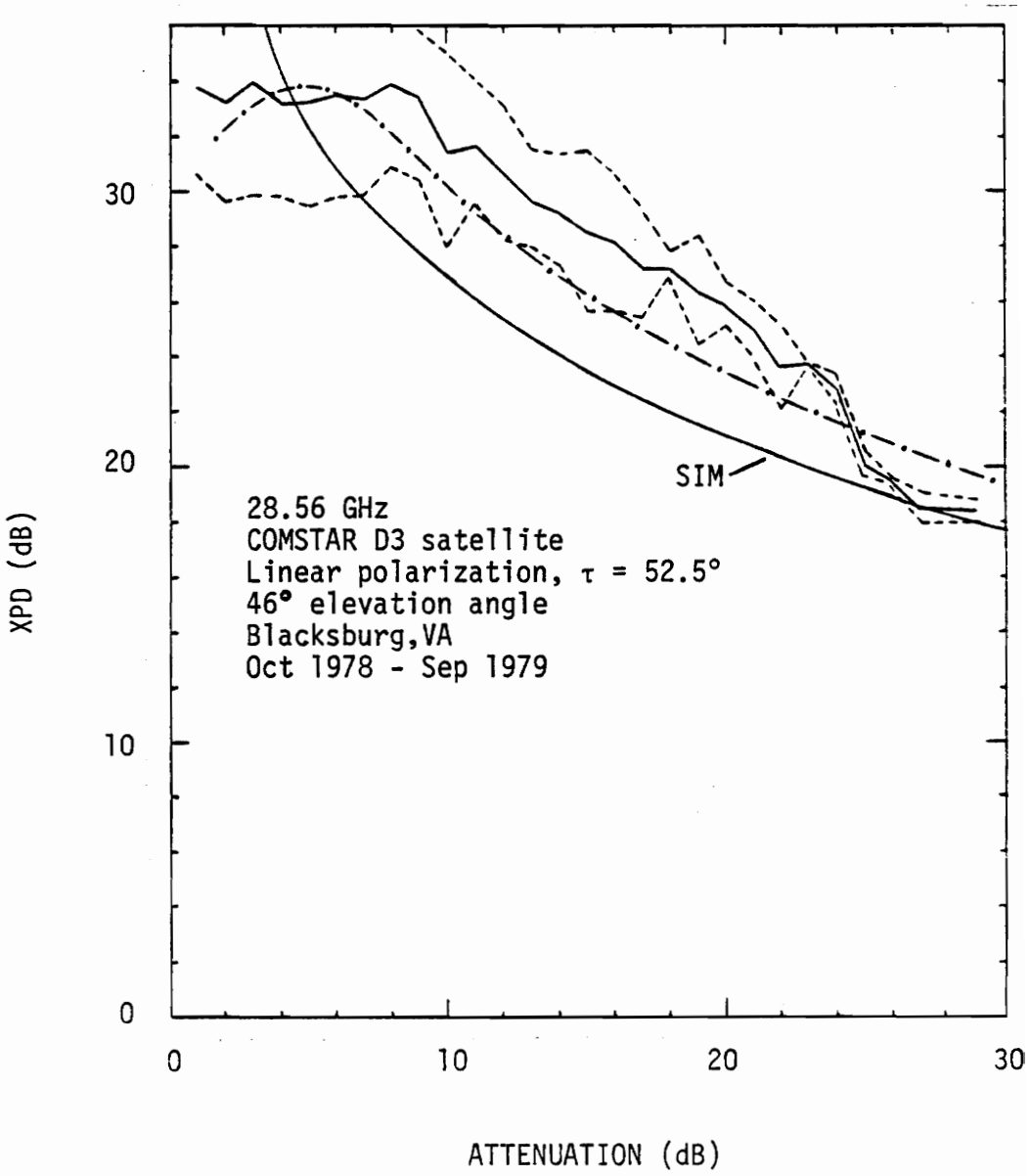

Figure 5-16. Comparison between simple isolation model and measured data set 13. Data quantities shown are: mean (——), mean and one standard deviation (----). Also predicted using the multiple scattering model with 30 dB receive antenna axial ratio is the curve (-·-·-).

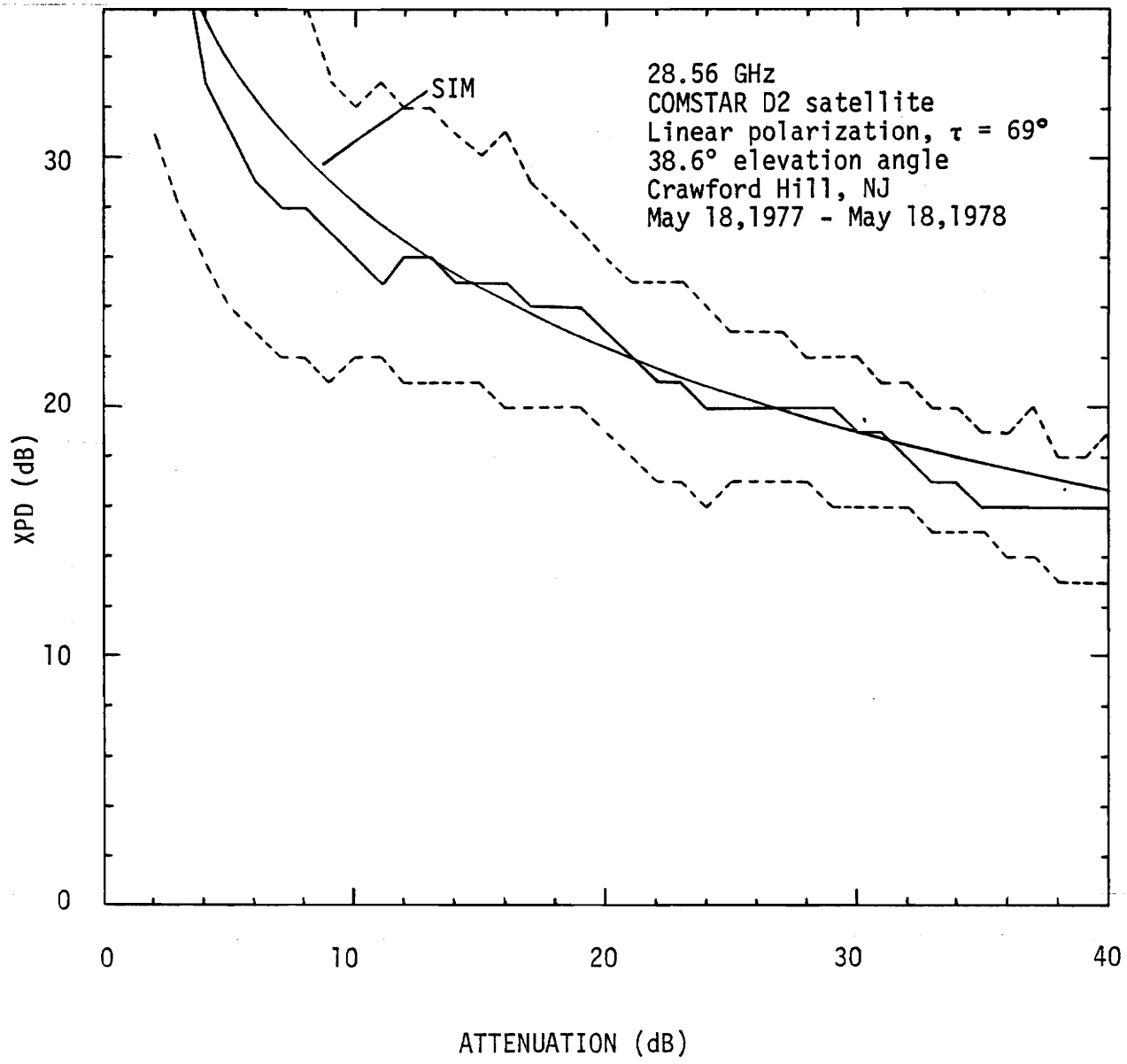

Figure 5-17. Comparison between the simple isolation model and measured data set 14. Data quantities shown are: median (——), 10%,90% occurrence levels (----).

parison of these data and predictions (including two other models in addition to SIM) is presented in the next section. Most deviations from SIM predictions are readily explained. For the cases of Martlesham Heath data (sets 1, 9, and 10 in Figs. 5-6, 12, and 13) and Blacksburg 28 GHz data (set 13, Figure 5-16) the data were apparently displaced due to antenna effects. This is illustrated by the dashed curve in Figure 5-16 which is a multiple scattering model calculation assuming an imperfect receiving antenna with a 30 dB axial ratio (this is consistent with clear weather observations). This calculation agrees quite well with the mean data.

A second source of deviation was the ice effects in the Blacksburg SIRIO data. This low elevation angle experiment had many ice events. These produced an experimental mean with lower XPD than predicted from SIM (see Figure 5-7 and 8).

5.6 EVALUATION OF PROPOSED MODELS

There are four simple models available to predict XPD as a function of attenuation (A). For ease of reference, we will call these models by the following: CCIR [1981], DHW [Dissanayake, Haworth, Watson, 1980], Chu [Chu,1982], and SIM (proposed Simple Isolation Model). All four models are for use in the frequency range from 10 to 30 GHz with addi-

CCIR

$$XPD = 30 \log(f) - 40 \log(\cos \varepsilon)$$

$$-10 \log \frac{1}{2}\left[1 - \cos(4\delta)\, e^{-p.0024\sigma_m^2}\right] + 0.0053\sigma_\theta^2$$

$$-V \log(A) \qquad (5.6\text{-}1)$$

$$\text{where } V = \begin{cases} 20 & 8 \le f \le 15 \text{ GHz} \\ 23 & 15 \le f \le 35 \text{ GHz} \end{cases}$$

DHW

$$XPD = B - 40 \log(\cos \varepsilon)$$

$$- 20 \log\left[\sin(2\delta)\right] + 0.0053\sigma_\theta^2$$

$$- 20 \log(A)$$

$$\text{where } B = 84.15 - 90.95\, xf^y + (52.56\, xf^y - 21.48) \log f \qquad (5.6\text{-}3)$$

$$\text{with } x = 0.625 \text{ and } y = 0.145$$

Chu

$$XPD_{CP} = 11.5 + 20 \log(f) - 40 \log(\cos \varepsilon) - 20 \log(A) \qquad (5.6\text{-}4)$$

$$XPD_{LP} = XPD_{CP} - 10 \log \frac{1}{2}\left[1 - \cos(4\delta)\, e^{-0.0024\sigma_m^2}\right]$$

$$\pm \frac{\Delta A}{2} \qquad (5.6\text{-}5)$$

$$\text{where } \Delta A = 0.15\, A \cos^2(\varepsilon) \cos(2\delta)$$

SIM

$$XPD = 9.5 + 17.3 \log(f) + 42 \log(\cos \varepsilon)$$
$$-10 \log \frac{1}{2} [1 - \cos(4\delta) e^{-0.0024\sigma_m^2}] + 0.0053\sigma_\theta^2$$
$$-20 \log(F_o) - 19 \log(A) \qquad (5.6\text{-}6)$$

tional frequncy application by the CCIR and DHW models below 10 GHz to 8 and 9 GHz, respectively. In addition, the four models follow the general form in (5.2-1), differing only by the analytic functions used to determine the coefficients U and V for a given set of site and system parameters. A summary of the four proposed models is given below. The angles ε, δ, σ_θ, and σ_m are in degrees, the frequency f in GHz, and XPD and A are in dB. The shape factor F_o in SIM is unitless.

Several characteristics should be noted about the analytical forms in the four models. We have found that the frequency term B in (5.6-3) for DHW may be accurately replaced with the curve fit

$$B = 8.16 + 21 \log (f) \qquad (5.6\text{-}7)$$

with $r^2 = 0.99$ for $10 \leqslant f \leqslant 30$ GHz. Including this substitution, the frequency dependence for the models are compared in Table 5-20.

Table 5-20

Frequency Dependent Terms for the Models

Model	Term
CCIR	30.0 log (f)
DHW	21.0 log (f)
Chu	20.0 log (f)
SIM	17.3 log (f)

The attenuation dependence is close to 20 log A in all models except for the additional linear polarization term $\Delta A/2$ in Chu's model where ΔA is the differential attenuation between quasi-vertical and quasi-horizontal polarizations. Plus and minus signs for $\Delta A/2$ in (5.6-5) should be applied to quasi-vertical and quasi-horizontal polarizations, respectively. The term, however, remains symmetric about $\delta = 45^\circ$ and has a minus sign for all values of δ.

The elevation angle dependence is close to 40 log ($\cos\varepsilon$) in all models.

The SIM model includes a variable fraction of oblate rain drops F_o while all others assume implicitly that F_o is 100%.

The rain parameters in all four models are taken to be constant for predictions under different system conditions. The parameter values suggested by the respective researchers of each model are given in Table 5-21.

Table 5-21

Suggested Rain Parameter Values

Model	$\langle\theta\rangle$	σ_θ	σ_m	F_o
CCIR	0°	0°	5°	
DHW	0°	25°		
Chu	0°		3°	
SIM	0°	12°	3°	0.65

It is interesting to note that an earlier form of Chu's model [Chu, 1980a, 1980b, 1981a] employed a term which was the same as the one used by SIM and DHW (DHW apparently borrowed their result). At that time, Chu proposed $\sigma_\theta = 30^\circ$ to be appropriate and added a 2 dB "correction factor" to his model to account for the discrepancy between his predicted results and measured data. He attributed this correction factor to the effects of ice depolarization. Later Chu [Chu, 1981b] presented the form (5.6-4,5) and stated that the constant term of value 11.5 dB is a linear function of σ_θ^2 but made no mention of the value he used for σ_θ.

The accuracy of the models is revealed by comparing model predictions to measured data. The technique chosen to accomplish the comparison was to sample the XPD data at equal attenuation increments and determine the deviation between

the predicted and measured XPD values. The deviation ΔX_i (in dB) is given by

$$\Delta X_i = XPD_i(\text{predicted}) - XPD_i(\text{measured}) \qquad (5.6\text{-}8)$$

In addition, the percent deviation was calculated for each sample value as

$$P_i = \frac{\Delta X_i}{XPD_i(\text{measured})} \cdot 100 \qquad (5.6\text{-}9)$$

The average (mean) and standard deviation (σ) of ΔX_i and P_i over each data set were calculated for all four models.

The data sets considered for the comparison are summarized in Table 4-1. Nine data sets were chosen from the 14 in the table. Data set numbers 2 and 3 were eliminated because ice effects were known to be significant for this unusually low elevation angle experiment and not one of the models presently account for this effect. Data set number 13 was eliminated because the antenna effects influencing the data illustrated in Section 5.5 were considered too severe. The simple models all assume near perfect antenna polarization characteristics. Data set pairs 4, 5 and 7, 8 respectively had overlapping time intervals for the same experiment and since the data did not significantly differ, only the longest data period was used in the comparison.

The measured data samples and the corresponding predicted XPD values are tabulated with the evaluation statistics for each data set in Tables 5-22 to 5-30. A summary of the statistics for each data set is given in Table 5-31. Predictions from all models were good, giving average deviations on the order of 1 dB, except for the CCIR model which showed larger deviations. One data set where the CCIR model performed poorly while the other models did well was data set number 11 at 19 GHz. Similar results occurred for data set number 12 at 19 GHz. The progressive increase in the deviations as the attenuation increased indicates that the slope coefficient (V) on Log (A) term is too large in the CCIR model. The value V=23 in the 20 GHz frequency range is quite different from the other models which have values of 19 and 20. In accordance with this modeling difference, the CCIR model had the largest value of σ at 28 GHz.

From the statistics in Table 5-31 the average value of the magnitude of the mean and standard deviations for the data sets were determined and are given in Table 5-32. This set of statistics reflects the overall agreement between the models for the data sets examined. From Table 5-32 we see similar performance between the SIM, DHW, and Chu models and a more obvious degraded performance by the CCIR model. The SIM model showed a slightly larger average deviation than

Table 5-22

Evaluation Statistics for the Model Predictions for 11.575 GHz at Martlesham Heath, U.K. (Data Set Number 1)

Measured Data		Predictions											
		SIM			CCIR			DHW			Chu		
	median		Deviation			Deviation			Deviation			Deviation	
A	XPD	XPD	ΔX_i	P_i	XPD	ΔX_i	P_i	XPD	ΔX_i	P_i	XPD	ΔX_i	P_i
3.5	32.5	32.4	-0.1	-0.3	30.4	-2.1	-6.5	33.0	0.5	1.5	31.9	-0.6	-1.8
4.5	31.8	30.3	-1.5	-4.7	28.2	-3.6	-11.3	30.8	-1.0	-3.1	29.7	-2.1	-6.6
5.5	30.8	28.7	-2.1	-6.8	26.5	-4.3	-14.0	29.0	-1.8	-5.8	27.9	-2.9	-9.4
6.5	29.1	27.3	-1.8	-6.2	25.1	-4.0	-13.7	27.6	-1.5	-5.2	26.4	-2.7	-9.3
7.5	27.5	26.1	-1.4	-5.1	23.8	-3.7	-13.5	26.3	-1.2	-4.4	25.1	-2.4	-8.7
8.5	25.8	25.1	-0.7	-2.7	22.7	-3.1	-12.0	25.2	-0.6	-2.3	24.0	-1.8	-7.0
9.5	25.8	24.2	-1.6	-6.2	21.8	-4.0	-15.5	24.3	-1.5	-5.8	23.0	-2.8	-10.9
10.5	25.3	23.4	-1.9	-7.5	20.9	-4.4	-17.4	23.4	-1.9	-7.5	22.0	-3.3	-13.0
		avg.	-1.39	-4.94	avg	-4.29	-12.99	avg	-1.13	-4.08	avg	-2.33	-8.34
		σ	0.67	2.39	σ	1.83	3.24	σ	0.78	2.78	σ	0.84	3.34

Table 5-23

Evaluation Statistics for the Model Predictions for 11.7 GHz at Austin, TX
(Data Set Number 5)

Measured Data		PREDICTIONS											
		SIM			CCIR			DHW			Chu		
			Deviation			Deviation			Deviation			Deviation	
A	median XPD	XPD	ΔX_i	P_i	XPD	ΔX_i	P_i	XPD	ΔX_i	P_i	XPD	ΔX_i	P_i
2	33	34.8	1.8	5.5	33.8	0.8	2.4	35.1	2.1	6.4	34.5	1.5	4.5
4	30	29.1	-0.9	-3.0	27.8	-2.2	-7.3	29.1	-0.9	-3.0	28.5	-1.5	-5.0
6	27	25.8	-1.2	-4.4	24.3	-2.7	-10.0	25.6	-1.4	-5.2	25.0	-2.0	-7.4
8	25	23.4	-1.6	-6.4	21.8	-3.2	-12.8	23.1	-1.9	-7.6	22.5	-2.5	-10.0
10	22	21.5	-0.5	-2.3	19.9	-2.1	-9.5	21.1	-0.9	-4.1	20.5	-1.5	-6.8
12	21	20.0	-1.0	-4.8	18.3	-2.7	-12.9	19.6	-1.4	-6.7	19.0	-2.0	-9.5
14	19	18.8	-0.2	-1.1	16.9	-2.1	-11.1	18.2	-0.8	-4.2	17.6	-1.4	-7.4
16	18	17.7	-0.3	-1.7	15.8	-2.2	-11.7	17.1	-0.9	-5.0	16.5	-1.5	-8.3
18	18	16.7	-1.3	-7.2	14.8	-3.2	-17.8	16.0	-2.0	-11.1	15.4	-2.6	-14.4
20	17	15.8	-1.2	-7.1	13.8	-3.2	-18.8	15.1	-1.9	-11.2	14.5	-2.5	-14.7
		avg	-0.64	-3.25	avg	-2.28	-10.95	avg	-1.00	-5.17	avg	-1.60	-7.90
		σ	0.97	3.78	σ	1.18	5.88	σ	1.18	4.95	σ	1.18	5.37

Table 5-24

Evaluation Statistics for the Model Predictions for 11.7 GHz at Blacksburg, VA
(Data Set Number 6)

Measured Data		PREDICTIONS											
		SIM			CCIR			DHW			Chu		
	(mean)		Deviation			Deviation			Deviation			Deviation	
A	XPD	XPD	ΔX_i	P_i	XPD	ΔX_i	P_i	XPD	ΔX_i	P_i	XPD	ΔX_i	P_i
2	32.2	30.0	-2.2	6.8	29.2	-3.0	-9.3	30.5	-1.7	5.3	29.9	-2.3	-7.1
4	27.6	24.3	-3.3	12.0	23.2	-4.4	-15.9	24.5	-3.1	-11.2	23.9	-3.7	-13.4
6	23.9	20.9	-3.0	12.6	19.7	-4.2	-17.6	21.0	-2.9	-12.1	20.4	-3.5	-14.6
8	22.6	18.5	-4.1	18.1	17.2	-5.4	-23.9	18.5	-4.1	-18.1	17.9	-4.7	-20.8
10	20.2	16.7	-3.5	17.3	15.2	-5.0	-24.8	16.5	-3.7	-18.3	15.9	-4.3	-21.3
12	18.5	15.2	-3.3	17.8	13.7	-4.8	-25.9	14.9	-3.6	-19.5	14.3	-4.2	-22.7
14	16.2	13.9	-2.3	14.2	12.3	-3.9	-24.1	13.6	-2.6	-16.0	13.0	-3.2	-19.8
16	15.6	12.8	-2.8	17.9	11.2	-4.4	-28.2	12.4	-3.2	-20.5	11.8	-3.8	-24.4
18	13.5	11.8	-1.7	12.6	10.1	-3.4	-25.2	11.4	-2.1	-15.6	10.8	-2.7	-20.0
20	13.5	11.0	-2.5	18.5	9.2	-4.3	-31.9	10.5	-3.0	-22.2	9.9	-3.6	-26.7
24	12.9	9.5	-3.4	26.4	7.6	-5.3	-41.1	8.9	-4.0	-31.0	8.3	-4.6	-35.7
		avg	-2.92	15.84	avg	-4.37	-24.35	avg	-3.09	-16.29	avg	-3.69	-14.10
		σ	0.70	5.04	σ	0.75	8.36	σ	0.75	8.93	σ	0.75	17.41

Table 5-25

Evaluation Statistics for the Model Predictions for 11.7 GHz at Crawford Hill N.J. (Data Set Number 8)

Measured Data		PREDICTIONS											
		SIM			CCIR			DHW			Chu		
	(median)		Deviation			Deviation			Deviation			Deviation	
A	XPD	XPD	ΔX_i	P_i	XPD	ΔX_i	P_i	XPD	ΔX_i	P_i	XPD	ΔX_i	P_i
2	23	28.9	5.9	25.7	28.2	5.2	22.6	29.5	6.5	28.3	28.8	5.8	25.2
4	21	23.2	2.2	10.5	22.1	1.1	5.2	23.4	2.4	11.4	22.8	1.8	8.6
6	19	19.8	0.8	4.2	18.6	-0.4	-2.1	19.9	0.9	4.7	19.3	0.3	1.6
8	18	17.4	-0.6	-3.3	16.1	-1.9	-10.6	17.4	-0.6	-3.3	16.8	-1.2	-6.7
10	15	15.6	0.6	4.0	14.2	-0.8	-5.3	15.5	0.5	3.3	14.9	-0.1	-0.7
12	14	14.1	0.1	0.7	12.6	-1.4	-10.0	13.9	0.1	0.7	13.3	-0.7	-5.0
14	12	12.8	0.8	6.7	11.3	-0.7	-5.8	12.6	0.6	5.0	11.9	-0.1	-0.8
16	11	11.7	0.7	6.4	10.1	-0.9	-8.2	11.4	0.4	3.6	10.8	-0.2	-1.8
18	9	10.7	1.7	18.9	9.1	0.1	1.1	10.4	1.4	15.6	9.8	0.8	8.9
20	9	9.9	0.9	10.0	8.2	-0.8	-8.9	9.5	0.5	5.6	8.8	-0.2	-2.2
22	11	9.1	-1.9	-17.3	7.3	-3.7	-33.6	8.6	-2.4	-21.8	8.0	-3.0	-27.3
24	10	8.4	-1.6	-16.0	6.6	-3.4	-34.0	7.9	-2.1	21.0	7.3	-2.7	-27.0
		avg	0.80	4.21	avg	-0.63	-7.47	avg	0.68	2.68	avg	0.04	-2.27
		σ	2.01	12.44	σ	2.28	15.31	σ	2.27	13.88	σ	2.25	14.40

Table 5-26

Evaluation Statistics for the Model Predictions for 11.793 GHz at Martlesham Heath, U.K. (Data Set Number 9)

Measured Data		PREDICTIONS											
		SIM			CCIR			DHW			Chu		
	(median)		Deviation			Deviation			Deviation			Deviation	
A	XPD	XPD	ΔX_i	P_i	XPD	ΔX_i	P_i	XPD	ΔX_i	P_i	XPD	ΔX_i	P_i
3.5	22.5	24.8	2.3	10.2	23.9	1.4	6.2	25.1	2.6	11.6	24.5	2.0	8.9
4.5	21.3	22.7	1.4	6.6	21.7	0.4	1.9	22.9	1.6	7.5	22.3	1.0	4.7
5.5	20.3	21.1	0.8	3.9	20.0	-0.3	-1.5	21.2	0.9	4.4	20.6	0.3	1.5
6.5	19.1	19.7	0.6	9.2	18.5	-0.6	-3.1	19.7	0.6	3.1	19.2	0.1	0.5
7.5	18.3	18.5	0.2	2.7	17.3	-1.0	-5.5	18.5	0.2	1.1	17.9	-0.4	-2.2
8.5	15.6	17.5	1.9	12.2	16.2	0.6	3.8	17.4	1.8	11.5	16.8	1.2	7.7
9.5	15.2	16.6	1.4	9.2	15.2	0.0	0.0	16.5	1.3	8.6	15.9	0.7	4.6
		avg	1.23	7.71	avg	0.07	0.26	avg	1.29	6.83	avg	0.70	3.67
		σ	0.74	3.46	σ	0.81	4.04	σ	0.81	4.10	σ	0.79	3.97

Table 5-27

Evaluation Statistics for the Model Predictions for 14.455 GHz at Martlesham Heath, U.K. (Data Set Number 10)

Measured Data		PREDICTIONS											
		SIM			CCIR			DHW			Chu		
	(median)		Deviation			Deviation			Deviation			Deviation	
A	XPD	XPD	ΔX_i	P_i	XPD	ΔX_i	P_i	XPD	ΔX_i	P_i	XPD	ΔX_i	P_i
3.5	26.3	26.3	0	0	26.5	0.2	0.8	26.6	0.3	1.1	26.3	0	0
4.5	25.5	24.3	-1.2	-4.7	24.4	-1.1	-4.3	24.4	-1.1	-4.3	24.1	-1.4	-5.5
5.5	24.0	22.6	-1.4	-5.8	22.6	-1.4	-5.8	22.6	-1.4	-5.8	22.4	-1.6	-6.7
6.5	21.6	21.2	-0.4	-1.9	21.2	-0.4	-1.9	21.2	-0.4	-1.9	20.9	-0.7	-3.2
7.5	19.5	20.1	0.6	3.1	19.9	0.4	2.1	20.0	0.5	2.6	19.7	0.2	3.6
8.5	18.7	19.0	0.3	1.6	18.8	0.1	0.5	18.9	0.2	1.1	18.6	0.1	0.5
9.5	17.3	18.1	0.8	4.6	17.9	0.6	3.5	17.9	0.6	3.5	17.6	0.3	1.7
10.5	16.6	17.3	0.9	5.4	17.0	0.4	2.4	17.0	0.4	2.4	16.8	0.2	1.2
11.5	14.8	16.5	1.7	11.5	16.2	1.4	9.5	16.2	1.4	9.5	16.0	1.2	8.1
12.5	13.7	15.8	2.1	15.3	15.5	1.8	13.1	15.5	1.8	13.1	15.2	1.5	10.9
		avg	0.34	2.91	avg	0.20	1.99	avg	0.23	2.13	avg	-0.02	1.06
		σ	1.14	6.70	σ	0.99	5.79	σ	0.99	5.77	σ	0.99	5.54

Table 5-28

Evaluation Statistics for the Model Predictions for 19.04 GHz at Crawford Hill, NJ (Data Set Number 11)

Measured Data		PREDICTIONS											
		SIM			CCIR			DHW			Chu		
	median		Deviation			Deviation			Deviation			Deviation	
A	XPD	XPD	ΔX_i	P_i	XPD	ΔX_i	P_i	XPD	ΔX_i	P_i	XPD	ΔX_i	P_i
2	37	38.4	1.4	3.8	39.2	2.2	5.9	39.1	2.1	5.7	38.8	1.8	4.9
4	29	32.7	3.7	12.8	32.3	3.3	11.4	33.0	4.0	13.8	32.7	3.7	12.8
6	26	29.3	3.3	12.7	28.2	2.2	8.5	29.5	3.5	13.5	29.1	3.1	11.9
8	26	27.0	1.0	3.8	25.4	-0.6	-2.3	27.0	1.0	3.8	26.5	0.5	1.9
10	24	25.1	1.1	4.6	23.1	-0.9	-3.8	25.1	1.1	4.6	24.5	0.5	2.1
12	22	23.6	1.6	7.3	21.3	-0.7	-3.2	23.5	1.5	6.8	22.9	0.9	4.1
14	21	22.4	1.4	6.7	19.8	-1.2	-5.7	22.2	1.2	5.7	21.5	0.5	2.4
16	20	21.3	1.3	6.5	18.4	-1.6	-8.0	21.0	1.0	5.0	20.2	0.2	1.0
18	19	20.3	1.3	6.8	17.3	-1.7	-8.9	20.0	1.0	5.3	19.1	0.1	0.5
20	18	19.4	1.4	7.8	16.2	-1.8	-10.0	19.1	1.1	6.1	18.2	0.2	1.1
22	18	18.6	1.6	8.9	15.3	-2.7	-15.0	18.2	0.2	1.1	17.3	-0.7	-3.9
24	17	17.9	1.9	11.2	14.4	-2.6	-15.3	17.5	0.5	2.9	16.4	-0.6	-3.5
26	16	17.2	1.2	7.5	13.6	-2.4	-15.0	16.8	0.8	5.0	15.7	-0.3	-1.9
28	16	16.6	0.6	3.8	12.8	-3.2	-20.0	16.1	0.1	0.6	15.0	-1.0	-6.3
30	16	16.1	0.1	0.6	12.2	-3.8	-23.0	15.5	-0.5	-3.1	14.3	-1.7	-10.6
32	15	15.5	0.5	3.3	11.5	-3.5	-23.3	15.0	0.0	0.0	13.7	-1.3	-8.7
34	14	15.0	1.0	7.1	10.9	-3.1	-22.1	14.4	0.4	2.9	13.1	-0.9	-6.4
36	14	14.6	0.6	1.7	10.3	-3.7	-26.4	14.0	0.0	0.0	12.5	-1.5	-10.7
38	14	14.1	0.1	0.7	9.8	-4.2	-30.0	13.5	-0.5	-3.6	12.0	-2.0	-14.3
40	14	13.7	-0.3	-2.1	9.3	-4.7	-33.6	13.0	-1.0	-7.1	11.5	-2.5	-17.9
		avg	1.24	5.78	avg	-1.74	-11.99	avg	0.88	3.45	avg	-0.05	-2.08
		σ	0.96	3.98	σ	2.20	12.64	σ	1.24	5.07	σ	1.59	8.00

Table 5-29

Evaluation Statistics for the Model Predictions for 19.04 GHz at Blacksburg, VA (Data Set Number 12)

Measured Data		PREDICTIONS											
		SIM			CCIR			DHW			Chu		
	(mean)		Deviation			Deviation			Deviation			Deviation	
A	XPD	XPD	ΔX_i	P_i	XPD	ΔX_i	P_i	XPD	ΔX_i	P_i	XPD	ΔX_i	P_i
2	34.5	37.0	2.5	7.3	37.9	3.4	9.9	37.6	3.1	9.0	37.4	2.9	8.4
4	28.7	31.3	2.6	9.1	31.0	2.3	8.0	31.6	2.9	10.1	31.3	2.6	9.1
6	26.6	28.0	1.4	5.3	26.9	0.3	1.1	28.1	1.5	5.6	27.8	1.2	4.5
8	25.7	25.6	-0.1	-0.4	24.1	-1.6	-6.2	25.6	-0.1	-0.4	25.3	-0.4	-1.6
10	25.5	23.8	-1.7	-6.7	21.8	-3.7	-14.5	23.6	-1.9	-7.5	23.3	-2.2	-8.6
12	23.4	22.3	-1.1	-9.2	20.0	-3.4	-14.5	22.0	-1.4	-6.0	21.7	-1.7	-7.3
14	23.9	21.0	-2.9	-12.1	18.5	-5.4	-22.6	20.7	-3.2	-13.4	20.4	-3.5	-14.6
		avg	0.10	-0.96	avg	-1.16	-5.54	avg	0.13	-0.37	avg	-0.16	-1.44
		σ	2.14	8.50	σ	3.28	12.37	σ	2.45	8.99	σ	2.47	9.15

Table 5-30

Evaluation Statistics for the Model Predictions for 28.56 GHz at Crawford Hill, NJ (Data Set Number 14)

Measured Data		PREDICTIONS											
		SIM			CCIR			DHW			Chu		
	median		Deviation			Deviation			Deviation			Deviation	
A	XPD	XPD	ΔX_i	P_i	XPD	ΔX_i	P_i	XPD	ΔX_i	P_i	XPD	ΔX_i	P_i
2													
4	33	35.7	2.7	8.2	37.6	4.6	13.9	37.3	4.3	13.0	36.2	3.2	9.7
6	29	32.4	3.4	11.7	33.5	4.5	15.5	33.8	4.8	16.6	32.6	3.6	12.4
8	28	30.0	2.0	7.1	30.6	2.6	9.3	31.3	3.3	11.8	30.1	2.1	7.5
10	26	28.2	2.2	8.5	28.4	2.4	9.2	29.3	3.3	12.7	28.0	2.0	7.7
12	26	26.7	0.7	2.7	26.6	0.6	2.3	27.7	1.7	6.5	26.4	0.4	1.5
14	25	25.4	0.4	1.6	25.1	0.1	0.4	26.4	1.4	5.6	25.0	0.0	0.0
16	25	24.3	-0.7	-2.8	23.7	-1.3	-5.2	25.2	0.2	0.8	23.8	-1.2	-4.8
18	24	23.3	-0.7	-2.9	22.5	-1.5	-6.3	24.2	0.2	0.8	22.7	-1.3	-5.4
20	23	22.5	-0.5	-2.2	21.5	-1.5	-6.5	23.3	0.3	1.3	21.7	-1.3	-5.7
22	21	21.7	0.7	3.3	20.5	-0.5	-2.4	22.5	1.5	7.1	20.8	-0.2	-1.0
24	20	21.0	1.0	5.0	19.7	-0.3	-1.5	21.7	1.7	8.5	20.0	0.0	0.0
26	20	20.3	0.3	1.5	18.9	-1.1	-5.5	21.0	1.0	5.0	21.5	1.5	7.5
28	20	19.7	-0.3	-1.5	18.1	-1.9	-9.5	20.4	0.4	2.0	18.8	-1.2	-6.0
30	19	19.1	0.1	0.5	17.4	-1.6	-8.4	19.8	0.8	4.2	17.8	-1.2	-6.3
32	18	18.6	0.6	3.3	16.8	-1.2	-6.7	19.2	1.2	6.7	17.2	-0.8	-4.4
34	17	18.1	1.1	6.5	16.2	-0.8	-4.7	18.7	1.7	10.0	16.6	-0.4	-2.4
36	16	17.6	1.6	10.0	15.6	-0.4	-2.5	18.2	2.2	13.8	16.0	0.0	0.0
38	16	17.2	1.2	7.5	15.1	-0.9	-5.6	17.7	1.7	10.6	15.5	-0.5	-3.1
40	16	16.7	0.7	4.4	14.6	-1.4	-8.8	17.3	1.3	8.1	15.0	-1.0	-6.3
		avg	0.81	3.81	avg	0.02	-1.21	avg	1.74	7.64	avg	0.19	0.71
		σ	1.13	4.42	σ	2.02	7.72	σ	1.33	4.69	σ	1.55	6.00

Table 5-31

Summary of Evaluation Statistics

Data Set No.	SIM				CCIR				DHW				Chu			
	ΔX_i		P_i		ΔX_i		P_i		ΔX_i		P_i		ΔX_i		P_i	
	avg	σ	avg	σ	avg	σ	avg	σ	avg	σ	avg	σ	avg	σ	avg	σ
1	-1.39	0.67	-4.94	2.39	-4.29	1.83	-12.99	3.24	-1.13	0.78	-4.08	2.78	-2.33	0.84	-8.34	3.34
5	-0.64	0.97	-3.25	3.78	-2.28	1.18	-10.95	5.88	-1.00	1.18	-5.17	4.95	-1.60	1.18	-7.90	5.37
6	-2.92	0.70	15.84	5.04	-4.37	0.75	-24.35	8.36	-3.09	0.75	-16.29	8.93	-3.69	0.75	-14.10	17.41
8	0.80	2.01	4.21	12.44	-0.63	2.28	-7.47	15.31	0.68	2.27	2.68	13.88	0.04	2.25	-2.27	14.40
9	1.23	0.74	7.71	3.46	0.07	0.81	0.26	4.04	1.29	0.81	6.83	4.10	0.70	0.79	3.67	3.97
10	0.34	1.14	2.91	6.70	0.20	0.99	1.99	5.79	0.23	0.99	2.13	5.77	-0.02	0.99	1.06	5.54
11	1.24	0.96	5.78	3.98	-1.74	2.20	-11.99	12.64	0.88	1.24	3.45	5.07	-0.05	1.59	-2.08	8.00
12	0.10	2.14	-0.96	8.50	-1.16	3.28	-5.54	12.37	0.13	2.45	-0.37	8.99	-0.16	2.47	-1.44	9.15
14	0.81	1.13	3.81	4.42	0.02	2.02	-1.21	7.72	1.74	1.33	7.64	4.69	0.19	1.55	0.71	6.00

Table 5-32

Average Evaluation Statistics for the Models

MODEL	ΔX		P	
	avg	σ	avg	σ
SIM	1.06	1.16	5.49	5.63
CCIR	1.64	1.70	9.44	8.37
DHW	1.13	1.31	5.40	6.57
Chu	0.98	1.38	4.62	8.13

the Chu model but a tighter bound on differences. The DHW model performed similar to the SIM model with an average deviation slightly larger than SIM but a bound tighter than the Chu model.

Although the number of data sets is relatively small compared to that available for attenuation modeling, they do span the frequency range of interest for a variety of system conditions. The final results indicate good performance by the SIM, Chu and DHW models and a less accurate performance by the CCIR model. The technique used to develop the SIM model was more rigorous than the others. This consideration in addition to the added flexibility of the shape factor term in the model suggests that some improvements can be made to the CCIR model. In particular,

$$30 \log(f)-40 \log(\cos\varepsilon)-V \log(A) \qquad (5.6\text{-}10)$$

of the current CCIR model should be replaced by

$$9.5+17.3 \log(f)-42 \log(\cos\varepsilon)-20 \log(F_o)-19 \log(A)$$

where $F_o = 0.65$.

5.7 DEGRADATION OF CARRIER TO NOISE RATIO ON DUAL POLARIZED DIGITAL COMMUNICATION LINKS

Reliability of the dual polarized satellite communication link is affected by the degradation of the carrier-to-noise ratio (CNR) due to cochannel fading and cochannel crosspolar interference. To accurately measure the fade margin required for a specified reliability it is necessary to examine the statistics of simultaneous pairs of attenuation (A) and cross polarization discrimination (XPD), the so-called joint statistics.

Two techniques for developing the joint statistics of XPD and A were discussed in Section 4.4. The definition that provides a more complete description of the simultaneous occurrence of the XPD and A data pairs was given in (4.4-3). This was defined as the fraction (or percent) time attenuation is greater than a fixed value a and XPD is less than a fixed value x ($P(A > a, X < x)$). The method chosen to represent the joint distribution is an XPD vs A plot with contours of constant joint percentage of time.

The minimum XPD determined for all A values over a particular joint statistics contour is the value determined from the marginal statistics for the same level of reliability as the contour. Similarly, the maximum A on a given contour is the value determined from the marginal statistics for the same reliability. However, XPD may be greater than X_{min} for other values of $A < A_{max}$.

The locus of (A, X) pairs where $X > X_{min}$ and $A < A_{max}$ occur simultaneously for a specified reliability defines the knee region of the contour for A close to A_{max}. We will show that the region of the knee defines the most significant values of XPD and A when determining the CNR margin for a specified reliability for a digital phase shift keying (PSK) system.

Expressions have been derived by Prabhu [1969] and Rosenbaum [1968] for the symbol error probability on a digital system using coherent PSK in terms of the carrier to noise ratio (CNR) and the carrier to interference ratio (CIR). The CIR corresponds to XPD since the only source of interference considered here is due to depolarization. For system calculations it is convenient to express the effects of interference as a degradation of a required CNR. The CNR degradation is defined as the difference between the CNR required to achieve a specified symbol probability of error for a given CIR and the CNR for the same symbol probability of error in the absence of the interference. The results of Prabhu [1969] and Rosenbaum [1968] show that the CNR degradation is a function of the specified symbol probability (or CNR) as well as CIR and the number of phase states M. Because calculation of the exact relationship for the CNR degradation is cumbersome, an upper bound on the CNR degrada-

tion was developed by Castle et al., [1979] using the upper bound on the symbol error probability developed by Juroshek [1977]. The upper bound on the CNR degradation is independent of the CNR and is a function of only the number of phase states in the M-ary PSK system and the CIR (taken here as XPD). The general form of the upper bound D_{ub} (in dB) is

$$D_{ub} = -20 \log \left[1 - \frac{R}{\sin (\pi/M)} \right] \qquad (5.7\text{-}1a)$$

where

$$R = 10^{-XPD/20} \qquad (5.7\text{-}1b)$$

with XPD in dB.

The CNR degradation may be used with the cochannel fade (or attenuation) A to express an effective attenuation [Castle et al., 1979] as

$$A_{eff} = A + D \qquad (5.7\text{-}2)$$

Where D is the degradation (in dB) determined using the exact expressions of symbol error probability. For a dual polarized system the degraded CNR due to cochannel fading and cochannel interference is the clear weather carrier to noise ration, CNR_o, reduced by the effective attenuation:

$$CNR = CNR_o - A_{eff}$$

$$CNR = CNR_o - A - D \qquad (5.7\text{-}3)$$

where all quantities are in dB.

We may define the system margin for propagation effects as

$$MAR = CNR_o - CNR \qquad (5.7\text{-}4)$$

where CNR is taken as the minimum CNR with which the system may operate. Substituting (5.7-3) into (5.7-4) gives

$$MAR = A + D \qquad (5.7\text{-}5)$$

again with all quantities in dB. Using (5.7-5) for fixed values of MAR, the pairs of A and D (or XPD) values equaling MAR generate constant MAR contours in the XPD vs A plane. Exact calculation of D using (5.7-5) will yield an accurate margin value. However, exact calculations of D (as a function of XPD, M, CNR) is rather complicated. For simplicity we shall use the simpler upper bound solution given in (5.7-1). This is justified by comparing the CNR degradation for a QPSK system (M=4) calculated using the upper bound and the exact values for different values of CNR and XPD shown in Table 5-33. We see very little difference between the upper bound and exact resuls for CNR = 25 dB. However, the difference increases as the CNR and XPD decrease. For rain depolarization, XPD decreases as A increases (or CNR de-

Table 5-33

Exact Values and Upper Bound of the CNR Degradation for a QPSK System as a Function of the CIR

	CNR DEGRADATION D					
		Exact (Prabhu)				
CIR (XPD)	Upper Bound (Castle et al.)	$(CNR)_o$ - A = 25 dB	$(CNR)_o$ - A = 20 dB	$(CNR)_o$ - A = 15 dB	$(CNR)_o$ - A = 10 dB	$(CNR)_o$ - A = 5 dB
5 dB	13.78 dB	13.37 dB	12.69 dB	11.28 dB	8.96 dB	6.42 dB
6	10.72	10.50	10.11	9.18	7.44	5.41
7	8.68	8.54	8.28	7.61	6.23	4.58
8	7.19	7.09	6.90	6.38	5.26	3.90
9	6.05	5.98	5.82	5.40	4.46	3.33
10	5.15	5.09	4.96	4.61	3.79	2.85
11	4.42	4.36	4.26	3.95	3.24	2.46
12	3.81	3.77	3.67	3.40	2.77	2.12
13	3.31	3.27	3.18	2.94	2.37	1.83
14	2.88	2.84	2.77	2.54	2.04	1.59
15	2.52	2.48	2.41	2.20	1.75	1.38
16	2.20	2.17	2.11	1.91	1.51	1.20
17	1.94	1.91	1.84	1.66	1.30	1.05
18	1.70	1.68	1.62	1.44	1.12	0.92
19	1.50	1.48	1.42	1.25	0.97	0.80
20	1.32	1.30	1.24	1.09	0.84	0.71
21	1.17	1.15	1.09	0.94	0.73	0.62
22	1.04	1.01	0.96	0.82	0.63	0.55
23	0.92	0.89	0.84	0.71	0.55	0.48
24	0.81	0.79	0.74	0.61	0.48	0.42
25	0.72	0.70	0.65	0.53	0.42	0.37
26	0.64	0.62	0.57	0.46	0.31	0.33
27	0.57	0.55	0.50	0.40	0.32	0.29
28	0.50	0.48	0.44	0.35	0.28	0.26
29	0.45	0.46	0.38	0.30	0.25	0.23
30	0.40	0.45	0.33	0.26	0.22	0.20

creases), so the expression for the upper bound is most accurate for the lower values of A. The accuracy, however, is dependent upon the clear weather CNR value. Typical values of CNR for operating PSK systems are in the range from 10 to 30 dB. The minimum value is typically on the order of 12 dB for an INTELSAT system with a maximum bit error rate (BER) of 10^{-5}. Consider the exact CNR degradation of 2.94 dB for XPD = 13 dB from the results of Prabhu [1969]. Then CNR_o -A = 15 dB (a total CNR of approximately 12 dB). The upper bound for the CNR degradation at XPD = 13 dB is 0.37 dB greater than the exact value. This small error is quite acceptable and is on the conservative side of the exact result. Using the upper bound for the CNR degradation for all CNR values 12 dB or greater yields a maximum conservative deviation of 0.4 dB from the exact result. The maximum deviation is 0.6 dB for all CNR values 10 dB or greater. Thus, the expression for the upper bound is sufficiently accurate for this application.

Using the upper bound for the CNR degradation and solving for XPD as a function of system margin and A gives

$$XPD = -20 \log [\sin (\pi/M)]$$

$$= -20 \log [1 - (10^{-[-(MAR - A)/10]})^{1/2}] \qquad (5.7\text{-}6)$$

For a BPSK system (M = 2)

$$XPD_{BPSK} = -20 \log \left[1 - 10^{[-(MAR - A)/10]}\right)^{1/2}] \qquad (5.7\text{-}7)$$

and for systems with M > 2

$$XPD = XPD_{BPSK} - 20 \log \left[\sin \left(\frac{\pi}{M} \right)\right] \qquad (5.7\text{-}8)$$

For QPSK (M = 4)

$$XPD_{QPSK} = XPD_{BPSK} + 3.01 \qquad (5.7\text{-}9)$$

and for 8-PSK (M = 8)

$$XPD_{8PSK} = XPD_{BPSK} + 8.34 \qquad (5.7\text{-}10)$$

Thus, an increase in the number of phase states requires a fixed increase in XPD for any system margin and attenuation. The value of XPD calculated using (5.7-6) is the minimum XPD for the specified margin and attenuation with which the system may operate. In the XPD vs A plane, we may plot contours of constant margin defining the minimum XPD as a function of A that satisfy the specified CNR margin.

A set of constant margin contours is plotted in Figure 5-18 for QPSK (M = 4) at 1 dB increments of CNR margin. This set of contours may be overlayed onto the contours of joint statistics to facilitate the determination of the reliability vs margin relationship for the set of joint sta-

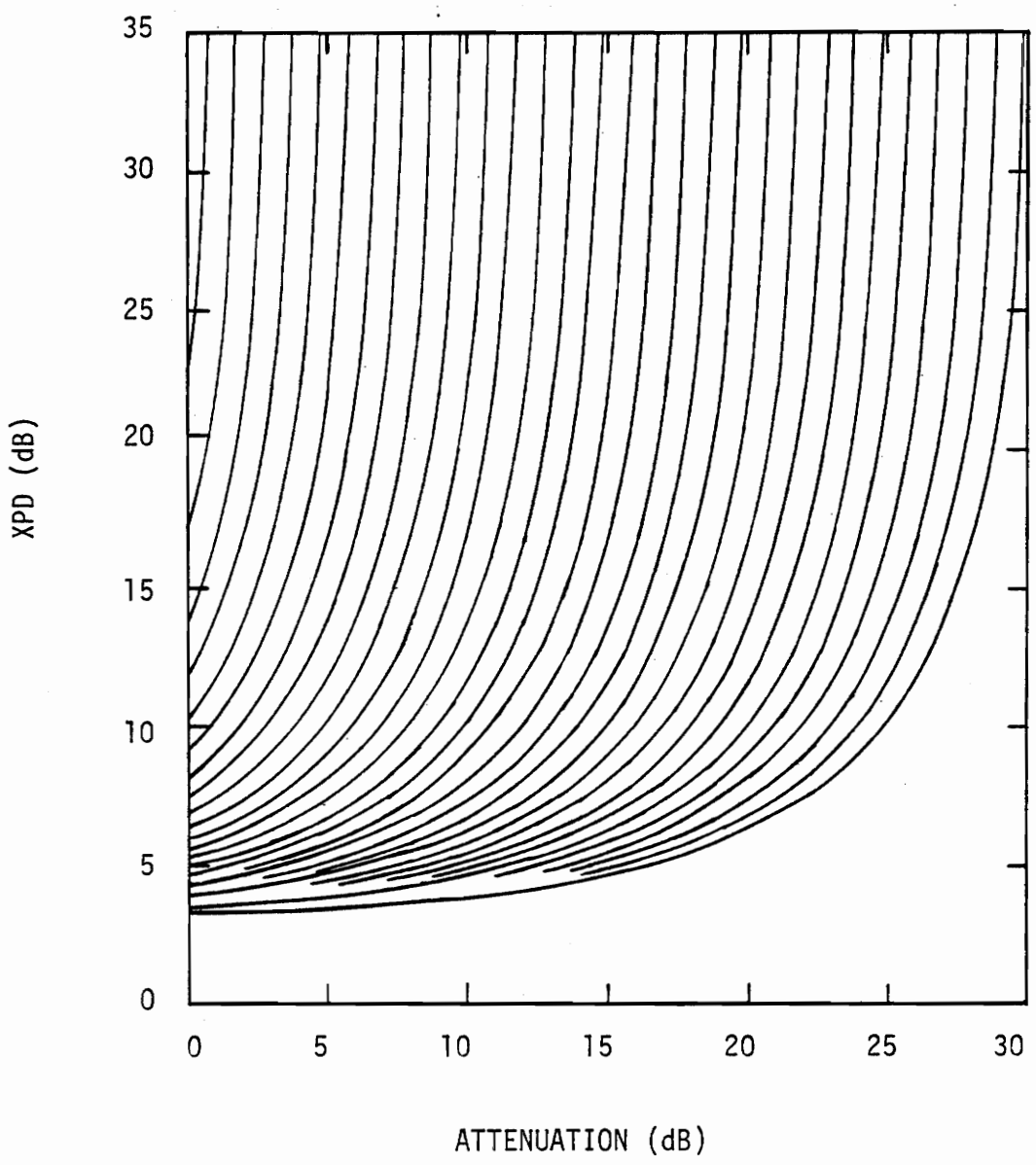

Figure 5-18. Contours of constant margin at 1 dB increments for QPSK.

tistics. A specified reliability is achieved when the corresponding joint statistics contour is completely bounded by the margin contour value used in the system design.

For a single polarized system (i.e. XPD $\rightarrow \infty$) the margin is equal to the cochannel attenuation. The additional margin required for the second channel of a dual polarized system is determined by the characteristic of the joint statistics. As an example, integer values of constant margin contours (QPSK) are overlayed on a few joint statistics contours in Figures 5-19 and 5-20. The joints statistics for the SIRIO remote site at 11.6 GHz shown in Figure 5-19 illustrates the effect of relatively low values of XPD as a function of A on the necessary margin required for a dual polarized system. Note that the knees of the joint statistic contours establish the required margin for the reliability given by the joint contour. As attenuation increases and the contour knee occurs at lower XPD values, the additional margin beyond that required for the single polarized system increases. This clearly is to compensate for the decreasing CIR caused by the depolarization. The mean XPD vs A relationship is also plotted in Figure 5-19. As was pointed out in Section 3.4, the mean relationship tends to follow the knees of the joint statistics contours. Therefore, the mean (or median) XPD vs A relationship has a close

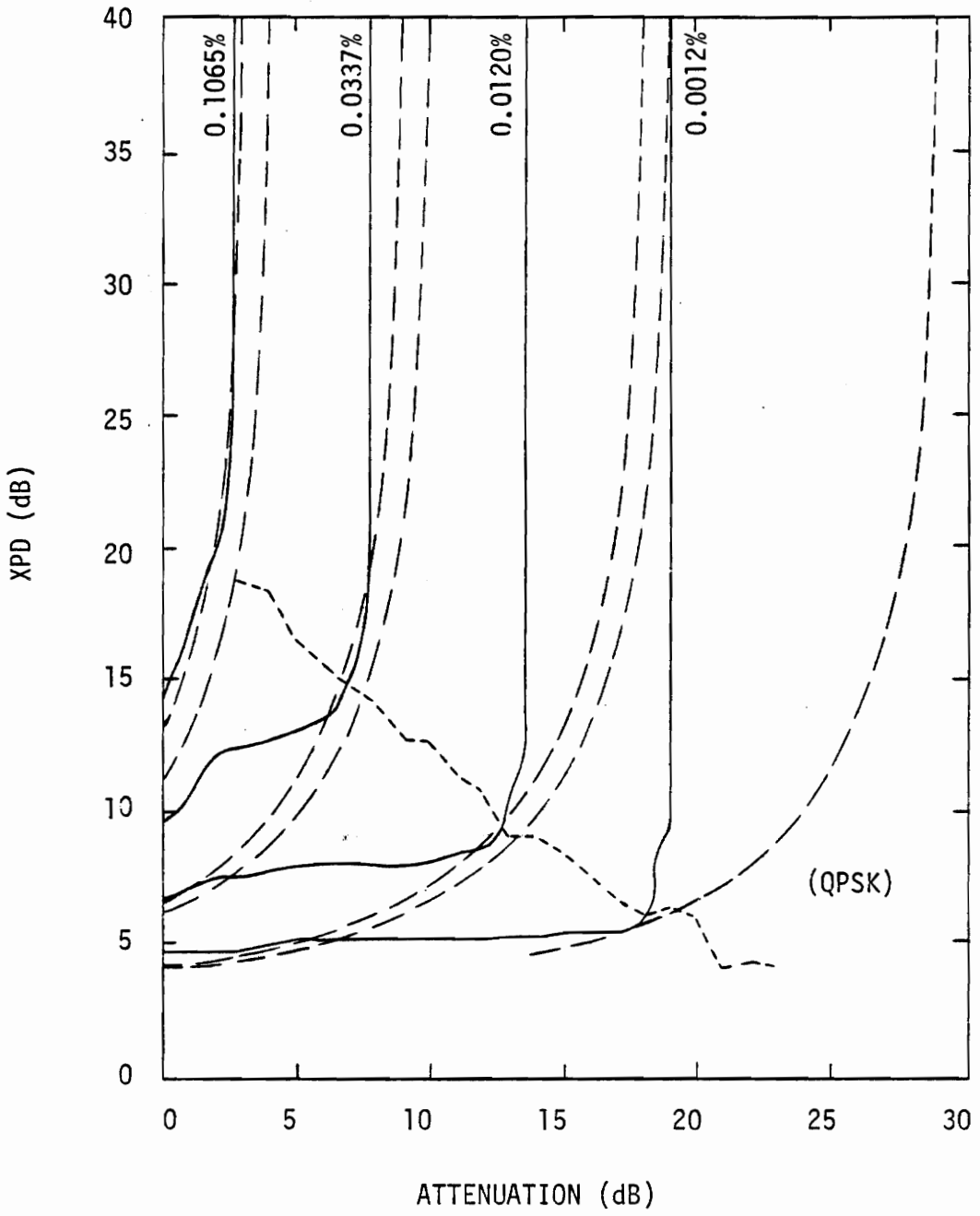

Figure 5-19. Contours of constant margin (— —) and contours of constant joint percent time (——) that A > a and X < x for the SIRIO remote site at 11.6 GHz. Also shown is the mean XPD vs A relationship (---).

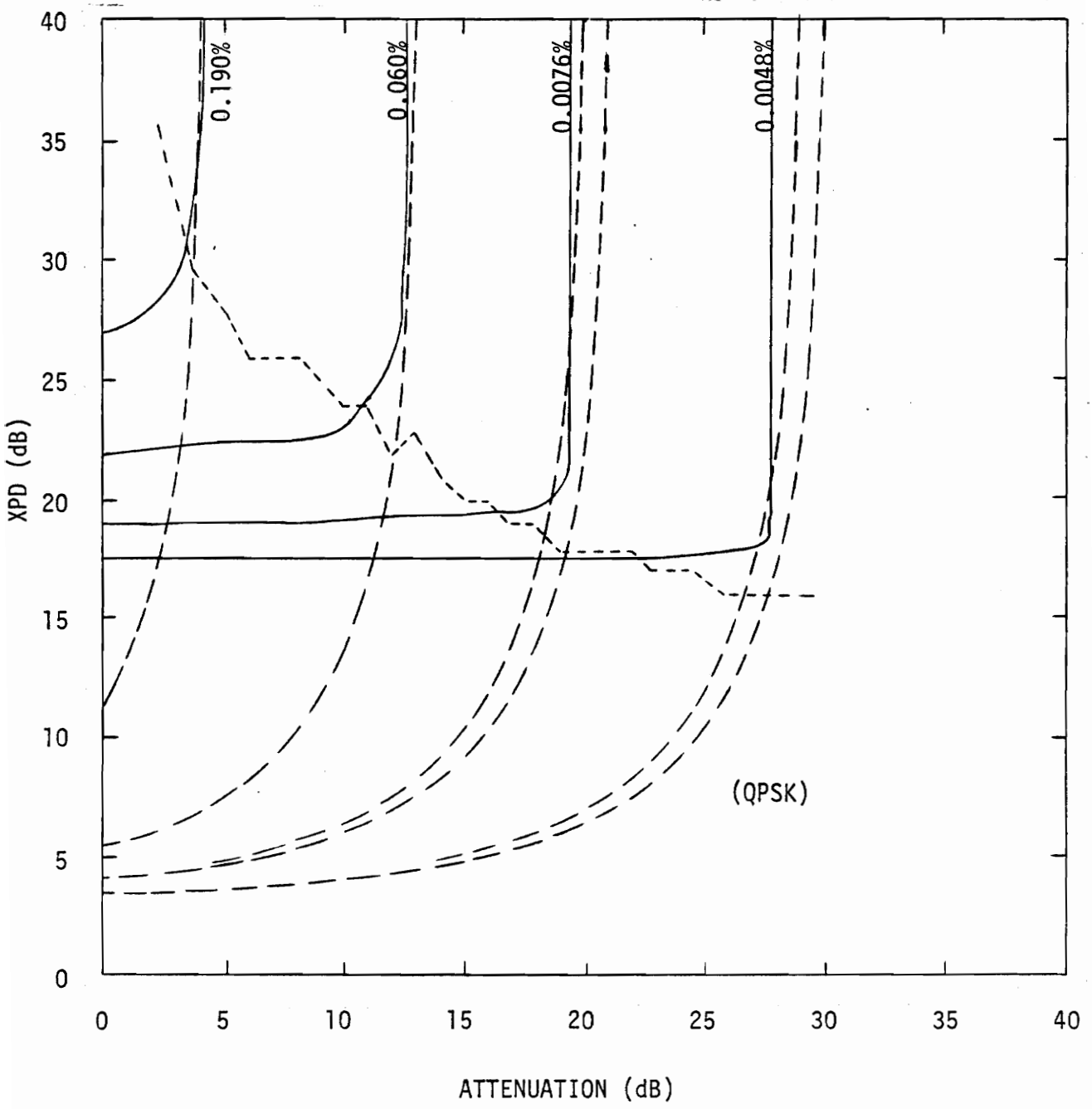

Figure 5-20. Contours of constant margin (— —) and contours of constant joint percent time (——) that A > a and X < x for Crawford Hill at 19 GHz. Also shown is the median XPD vs A relationship (---).

correlation with the joint statistics in determining the margin on a dual polarized system.

We may construct a vertical contour associated with the marginal attenuation statistics down from the top of the plot to the point of intersection with the mean XPD relationship. This establishes the mean XPD occurring for the attenuation of the specified attenuation exceedance. As we will show later, the margin determined using this (A, X) pair usually does not differ much from that determined directly from the joint statistics. The sensitivity of the CNR degradation in (5.7-1) to small changes in XPD is rather mild. An additional note about the joint-margin relationship is that the severe ice depolarization occurring at the low values of attenuation does not play a role in the margin determination. The margin is essentially attenuation limited in this region.

Next, we focus our attention on the joint statistcs for Crawford Hill, NJ at 19.04 GHz shown in Figure 5-20. As in the previous case, the joint statistics contour knees establish the margin required to achieve the contour reliability. However, in this case the corresponding knees occur at much higher values of XPD. Because of the high XPD values, the margin is essentially attenuation limited for attenuations less than 10 dB. Relatively small values of additional CNR

margin are required for a dual polarized system at this frequency for larger attenuations. Again note that the median XPD vs A relationship tends to follow the knees of the joint contours. However, a discrepancy occurs for the lowest contour at XPD equal to approximately 18 dB. The horizontal portion of the contours for XPD $\leq$ 18 dB showed errors (~ 1.5 dB) when compared to the marginal XPD statistics presented by Cox [1982]. This is because there were data outside the plot boundaries (i.e. A > 40 dB) which in turn distorted contours for XPD > 18 dB. It is felt that had this data not been present, better agreement would have been found with the knees and the median in this region. The data for XPD > 18 dB agreed very well with the published marginal statistics and the contours are accurate.

In Section 3.4 we saw that the equiprobable XPD vs A relationship may be below the mean when ice depolarization and/or measurement errors are present. In this case if the equiprobable relationship is used with the marginal attenuation statistics to specify the CNR margin, the result would require a more pessimistic margin than that found using the mean. For this reason we discourage the use of the equiprobable relationship.

We will now illustrate with data that very good agreement is found between the CNR margin determined using the mean

(or median) XPD relationship in conjunction with the attenuation statistics and the margin determined directly from the joint statistics.

The percent time that the value of the CNR margin is exceeded vs margin is shown for the SIRIO main site in Figure 5-21 for several methods of determining margin statistics. For the single polarized system, the margin exceedance is equal to the attenuation exceedance (this is the solid curve). Also plotted is the margin determined using the joint statistics directly. A third approach shown is the technique using the attenuation marginal statistics and the mean XPD vs A relationship. Very good agreement is found between the last two methods. Shown in Figure 5-22 are the same curves for the data taken at Crawford Hill. Here again we see very good agreement between the techniques for determining the margin for dual polarized systems. We note, though, that the additional margin for the second channel is relatively small. Also, the margin determined using the marginal statistics and XPD vs A relationship is on the conservative side of that determined using the joint statistics.

These data sets suggest that the joint statistics are not necessary to determine the CNR margin required for dual polarized system operation. All that is required is the mar-

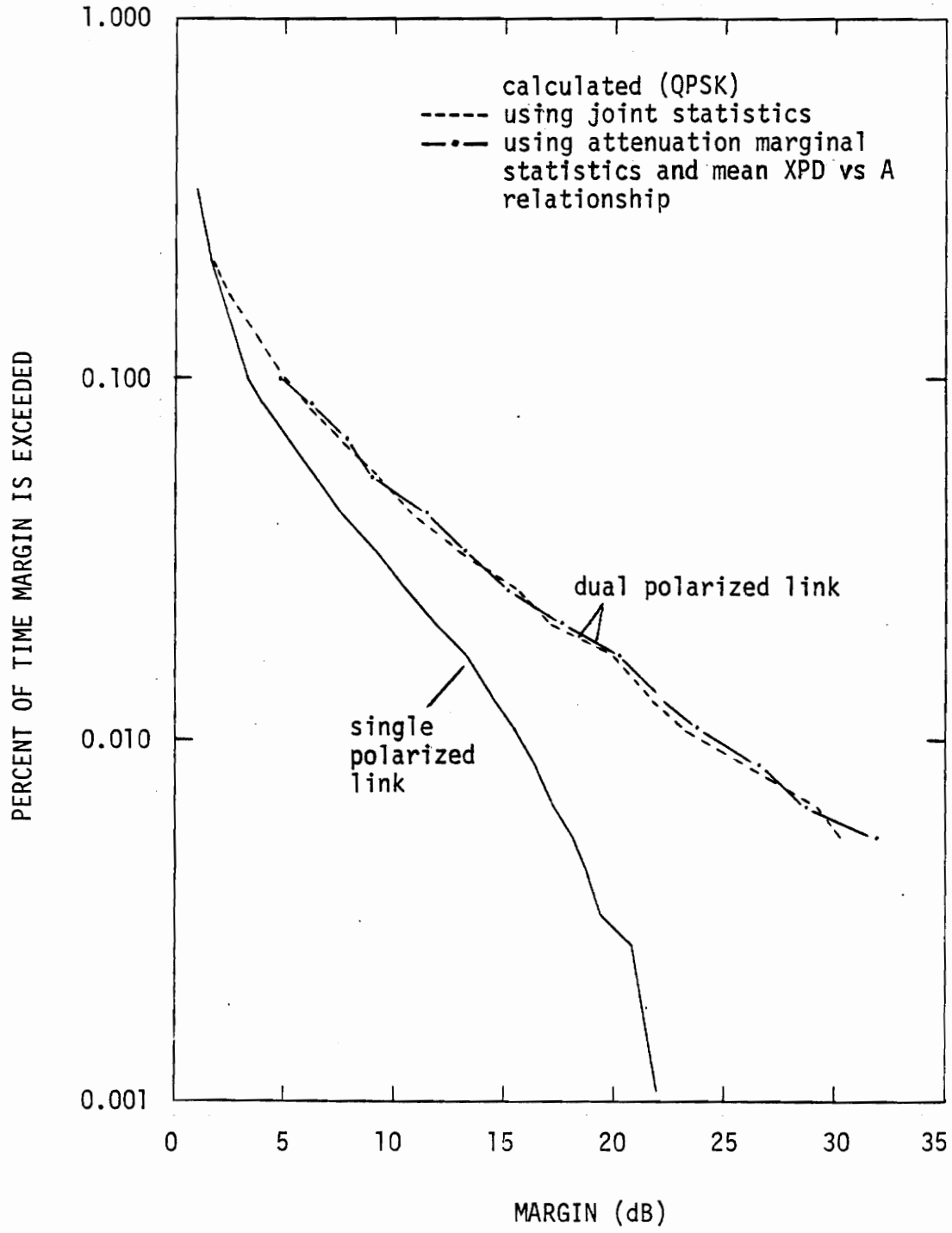

Figure 5-21. Carrier to noise ratio margin statistics for the SIRIO main site at 11.6 GHz at Blacksburg, VA.

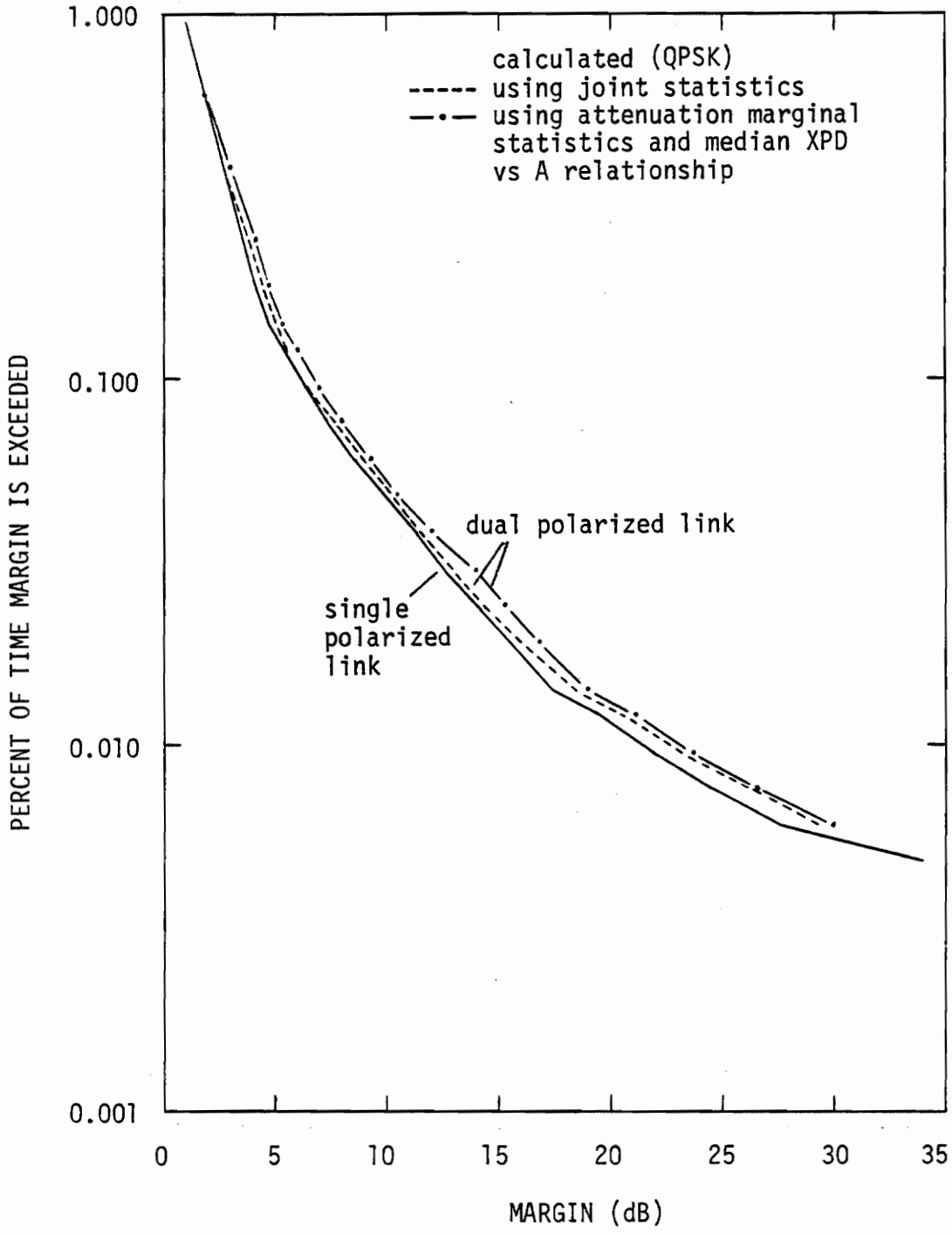

Figure 5-22. Carrier to noise ratio margin statistics for COMSTAR D2 at 19.04 GHz at Crawford Hill, NJ.

ginal attenuation statistics and the corresponding XPD vs A relationship to accurately predict the CNR margin. This further suggests a next step, which is to use the SIM model for the XPD vs A relationship. We have established good agreement between the predicted XPD using SIM and measured mean (or median) XPD data in Sections 5.4 and 5.5 and would expect similar performance in this application. Examples of this follow.

Margin statistics found from measured attenuation statistics and the SIM model are shown in Figures 5-23 to 5-25. The margin statistics for CTS at 11.7 GHz at Crawford Hill, NJ are shown in Figure 5-23. [Rustako, 1982] The single polarization margin in addition to the SIM are given. Significant additional margin is required for these conditions for the addition of the second channel and the predicted results compare very well with that using the measured data. Figure 5-24 shows statistics for the same satellite at Austin, Texas. [Vogel, 1982] The elevation angle of 50° is seen to require less margin than at Crawford Hill for 27° elevation angle. Only the dual polarized margin determined using SIM is shown because the maximum deviaiton from that determined using the data was 0.3 dB for $A \leq 20$ dB. Figure 5-25 shows data for COMSTAR D2 taken at Crawford Hill at 28.56 GHz and an elevation angle of 38.6°. [Arnold et al.,

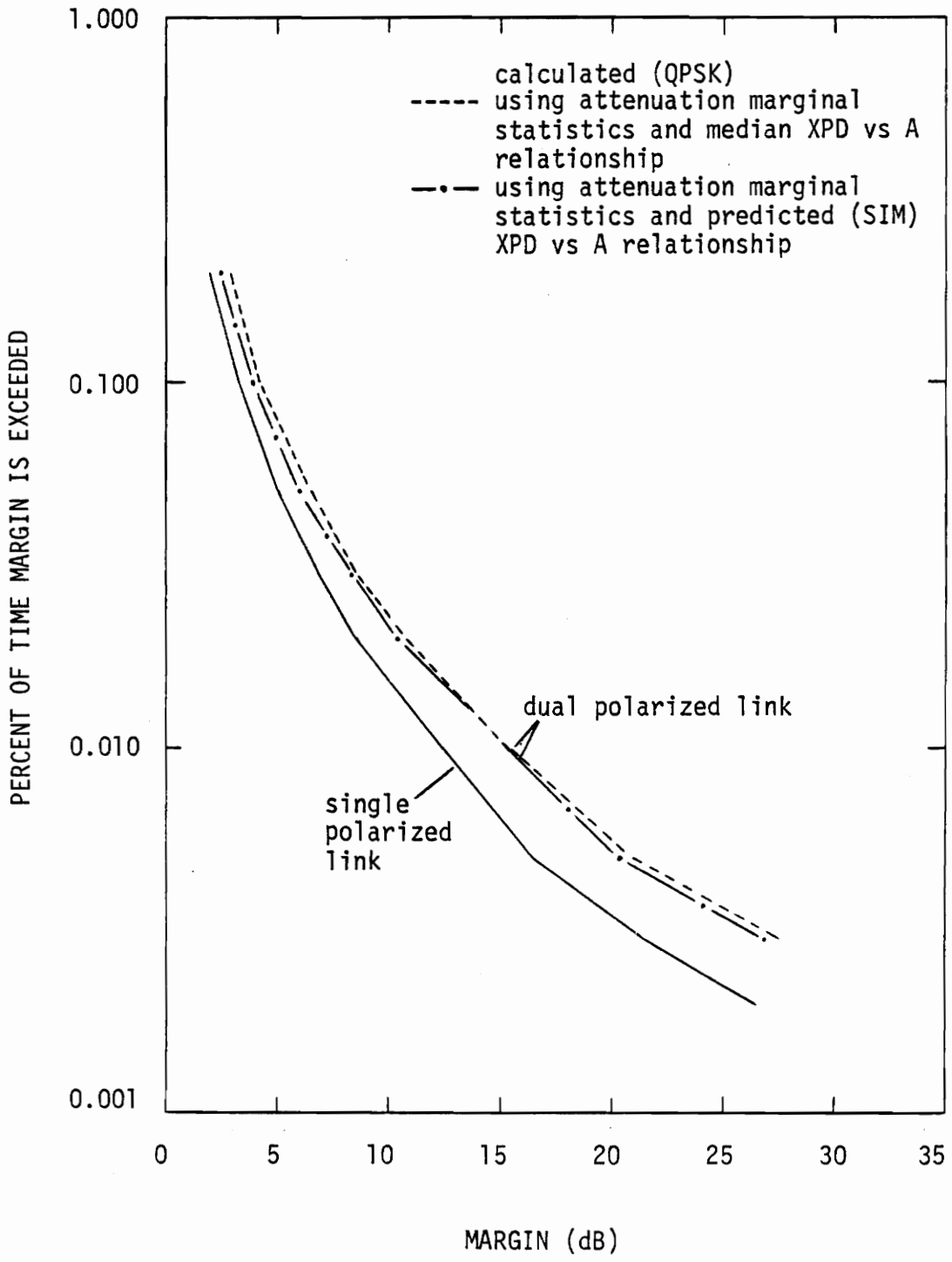

Figure 5-23. Carrier to noise ratio margin statistics for CTS at 11.7 GHz at Crawford Hill, NJ.

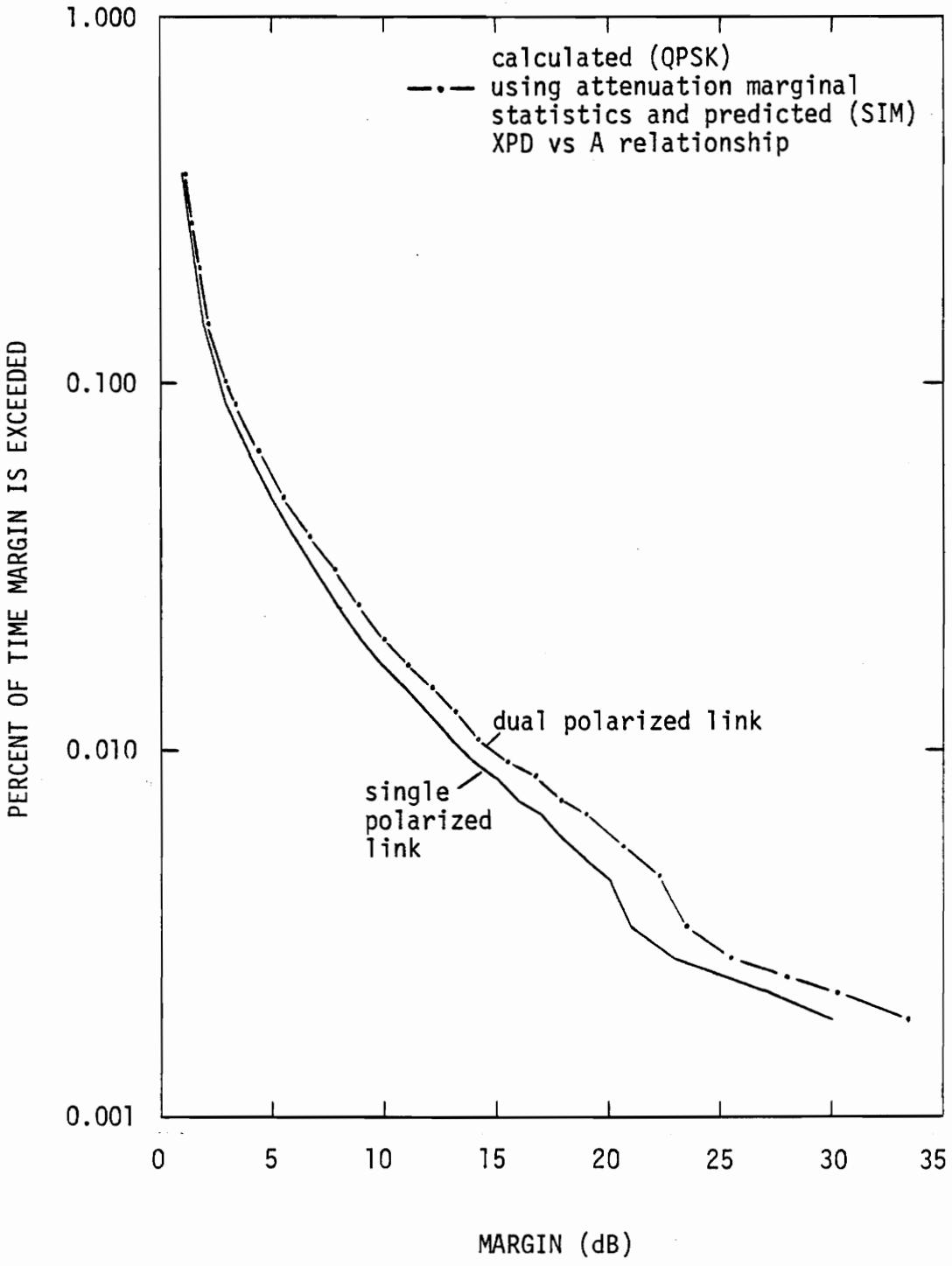

Figure 5-24. Carrier to noise ratio margin statistics for CTS at 11.7 GHz at Austin, TX.

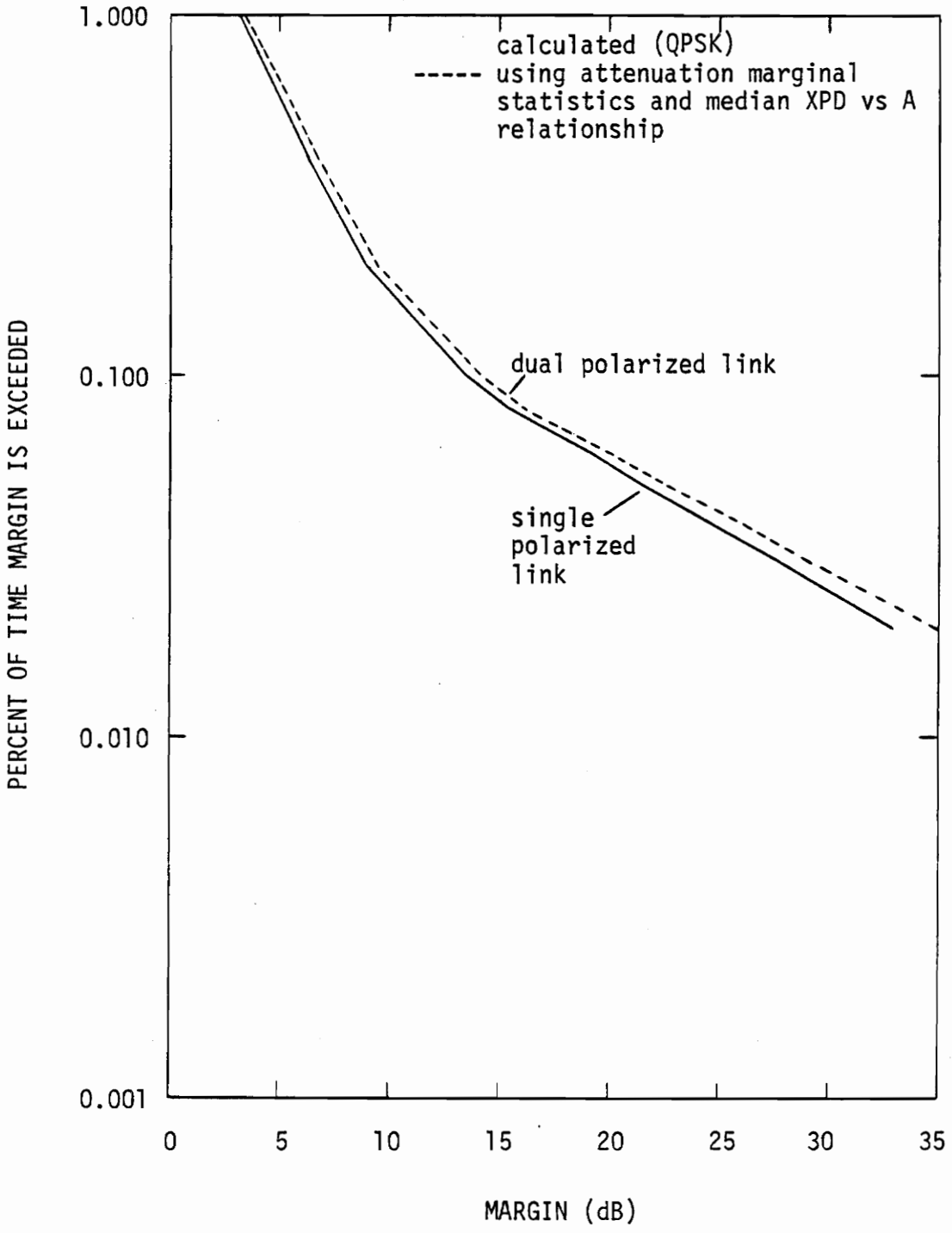

Figure 5-25. Carrier to noise ratio margin statistics for COMSTAR D2 at 28.56 GHz at Crawford Hill, NJ.

1980] The dual polarized margin shown is that determined from the measured data. The maximum deviation of 0.1 dB for $A \leqslant 30$ dB and 0.3 dB for $A > 30$ dB. Note that the statistics are essentially attenuation limited.

The three data sets illustrate that the proposed XPD vs A model used in conjunction with attenuation statistics and (5.7-1) will provide accurate predictions of the CNR margin required for dual polarized system operation. The prediction accuracy, however, is tied closely to the accuracy of the attenuation statistics. If an attenuation model is used to generate the marginal attenuation statistics, inaccuracies in the predicted attenuation will be amplified in the prediction of the dual polarized margin because the predicted XPD used in (5.7-1) is a function of the attenuation.

5.8 FREQUENCY SCALING

THe study of frequency scaling of XPD and A is now simplified through the use of (5.2-1). For two different frequencies (with all other parameters the same) we may write

$$XPD_1 = U(f_1) - V(f_1)\log(A_1) \qquad (5.8\text{-}1)$$

$$XPD_2 = U(f_2) - V(f_2)\log(A_2) \qquad (5.8\text{-}2)$$

Taking the difference we have

$$XPD_2 - XPD_1 = [U(f_2) - U(f_1)] - [V(f_2)\log(A_2) - V(f_1)\log(A_1)]. \qquad (5.8\text{-}3)$$

If

$$V(f_2) = V(f_1) = V \qquad (5.8\text{-}4)$$

then (5.8-3) reduces to

$$XPD_2 - XPD_1 = [U(f_2) - U(f_1)] - V \log\left(\frac{A_2}{A_1}\right) \qquad (5.8\text{-}5)$$

From (5.3-2) we found that for a fixed rainrate

$$XPD_1 - XPD_2 = -\beta \log\left(\frac{f_2}{f_1}\right) \qquad (5.8\text{-}6)$$

And under the assumption of (5.8-4) we determined (5.3-4) was accurately described by

$$U(f_2) - U(f_1) = \alpha \log\left(\frac{f_2}{f_1}\right) \qquad (5.8\text{-}7)$$

Substituting (5.8-6) and (5.8-7) into (5.8-5) yields

$$-\beta \log\left(\frac{f_2}{f_1}\right) = \alpha \log\left(\frac{f_2}{f_1}\right) - V \log\left(\frac{A_2}{A_1}\right) \qquad (5.8\text{-}8)$$

or

$$V \log\left(\frac{A_2}{A_1}\right) = (\alpha + \beta) \log\left(\frac{f_2}{f_1}\right) \qquad (5.8\text{-}9)$$

Equation (5.8-9) may be solved for A_2/A_1 giving

$$\frac{A_2}{A_1} = \left(\frac{f_2}{f_1}\right)^{\left(\frac{\alpha + \beta}{V}\right)} \tag{5.8-10}$$

Thus we have derived a formula for scaling attenuation values from one frequency to another, which may be rewritten as

$$A_2 = A_1 \left(\frac{f_2}{f_1}\right)^{\left(\frac{\alpha + \beta}{V}\right)} \tag{5.8-11}$$

From the analysis in Section 5.3 we determined reasonable values of $\alpha = 17.27$, $\beta = 20.5$ and $V = 19.0$. Substituting these values into (5.8-11) yields

$$A_2 = A_1 \left(\frac{f_2}{f_1}\right)^{1.99} \tag{5.8-12}$$

From (5.3-2) we determine

$$XPD_2 = XPD_1 - 20.5 \log \left(\frac{f_2}{f_1}\right) \tag{5.8-13}$$

Using (5.8-12) and 5.8-13) provides a two step procedure for the frequency scaling of XPD vs A data pairs occurring simultaneously for a fixed rainrate.

The application of (5.8-12) and (5.8-13) is not limited to instantaneous data pairs. For example, the relations may be used to scale mean (or median) XPD values given as a function of attenuation. In this case, the scaled instantaneous (A,X) pairs would yield the same mean (or median) values as those determined by scaling the mean (or median) directly.

The COMSTAR D2 experiment at Crawford Hill, NJ provided measurements for 19.04 GHz and 28.56 GHz over the same data period from May 18, 1977 to May 18, 1978. All other experiment parameters were the same for the two frequencies. The ratio of the 19 GHz attenuation to the 28 GHz attenuation was calculated by Cox et al., [1982] for the instantaneous data and the median and 10%, 90% values presented. The best fit factor for the median of instantaneous ratio values was found to be 0.476 for A_{19}/A_{28}. The factor predicted using (5.8-12) is 0.446. The 28 GHz attenuation calculated for A_{19} = 10 dB is 21.0 dB using the best fit factor of the measured data and 22.4 dB using the prediction factor. The difference between the predicted and measured attenuations is less than 7% of the measured value. This difference li-

nearly decreases for smaller 28 GHz attenuations. We may conclude that very good agreement exists between the measured data and the predictions using the scaling factor.

Both frequency scaling equations were used to scale the median XPD vs A data at 28.56 GHz to 19.04 GHz. The data scaled from 28 GHz and the measured 19 GHz data for the median values is shown in Figure 5-26. This preliminary investigation into the accuracy of (5.8-12) and (5.8-13) indicates good agreement between measured data and predicted results. Further testing is required for other frequency ranges and conditions.

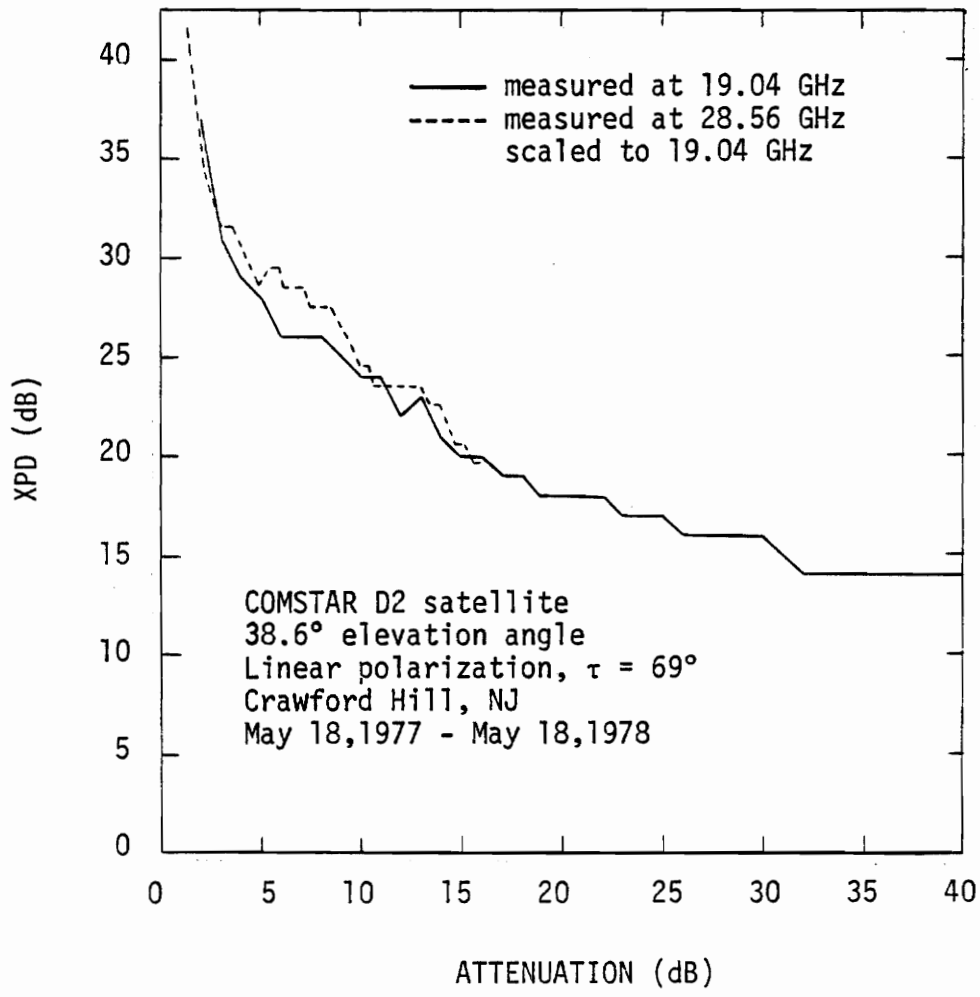

Figure 5-26. Comparison between median XPD vs A relationships using frequency scaling theory.

Chapter VI

ICE EFFECTS

We have seen that ice depolarization occurring in the absence of significant attenuation plays an insignificant role in the determination of the system margin for digital PSK systems. Modeling depolarization due to rain only has been shown to be sufficiently accurate for most conditions (i.e. moderate elevation angles). However, the low elevation angle experiment at 10.7° at Blacksburg, Virginia using the circularly polarized SIRIO beacon (see Section 5.5) has shown a need to account for ice depolarization occurring simultaneously with significant rain attenuation.

6.1 THEORY

Ice effects can be included in the multiple scattering model by the addition of a slab of ice particles located above the rain (i.e. above the 0°C isotherm layer). In this manner, the plane wave output of one medium may be applied to the other as input. Then the depolarization matrix for the multiple scattering model is

$$\underline{D}_d = \underline{D}_R\underline{D}_I = [e^{-j\underline{k}_R}][e^{-j\underline{k}_I}] \qquad (6.1\text{-}1)$$

for a downlink and

$$\underline{D}_u = \underline{D}_I\underline{D}_R = [e^{-j\underline{k}_I}][e^{-j\underline{k}_R}] \qquad (6.1\text{-}2)$$

for an uplink.

The System Equation for Rain-Ice Calculations

On the downlink the system equation, from (2.1-11), is

$$\underline{V}_R = \underline{A}_R^* \, \underline{D}_R \, \underline{D}_I \, \underline{A}_T^T \, \underline{V}_T \qquad (6.1\text{-}3)$$

and on the uplink

$$\underline{V}_R = \underline{A}_R^* \, \underline{D}_I \, \underline{D}_R \, \underline{A}_T^T \, \underline{V}_T \qquad (6.1\text{-}4)$$

where the receive and transmit antenna matrices for the two links are not necessarily the same. For medium-induced effects when rain and ice are both present we will consider the relationship between

$$\underline{D}_d = \underline{D}_R \, \underline{D}_I \qquad (6.1\text{-}5)$$

for the downlink and

$$\underline{D}_u = \underline{D}_I \, \underline{D}_R \qquad (6.1\text{-}6)$$

for the uplink along the same path.

Both depolarization matrices $\underline{D}_R$ and $\underline{D}_I$ have been modeled with off-diagonal symmetry, so in general we may write

$$\underline{D}_R = \begin{bmatrix} D_{11}^r & D_{12}^r \\ D_{12}^r & D_{22}^r \end{bmatrix} \tag{6.1-7}$$

and

$$\underline{D}_I = \begin{bmatrix} D_{11}^i & D_{12}^i \\ D_{12}^i & D_{22}^i \end{bmatrix} \tag{6.1-8}$$

where the matrix entries are complex quantities. Then the downlink depolarization matrix is

$$\underline{D}_d = \begin{bmatrix} D_{11}^r D_{11}^i + D_{12}^r D_{12}^i & D_{11}^r D_{12}^i + D_{12}^r D_{22}^i \\ D_{12}^r D_{11}^i + D_{22}^r D_{12}^i & D_{12}^r D_{12}^i + D_{22}^r D_{22}^i \end{bmatrix} \tag{6.1-9}$$

and the uplink depolarization matrix is

$$\underline{D}_u = \begin{bmatrix} D_{11}^i D_{11}^r + D_{12}^i D_{12}^r & D_{11}^i D_{12}^r + D_{12}^i D_{22}^r \\ D_{12}^i D_{11}^r + D_{22}^i D_{12}^r & D_{12}^i D_{12}^r + D_{22}^i D_{22}^r \end{bmatrix} \tag{6.1-10}$$

In general, then

$$\underline{D}_u = \underline{D}_d^{\tau} \qquad (6.1\text{-}11)$$

where $^{\tau}$ denotes the transpose of the matrix. The case where

$$\underline{D}_u = \underline{D}_d \qquad (6.1\text{-}12)$$

occurs in the specific situation when

$$\frac{D_{12}^i}{D_{12}^r} = \frac{D_{22}^i - D_{11}^i}{D_{22}^r - D_{11}^r} \qquad (6.1\text{-}13)$$

or when the off-diagonal entries in $\underline{D}$ are zero.

The condition for zero values for the off-diagonal entries in $\underline{D}$ results when the off-diagonal entries in $\underline{D}_R$ and $\underline{D}_I$ are zero. The case where $<\theta> = 0°$ give $D_{12}^r = 0$ for rain. The case where $<\psi> = 0$ for ice plates gives $D_{12}^r = 0$ for a 100% plates media and the $<\phi> - <\psi> = n\frac{\pi}{2}$, n = 0, 1 condition for an ice plates and/or needles media when $<\phi> = 0°$.

If we examine XPD and XPI due to medium effects alone (for channel 1) we see that for the downlink from (2.1-16), (2.1-19), and (6.1-9) for ideal antennas

$$xpd_d = \frac{\left| D_{11}^r \, D_{11}^i + D_{12}^r \, D_{12}^i \right|}{\left| D_{12}^r \, D_{11}^i + D_{22}^r \, D_{12}^i \right|} \qquad (6.1\text{-}14)$$

$$xpi_d = \frac{\left| D_{11}^r \, D_{11}^i + D_{12}^r \, D_{12}^i \right|}{\left| D_{11}^r \, D_{12}^i + D_{12}^r \, D_{22}^i \right|} \qquad (6.1\text{-}15)$$

and for the uplink from (6.1-10),

$$xpd_u = \frac{\left| D_{11}^i \, D_{11}^r + D_{12}^i \, D_{12}^r \right|}{\left| D_{12}^i \, D_{11}^r + D_{22}^i \, D_{12}^r \right|} \qquad (6.1\text{-}16)$$

$$xpi_u = \frac{\left| D_{11}^i \, D_{11}^r + D_{12}^i \, D_{12}^r \right|}{\left| D_{11}^i \, D_{12}^r + D_{12}^i \, D_{22}^r \right|} \qquad (6.1\text{-}17)$$

From the above expressions we find for medium effects that

$$XPD_d = XPI_u \qquad (6.1\text{-}18)$$

and

$$XPI_d = XPD_u \qquad (6.1\text{-}19)$$

Single Particle Scattering Matrices

The geometry used for single ice particle scattering is similar to the approach of Haworth, Watson and McEwan [1977]. A 3-dimensional directional coordinate system with unit vectors $\hat{n}$, $\hat{\ell}$, and $\hat{m}$ is defined such that the unit vectors $\hat{\ell}$ and $\hat{m}$ define the azimuthal plane (see Figure 6-1). A unit vector $\hat{o}$ lies in the azimuthal plane making an angle with respect to $\hat{\ell}$. The unit vector $\hat{o}$ is given in terms of $\hat{\ell}$ and $\hat{m}$ by

$$\hat{o} = \cos\phi\,\hat{\ell} + \sin\phi\,\hat{m} \qquad (6.1\text{-}20)$$

The orientation of the principal axis of the ice particle will be described in the above system.

A second directional coordinate system is defined with unit vectors $\hat{x}$, $\hat{y}$, and $\hat{z}$ in which the characteristics of the plane wave propagation are described (see Figure 6-2). The plane of incidence is defined by vectors $\hat{x}$, $\hat{y}$ and the direction of propagation of the plane wave is $\hat{z}$. The vector $\hat{x}$ is taken parallel to the local horizontal. The two systems are defined such that $\hat{\ell}\cdot\hat{z} = 0$ which requires $\hat{\ell}$ to lie in the plane parallel to the plane of incidence.

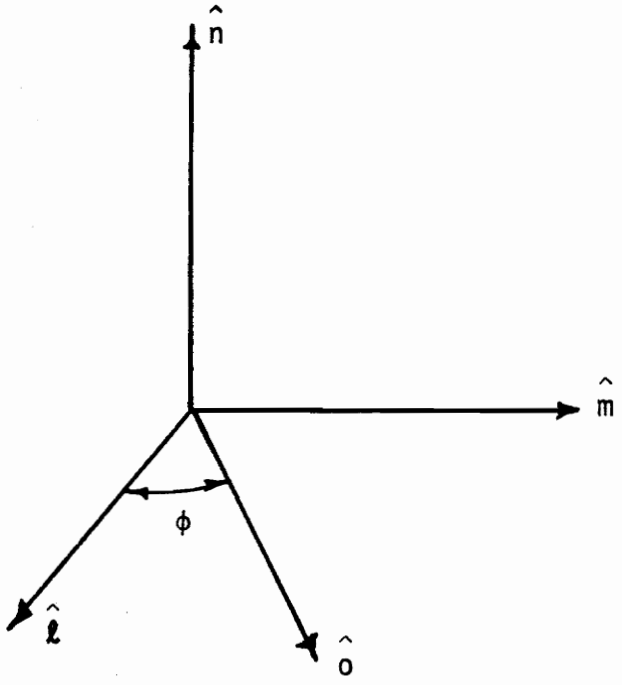

Figure 6-1. Geometry for the orientation of the principal axis of the ice particle.

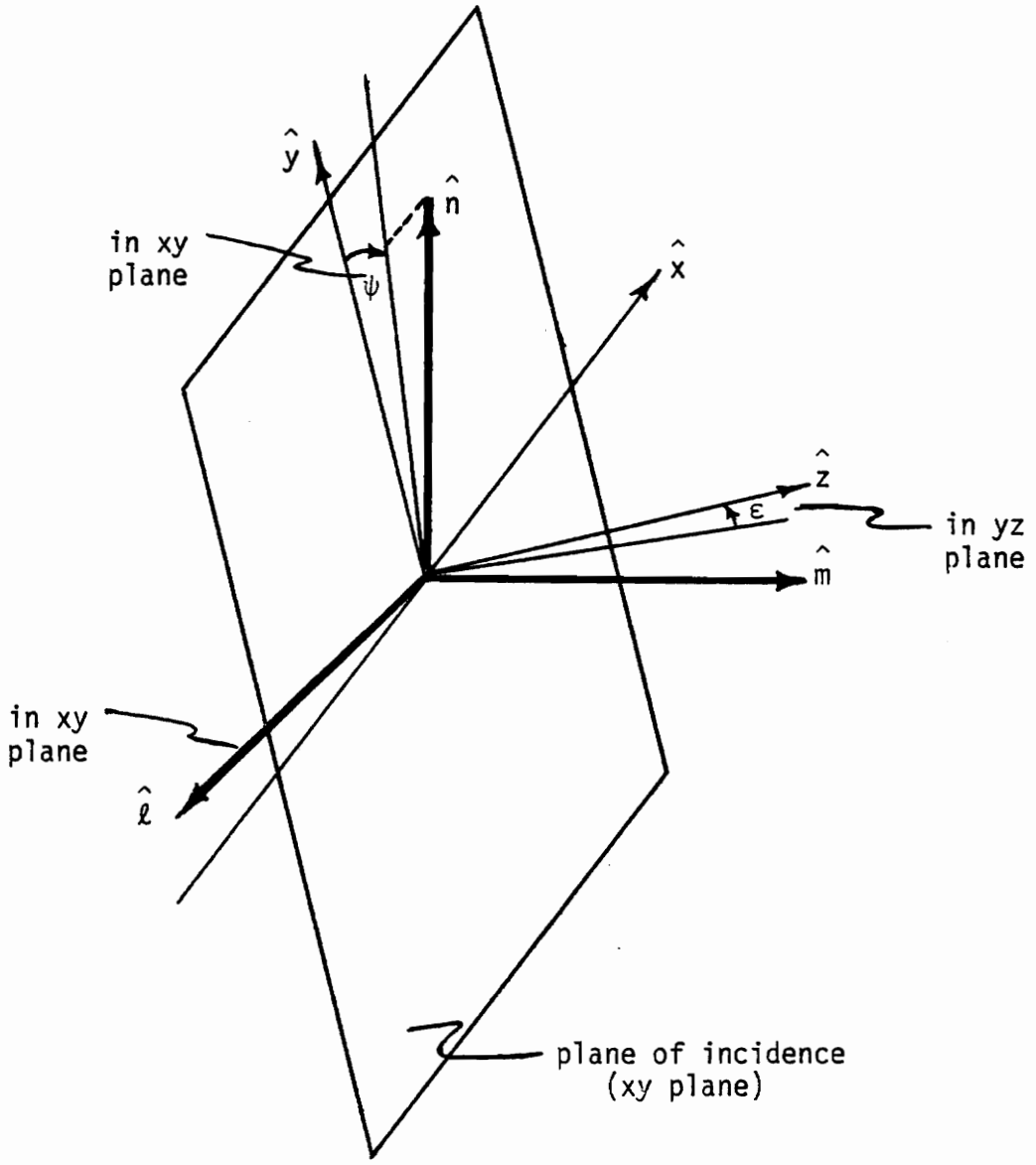

Figure 6-2. Geometry for plane wave interaction with ice particle.

The directional relationship between the unit vectors of the two systems may be described in terms of $\hat{x}$, $\hat{y}$ and $\hat{z}$ by the angles ψ and ε. The angle ψ is the angle measured from $\hat{y}$ toward $\hat{x}$ described by the projection of $\hat{n}$ onto the plane of incidence. (Here, we are assuming that the particle axes are all aligned so that $\theta_{ip} = \theta_{in} = \psi$; see Section 2.3) The angle between $\hat{n}$ and the direction of propagation $\hat{z}$ when $\psi = 0$ is the complement of the elevation angle ε. The angle ε is the projection of $\hat{m}$ onto the y,z plane measured from $\hat{z}$. The unit vectors $\hat{n}$ and $\hat{\ell}$ are given in terms of the unit vectors $\hat{x}$, $\hat{y}$ and $\hat{z}$ by

$$\begin{aligned} n &= n_x\hat{x} + n_y\hat{y} + n_z\hat{z} \\ &= \cos\varepsilon \sin\psi\,\hat{x} + \cos\varepsilon\cos\psi\,\hat{y} + \sin\varepsilon\,\hat{z} \end{aligned} \tag{6.1-21}$$

$$\begin{aligned} \hat{\ell} &= \ell_x\hat{x} + \ell_y\hat{y} + \ell_z\hat{z} \\ &= -\cos\psi\,\hat{x} + \sin\psi\,\hat{y} \end{aligned} \tag{6.1-22}$$

The unit vector $\hat{m}$ is determined by $\hat{m} = \hat{n} \times \hat{\ell}$ which gives

$$\begin{aligned} m &= m_x\hat{x} + m_y\hat{y} + m_z\hat{z} \\ &= -\sin\varepsilon\cos\psi\,\hat{x} - \sin\varepsilon\cos\psi\,\hat{y} + \cos\varepsilon\,\hat{z} \end{aligned} \tag{6.1-23}$$

From (6.1-20), (6.1-22) and (6.1-23)

$$\hat{o} = o_x \hat{x} + o_y \hat{y} + o_z \hat{z}$$

$$= (-\cos\psi \cos\phi - \sin\varepsilon \sin\psi \sin\phi)\,\hat{x}$$

$$+ (\sin\psi \cos\phi - \sin\varepsilon \cos\psi \sin\phi)\,\hat{y}$$

$$+ \cos\varepsilon \sin\phi\,\hat{z} \qquad (6.1\text{-}24)$$

The orientation of the oblate spheroid is taken such that $\hat{n}$ is the direction of the spheriod axis of revolution (see Figure 6-3). Then the scattering matrix of the oblate spheroid (eccentricity = 1) in terms of $\hat{n}$ is given by [Stutzman, et al., 1981]

$$[f']_{plate} = (m^2 - 1) \begin{bmatrix} \frac{1 - m^2}{m^2} n_x^2 + 1 & \frac{1 - m^2}{m^2} n_x n_y \\ \frac{1 - m^2}{m^2} n_x n_y & \frac{1 - m^2}{m^2} n_y^2 + 1 \end{bmatrix}$$

(6.1-25)

where V is the volume of the spheroid and m is the complex index of refraction of ice. The $\hat{n}$ components in the above equation may be written in the form

$$n_x^2 = \frac{1}{2} \cos^2 \varepsilon \, (1 - \cos 2\psi) \qquad (6.1\text{-}26a)$$

$$n_y^2 = \frac{1}{2} \cos^2 \varepsilon \, (1 + \cos 2\psi) \qquad (6.1\text{-}26b)$$

$$n_x n_y = \frac{1}{2} \cos^2 \varepsilon \sin 2\psi \qquad (6.1\text{-}26c)$$

Similarly, the orientation of the prolate spheroid is taken such that $\hat{o}$ is the direction of the spheroid axis of revolution (see Figure 6-3). Then the scattering matrix of the prolate spheroid (eccentricity = 1) in terms of $\hat{o}$ is given by [Stutzman, et al., 1981]

$$[f']_{needle} = \frac{m^2 - 1}{m^2 + 1} \begin{bmatrix} (m^2 - 1)\, o_x^2 + 2 & (m^2 - 1)\, o_x o_y \\ (m^2 - 1)\, o_x o_y & (m^2 - 1)\, o_y^2 + 2 \end{bmatrix} \qquad (6.1\text{-}27)$$

The $\hat{o}$ components in the above equation may be written in the form

$$o_x^2 = \frac{1}{4} \{1 + \cos^2 \varepsilon \, (\cos 2\phi + \cos 2\psi) + \cos 2\psi \cos 2\phi \, (1 + \sin^2 \varepsilon) + \sin^2 \varepsilon + 2 \sin 2\psi \sin 2\phi \sin \varepsilon\} \qquad (6.1\text{-}28a)$$

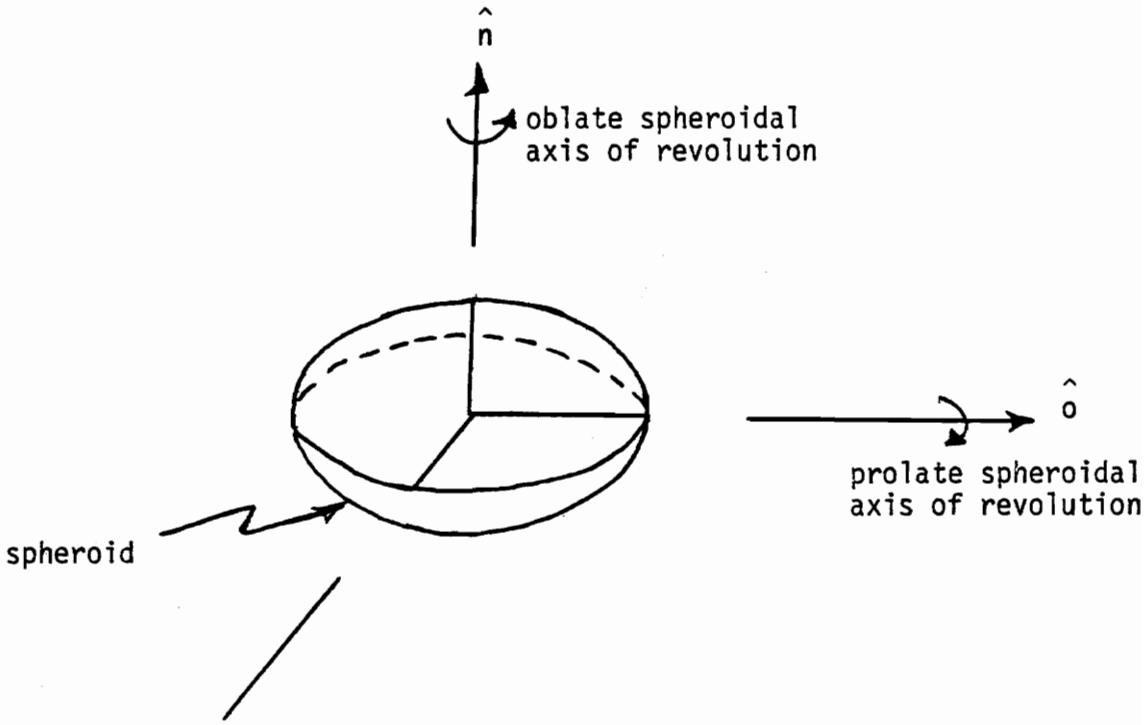

Figure 6-3. Geometry for the principal axis of oblate and prolate spheroids.

$$o_y^2 = \frac{1}{4}\{1 + \cos^2\varepsilon\,(\cos 2\phi - \cos 2\psi) - \cos 2\psi \cos 2\phi\,(1 + \sin^2\varepsilon) + \sin^2\varepsilon - 2\sin 2\psi \sin 2\phi \sin\varepsilon\} \quad (6.1\text{-}28b)$$

$$o_x o_y = \frac{1}{4}\{2\cos 2\psi \sin 2\phi \sin\varepsilon - 2\sin 2\psi \cos 2\phi\,(1 + \sin^2\varepsilon) - \sin 2\psi \cos^2\varepsilon\} \quad (6.1\text{-}28c)$$

Ice Medium Calculations

We assume that the ice particles are distributed homogeneously along the propagation direction (z), so that $n(z, \omega)$ is independent of z. We also assume $n(z, \omega)$ is composed of statistically independent distributions over shape, azimuth angle, and tilt angle onto the xy plane. The shape distribution is bimodal with P being the fraction of plates and 1-P being the fraction of needles. The orientation angle in the azimuth plane, ϕ, is assumed to be Gaussian distributed with mean $\langle\phi\rangle$ and standard deviation σ_ϕ. Similarly, the tilt angle onto the xy plane, ψ, is assumed to be Gaussian distributed with mean $\langle\psi\rangle$ and standard deviation σ_ψ. It turns out that the size distribution need not be specified. Then the scattering matrix for a slab of ice particles with distributions of shapes and orientation angles is given as [Stutzman, et al., 1981]

$$\underline{k}_I = \frac{k_o}{2} \rho L \langle V \rangle \left\{ P \langle [f']_{plate} + (1 - P) \langle [f']_{needle} \rangle \right\} \tag{6.1-29}$$

where <[f']plate> and <[f']needle> are found from (6.1-25) to (6.1-28) with the following replacements:

$$\cos 2\psi \rightarrow e^{-2\sigma_\psi^2} \cos (2 \langle \psi \rangle) \tag{6.1-30a}$$

$$\sin 2\psi \rightarrow e^{-2\sigma_\psi^2} \sin (2 \langle \psi \rangle) \tag{6.1-30b}$$

$$\cos 2\phi \rightarrow e^{-2\sigma_\phi^2} \cos (2 \langle \phi \rangle) \tag{6.1-30c}$$

$$\sin 2\phi \rightarrow e^{-2\sigma_\phi^2} \sin (2 \langle \phi \rangle) \tag{6.1-30d}$$

Here ρ is the ice particle density (number per m^3 of volume), L is the thickness of the ice cloud (in m), and <V> is the average ice particle volume. It is convenient to define ice content as

$$IC = \rho L \langle V \rangle \tag{6.1-31}$$

It is a measure of the total ice encountered by a wave passing through the cloud (or slab). Introduction of this parameter combines three unknowns into one, reducing the complexity of the problem.

The multiple scattering model (statement listing in Appendix C) has been computer programmed with the capability of making rain only, ice only, and rain and ice medium calculations.

6.2 PRELIMINARY CALCULATIONS

Calculations for a rain/ice medium involves six parameters to characterize the ice ensemble in addition to the rain and system parameters. Currently there is insufficient data to establish the appropriate values for the ice parameters. The ice medium along an earth-space path is even more difficult to characterize than rain. Here we will present several general observations.

The ice content (IC) is a function of the thickness of the ice cloud along the propagation path. If we assume a stratiform layer of ice particles above the rain then the path length through the ice cloud, and consequently the ice content, will vary with elevation angle. This variation may be simply modeled by a geometrical relation of the form

$$IC = IC_1 \frac{\csc(\varepsilon)}{\csc(\varepsilon_1)} \qquad (6.2\text{-}1)$$

where IC_1 is determined empirically at elevation angle ε_1. Without this variation, calcualtions show for a constant ice content that ice depolarizaiton has a greater in-

fluence on the overall depolarization value as the elevation angle increases. This is physically unrealistic and does not agree with experimental results.

The XPD vs A relationship obtained from the multiple scattering program and incorporating (6.2-1) at 11 GHz with IC_1 = 0.001 and ε_1 10.7° is shown in Figure 6-4. In this case, the theory predicts that rain depolarization begins to dominate as attenuation icreases. This effect becomes more significant as the elevation angle increases (and IC decreases). At higher elevation angles the 100% ice needle condition produces the greatest depolarization and at the low elevation angles the 100% plate condition produces the greatest depolarization.

In these calculations we have assumed the ice particles to be completely aligned. Furthermore, we have assumed alignment with the raindrops which renders the total medium reciprocal (i.e. XPD is identical for uplink and downlink cases).

Several combinations of ice parameters representing mixtures of ice plates and ice needles can produce similar results. The available XPD vs A data base is not complete enough to allow reliable inferences about appropriate parameter values. Remote sensing in the form of a meterological dual-polarized radar operating in conjunction with a low

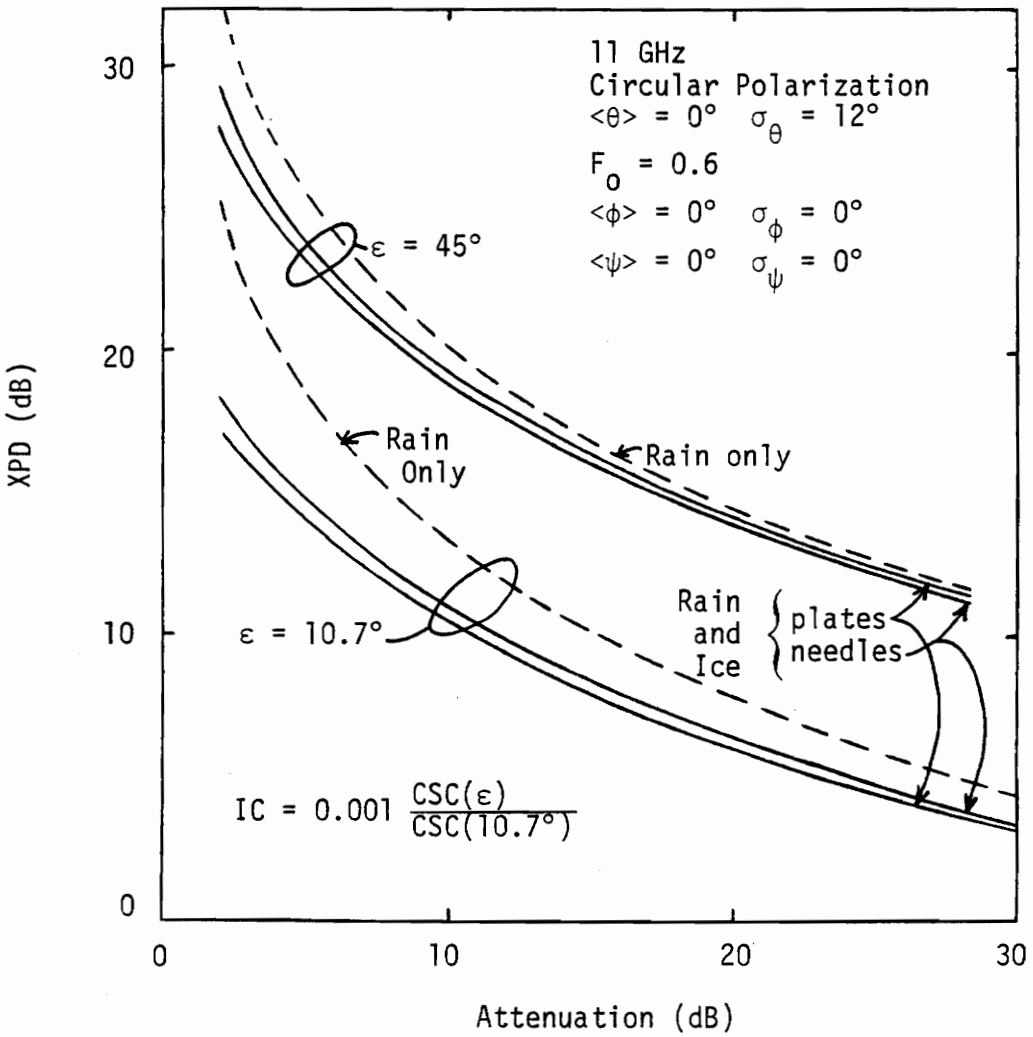

Figure 6-4. XPD vs A calculated at 11 GHz using the multiple scattering model for elevation angles of 10.7° and 45°. An ice layer is included above the rain with an ice content given by (6.2-1).

elevation angle beacon experiment is the type of system required to derive the information necessary to develop an accurate model of this form.

Other variations in the ice cloud model may also be required to accurately represent the phenomena. We might suggest that the ice content is linked to rainrate. As rainrate increases above some threshold, it is reasonable to assume the ice content decreases. This decrease could be investigated by correlating the ice content variation with attenuation or directly with rainrate. Also, in the theory presented in Section 6.1 we assumed that the ice particles were homogeneously distributed along the path length. For ice media (which introduce significant phase shifts) the XPD vs A relationship may no longer be independent of the spatial distribution of hydrometeors. Radar studies would also be helpful in resolving this issue.

Ice depolarization requires further experimental and theoretical research. The theory presented in this report provides only a basis for future work on this problem.

Chapter VII

CONCLUSIONS

Accurate estimation of the depolarizing effects due to rain and ice is an essential part of system calculations for a dual polarized link. A simple model that can be used to determine crosspolarization discrimination due to rain from co-polar attenuation has been presented. The model was compared to existing data for several locations and conditions. Finally, the model was compared to several other XPD models. The technique used to develop the proposed simple model was more rigorous than the others and the resulting model has additional flexibility through inclusion of the particle shape factor term.

The various methods for XPD data display were examined and evaluated. The mean and median were found to be equivalent measures whereas the equiprobable value of data is to be used with caution. Two methods of defining the joint distribution were examined and compared. The AND condition joint distribution was found to be preferable over the OR condition joint distribution. In addition, the relationship between the joint distribution and the other measures were established.

The relationship of attenuation and depolarization from the system reliability standpoint was examined for a phase-shift-keying (PSK) system and a method to predict the system margin for propagation effects was proposed using the simple model.

An investigation into the theoretical prediction of crosspolarization discrimination due to simultaneous rain and ice effects was initiated. Recommendations for future work include a refinement of the simple model to include ice effects. This aspect of the model would provide prediction accuracy for the low elevation angle conditions susceptible to significant reduction of crosspolarization discrimination due to rain/ice influence.

Chapter VIII

APPENDIX A: DUAL POLARIZED ANTENNA-WAVE INTERACTION COMPUTATION USING THE COMPLEX-VECTOR REPRESENTATION

The Receive Antenna

First consider a receive antenna with a single polarization state. The receive antenna channel output may be represented by a complex voltage which accounts for the incoming wave polarization state interaction with the antenna polarization response. The voltage is defined using the notation of Stutzman [1977] as

$$V(w, a^r) = C \vec{E}_w \cdot \hat{a}^{r*} \qquad (8\text{-}1)$$

where $\vec{E}_w$ is the complex-vector electric field representation of the incoming wave and $\hat{a}^{r*}$ is the unit complex-vector representation of the receive antenna. Using the IEEE definition, C is the effective length of a linearly polarized antenna receiving a plane wave from a given direction. This constant of proportionality is the ratio of the open circuit voltage developed at the antenna terminals to the electric field strength in the direction of the antenna polarization. The definition of the effective length is equally applicable to the circularly polarized wave and antenna. Stutzman [1977] has shown that C is given by $\sqrt{R_a A_e/2\eta}$ for a match

loaded antenna of radiation resistance R_a and effective aperture A_e (η = intrinsic impedance of free space).

The definition in (8-1) is complete when the wave and the antenna polarization states are both described in the coordinate system of the incoming wave. Referencing the polarization states in different coordinate systems requires a translation before this formulation may be used [Overstreet, 1978; Hollis, et al., 1971]. A common convention is the xyz right-handed coordinate system with the positive z-axis in the direction of propagation of the wave and the xy coordinate plane fixed in space.

A derivation for an arbitrary wave state incident upon a dual polarized receive antenna was presented by Stutzman [1980] using the complex vector notation. This derivation will be repeated here to include the antenna effective lengths to allow for different effective apertures. The dual polarized receiving antenna has two channels or polarization states which will be specified as $\hat{a}_1$ and $\hat{a}_2$. From (8-1) the complex receive voltages are then

$$V_1^r = V(w, a_1^r) = C_1^r \vec{E}_w \cdot \hat{a}_1^{r\,*} \tag{8-2}$$

and

$$V_2^r = V(w, a_2^r) = C_2^r \vec{E}_w \cdot a_2^{r\,*} \tag{8-3}$$

Expanding (8-2) and (8-3)

$$V_1^r = C_1^r \; E_{wx} \; a_{1x}^* + C_1^r \; E_{wy} \; a_{1y}^* \tag{8-4}$$

$$V_2^r = C_2^r \; E_{wx} \; a_{2x}^* + C_2^r \; E_{wy} \; a_{2y}^* \tag{8-5}$$

Equations (8-4) and (8-5) may be written in matrix form as

$$\begin{bmatrix} V_1^r \\ V_2^r \end{bmatrix} = \begin{bmatrix} C_1^r & 0 \\ 0 & C_2^r \end{bmatrix} \begin{bmatrix} a_{1x}^r & a_{1y}^r \\ a_{2x}^r & a_{2y}^r \end{bmatrix}^* \begin{bmatrix} E_{wx} \\ E_{wy} \end{bmatrix} \tag{8-6}$$

or

$$[V_R] = [C_R][A_R]^*[E_w] \; . \tag{8-7}$$

The entries of $[A_R]$ are obtained from (2.1-5) as

$$[A_R] = \begin{bmatrix} \cos \gamma_1^r & \sin \gamma_1^r \; e^{j\delta_1^r} \\ \cos \gamma_2^r & \sin \gamma_2^r \; e^{j\delta_2^r} \end{bmatrix} \tag{8-8}$$

where the receive antenna polarization states for channel 1 and channel 2 are (γ_1^r, δ_1^r) and (γ_2^r, δ_2^r).

The receive antenna effective length matrix $[C_R]$ may be replaced by a constant when a single aperture is illuminated with a dual polarized feed structure which results in the same effective lengths for the two channels.

The Transmit Antenna

Consider again the single polarization antenna system. When the wave and antenna polarization states are expressed in the same fixed coordinate system, then the receive antenna polarization state is the conjugate of the transmit antenna polarization. [Overstreet, 1978; Hollis, et. al., 1971]. The complex electric field transmitted may be determined using

$$\begin{bmatrix} E_{wx} \\ \\ E_{wy} \end{bmatrix} = \frac{1}{C^t} V^t \begin{bmatrix} a_x^t \\ \\ a_y^t \end{bmatrix} \qquad (8\text{-}9)$$

or

$$\vec{E}_w = \frac{1}{C^t} V^t \hat{a}^t \qquad (8\text{-}10)$$

where $\hat{a}^t$ is the unit complex vector representation of the transmit antenna, C^t is effective length and V^t is the impressed voltage at the antenna terminals.

The dual polarized transmit antenna formulation is found by a similar procedure as the receive condition. From (8-9) the transmitted wave field components from channel 1 and channel 2 may be written as

$$E_{w1x} = \frac{1}{C_1^t} \; V_1^t \; a_{1x}^t \tag{8-11}$$

$$E_{w1y} = \frac{1}{C_1^t} \; V_1^t \; a_{1y}^t \tag{8-12}$$

$$E_{w2x} = \frac{1}{C_2^t} \; V_2^t \; a_{2x}^t \tag{8-13}$$

$$E_{w2y} = \frac{1}{C_2^t} \; V_2^t \; a_{2y}^t \tag{8-14}$$

The wave components may be written as the sum of the contributions from the respective channels in the form

$$E_{wx} = E_{w1x} + E_{w2x} \tag{8-15}$$

$$E_{wy} = E_{w1y} + E_{w2y} \tag{8-16}$$

or

$$E_{wx} = \frac{1}{C_1^t} \; V_1^t \; a_{1x}^t + \frac{1}{C_2^t} \; V_2^t \; a_{2x}^t \tag{8-17}$$

$$E_{wy} = \frac{1}{C_2^t} \; V_1^t \; a_{2y}^t + \frac{1}{C_2^t} \; V_2^t \; a_{2y}^t \tag{8-18}$$

The equations (8-17) and (8-18) may be written in matrix form as

$$\begin{bmatrix} E_{wx} \\ \\ E_{wy} \end{bmatrix} = \begin{bmatrix} a_{1x}^t & a_{2x}^t \\ \\ a_{1y}^t & a_{2y}^t \end{bmatrix} \begin{bmatrix} \frac{1}{C_1^t} & 0 \\ \\ 0 & \frac{1}{C_2^t} \end{bmatrix} \begin{bmatrix} V_1^t \\ \\ V_2^t \end{bmatrix} \tag{8-19}$$

or

$$\begin{bmatrix} E_{wx} \\ \\ E_{wy} \end{bmatrix} = \begin{bmatrix} a_{1x}^t & a_{1y}^t \\ \\ a_{2x}^t & a_{2y}^t \end{bmatrix}^{\tau} \begin{bmatrix} C_1^t & 0 \\ \\ 0 & C_2^t \end{bmatrix}^{-1} \begin{bmatrix} V_1^t \\ \\ V_2^t \end{bmatrix} \tag{8-20}$$

where the matrix superscript τ indicates the transpose of the matrix. The system in (8-20) can be written

$$[E_w] = [A_T]^{\tau} \; [C_T]^{-1} \; [V_T] \tag{8-21}$$

and the entries for $[A_T]$ are

$$[A_T] = \begin{bmatrix} \cos \gamma_1^t & \sin \gamma_1^t \; e^{j\delta_1 t} \\ \\ \cos \gamma_2^t & \sin \gamma_2^t \; e^{j\delta_2 t} \end{bmatrix} \tag{8-22}$$

Chapter IX

APPENDIX B: REGRESSION ANALYSIS

If experimental observations of a given system are available as paired values of the variables (x_i, y_i) it is sometimes possible to determine what analytic formula best describes the relationship between the variables x and y. One approach is to use the linear equation $y = a_1 x + a_o$. The technique used is linear regression by the method of least square error. A measure of the quality of fit to the data is the coefficient of determination r^2 which ranges in value from 0 to 1. The closer the value of r^2 is to 1, the better the fit.

The regression constants a_1 and a_o are determined by

$$a_1 = \frac{\sum_{i=1}^{n} x_i y_i - \frac{1}{n} \sum_{i=1}^{n} x_i \sum_{i=1}^{n} y_i}{\sum_{i=1}^{n} x_i^2 - \frac{1}{n} \left(\sum_{i=1}^{n} x_i \right)^2} \qquad (9\text{-}1)$$

$$a_0 = \bar{y} - a_1 \bar{x}$$

where $\bar{x}$ and $\bar{y}$ are the mean values of x and y, respectively, and are

$$\bar{x} = \frac{1}{n} \sum_{i=1}^{n} x_i \qquad (9\text{-}3)$$

$$\bar{y} = \frac{1}{n} \sum_{i=1}^{n} y_i \qquad (9\text{-}4)$$

The coefficient of determination is

$$r^2 = \frac{\left[\sum_{i=1}^{n} x_i y_i - \frac{1}{n} \sum_{i=1}^{n} x_i \sum_{i=1}^{n} y_i\right]^2}{\left[\sum_{i=1}^{n} x_i^2 - \frac{1}{n}\left(\sum_{i=1}^{n} x_i\right)^2\right]\left[\sum_{i=1}^{n} y_i^2 - \frac{1}{n}\left(\sum_{i=1}^{n} y_i\right)^2\right]} \qquad (9\text{-}5)$$

Other forms of equations may be used in the curve fit routine. Of specific interest is (5.1-1) where

$$XPD_{dB} = U - V \log_{10}(A_{dB}) \qquad (9\text{-}6)$$

If we let $x = \log_{10}(A_{dB})$ and $y = XPD_{dB}$ then $a_o = U$ and $a_1 = -V$ and a logarithmic curve fit is accomplished using a regression analysis of linear form. Other mathematical formulas may be used for the variables x and y to perform a variety of functional curve fits.

Chapter X

APPENDIX C: FORTRAN CODE OF THE MULTIPLE SCATTERING MODEL

The multiple scattering model has been changed from its original version [Tsolakis, 1982] to include the exponential rainrate profile and also the capability of computing the effects of an ice layer (alone or along with rain). In this chapter we give the complete statement listing of the Fortran code.

The program is very similar to that published by Tsolakis [1982] but has been reorganized slightly to correspond more closely to the theoretical derivation in Secton 3.1. The elements of the $\underline{k}$ matrix in (3.1-9) involve summations of the form (see (3.1-34)):

$$\mathcal{L}_{U}^{L} = \underbrace{N_o}_{\text{KMATR}} \underbrace{\sum_{q=1}^{5}}_{} \underbrace{\sum_{n=0}^{5} \alpha_{nq}}_{\text{COEF}} \underbrace{\sum_{m=0}^{n} G_{mq}}_{\text{INTR}} \qquad (10\text{-}1)$$

Shown below each sum in the above equation are the names of the subroutines used to evaluate the sums.

```
C*********************************************************************
C*********************************************************************
C
C              RAIN AND ICE MULTIPLE SCATTERING PROGRAM
C
C                     DUAL POLARIZED SYSTEM
C
C    LATEST REVISION:  8DEC82              PROGRAMMER: D.L.RUNYON
C
C*********************************************************************
C*********************************************************************
C
C      THE SCATTERING STATUS:
C
C    ISCAT=1    MULTIPLE SCATTERING (RAIN ONLY)
C    ISCAT=2    MULTIPLE SCATTERING (RAIN AND ICE)
C    ISCAT=3    MULTIPLE SCATTERING (ICE ONLY)
C
C      THE RAIN RATE SPATIAL DISTRIBUTION STATUS:
C
C    ISTAT=1    UNIFORM
C    ISTAT=2    PIECE-WISE UNIFORM
C    ISTAT=3    EXPONENTIAL
C
C      RAINRATE OPTION:
C
C    IRAIN=1    RAINRATE VARIATION FROM 5 TO 150 BY 5 (MM/HR)
C    IRAIN=2    RAINRATE VARIATION FROM 1 TO 40 BY 1 (MM/HR)
C
C      INPUT PARAMETERS:
C
C    ELEV       THE ELEVATION ANGLE OF THE PATH
C    FREQ       THE FREQUENCY OF THE WAVE IN GHZ (4,6,11,14,20,30 GHZ ONLY
C    LAT        THE LATITUDE OF THE RECEIVER LOCATION (DEG.)  (ISTAT=2,3)
C    HO         THE HEIGHT AMSL OF THE RECEIVER LOCATION (METERS)(ISTAT=3)
C    L          THE RAIN CELL THICKNESS (METERS) (ISTAT=1)
C
C      INPUT PARAMETERS: RAIN
C
C    SIGMA      THE STANDARD DEVIATION OF THE RAINDROP CANTING ANGLE
C    THETA      THE MEAN RAIN DROP CANTING ANGLE
C    P1         THE FRACTION OF SPHERICAL RAINDROPS, P1+P2=1
C    P2         THE FRACTION OF OBLATE SPHEROIDAL RAINDROPS (COMPUTED)
C
C      INPUT PARAMETERS: ICE
C
C    ICO        THE ICE CONTENT FOR THE ICE CLOUD. DEFINED AS THE
C                AVERAGE VOLUME OF ICE PER UNIT VOLUME OF AIR TIMES THE
C                THICKNESS OF THE ICE CLOUD.
C    PHI        THE MEAN AZIMUTHAL ROTATION ANGLE OF THE AXIS OF
C                SYMMETRY FOR THE ICE NEEDLES.
C    SIGPHI     THE STANDARD DEVIATION OF THE DISTRIBUTION ABOUT THE
C                MEAN AZIMUTHAL ROTATION ANGLE.
```

```
C   PSI        THE MEAN PROJECTION OF THE TILT ANGLE OF THE ICE
C               PARTICLE ONTO THE XY PLANE (FOR BOTH PLATES AND NEEDLES).
C   SIGPSI     THE STANDARD DEVIATION OF THE DISTRIBUTION ABOUT THE
C               MEAN PROJECTION OF THE TILT ANGLE.
C   PN         THE FRACTION OF ICE NEEDLES IN THE ICE CLOUD (PN+PP=1).
C   PP         THE FRACTION OF ICE PLATES IN THE ICE CLOUD (COMPUTED).
C
C
C     INPUT:  POLARIZATION PARAMETERS (EPSILON AND TAU REPRESENTATION)
C
C   EPS1T      THE CHANNEL 1 TRANSMIT ANTENNA EPSILON
C   TAU1T      THE CHANNEL 1 TRANSMIT ANTENNA TILT ANGLE TAU
C   EPS2T      THE CHANNEL 2 TRANSMIT ANTENNA EPSILON
C   TAU2T      THE CHANNEL 2 TRANSMIT ANTENNA TILT ANGLE TAU
C
C   EPS1R      THE CHANNEL 1 RECEIVE ANTENNA EPSILON
C   TAU1R      THE CHANNEL 1 RECEIVE ANTENNA TILT ANGLE TAU
C   EPS2R      THE CHANNEL 2 RECEIVE ANTENNA EPSILON
C   TAU2R      THE CHANNEL 2 RECEIVE ANTENNA TILT ANGLE TAU
C
C   NOTES:
C
C      1) CASES HAVING THETA+TAU1T(OR TAU2T)=CONSTANT GIVES SAME
C         RESULTS AS TAU1T(OR TAU2T)=CONSTANT AND THETA=0.
C      2) CASES HAVING PSI+TAU1T(OR TAU2T)=CONSTANT GIVES SAME
C         RESULTS AS TAU1T(OR TAU2T)=CONSTANT AND PSI=0 FOR ICE PLATES.
C         THIS RELATIONSHIP DOES NOT HOLD FOR ICE NEEDLES.
C      3) FOR ICE ONLY MEDIUM (ISCAT=3) THE FREQUENCY IS NOT LIMITED
C         TO 4,6,11,14,20, OR 30 GHZ.
C
C*************************************************************************
0001        COMPLEX KR(2,2),KI(2,2),EI(2,2),EFIN(2,2),D(2,2),DI(2,2),DR(2,2)
0002        COMPLEX MINUSJ,AT(2,2),AR(2,2),ARC(2,2)
0003        REAL ARDB1(40),TAU1(40),ARDB2(40),TAU2(40)
0004        REAL ATTEN(2),XPI(2),XPD(2),PHASE(2)
0005        REAL ATTEN1(40),XPI1(40),XPD1(40),PHASE1(40),RATE(40)
0006        REAL ATTEN2(40),XPI2(40),XPD2(40),PHASE2(40)
0007        REAL KO,L,LAT,LAM,ISOLDB,ICO,ICO
0008        COMMON/VAR/ ATTEN1,ATTEN2,XPI1,XPI2,XPD1,XPD2,RATE
0009        COMMON/BLOC1/ MINUSJ,CONV
0010        COMMON/BLOC2/ VWACM
0011        COMMON/BLOC3/ FREQ,KO,L,ELEV,P1,P2,ISTAT,PI,THE,SIGM,PN,PP,PSI,
           $SIGPSI,PHI,SIGPHI
C
C   INITIALIZE CONSTANTS
C
0012        MINUSJ=(0.0,-1.0)
0013        PI=3.1415927
0014        CONV=PI/180.0
C
C   READ IN THE INPUT PARAMETERS.  ENTER 0.0 FOR QUANTITIES NOT REQUIRED
C   FOR THE DESIRED STATUS.
C
```

```
0015              1    READ(5,510,END=999) ELEV,FREQ,LAT,HO
0016                   READ(5,510) THETA,SIGMA,ICO,PHI,SIGPHI,PSI,SIGPSI
0017                   READ(5,510) EPS1T,TAU1T,EPS2T,TAU2T
0018                   READ(5,510) EPS1R,TAU1R,EPS2R,TAU2R
0019               510 FORMAT(7F10.4)
0020                   READ(5,520) P1,PN,ISCAT,ISTAT,IRAIN,L
0021               520 FORMAT(2(F10.4),I1,1X,I1,1X,I1,F10.4)
                   C
                   C   COMPUTE THE PERCENT OF OBLATE SPHEROIDAL RAIN DROPS
                   C
0022                   P2=1.-P1
0023                   P1P=P1*100.
0024                   P2P=P2*100.
                   C
                   C   COMPUTE THE PERCENT OF ICE PLATES IN THE ICE CLOUD
                   C
0025                   PP=1.-PN
0026                   PNP=PN*100.
0027                   PPP=PP*100.
                   C
                   C   COMPUTE THE ICE CONTENT ELEVATION ANGLE DEPENDENCE
                   C
                   C     ICO=ICO*SIN(CONV*10.7)/SIN(CONV*ELEV)
                   C
                   C PRINT OUT THE PARAMETERS
                   C
0028                   IF(ISCAT.LT.3) WRITE(6,610) FREQ,ELEV,HO,LAT
0029               610 FORMAT(1H1,4X,'THE LOCATION PARAMETERS ARE',//,10X,'FREQUENCY',11X
                  $,F10.3,' GHZ',/,10X,'ELEVATION',11X,F10.3,' DEG.',/,10X,'HEIGHT',
                  $14X,F10.3,/,10X,'LATITUDE',12X,F10.3,//)
0030                   IF(ISCAT.EQ.3) WRITE(6,611) FREQ,ELEV
0031               611 FORMAT(1H1,4X,'THE LOCATION PARAMETERS ARE',//,10X,'FREQUENCY',11X
                  $,F10.3,' GHZ',/,10X,'ELEVATION',11X,F10.3,' DEG.',//)
0032                   IF (ISCAT.LT.3) WRITE(6,620) THETA,SIGMA,P1P,P2P
0033               620 FORMAT(5X,'THE RAINDROP PARAMETERS ARE',//,10X,'THETA',15X,F10.3,/
                  $,10X,'SIGMA',15X,F10.3,/,10X,'% SPHERICAL',9X,F10.3,/,10X,
                  $'% OBLATE',12X,F10.3,//)
0034                   IF(ISCAT.EQ.2) WRITE(6,625) PHI,SIGPHI,PSI,SIGPSI,PNP,PPP,ICO
0035               625 FORMAT(5X,'THE ICE PARAMETERS ARE',//
                  $,10X,'PHI',17X,F10.3,/,10X,'SIGPHI',14X,F10.3,/
                  $,10X,'PSI',17X,F10.3,/,10X,'SIGPSI',14X,F10.3,/
                  $,10X,'% NEEDLES',11X,F10.3,/,10X,'% PLATES',12X,F10.3,/
                  $,10X,'ICO',18X,F10.8,//)
0036                   IF(ISCAT.EQ.3) WRITE(6,626) PHI,SIGPHI,PSI,SIGPSI,PNP,PPP
0037               626 FORMAT(5X,'THE ICE PARAMETERS ARE',//
                  $,10X,'PHI',17X,F10.3,/,10X,'SIGPHI',14X,F10.3,/
                  $,10X,'PSI',17X,F10.3,/,10X,'SIGPSI',14X,F10.3,/
                  $,10X,'% NEEDLES',11X,F10.3,/,10X,'% PLATES',12X,F10.3,//)
0038                   WRITE(6,630) EPS1T,TAU1T,EPS2T,TAU2T
0039               630 FORMAT(5X,'THE TRANSMIT ANTENNA POLARIZATION PARAMETERS ARE',//,
                  $10X,'EPS1T',16X,F10.4,/,10X,'TAU1T',16X,F10.4,/,10X,'EPS2T',16X,
                  $F10.4,/,10X,'TAU2T',16X,F10.4,//)
0040                   WRITE(6,635) EPS1R,TAU1R,EPS2R,TAU2R
```

```
0041            635  FORMAT(5X,'THE RECEIVE ANTENNA POLARIZATION PARAMETERS ARE',//,
                $10X,'EPS1R',16X,F10.4,/,10X,'TAU1R',16X,F10.4,/,10X,'EPS2R',16X,
                $F10.4,/,10X,'TAU2R',16X,F10.4,//)
0042                 IF(ISTAT.EQ.1) WRITE(6,640) L
0043                 IF(ISCAT.EQ.3) GO TO 5
0044            640  FORMAT(5X,'THE RAINRATE SPATIAL DISTRIBUTION IS UNIFORM',//,
                $5X,'THE PATH LENGTH IS ',F10.2,' METERS')
                C
                C   IF THE RAIN RATE HAS A PIECE-WISE UNIFORM SPATIAL DISTRIBUTION
                C   COMPUTE THE LENGTH OF THE RAIN MEDIUM.
                C
0045                 IF(ISTAT.EQ.2) CALL LENGTH(L,ELEV,LAT,HO,RO,ISTAT)
0046                 IF(ISTAT.EQ.2) WRITE(6,650) L
0047            650  FORMAT(5X,'THE RAINRATE SPATIAL DISTRIBUTION IS PIECE-WISE ',
                $'UNIFORM',//,5X,'THE PATH LENGTH IS ',F10.2,'METERS')
0048                 IF(ISTAT.EQ.3) WRITE(6,660)
0049            660  FORMAT(5X,'THE RAINRATE SPATIAL DISTRIBUTION IS EXPONENTIAL')
0050              5  CONTINUE
                C
                C PRINT HEADER
                C
0051                 IF(ISCAT.EQ.1) WRITE(6,668)
0052            668  FORMAT(1H1,10X,'MULTIPLE SCATTERING (RAIN ONLY)',//)
0053                 IF(ISCAT.EQ.2) WRITE(6,669)
0054            669  FORMAT(1H1,10X,'MULTIPLE SCATTERING (RAIN AND ICE)',//)
0055                 IF(ISCAT.EQ.3) WRITE(6,670)
0056            670  FORMAT(1H1,10X,'MULTIPLE SCATTERING (ICE ONLY)',//)
0057                 IF (ISCAT.LT.3) WRITE(6,671)
0058            671  FORMAT(1X,'RESULTS',//,4X,'RATE',5X,'ATTEN1',5X,'XPI1',5X,
                $'XPD1',5X,'PHASE1',5X,'ARDB1',5X,'TAU1',5X,'ATTEN2',5X,'XPI2',
                $5X,'XPD2',5X,'PHASE2',5X,'ARDB2',5X,'TAU2')
0059                 IF (ISCAT.EQ.3) WRITE(6,672)
0060            672  FORMAT(1X,'RESULTS',//,4X,'ICO ',5X,'ATTEN1',5X,'XPI1',5X,
                $'XPD1',5X,'PHASE1',5X,'ARDB1',5X,'TAU1',5X,'ATTEN2',5X,'XPI2',
                $5X,'XPD2',5X,'PHASE2',5X,'ARDB2',5X,'TAU2')
0061                 WRITE(6,673)
0062            673  FORMAT(4X,'----',5X,'------',5X,'----',5X,'----',5X,'------',
                $5X,'------',4X,'----',5X,'------',5X,'----',/)
                C
                C BEGIN
                C
0063                 ELEV=ELEV*CONV
0064                 THE=THETA*CONV
0065                 SIGM=SIGMA*CONV
0066                 PHI=PHI*CONV
0067                 SIGPHI=SIGPHI*CONV
0068                 PSI=PSI*CONV
0069                 SIGPSI=SIGPSI*CONV
0070                 LAM=0.3/FREQ
0071                 KO=2.*PI/LAM
                C
                C
                C   COMPUTE THE TRANSMIT ANTENNA AND THE RECEIVE ANTENNA CO AND CROSS
```

```
C   X AND Y COMPONENTS.
C
0072          CALL COMPNT(EPS1T,TAU1T,AT(1,1),AT(1,2))
0073          CALL COMPNT(EPS2T,TAU2T,AT(2,1),AT(2,2))
0074          CALL COMPNT(EPS1R,TAU1R,AR(1,1),AR(1,2))
0075          CALL COMPNT(EPS2R,TAU2R,AR(2,1),AR(2,2))
C
C   COMPUTE THE TRANSPOSE OF THE TRANSMIT ANTENNA MATRIX.
C   ASSUMING THE CO AND CROSS EFFECTIVE APERTURES ARE EQUAL
C   THEN EI=TRANSPOSE(AT)*VT WHERE VT IS THE TRANSMIT VOLTAGE
C   TENSOR WHICH WILL NOT BE MULTIPLIED .
C
0076          CALL TPOSE(AT,EI,2)
C
C   COMPUTE THE COMPLEX CONJUGATE OF THE RECEIVE ANTENNA MATRIX.
C
0077          CALL MCONJG(AR,ARC,2,2)
C
C   COMPUTE ISOLATON AND ATTENUATION FOR DIFFERENT RAIN RATES  RO.
C   OR FOR DIFFERENT ICE CONTENTS ICO
C
0078          IF(ISCAT.LT.3.AND.IRAIN.EQ.1) ICOUNT=30
0079          IF(ISCAT.LT.3.AND.IRAIN.EQ.2) ICOUNT=40
0080          IF(ISCAT.EQ.3) ICOUNT=20
0081          ICO=ICO
0082          DO 70 J=1,ICOUNT
0083          IF(ISCAT.LT.3.AND.IRAIN.EQ.1) RO=5.+5.*(J-1)
0084          IF(ISCAT.LT.3.AND.IRAIN.EQ.2) RO=1.+1.*(J-1)
0085          IF(ISCAT.EQ.3) ICO=0.0005+0.0005*(J-1)
C
C   FOR RAIN ONLY GO TO 20
C
0086          IF(ISCAT.EQ.1) GO TO 20
C
C   COMPUTE THE RAINRATE DEPENDENCE OF THE ICE CONTENT
C
C     IF(ISCAT.EQ.2) ICO=ICO*(1.202-EXP(-.06404*RO))
C
C   COMPUTE THE SCATTERING MATRIX KI OF THE ICE LAYER
C
0087          CALL KMATI(ICO,KI)
C
C   COMPUTE THE MATRIX DI FOR THE ICE LAYER.
C   THE EXPONENTIAL OF THE PROPAGATION TENSOR KI, DI=EXP(MINUSJ*KI)
C
0088          CALL EXPON(KI,DI)
C
C   FOR ICE ONLY MEDIUM GO TO 50
C
0089          IF(ISCAT.EQ.3) GO TO 50
0090        20  CONTINUE
C
C   IF THE RAIN RATE HAS AN EXPONENTIAL SPATIAL DISTRIBUTION COMPUTE
```

```
C   THE LENGTH OF THE RAIN MEDIUM.
C
0091        IF(ISTAT.EQ.3) CALL LENGTH(L,ELEV,LAT,HO,RO,ISTAT)
C
C   COMPUTE THE SCATTERING MATRIX KR OF THE RAIN MEDIUM.
C
0092        CALL KMATR(RO,KR)
C
C   COMPUTE THE MATRIX DR FOR THE RAIN MEDIUM.
C   THE EXPONENTIAL OF THE PROPAGATION TENSOR KR, DR=EXP(MINUSJ*KR)
C
0093        CALL EXPON(KR,DR)
C
C   FOR RAIN ONLY GO TO 30
C
0094        IF(ISCAT.EQ.1) GO TO 30
C
C   COMPUTE THE TOTAL MEDIUM TRANSMISSION MATRIX D,  D = DR * DI
C
0095        CALL MULT(DR,2,2,DI,2,D)
0096        GO TO 60
0097     30 CONTINUE
C
C   FOR RAIN ONLY, D = DR
C
0098        D(1,1)=DR(1,1)
0099        D(2,2)=DR(2,2)
0100        D(1,2)=DR(1,2)
0101        D(2,1)=DR(2,1)
0102        GO TO 60
0103     50 CONTINUE
C
C   FOR RAIN ONLY, D = DI
C
0104        D(1,1)=DI(1,1)
0105        D(2,2)=DI(2,2)
0106        D(1,2)=DI(1,2)
0107        D(2,1)=DI(2,1)
0108     60 CONTINUE
C
C   COMPUTE THE RECEIVED FIELD   EFIN=D*EI .  EI IS THE INCIDENT
C   ELECTRIC FIELD AND D IS THE SCATTERING TENSOR OF THE RAIN SLAB.
C
0109        CALL MULT(D,2,2,EI,2,EFIN)
C
C   COMPUTE THE WAVE STATE PARAMETERS FOR CHANNELS 1 AND 2
C
0110        CALL WAVE(EFIN(1,1),EFIN(2,1),ARDBC1,TAUC1)
0111        CALL WAVE(EFIN(1,2),EFIN(2,2),ARDBC2,TAUC2)
0112        ARDB1(J)=ARDBC1
0113        TAU1(J)=TAUC1
0114        ARDB2(J)=ARDBC2
0115        TAU2(J)=TAUC2
```

```
                C
                C   COMPUTE THE ATTENUATION, ISOLATON, AND PHASE FOR THE GIVEN RAINRATE
                C   OR ICE CONTENT
                C
0116                  CALL OUTANT(EI,EFIN,ARC,ATTEN,XPI,XPD,PHASE)
0117                  ATTEN1(J)=ATTEN(1)
0118                  ATTEN2(J)=ATTEN(2)
0119                  XPI1(J)=XPI(1)
0120                  XPI2(J)=XPI(2)
0121                  XPD1(J)=XPD(2)
0122                  XPD2(J)=XPD(2)
0123                  PHASE1(J)=PHASE(1)
0124                  PHASE2(J)=PHASE(2)
0125                  IF(ISCAT.LT.3) RATE(J)=RO
0126                  IF(ISCAT.EQ.3) RATE(J)=ICO
                C
                C PRINT RESULTS
                C
0127                  WRITE(6,680) RATE(J),ATTEN1(J),XPI1(J),XPD1(J),PHASE1(J),
                     $ARDB1(J),TAU1(J),ATTEN2(J),XPI2(J),XPD2(J),PHASE2(J),
                     $ARDB2(J),TAU2(J)
0128             680  FORMAT(1X,F9.4,2X,F7.3,3X,F7.3,2X,F7.3,3X,F7.3,4X,F7.3,3X,F7.3,
                     $2X,F7.3,3X,F7.3,3X,F7.3,3X,F7.3,3X,F7.3,3X,F7.3)
0129              70  CONTINUE
0130                  IF(ISCAT.GT.2) GO TO 80
                C
                C   COMPUTE THE CURVE FIT PARAMETERS U AND V OF I=U+V*ALOG10(A)
                C
0131                  CALL FIT(ATTEN1,XPD1,U1,V1,R1)
0132                  CALL FIT(ATTEN2,XPD2,U2,V2,R2)
0133                  V1=-V1
0134                  V2=-V2
0135                  WRITE(6,690) U1,V1,R1,U2,V2,R2
0136             690  FORMAT(/////,10X,'THE LEAST SQUARES FIT OF XPD=U-V*ALOG10(A)',//,
                     $10X,'U1=',F10.4,5X,'V1=',F10.4,5X,'RSQ1=',F10.4,/,
                     $10X,'U2=',F10.4,5X,'V2=',F10.4,5X,'RSQ2=',F10.4)
0137              80  CONTINUE
0138                  GO TO 1
0139             999  CONTINUE
0140                  STOP
0141                  END
```

```
C*************************************************************************
C
0001        SUBROUTINE COMPNT(EPS,TAU,EX,EY)
C
C     THIS SUBROUTINE RETURNS THE X AND Y COMPONENTS GIVEN AN EPSILON
C     AND TAU (IN DEGREES) DESCRIBING AN ARBITRARY POLARIZATION STATE.
C
0002        COMPLEX  EX,EY
0003        COMPLEX MINUSJ
0004        COMMON/BLOC1/ MINUSJ,CONV
0005        EPSR=EPS*CONV
0006        TAUR=TAU*CONV
0007        IF(ABS(EPSR).EQ.(45.*CONV)) GO TO 10
C           IF(EPSR.EQ.0.) GO TO 20
0008        IF(TAUR.EQ.0.) GO TO 30
0009        IF(TAUR.EQ.(90.*CONV)) GO TO 40
0010        T1=TAN(2.*EPSR)
0011        T2=SIN(2.*TAUR)
0012        DELTR=ATAN2(T1,T2)
0013        GAMR=0.5*ARCOS(COS(2.*EPSR)*COS(2.*TAUR))
0014        GO TO 50
0015      10  DELTR=2.*EPSR
0016        GAMR=45.*CONV
0017        GO TO 50
C 20    DELTR=0.
C       GAMR=TAUR
C       GO TO 50
0018      30  DELTR=SIGN(1.,EPSR)*90.*CONV
0019        GAMR=ABS(EPSR)
0020        GO TO 50
0021      40  DELTR=SIGN(1.,EPSR)*90.*CONV
0022        GAMR=90.*CONV-ABS(EPSR)
0023      50  CONTINUE
0024        EX=COS(GAMR)
0025        EY=SIN(GAMR)*CEXP(-MINUSJ*DELTR)
0026        RETURN
0027        END

C*************************************************************************
C
0001        SUBROUTINE TPOSE(A,TPA,N)
C
C   THIS ROUTINE RETURNS THE TRANSPOSE OF THE NXN COMPLEX MATRIX A.
C
0002        COMPLEX A(N,N),TPA(N,N)
0003        DO 10 J=1,N
0004        DO 10 K=1,N
0005        TPA(J,K)=A(K,J)
0006      10  CONTINUE
0007        RETURN
0008        END
```

```
C*************************************************************************
C
0001            SUBROUTINE LENGTH(L,ELEV,LAT,HO,RO,ISTAT)
C
C   THIS ROUTINE COMPUTES THE LENGTH (METERS)  OF THE RAIN MEDIUM
C   DEPENDING ON THE MODEL OF THE RAIN: PIECE-WISE UNIFORM, EXPONENTIAL.
C
0002            REAL L,LAT
0003            IF(ISTAT.EQ.3) GO TO 10
C
C   PIECE-WISE UNIFORM
C
0004            H=4000.0
0005            IF(LAT.GT.40.) H=3500.0
0006            IF(LAT.LT.33.) H=4500.0
0007            EO=ATAN(H/10500.0)
0008            L=H/SIN(ELEV)
0009            IF(ELEV.LT.EO) L=10500.0/COS(ELEV)
0010            RETURN
C
C   EXPONENTIAL
C
0011          10  IF(LAT.LE.30.) HI=4.8
0012              IF(LAT.GT.30.) HI=7.8-0.1*ABS(LAT)
0013              IF(RO.LE.10.) HE=HI
0014              IF(RO.GT.10.) HE=HI+ALOG10(RO/10.)
0015              HE=HE*1000.
0016              L=(HE-HO)/SIN(ELEV)
0017              RETURN
0018              END
```

```
C*************************************************************************
C
0001            SUBROUTINE MCONJG(A,AC,M,N)
C
C   THIS ROUTINE RETURNS THE COMPLEX CONJUGATE OF THE MXN MATRIX A
C   AS THE MATRIX AC.
C
0002            COMPLEX A(M,N),AC(M,N)
0003            DO 10 J=1,M
0004            DO 10 K=1,N
0005            AC(J,K)=CONJG(A(J,K))
0006          10  CONTINUE
0007              RETURN
0008              END
```

```
C*********************************************************************
C
0001          SUBROUTINE KMATR(RO,KR)
C
C   THIS SUBROUTINE COMPUTES THE SCATTERING MATRIX OF A RAIN
C   MEDIUM WITH UNIFORM (ISTAT=1), PIECE-WISE UNIFORM (ISTAT=2), OR
C   EXPONENTIAL (ISTAT=3) RAINRATE SPATIAL DISTRIBUTION.
C
0002          COMPLEX F(2,2),FV1,FH1,DIFF1,FV2,FH2,DIFF2,FSH1,FSH2
             C,FV,FH,FSH,DIFF,KR(2,2)
0003          REAL AMODE(6)
0004          REAL KO,NO,L
0005          INTEGER Q
0006          COMMON/BLOC3/ FREQ,KO,L,ELEV,P1,P2,ISTAT,PI,THE,SIGM,PN,PP,PSI,
             $SIGPSI,PHI,SIGPHI
C
C   THE AMODE VALUES ARE THE RAINDROP RADIUS (MM) THAT FORM THE
C   INTERVALS FOR THE SINGLE DROP SCATTERING COEFFICIENTS POLYNOMIAL
C   CURVE FITS.
C
0007          DATA AMODE/0.0,0.25,1.0,2.0,2.5,3.5/
0008          NO=16000.
C
C   INITIALIZE THE SCATTERING MATRIX F TO THE ZERO MATRIX
C
0009          DO 10 I=1,2
0010          DO 10 J=1,2
0011       10 F(I,J)=(0.0,0.0)
C
C   COMPUTE THE AVERAGE OF COS(2.0*THETA) , SIN(2.*THETA)
C
0012          CTHE=EXP(-2.*SIGM**2)*COS(2.*THE)
0013          STHE=EXP(-2.*SIGM**2)*SIN(2.*THE)
C
C   CHECK FOR EXPONENTIAL RAIN SPATIAL DISTRIBUTION
C
0014          J=0
0015          IF(ISTAT.EQ.3) GO TO 20
C
C   COMPUTE THE SCATTERING MATRIX F FOR THE UNIFORM, OR PIECE-WISE
C   UNIFORM RAIN SPATIAL DISTRIBUTION.
C
0016       15 J=J+1
0017          AL=L
0018          R=RO*((RO/10.)**(-(J-1.)*0.66))
0019          IF(ISTAT.EQ.2) AL=L*0.2
0020          IF(J.EQ.2) AL=0.8*L
0021          GO TO 30
C
C   COMPUTE THE SCATTERING MATRIX F FOR THE EXPONENTIAL RAIN
C   SPATIAL DISTRIBUTION.
C
0022       20 CONTINUE
```

```
0023                  AL=L
0024                  R=RO
0025               30 CONTINUE
0026                  DO 40 Q=1,5
0027                  AMODE1=AMODE(Q)+0.001
0028                  AMODE2=AMODE(Q+1)
                   C
                   C   THE FIRST CALL TO COEFF COMPUTES FOR THE LOWER LIMIT AMODE1 IN
                   C   THE INTERVAL Q.
                   C
0029                  CALL COEF(FREQ,AMODE1,FV1,FH1,FSH1,DIFF1,ELEV,R,AL,ISTAT)
                   C
                   C   THE SECOND CALL TO COEFF COMPUTES FOR THE UPPER LIMIT AMODE2 IN
                   C   THE INTERVAL Q.
                   C
0030                  CALL COEF(FREQ,AMODE2,FV2,FH2,FSH2,DIFF2,ELEV,R,AL,ISTAT)
                   C
                   C   THE INTEGRATION OVER THE AMODE INTERVAL Q IS PERFORMED BY
                   C   SUBTRACTING THE RESULTS FROM THE LOWER INTERVAL LIMIT FROM
                   C   THE RESULTS FROM THE UPPER INTERVAL LIMIT.
                   C
0031                  FV=FV2-FV1
0032                  FH=FH2-FH1
0033                  FSH=FSH2-FSH1
0034                  DIFF=DIFF2-DIFF1
                   C
                   C   SUM THE COMPUTATIONS OF THE INTERVALS.
                   C
0035                  F(1,1)=F(1,1)+(P1*FSH+P2*((FH+FV)/2.-DIFF*CTHE/2.))*NO
0036                  F(2,2)=F(2,2)+(P1*FSH+P2*((FV+FH)/2.+DIFF*CTHE/2.))*NO
0037                  F(1,2)=F(1,2)+(P2*DIFF )*(STHE/2.)*NO
0038                  F(2,1)=F(1,2)
0039               40 CONTINUE
0040                  IF(ISTAT.NE.3.AND.J.NE.ISTAT) GO TO 15
                   C
                   C   COMPUTE THE SCATTERING MATRIX K.
                   C
0041                  KR(1,1)=2.*PI*F(1,1)/KO
0042                  KR(2,2)=2.*PI*F(2,2)/KO
0043                  KR(2,1)=2.*PI*F(2,1)/KO
0044                  KR(1,2)=KR(2,1)
0045                  RETURN
0046                  END
```

```
                C*********************************************************************
                C
0001                  SUBROUTINE KMATI(ICO,KI)
                C
                C   THIS SUBROUTINE COMPUTES THE SCATTERING MATRIX OF AN ICE CLOUD
                C   WITH ICE CONTENT ICO.
                C
0002                  COMMON/BLOC3/ FREQ,KO,L,ELEV,P1,P2,ISTAT,PI,THE,SIGM,PN,PP,PSI,
                     $SIGPSI,PHI,SIGPHI
0003                  COMPLEX FP(2,2),FN(2,2),KI(2,2),M,MSQ,F(2,2)
0004                  REAL ICO,KO,L,NXNX,NYNY,NXNY
                C
                C   M IS THE COMPLEX INDEX OF REFRACTION OF ICE
                C
0005                  M=(1.78,-0.0024)
0006                  MSQ=M*M
                C
                C   COMPUTE THE AVERAGE OF COS(2.0*PHI) ,SIN(2.0*PHI)
                C
0007                  CPHI=EXP(-2.*(SIGPHI**2))*COS(2.*PHI)
0008                  SPHI=EXP(-2.*(SIGPHI**2))*SIN(2.*PHI)
                C
                C   COMPUTE THE AVERAGE OF COS(2.0*PSI) ,SIN(2.0*PSI)
                C
0009                  CPSI=EXP(-2.*(SIGPSI**2))*COS(2.*PSI)
0010                  SPSI=EXP(-2.*(SIGPSI**2))*SIN(2.*PSI)
                C
                C   COMPUTE THE SCATTERING  MATRIX FP FOR ICE PLATES
                C
0011                  NXNX=COS(ELEV)*COS(ELEV)*(1.-CPSI)/2.
0012                  NYNY=COS(ELEV)*COS(ELEV)*(1.+CPSI)/2.
0013                  NXNY=COS(ELEV)*COS(ELEV)*SPSI/2.
                C
0014                  FP(1,1)=(MSQ-1.)*(1.+(1.-MSQ)/MSQ*NXNX)
0015                  FP(2,2)=(MSQ-1.)*(1.+(1.-MSQ)/MSQ*NYNY)
0016                  FP(1,2)=(MSQ-1.)*((1.-MSQ)/MSQ*NXNY)
0017                  FP(2,1)=FP(1,2)
                C
                C   COMPUTE THE SCATTERING MATRIX FN FOR ICE NEERDLES
                C
0018                  OXOX=(1.+COS(ELEV)*COS(ELEV)*(CPHI+CPSI)+CPSI*CPHI*(1.+SIN(ELEV)*
                     $SIN(ELEV))+SIN(ELEV)*SIN(ELEV)+2.*SPSI*SPHI*SIN(ELEV))/4.
0019                  OYOY=(1.+COS(ELEV)*COS(ELEV)*(CPHI-CPSI)-CPSI*CPHI*(1.+SIN(ELEV)*
                     $SIN(ELEV))+SIN(ELEV)*SIN(ELEV)-2.*SPSI*SPHI*SIN(ELEV))/4.
0020                  OXOY=(2.*CPSI*SPHI*SIN(ELEV)-SPSI*CPHI*(1.+SIN(ELEV)*SIN(ELEV))
                     $-SPSI*COS(ELEV)*COS(ELEV))/4.
                C
0021                  FN(1,1)=2.*(MSQ-1.)/(MSQ+1.)*(1.+(MSQ-1.)/2.*OXOX)
0022                  FN(2,2)=2.*(MSQ-1.)/(MSQ+1.)*(1.+(MSQ-1.)/2.*OYOY)
0023                  FN(1,2)=2.*(MSQ-1.)/(MSQ+1.)*(MSQ-1.)/2.*OXOY
0024                  FN(2,1)=FN(1,2)
                C
                C   COMPUTE THE SCATTERING MATRIX KI
```

```
C
      DO 20 I=1,2
      DO 10 J=1,2
      KI(I,J)=0.5*KO*ICO*(PP*FP(I,J)+PN*FN(I,J))
   10 CONTINUE
   20 CONTINUE
      RETURN
      END
```

```
                C*********************************************************************
                C
0001                  SUBROUTINE COEF(FREQ,AMODE,FV,FH,FSPH,DIFF,ELEV,R,AL,ISTAT)
                C
                C     THIS SUBROUTINE RETURNS TO THE CALLING PROGRAM THE SCATTERING
                C     COEFFICIENTS FOR SPHERICAL AND OBLATE RAIN DROPS.
                C     THE COEFFICIENTS ARE A FUNCTION OF FREQUENCY AND DROP SIZE
                C     AND ELEVATION ANGLE.  THE COEFFICIENTS USED ARE THOSE OF UZUNOGLU,
                C     EVANS AND HOLT. THIS IS A MODIFIED VERSION OF THE
                C     SUBROUTINE DEVELOPED BY PERSINGER AND STUTZMAN.
                C
0002                  COMPLEX CMPLX
0003                  COMPLEX FV,FH,FSPH,DIFF
0004                  REAL U(6)
                C
                C   FIND THE VALUES OF POWERS OF THE EQUIVOLUMETRIC RADIUS
                C   AVERAGED OVER THE DISTRIBUTION OF THE RAINDROPS WITH
                C   RESPECT TO POSITION AND SIZE.
                C
0005                  CALL INTGR(FREQ,AMODE,R,AL,ELEV,ISTAT,U)
                C
                C   U0,U1,U2,U3,U4,U5, ARE THE ZERO FIRST,SECOND ETC AVERAGED POWERS
                C   OF THE EQUIVOLUMETRIC RADIUS.
                C
0006                  U0=U(1)
0007                  U1=U(2)
0008                  U2=U(3)
0009                  U3=U(4)
0010                  U4=U(5)
0011                  U5=U(6)
                C
                C   NOTE: THE POLYNOMIAL FITS ARE 10 TIMES LARGER THAN EVANS AND HOLT
                C         SINGLE DROP COEFFICIENTS.
                C
                C   NOTE: THE DIFFERENTIAL COEFFICIENTS DIFFR,DIFFI ARE FH-FV FROM EVANS
                C         AND HOLT.
                C
                C---------------------------------------------------------------------
                C
                C     4.0 GHZ COEFFICIENTS
                C---------------------------------------------------------------------
0012                  IF(INT(FREQ).NE.4) GO TO 100
                C
                C     SPHERICAL DROP COEFFICIENTS
                C
0013                  IF(AMODE.GT.1.25) GO TO 110
                C
0014                  EOR=U0*3.2E-5-2.862666666E-4*U1+9.064E-4*U2+5.469866666E-3*U3
                     1+.001088*U4
0015                  EOI=U0*7.34E-6-6.566533333E-5*U1+2.07632E-4*U2-2.354986667E-4*U3
                     1+1.80992E-4*U4
0016                  GO TO 111
0017             110  CONTINUE
```

```
                C
0018                 EOR=-U0*.5283066839+1.408094137*U1-1.457767235*U2+.7388385363*U3
                    1-.1781248717*U4+.01710865643*U5
0019                 EOI=-U0*.1845101396+.4974350688*U1-.5232270887*U2+.2687056659*U3
                    1-6.753081628E-2*U4+6.732065313E-3*U5
                C
0020                 GO TO 112
0021              111  CONTINUE
                C-------------------------------------------------------------------
                C     OBLATE DROP COEFFICIENTS
                C
0022                 EV90R=U0*2.9E-5-2.545333334E-4*U1+7.878666668E-4*U2+5.666133333E-3
                    1*U3+1.68533333333E-4*U4
0023                 EV90I=U0*7.285E-6-6.4463E-5*U1+2.00938E-4*U2-2.22288E-4*U3
                    1+1.59328E-4*U4
0024                 EH90R=U0*3.5E-5-3.18E-4*U1+1.026933333E-3*U2+.0052736*U3
                    1+1.207466667E-3*U4
0025                 EH90I=U0*9.745E-6-8.6791E-5*U1+2.722126667E-4*U2-3.20336E-4*U3
                    1+2.236693333E-4*U4
0026                 DIFFR=U0*6.0E-6-6.346666664E-5*U1+2.390666666E-4*U2-3.925333333E-4
                    1*U3+1.038933333E-3*U4
0027                 DIFFI=U0*2.86E-6-2.566133333E-5*U1+8.0608E-5*U2-1.087146667E-4*U3
                    1+6.8608E-5*U4
                C
0028                 GO TO 1000
0029              112  CONTINUE
                C
0030                 EV90R=-U0*.76216002+2.027068821*U1-2.09378577*U2+1.055413358*U3
                    1-.255028577*U4+2.410361953E-2*U5
0031                 EV90I=-U0*.1887390064+.5084448775*U1-.5341877846*U2+.2738404511*U3
                    1-6.863368402E-2*U4+6.804241398E-3*U5
0032                 EH90R=-U0*.5876866863+1.569955667*U1-1.63198314*U2+.8322340943*U3
                    1-.203470904*U4+1.998967235E-2*U5
0033                 EH90I=-U0*.732168559+1.988465191*U1-2.109866324*U2+1.094172886*U3
                    1-.2778837732*U4+2.781064856E-2*U5
0034                 DIFFR=U0*.174473338-.4571131539*U1+.4618026564*U2-.2231792645*U3
                    1+5.155767301E-2*U4-4.113947188E-3*U5
0035                 DIFFI=-U0*.5434295527+1.480020313*U1-1.575678539*U2+.8203324351*U3
                    1-.2092500892*U4+2.100640716E-2*U5
                C
                C     IF((AMODE.GE.1.5).AND.(AMODE.LE.2.0)) DIFFI=U0*.13455E-3+1.2488E-3
                C    1*(U1-1.5)
                C
0036                 GO TO 1000
0037              100  CONTINUE
                C-------------------------------------------------------------------
                C
                C     6 GHZ COEFFICIENTS
                C-------------------------------------------------------------------
0038                 IF(INT(FREQ).NE.6) GO TO 200
                C
                C     SPHERICAL DROP COEFFICIENTS
                C
```

```
0039                  IF(AMODE.GT.1.25) GO TO 210
                C
0040                  EOR=U0*1.435E-4-1.293966667E-3*U1+4.154466668E-3*U2+9.189866666E-3
                     1*U3+4.466133333E-3*U4
0041                  EOI=U0*9.745E-5-8.5481E-4*U1+2.615206667E-3*U2-3.29008E-3*U3
                     1+1.904533333E-3*U4
0042                  GO TO 211
0043           210    CONTINUE
0044                  EOR=-U0*5.495760154+14.33206152*U1-14.41237337*U2+6.970435718*U3
                     1-1.601631782*U4+.1408985428*U5
0045                  EOI=U0*4.168678146-11.40369894*U1+12.16403153*U2-6.309677488*U3
                     1+1.585440986*U4-.1527419458*U5
                C
                C     IF(AMODE.LE.1.5) EOI=U0*.1339E-2+8.4372E-3*(U1-1.25)
                C
0046                  GO TO 212
0047           211    CONTINUE
                C-----------------------------------------------------------------------
                C     OBLATE DROP COEFFICIENTS
                C
0048                  EV90R=U0*1.59E-4-.0013962*U1+4.309199999E-3*U2+9.276799999E-3*U3
                     1+.0024512*U4
0049                  EV90I=U0*9.12E-5-8.004933333E-4*U1+2.452066667E-3*U2-3.081386667E-
                     13*U3+1.760213333E-3*U4
0050                  EH90R=U0*2.035E-4-1.811966667E-3*U1+.0056958*U2+7.237866665E-3*U3
                     1+.0054048*U4
0051                  EH90I=U0*1.349E-4-.00117752*U1+3.571306667E-3*U2-.0044864*U3
                     1+2.461013333E-3*U4
0052                  DIFFR=U0*4.45E-5-4.157666667E-4*U1+.0013866*U2-2.038933333E-3*U3
                     1+.0029536*U4
0053                  DIFFI=U0*4.37E-5-3.770266667E-4*U1+1.11924E-3*U2-1.405013333E-3*U3
                     1+7.008E-4*U4
                C
                C     IF(AMODE.LE.0.5) DIFFI=U0*.18E-6+1.196E-5*(U1-.25)
0054                  GO TO 1000
0055           212    CONTINUE
                C
0056                  EV90R=-U0*5.329666816+13.91794322*U1-14.01487548*U2+6.785896455*U3
                     1-1.561197919*U4+.136821167*U5
0057                  EV90I=U0*4.267152149-11.67086117*U1+12.44813368*U2-6.458176158*U3
                     1+1.623786702*U4-.156723203*U5
0058                  EH90R=-U0*12.89499372+34.08624828*U1-34.88670275*U2+17.24582856*U3
                     1-4.092570461*U4+.3736189707*U5
0059                  EH90I=-U0*5.636522125+14.02279601*U1-13.28152624*U2+5.944722798*U3
                     1-1.250844791*U4+.09992091678*U5
0060                  DIFFR=-U0*7.565326904+20.16830506*U1-20.87182727*U2+10.4599321*U3
                     1-2.531372542*U4+.2367978037*U5
                C
                C     IF(AMODE.LE.1.5) EV90I=U0*.1201E-2+7.6708E-3*(U1-1.25)
                C     IF((AMODE.GE.1.5).AND.(AMODE.LE.2.0)) EH90I=U0*.4049E-2+.041298*
                C    1(U1-1.5)
                C     IF(AMODE.LE.1.5) DIFFI=U0*2.88E-5+2.568E-4*(U1-1.25)
                C     IF((AMODE.GT.1.5).AND.(AMODE.LE.2.0)) DIFFI=U0*9.3E-5+1.154E-3*
```

```
C     1(U1-1.5)
C      IF((AMODE.GT.2.0).AND.(AMODE.LE.2.5)) DIFFI=U0*6.7E-4+.01626*
C     1(U1-2.0)
C      IF((AMODE.GT.2.5).AND.(AMODE.LE.3.0)) DIFFI=U0*8.8E-3-.016*
C     1(U1-2.5)
C      IF((AMODE.GT.3.0).AND.(AMODE.LE.3.5)) DIFFI=U0*8.0E-4+4.4E-3*
C     1(U1-3.0)
0061        DIFFI=EH90I-EV90I
C
0062        GO TO 1000
C
0063    200 CONTINUE
C-------------------------------------------------------------------------
C
C     11.0 GHZ COEFFICIENTS
C-------------------------------------------------------------------------
0064        IF(INT(FREQ).NE.11) GO TO 1
C
C     SPHERICAL DROP COEFFICIENTS
C
0065        IF(AMODE.GT.1.00) GO TO 10
C
0066        EOR=-U0*0.0020548+0.01638947*U1-0.0417568*U2+0.08832213*U3
0067        EOI=-U0*0.0025154+0.01928553*U1-0.0456816*U2+0.03655147*U3
0068        GO TO 11
0069     10 CONTINUE
C
0070        EOR=-U0*1.28155706+2.83287718*U1-2.07399678*U2+0.60190887*U3
           1-0.00984194*U4-0.01096165*U5
0071        EOI=U0*2.60278025-7.52434662*U1+8.14691632*U2-4.12133971*U3
           1+0.99089467*U4-0.08731788*U5
C
0072        GO TO 12
0073     11 CONTINUE
C-------------------------------------------------------------------------
C     OBLATE DROP COEFFICIENTS
C
0074        EV90R=-U0*0.001322+0.01036867*U1-0.025372*U2+0.07072533*U3
0075        EV90I=-U0*0.0024306+0.01861967*U1-0.0440232*U2+0.03507413*U3
0076        EH90R=-U0*0.0023684+0.01878307*U1-0.0473704*U2+0.09255573*U3
0077        EH90I=-U0*0.0030366+0.02320527*U1-0.0546296*U2+0.04299093*U3
0078        DIFFR=-U0*0.0010464+0.0084144*U1-0.0219984*U2+0.0218304*U3
0079        DIFFI=-U0*0.000606+0.0045856*U1-0.0106064*U2+0.0079168*U3
C
0080        GO TO 1000
0081     12 CONTINUE
C
0082        EV90R=-U0*0.3653892+0.32540943*U1+0.45280976*U2-0.53907398*U3
           1+0.20309215*U4-0.02432204*U5
0083        EV90I=U0*2.20618555-6.19251766*U1+6.43873903*U2-3.090414*U3
           1+0.70600211*U4-0.0607173*U5
0084        EH90R=U0*2.09022706-7.07345119*U1+9.03639726*U2-5.33156215*U3
           1+1.49716423*U4-0.15747063*U5
```

```
0085                EH90I=U0*3.28654422-9.68217951*U1+10.71102231*U2-5.5491184*U3
                   1+1.36694565*U4-0.12512466*U5
0086                DIFFI=U0*1.08034369-3.48962081*U1+4.2722407*U2-2.45868344*U3
                   1+0.66093861*U4-0.06440692*U5
                C
0087                IF(AMODE.GT.2.0) GO TO 120
                C
0088                DIFFR=-U0*0.32599997+0.7531995*U1-0.57039996*U2+0.15039999*U3
0089                GO TO 1000
                C
0090              120 CONTINUE
                C
0091                DIFFR=U0*11.94200847-14.59334299*U1+5.80600359*U2-0.7346671*U3
                C
0092                GO TO 1000
                C
0093                1 CONTINUE
                C-----------------------------------------------------------------------
                C
                C     14 GHZ COEFFICIENTS
                C-----------------------------------------------------------------------
0094                IF(INT(FREQ).NE.14) GO TO 2
                C
                C     SPHERICAL DROP COEFFECIENTS
                C
0095                IF(AMODE.GT.1.00) GO TO 20
                C
0096                EOR=-U0*0.001376+0.012776*U1-0.040136*U2+0.128736*U3
0097                EOI=-U0*0.008796+0.06731467*U1-0.1588*U2+0.12418133*U3
                C
0098                GO TO 21
0099              20 CONTINUE
                C
0100                EOR=-U0*12.13707993+34.85683676*U1-37.84887378*U2+19.48995359*U3
                   1-4.69149894*U4+0.42548477*U5
0101                EOI=-U0*8.4550178+22.97909617*U1-23.38444001*U2+11.09553161*U3
                   1-2.41694538*U4+0.19907664*U5
                C
0102                GO TO 22
0103              21 CONTINUE
                C-----------------------------------------------------------------------
                C     OBLATE DROP COEFFICIENTS
                C
0104                EV90R=-U0*0.000248+0.00335467*U1-0.013928*U2+0.10002133*U3
0105                EV90I=-U0*0.008436+0.06455867*U1-0.152256*U2+0.11893333*U3
0106                EH90R=-U0*0.000656+0.007656*U1-0.029656*U2+0.122656*U3
0107                EH90I=-U0*0.010366+0.079154*U1-0.18596*U2+0.143872*U3
0108                DIFFR=-U0*0.000408+0.00430133*U1-0.015728*U2+0.02263467*U3
0109                DIFFI=-U0*0.00193+0.01459533*U1-0.033704*U2+0.02493867*U3
                C
0110                GO TO 1000
0111              22 CONTINUE
                C
```

```
0112                EV90R=-U0*4.48493663+12.45481829*U1-12.90182271*U2+6.32901913*U3
                   1-1.42805671*U4+0.11875301*U5
0113                EV90I=-U0*0.1923376+0.3425132*U1-0.196242*U2+0.07468968*U3
                C
0114                IF(AMODE.GT.2.5) GO TO 24
                C
0115                EH90I=U0*1.10278458-3.74696237*U1+4.48042001*U2-2.22964317*U3
                   1+0.42010037*U4
0116                DIFFR=-U0*0.15268404+0.39830845*U1-0.3527577*U2+0.11767014*U3
0117                DIFFI=-U0*1.29960041+2.93303524*U1-2.15255009*U2+0.5206384*U3
                C
0118                IF(AMODE.GT.2.00) GO TO 25
                C
0119                EH90R=-U0*1.02599992+2.30733317*U1-1.60799988*U2+0.4266664*U3
                C
0120                GO TO 1000
0121             24 CONTINUE
                C
0122                EH90I=U0*2.51000033-2.03000022*U1+0.62000004*U2
0123                DIFFR=-U0*15.85152202+18.27189723*U1-6.68140666*U2+0.79411153*U3
0124                DIFFI=U0*22.32321586-44.48681458*U1+30.17926125*U2-8.46925565*U3
                   1+0.85300427*U4
                C
0125                GO TO 1000
0126             25 CONTINUE
                C
0127                EH90R=-U0*19.65+20.6567*U1-6.66*U2+0.6933*U3
                C
0128                GO TO 1000
0129              2 CONTINUE
                C-----------------------------------------------------------------------
                C
                C     20 GHZ COEFFICIENTS
                C-----------------------------------------------------------------------
0130                IF(INT(FREQ).NE.20) GO TO 3
                C
                C     SPHERICAL DROP COEFFICIENTS
                C
0131                IF(AMODE.GT.1.0) GO TO 30
                C
0132                EOR=U0*0.020296-0.145276*U1+0.297656*U2+0.008224*U3
                C
0133                EOI=-U0*0.015488+0.12709133*U1-0.334568*U2+0.30583467*U3
                C
0134                GO TO 31
0135             30 CONTINUE
                C
0136                EOR=U0*3.35567152-8.61818659*U1+7.8157989*U2-2.68217917*U3
                   1+0.3108073*U4
0137                EOI=U0*1.85636463-3.70750898*U1+2.19599302*U2-0.25148145*U3
                C
0138                GO TO 32
0139             31 CONTINUE
```

```
C-----------------------------------------------------------------------
C     OBLATE DROP COEFFICIENTS
C
      EV90R=U0*0.02454800-0.17912133*U1+0.384448*U2-0.07447467*U3
      EV90I=-U0*0.013492+0.11190533*U1-0.299032*U2+0.27853867*U3
      EH90R=U0*0.02282-0.16596667*U1+0.34976*U2-0.03061333*U3
      EH90I=-U0*0.015178+0.12623933*U1-0.33848*U2+0.31533867*U3
      DIFFR=U0*0.000072+0.00175467*U1-0.015488*U2+0.03426133*U3
      DIFFI=-U0*0.001686+0.014334*U1-0.039448*U2+0.0368*U3
C
      GO TO 1000
   32 CONTINUE
C
      EV90R=U0*1.56037246-3.97019757*U1+3.66524972*U2-1.24458239*U3
     1+0.14526662*U4
      EV90I=U0*4.77376463-13.63610787*U1+14.83397997*U2
     1-7.66136891*U3+1.96881573*U4-0.19749381*U5
      EH90R=U0*4.63026679-11.97374109*U1+11.0254653*U2
     1-4.0050613*U3+0.50244373*U4
      EH90I=-U0*1.5390057+6.3417866*U1-9.35328879*U2+6.20987895*U3
     1-1.74544867*U4+0.17820925*U5
      DIFFR=U0*3.06989428-8.00354339*U1+7.36021547*U2
     1-2.76047886*U3+0.3571771*U4
      DIFFI=-U0*6.31274803+19.97783334*U1-24.1872053*U2+13.8712166*U3
     1-3.71425705*U4+0.3757024*U5
C
      GO TO 1000
    3 CONTINUE
C
      IF(INT(FREQ).NE.30) GO TO 2000
C-----------------------------------------------------------------------
C
C     30 GHZ COEFFICIENTS
C-----------------------------------------------------------------------
C
C     SPHERICAL DROP COEFFICIENTS
C
      IF(AMODE.GT.1.0) GO TO 40
C
      EOR=U0*0.028004-0.221564*U1+0.530744*U2+0.022816*U3
      EOI=-U0*0.007072+0.09329866*U1-0.390112*U2+0.55688533*U3
C
      GO TO 41
   40 CONTINUE
C
      EOR=-U0*1.95096901+3.4107597*U1-0.82790307*U2-0.39982485*U3
     1+0.1291964*U4
      EOI=U0*5.77798866-16.3876166*U1+16.10102407*U2-6.06482662*U3
     1+0.82747918*U4
C
      GO TO 42
   41 CONTINUE
C-----------------------------------------------------------------------
```

```
C      OBLATE DROP COEFFICIENTS
C
0166        EV90R=U0*0.03542-0.2838733*U1+0.7038*U2-0.15834666*U3
0167        EV90I=U0*0.013876-0.064756*U1-0.026904*U2+0.290784*U3
0168        EH90R=U0*0.031652-0.252652*U1+0.614952*U2-0.049952*U3
0169        EH90I=-U0*0.000532+0.04746533*U1-0.299512*U2+0.50957867*U3
0170        DIFFR=-U0*0.003768+0.03122133*U1-0.088848*U2+0.10839467*U3
0171        DIFFI=-U0*0.014408+0.11222133*U1-0.272608*U2+0.21879467*U3
C
0172        GO TO 1000
0173     42 CONTINUE
C
0174        EV90R=U0*3.93161268-10.97208846*U1+11.43870068*U2
           1-4.78953064*U3+0.69447892*U4
0175        EV90I=U0*3.12729055-9.08249632*U1+9.16246329*U2
           1-3.47227982*U3+0.47789632*U4
0176        EH90R=-U0*6.97583584+16.79179963*U1-13.53607686*U2
           1+4.63811854*U3-0.57535653*U4
0177        EH90I=-U0*1.39373246+1.72736066*U1-0.14076091*U2+0.05474057*U3
0178        DIFFR=-U0*10.90744851+27.76388807*U1-24.97477753*U2
           1+9.42764918*U3-1.26983545*U4
0179        DIFFI=U0*5.33984552-17.20920477*U1+20.7812541*U2
           1-11.64360435*U3+3.07942984*U4-0.30370378*U5
C-----------------------------------------------------------------------
0180     1000 CONTINUE
C
C   A FACTOR OF 0.001 IS REQUIRED TO RECOVER THE 10 OFFSET FROM EVANS
C   AND HOLT AND THE 100 FACTOR DIFFERENCE (AND CONJUGATE) FROM OGUCHI'S
C   NOTATION WHICH WE USE.
C
0181        EOR=0.001*EOR
0182        EOI=-0.001*EOI
0183        EV90R=0.001*EV90R
0184        EV90I=-0.001*EV90I
0185        EH90R=0.001*EH90R
0186        EH90I=-0.001*EH90I
C
C   THERE IS ANOTHER MINUS SIGN INTRODUCED IN THE DIFFERENTIAL
C   COEFFICIENTS TO GET FV-FH INSTEAD OF FH-FV FROM EVANS AND HOLT.
C
0187        DIFFR=-0.001*DIFFR
0188        DIFFI=0.001*DIFFI
C
0189        ALPH=1.576796-ELEV
0190        CSLA=COS(ALPH)**2
0191        SNLA=SIN(ALPH)**2
C
0192        FVR=CSLA*EOR+SNLA*EV90R
0193        FVI=CSLA*EOI+SNLA*EV90I
0194        FHR=CSLA*EOR+SNLA*EH90R
0195        FHI=CSLA*EOI+SNLA*EH90I
0196        DIFFR=SNLA*DIFFR
0197        DIFFI=SNLA*DIFFI
```

```
                C
0198                  FV=CMPLX(FVR,FVI)
0199                  FH=CMPLX(FHR,FHI)
0200                  FSPH=CMPLX(EOR,EOI)
0201                  DIFF=CMPLX(DIFFR,DIFFI)
                C
0202                  GO TO 3000
                C
0203               2000 WRITE(6,2001)
0204               2001 FORMAT(//,3X,'FREQUENCY NOT ALLOWED, ONLY 4,6,11,14,20,30 GHZ ',
                     1'ALLOWED')
                C
0205                  STOP
0206               3000 CONTINUE
                C
0207                  RETURN
0208                  END
```

```
C*********************************************************************
C
0001        SUBROUTINE INTGR(FREQ,AMODE,R,AL,ELEV,ISTAT,U)
C
C   THIS SUBROUTINE COMPUTES THE VALUES OF POWERS OF THE
C   EQUIVOLUMETRIC RADIUS AVERAGED OVER THE DISTRIBUTION
C   OF THE RAINDROPS WITH RESPECT TO POSITION AND SIZE.
C
0002        DOUBLE PRECISION EI,MMDEI,ARG
0003        REAL U(6),AI(2)
0004        AMODE1=AMODE
C
0005        IF(AMODE.LT.0.25) AMODE=0.25
0006        IF(AMODE.LE.0.25) GO TO 30
0007        IF((INT(FREQ).EQ.4).AND.(AMODE.GT.3.5)) AMODE=3.5
0008        IF((INT(FREQ).EQ.6).AND.(AMODE.GT.3.5)) AMODE=3.5
0009        IF((INT(FREQ).EQ.11).AND.(AMODE.GT.3.5)) AMODE=3.5
0010        IF((INT(FREQ).EQ.14).AND.(AMODE.GT.3.5)) AMODE=3.5
0011        IF((INT(FREQ).EQ.20).AND.(AMODE.GT.3.0)) AMODE=3.0
0012        IF((INT(FREQ).EQ.30).AND.(AMODE.GT.3.0)) AMODE=3.0
0013        IF((INT(FREQ).EQ.20).AND.(AMODE.GT.3.0)) GO TO 30
0014        IF((INT(FREQ).EQ.30).AND.(AMODE.GT.3.0)) GO TO 30
C
C   CHECK FOR EXPONENTIAL RAIN SPATIAL DISTRIBUTION (R>10 MM/HR).
C
0015        IF(ISTAT.EQ.3.AND.R.GT.10.) GO TO 50
C
C   COMPUTE FOR UNIFORM, PIECE-WISE UNIFORM, AND EXPONENTIAL
C   (R<=10 MM/HR) RAIN SPATIAL DISTRIBUTION.
C
0016        AC=-8.2*R**(-0.21)
0017        EXPON=EXP(AC*AMODE)
0018        U(1)=AL*EXPON/AC
0019        DO 20 N=1,5
0020        SUM=0.0
0021        DO 10 M=1,N
0022        SUM=SUM+GAMMA(N+1.)*(AMODE**(N-M))*(-1.0/AC)**M/GAMMA(N-M+1.)
0023   10   CONTINUE
0024        U(N+1)=(SUM+(AMODE**N))*U(1)
0025   20   CONTINUE
0026        RETURN
C
C   FOR  AMODE<=0.25, THE INTEGRAL IS THE FOLLOWING
C
0027   30   IF(ISTAT.EQ.3.AND.R.GT.10.) GO TO 110
0028        AC=-8.2*R**(-0.21)
0029        EXPON=EXP(AC*AMODE1)
0030        DO 40 N=1,6
0031   40   U(N)=(AMODE**N)*AL*EXPON/AC
0032        RETURN
C
C   COMPUTE FOR THE EXPONENTIAL SPATIAL RAINRATE DISTRIBUTION.
C   FOR RAINRATE>10 MM/HR
```

```
                C
0033              50  CONTINUE
0034                  AK=(0.21/22000.)*ALOG(R/10.)*COS(ELEV)
0035                  AC=-8.2*R**(-0.21)
0036                  DO 60 J=1,2
0037                  UP=EXP(AK*AL*(J-1))
0038                  ARG=AC*AMODE*UP
                C
                C   MMDEI IS THE IMSL ROUTINE FOR THE EXPONENTIAL INTEGRAL
                C   FUNCTION EI(ARG)
                C
0039                  EI=MMDEI(1,ARG,IER)
0040                  AI(J)=-EXP(AC*AMODE*UP)/UP+AC*AMODE*EI
0041              60  CONTINUE
0042                  U(1)=(AI(2)-AI(1))/(AK*AC)
0043                  DO 100 N=1,5
0044                  SUM2=0.0
0045                  DO 90 M=1,N
0046                  ASUM=GAMMA(N+1.)*((-1.0)**M)*(AMODE**(N-M))/GAMMA(N-M+1.)
0047                  DO 80 J=1,2
0048                  UP=EXP(AK*AL*(J-1))
0049                  MP1=M+1
0050                  SUM1=0.0
0051                  DO 70 L=1,MP1
0052              70  SUM1=SUM1+GAMMA(M+2.-L)*(AC*AMODE)**(L-1)/(UP**(M+2-L))
0053                  ARG=AC*AMODE*UP
0054                  EI=MMDEI(1,ARG,IER)
0055                  AI(J)=-EXP(AC*AMODE*UP)*SUM1+((AC*AMODE)**MP1)*EI
0056              80  CONTINUE
0057                  BSUM=(AI(2)-AI(1))/(AK*(AC**MP1)*GAMMA(M+2.))
0058                  SUM2=SUM2+ASUM*BSUM
0059              90  CONTINUE
0060                  U(N+1)=SUM2+(AMODE**N)*U(1)
0061             100  CONTINUE
0062                  RETURN
                C
                C   FOR AMODE<=0.25 THE INTEGRAL BECOMES THE FOLLOWING
                C   FOR RAINRATE>10 MM/HR
                C
0063             110  CONTINUE
0064                  AC=-8.2*R**(-0.21)
0065                  AK=(0.21/22000.)*ALOG(R/10.)*COS(ELEV)
0066                  DO 115 J=1,2
0067                  ARG=AC*AMODE1*EXP(AK*AL*(J-1))
0068                  EI=MMDEI(1,ARG,IER)
0069                  AI(J)=EI
0070             115  CONTINUE
0071                  AEI=(AI(2)-AI(1))/AC
0072                  DO 120 N=1,6
0073             120  U(N)=(AMODE**N)*AEI
0074                  RETURN
0075                  END
```

```
C*********************************************************************
C
0001        SUBROUTINE EXPON(K,D)
C
C   THIS SUBROUTINE COMPUTES THE EXPONENTIAL OF THE PROPAGATION
C   MATRIX.  IT USES AN EIGENVALUE-EIGENVECTOR METHOD DISCRIBED
C   IN THE FINAL REPORT OF ICE DEPOLARIZATION.
C
0002        COMPLEX K(2,2),D(2,2)
0003        COMPLEX MINUSJ,DIF,LAM1,LAM2,EX1,EX2
0004        COMMON/BLOC1/ MINUSJ,CONV
0005        DIF=CSQRT((K(1,1)-K(2,2))**2+(2.*K(1,2))**2)
0006        LAM1=0.5*(K(1,1)+K(2,2)+DIF)
0007        LAM2=0.5*(K(1,1)+K(2,2)-DIF)
0008        EX1=CEXP(MINUSJ*LAM1)
C
C  CHECK FOR ALL SPHERICAL DROPS.
C
0009        IF(REAL(LAM1).EQ.REAL(LAM2).AND.AIMAG(LAM1).EQ.AIMAG(LAM2))GOTO 10
C
0010        EX2=CEXP(MINUSJ*LAM2)
0011        D(1,1)=((K(2,2)-LAM2)*EX2-(K(2,2)-LAM1)*EX1)/DIF
0012        D(2,2)=((K(2,2)-LAM2)*EX1-(K(2,2)-LAM1)*EX2)/DIF
0013        D(1,2)=K(1,2)*(EX1-EX2)/DIF
0014        GO TO 20
C
C   FOR ALL SPHERICAL DROPS.
C
0015      10  D(1,1)=EX1
0016        D(2,2)=D(1,1)
0017        D(1,2)=(0.0,0.0)
0018      20  D(2,1)=D(1,2)
0019        RETURN
0020        END

C*********************************************************************
C
0001        SUBROUTINE  MULT(A,N,M,B,M1,C)
C
C   THIS SUBROUTINE MULTIPLIES TWO COMPLEX MATRICES
C
0002        COMPLEX A(N,M),B(M,M1),C(N,M1),SUM
0003        DO 20 I=1,N
0004        DO 20 J=1,M1
0005        SUM=(0.0,0.0)
0006        DO 10 IJ=1,M
0007      10  SUM=SUM+A(I,IJ)*B(IJ,J)
0008        C(I,J)=SUM
0009      20  CONTINUE
0010        RETURN
0011        END
```

```
C*************************************************************************
C
0001        SUBROUTINE WAVE(EXP,EYP,ARDB,TAUW)
C
C   THIS SUBROUTINE COMPUTES THE AXIAL RATIO IN DB AND THE TILT ANGLE
C   TAUW OF A WAVE WITH COMPONENTS EXP AND EYP.
C
0002        COMMON/BLOC1/ MINUSJ,CONV
0003        COMPLEX EXP,EYP
0004        EXPMAG=CABS(EXP)
0005        EXPR=REAL(EXP)
0006        EXPI=AIMAG(EXP)
0007        IF(EXPR.EQ.0.0.AND.EXPI.EQ.0.0) GO TO 10
0008        PHASEX=ATAN2(EXPI,EXPR)
0009        GO TO 20
0010      10  CONTINUE
0011        PHASEX=0.0
0012      20  CONTINUE
0013        EYPMAG=CABS(EYP)
0014        EYPR=REAL(EYP)
0015        EYPI=AIMAG(EYP)
0016        IF(EYPR.EQ.0.0.AND.EYPI.EQ.0.0) GO TO 30
0017        PHASEY=ATAN2(EYPI,EYPR)
0018        GO TO 40
0019      30  CONTINUE
0020        PHASEY=0.0
0021      40  CONTINUE
0022        DELTA=PHASEY-PHASEX
0023        GAMMA=ARCOS(EXPMAG/SQRT(EXPMAG*EXPMAG+EYPMAG*EYPMAG))
0024        EPS=0.5*ARSIN(SIN(2.*GAMMA)*SIN(DELTA))
0025        T1=SIN(2.*GAMMA)*COS(DELTA)
0026        T2=COS(2.*GAMMA)
0027        TAUW=0.5*ATAN2(T1,T2)/CONV
0028        AR=ABS(1./TAN(EPS))
0029        ARDB=20.*ALOG10(AR)
0030        RETURN
0031        END
```

```
                C*********************************************************************
                C
0001                  SUBROUTINE OUTANT(EI,EFIN,ARC,ATTEN,XPI,XPD,PHASE)
                C
                C     THIS SUBROUTINE TAKES THE X AND Y COMPONENTS OF THE WAVE EXITING
                C     THE RAIN CELL FOR EACH CHANNEL (1 AND 2) AND COMPUTES THE VALUES
                C     FOR ATTENUATION, ISOLATON, AND PHASE AS A RESULT OF THE TRANSMIT
                C     ANTENNA POLARIZATIONS,THE MEDIUM, AND THE POLARIZATION MISMATCH
                C     EFFECTS OF THE RECEIVE ANTENNA.
                C
0002                  COMPLEX EI(2,2),EFIN(2,2),ARC(2,2),TC(2,2),T(2,2)
0003                  COMPLEX  MINUSJ
0004                  REAL  ATTEN(2),XPI(2),XPD(2),PHASE(2)
0005                  COMMON/BLOC1/ MINUSJ,CONV
                C
                C   COMPUTE THE "CLEAR WEATHER" TRANSMISSION MATRIX TO INCLUDE THE
                C   RECEIVE ANTENNA EFFECTS.   VR = TC * VT
                C
0006                  CALL MULT(ARC,2,2,EI,2,TC )
                C
                C   COMPUTE THE MEDIA TRANSMISSION MATRIX TO INCLUDE THE RECEIVE
                C   ANTENNA EFFECTS.   VR = T * VT
                C
0007                  CALL MULT(ARC,2,2,EFIN,2,T)
                C
                C   COMPUTE THE ATTENUATION FOR CHANNEL 1 AND CHANNEL 2.
                C   ALL IN DB.
                C
0008                  ATTEN(1)=20.*ALOG10(CABS(TC(1,1))/CABS(T(1,1)))
0009                  ATTEN(2)=20.*ALOG10(CABS(TC(2,2))/CABS(T(2,2)))
                C
                C   COMPUTE THE PHASE,XPI, AND XPD
                C
                C   CHANNEL 1
                C
0010                  V1CR=REAL(T(1,1))
0011                  V1CI=AIMAG(T(1,1))
0012                  V1CP=ATAN2(V1CI,V1CR)/CONV
0013                  V1XR=REAL(T(1,2))
0014                  V1XI=AIMAG(T(1,2))
0015                  IF(CABS(T(1,2)).EQ.0.0) GO TO 10
0016                  V1XP=ATAN2(V1XI,V1XR)/CONV
0017                  XPI(1)=20.*ALOG10(CABS(T(1,1))/CABS(T(1,2)))
0018                  XPD(2)=20.*ALOG10(CABS(T(2,2))/CABS(T(1,2)))
0019                  IF(XPI(1).GT.100.) XPI(1)=999.00
0020                  IF(XPD(2).GT.100.) XPD(2)=999.00
0021                  GO TO 20
0022                10  CONTINUE
0023                  V1XP=0.0
0024                  XPI(1)=999.99
0025                  XPD(2)=999.99
0026                20  CONTINUE
                C
```

```
C    CHANNEL 2
C
0027        V2CR=REAL(T(2,2))
0028        V2CI=AIMAG(T(2,2))
0029        V2CP=ATAN2(V2CI,V2CR)/CONV
0030        V2XR=REAL(T(2,1))
0031        V2XI=AIMAG(T(2,1))
0032        IF(CABS(T(2,1)).EQ.0.0) GO TO 30
0033        V2XP=ATAN2(V2XI,V2XR)/CONV
0034        XPD(1)=20.*ALOG10(CABS(T(1,1))/CABS(T(2,1)))
0035        XPI(2)=20.*ALOG10(CABS(T(2,2))/CABS(T(2,1)))
0036        IF(XPD(1).GT.100.) XPD(1)=999.00
0037        IF(XPI(2).GT.100.) XPI(2)=999.00
0038        GO TO 40
0039     30 CONTINUE
0040        V2XP=0.0
0041        XPD(1)=999.99
0042        XPI(2)=999.99
0043     40 CONTINUE
C
C    THE PHASE COMPUTED IS 'XPD' PHASE
C
0044        PHASE(1)=V2XP-V1CP
0045        IF(PHASE(1).LT.0.0) PHASE(1)=PHASE(1)+360.0
0046        PHASE(2)=V1XP-V2CP
0047        IF(PHASE(2).LT.0.0) PHASE(2)=PHASE(2)+360.0
0048        RETURN
0049        END
```

```
C*************************************************************************
C
0001        SUBROUTINE FIT(X,Y,U,V,R)
0002        DIMENSION X(40),Y(40)
0003        X1=0.0
0004        X2=0.0
0005        Y1=0.0
0006        Y2=0.0
0007        XY=0.0
0008        N=0
0009        DO 10 I=1,30
0010        IF(X(I).LT.1.0) GO TO 10
0011        IF(Y(I).LT.0.0) GO TO 10
0012        N=N+1
0013        XX=ALOG10(X(I))
0014        YY=Y(I)
0015        X1=X1+XX
0016        X2=X2+XX*XX
0017        Y1=Y1+YY
0018        Y2=Y2+YY*YY
0019        XY=XY+XX*YY
0020     10 CONTINUE
0021        IF(N.EQ.0) GO TO 20
0022        XN=FLOAT(N)
0023        V=(XN*XY-X1*Y1)/(XN*X2-X1*X1)
0024        U=Y1/XN-V*X1/XN
0025        R=(XN*XY-X1*Y1)**2/((XN*X2-X1*X1)*(XN*Y2-Y1*Y1))
0026        RETURN
0027     20 CONTINUE
0028        V=0.0
0029        U=0.0
0030        R=0.0
0031        RETURN
0032        END
```

Chapter XI

REFERENCES

Arnold, H. W., Cox, D. C., Wazowicz, M. F., Hoffman, H. H. (1982), 19-GHz space-earth depolarization measurements at 4° polarization, IEEE Trans. on Ant. and Prop., Vol. AP-30, pp. 811-814, July 1982.

Arnold, H. W., Cox, D. C., Hoffman, H. H., and Leck, R. P., (1980), Characterisitcs of rain and ice depolarization for a 19- and 28-GHz propagation path from a Comstar stellite, IEEE Trans. on Ant. and Prop., Vol. AP-28, pp. 22-27, Jan. 1980.

Bostian, C. W., Stutzman, W. L., Gaines, J. M. (1982), A review of depolarization modeling for earth-space radio paths at frequencies above 10 GHz, Radio Science, Vol. 17, pp. 1231-1241, Sept./Oct. 1982.

Bostian, C. W., and Allnutt, J. E. (1979), Ice-crystal depolarization on satellite-earth microwave radio paths, Proc. IEE (London), Vol. 126, pp. 951-960, Oct. 1979.

CCIR (1977), Techniques for the prediction of rain depolarization statistics at microwave and millimeter wavelengths, CCIR Study Group Report, Doc. 5/206-E, Canada, May 20, 1977.

CCIR (1981), Cross-polarization due to the atmosphere, CCIR Study Group Report 722, Doc. 5/5005-E. September 7, 1981.

Cox, D. C. (1981), Depolarization of radio waves by atmospheric hydrometeors in earth-space paths: A review, Radio Science, Vol. 16, pp. 781-812, Sept./Oct. 1981.

Cox, D. C., and Arnold, H. W. (1982), Results from the 19-28-GHz Comstar satellite propagation experiments at Crawford Hill, Proc. IEEE, Vol. 70, pp. 458-488, May 1982.

Chu, T. S. (1974), Rain-induced cross-polarization at centimeter and millimeter wavelengths, B.S.T.J., Vol. 53, pp. 1557-1579, Oct. 1974.

Chu, T. S. (1980a), Microwave depolarization of an earth-space path, B.S.T.J., Vol. 59, pp. 987-1007, July/Aug. 1980.

Chu, T. S. (1980b), Analysis and prediction of cross-polarization on earth-space links, "Open-Symposium on Effects of the Lower Atmosphere on Radio Frequencies Above 1 GHz," Lennoxville Canada, pp. 6.8.1-6.8.7, May 1980.

Chu, T. S. (1981a), Analysis and prediction of cross-polarization on earth-space links, Ann. Telecommunic., Vol. 36, 1981.

Chu, T. S. (1981b), A semi-empirical formula for depolarization versus attenuation, URSI XXth General Assembly, Washington, D.C., August 10-19, 1981.

Chu, T. S. (1982), A semi-empirical formula for microwave depolarization versus rain attenuation on earth-space paths, IEEE Trans. on Comm., Vol. COM-30, pp. 2550-2554, Dec. 1982.

Castle, R. E., Bostian, C. W. (1979), Combining the effects of rain-induced attenuation and depolarization in digital satellite systems, IEEE Trans. on Aerospace and Electronic Systems, Vol. AES-15, March 1979.

Dishman, W.K. and Stutzman, W. L. (1982), Estimation of Rain Attenuation on Earth-Space Millimeter Wave Communication Links, Virginia Tech EE Dept Technical Report under NASA/JPL Contract No. 944954, May 1982.

Dissananyake, A. W., Haworth, D. P., and Watson, P. A. (1981), Analytical models for cross-polarization on earth-space radio paths for frequency range 9-30 GHz, Ann. Telecommunic., Vol. 35, pp. 398-404, 1980.

Edelson, B. J., and Cooper, R. S. (1982), Business use of satellite communications, Science, Vol. 215, pp. 837-842, February 12, 1982.

Gaines, J. M., and Bostian, C. W. (1982), Modeling the joint statistics of satellite path XPD and attenuation, IEEE Trans. on Ant. and Prop., Vol. AP-30, pp. 815-817, July 1982.

Gradshteyn, I. S. and Ryzhik, I. M. (1980), Table of Integrals, Series, and Products, Academic Press, p. 92.

Haworth, D. P., Watson, P. A., and McEwan, N. J. (1977), Model for the effect of electric fields on satellite-earth microwave radio propagation, Elec. Letters, Vol. 13, pp. 562-564, September 15, 1977.

Holt, A. R. and Evans, B. G. (1977), Some resonance effects in scattering of microwaves by hydrometeors, Proc. IEE, Vol. 124, pp. 1114-1116, Dec. 1977.

Howell, R. G., Thirlwell, J., Emerson, D. J. (1982), Long term cross-polar statistics at 12 and 14 GHz on a 30° slant path, presented at AGARD Conference on "Propagation Aspects of Frequency Sharing, Interference, and System Diversity," Issy-les-Moulineaux, France, Preprint No. 332, Oct. 1982.

Ippolito, L. J. (1981), Radio propagation for space communication systems, Proc. IEEE, Vol. 69, pp. 697-727, June 1981.

Ishimaru, A. (1977), Theory and application of wave propagation and scattering in random media, Proc. IEEE, Vol. 65, pp. 1030-1061, July 1977.

Jones, D. M. A. (1959), The shapes of raindrops, Journal of Meteorology, Vol. 16, pp. 504-510, Oct. 1959.

Juroshek, J. R. (1977), An Approximate Method for Calculating the Performance of CPSK and NCFSK Modems in Gaussian Noise and Interference OT-Report 77-109, U. S. Dept. of Commerce, Office of Telecommunications, Boulder, Colorado, January 1977.

Kanellopoulos, J. D., and Clarke, R. H. (1981), A study of the joint statistics of rain depolarization and attenuation applied to the prediction of radio link performance, Radio Science, Vol. 16, pp. 203-211, March/April 1981.

Lin, S. H., Statistical behavior of rain attenuation, B.S.T.J. Vol. 52, pp. 557-581, April 1973.

Nowland, W. L., Olsen, R. L. and Shkarofsky, I. P. (1977), Theoretical relationship between rain depolarization and attenuation, Elec. Letters, Vol. 13, pp. 676-678, Oct. 27, 1977.

Olsen, R. L. (1981), Cross polarization during precipitation on terrestrial links: A review, Radio Science, Vol. 16, pp. 761-779, Sept./Oct. 1981.

Olsen, R. L. (1982), A review of coherent radio wave propagation through precipitation media of randomly oriented scatterers, and the role of multiple scattering, Radio Science, Vol. 17, pp. 913-928, Sept./Oct. 1982.

Olsen, R. L. and Nowland, W. L. (1978), Semi-empirical relations for the prediction of rain depolarization statistics: Their theoretical and experimental basis, Proc. of the International Symposium on Ant. and Prop., Japan.

Oguchi, T. (1977), Scattering properties of Pruppacher-and-Pitter form raindrops and cross polarization due to rain: Calculations at 11, 13, 19.3 and 34.8 GHz, Radio Science, Vol. 12, pp. 41-51, Jan./Feb. 1977.

Oguchi, T. (1981a), Scattering from hydrometeors: A survey, Radio Science, Vol. 16, pp. 691-730, Sept./Oct. 1981.

Oguchi, T. (1981b), Summary of studies on scattering of centimetre and millimetre waves due to rain and hail, Ann. Telecommunic., Vol. 36, pp. 383-399, July/Aug. 1981.

Osterberg, K. (1976), Effect of drop canting angle distribution on depolarization of microwaves in rain, FOA Report, Vol. 10, pp. 1-8.

Persinger, R. P. and Stutzman, W. L. (1978), Millimeter Wave Propagation Modeling of Inhomogeneous Rain Media for Satellite Communication Systems," Interim Report under NASA Goddard Contract NAS5-22577 and U. S. Army Research Office Grant DAAG29-77-G-0083, June 1978.

Persinger, R. P., Stutzman, W. L., Castle, R. E., and Bostian, C. W. (1980), Millimeter wave attenuation prediction using a piecewise uniform rain rate model, IEEE Trans. on Ant. and Prop., Vol. AP-28, pp. 149-153, March 1980.

Prabhu, V. K. (1969), Error rate considerations for coherent PSK systems with co-channel interference, B.S.T.J., March 1969.

Pruppacher, H. R., and Pitter, R. L. (1971), A semi-empirical determination of the shape of cloud and rain drops, J. of Atmospheric Sciences, Vol. 28, pp. 86-94, Jan. 1971.

Rogers, D. V. and Osen, R. L. (1976), "Calculation of Radiowave Attenuation due to Rain at Frequencies up to 1000 GHz," CRC Report 1299, Communication Research Centre, Ottawa, Canada, Nov. 1976.

Rosenbaum, A. S. (1968), PSK error performance with gaussian noise and interference, B.S.T.J., Feb. 1968.

Rustako, A. J. (1982), Rain attenuation and depolarization over an earth-space path at 12 GHz: Experimental results using the CTS satellite beacon, IEEE Trans. on Ant. and Prop., Vol. AP-30., July 1982.

Smith, E. K. (1982), Centimeter and millimeter wave attenuation and brightness temperature due to atmospheric oxygen and water vapor, Radio Science, pp. 1455-1464, Nov./Dec. 1982.

Stutzman, W. L. (1980), "A Review of Theoretical Modeling of Millimeter Wave Propagation Through Precipitation," Interim Report for NASA under Contract NAS5-22577, May 1980.

Stutzman, W. L., Tsolakis, A. and Dishman, W. K. (1982), Millimeter Wave Satellite Communication Studies - Results of the 1981 Propagation Modeling Effort, Virginia Tech EE Dept. Technical Report under NASA/JPL Contract No. 955954, Dec. 1982.

Stutzman, W. L. and Dishman, W. K. (1982), A simple model for the estimation of rain-induced attenuation along earth-space paths at millimeter wavelengths, Radio Science, Vol. 17, pp. 1465-1476, Nov./Dec. 1982.

Stutzman, W. L., Bostian, C. W., Tsolakis, A. and Pratt, T., (1983), The impact of ice on 11 GHz depolarization along satellite to earth paths, submitted for publication.

Stutzman, W. L., Overstreet, W. P., Bostian, C. W., Tsolakis, A. and Manus, E. A. (1981), Final Report on Ice Depolarization on Satellite Radio Paths, Virginia Tech EE Dept. Technical Report under INTELSAT Contract No. INTEL-123, April 1981.

Tsolakis, A. (1982), "Multiple Scattering of Electromagnetic Waves by Distributions of Particles with Applications to Radio Wave Propagation Through Precipitation," Ph.D. Dissertation, VPI&SU, Jan. 1982.

Tsolakis, A. and Stutzman, W. L. (1982), Multiple scattering of electromagnetic waves by rain, Radio Science, Vol. 17, pp. 1495-1502, Nov./Dec. 1982.

Towner, G. C., Marshall, R. E., Stutzman, W. L., Bostian, C. W., Pratt, T., Manus, E. A. and Wiley, P. H. (1982), Initial results from the VPI&SU SIRIO diversity experiment, Radio Science, Vol. 17, pp. 1489-1494, Nov./Dec. 1982.

Thirlwell, J. and Howell, R. G. (1980), 20 and 30 GHz slant path propagation measurements at Marthesham Heath, U.K., AGARD Conference Preprint No. 284 on "Propagtion Effects in Space/Earth Paths," London, pp. 10.1-10.9, May 1980.

Vogel, W. J. (1979), CTS Attenuation and Cross Polarization Measurements at 11.7 GHz, Final Report for Feb. 1978 to Jan. 1979 under NASA Goddard Contract No. NAS5-22576, May, 1979.

Vogel, W. J. (1980), CTS Attenuation and Cross Polarization Measurements at 11.7 GHz, Final Report for June 1976 to June 1979 under NASA Goddard Contract No. NAS5-22576, June 1980.

Watson, P. A. and Arbabi, M. (1973), Crosspolarization isolation and discrimination, Elec. Letters, Vol. 9, pp. 516-517, Nov. 1973.

VITA

Donald L. Runyon Jr. was born March 4, 1958 in Charleston, West Virginia. He attended South Charleston High School, in South Charleston, West Virginia from 1973 to 1976. He attended VPI&SU in Blacksburg, Virginia from 1976 to 1981 and received the Bachelor of Science degree in Electrical Engineering. While pursuing the B.S. degree Don participated in the Co-operative-Education Program. He worked at Westinghouse, Inc. in South Boston, Virginia during one work period and at Motorola, Inc. in Fort Lauderdale, Florida for the remaining three assigned work periods. From 1981 to 1983 Don attended the graduate program at VPI&SU in Electrical Engineering. He also worked as a research assistant in the Satellite Communications Group during that time. Don received the Master of Science degree in Electrical Engineering on March 19, 1983.

A SIMPLE MODEL FOR THE DEPOLARIZING EFFECTS OF RAIN AND ICE ON EARTH SATELLITE LINKS IN THE 10 TO 30 GHz FREQUENCY RANGE

by

Donald Lawson Runyon, Jr.

(ABSTRACT)

This thesis reports the results of a thorough study into the effects of rain and ice on the polarization resuse technique for earth-space communications. Precipitation in the form of rain and ice leads to significant depolarization and attenuation of dual polarized signals above about 10 GHz. The depolarization versus attenuation relationship is examined in depth using a rigorous multiple scattering model. This relationship for rain is expressed in the form of a simple function similar to that used by the CCIR. Prediction accuracy using this simple model is quantified by comparisons to measured data and other model values. The impact of depolarization effects on the carrier-to-noise ratio for digital PSK systems is also addressed. Preliminary results for ice layer effects are presented.